Matter, Dark Matter and Gravitational Waves from a GUT-Scale $U(1)$ Phase Transition

Dissertation

zur Erlangung des Doktorgrades

des Fachbereichs Physik

der Universität Hamburg

vorgelegt von

Valerie Domcke

aus München

Hamburg

2013

Gutachter der Dissertation:	Prof. Dr. Wilfried Buchmüller Prof. Dr. Jan Louis Prof. Dr. Juan Garcia-Bellido
Gutachter der Disputation:	Prof. Dr. Wilfried Buchmüller Prof. Dr. Günter Sigl
Datum der Disputation:	10. Juli 2013
Vorsitzender des Prüfungsausschusses:	Prof. Dr. Georg Steinbrück
Vorsitzender des Promotionsausschusses:	Prof. Dr. Peter Hauschildt
Dekan der Fakultät für Mathematik, Informatik und Naturwissenschaften:	Prof. Dr. Heinrich Graener

Abstract

The cosmological realization of the spontaneous breaking of $B-L$, the difference of baryon and lepton number, can generate the initial conditions for the hot early universe. In particular, we show that entropy, dark matter and a matter-antimatter asymmetry can be produced in accordance with current observations. If $B-L$ is broken at the grand unification scale, F-term hybrid inflation can be realized in the false vacuum of unbroken $B-L$. The phase transition at the end of inflation, governed by tachyonic preheating, spontaneously breaks the $U(1)_{B-L}$ symmetry and sets the initial conditions for the following perturbative reheating phase. We provide a detailed, time-resolved picture of the reheating process. The competition of cosmic expansion and entropy production leads to an intermediate plateau of constant temperature, which controls both the generated lepton asymmetry and the dark matter abundance. This enables us to establish relations between the neutrino and superparticle mass spectrum, rendering this mechanism testable. Moreover, we calculate the entire gravitational wave spectrum for this setup. This yields a promising possibility to probe cosmological $B-L$ breaking with forthcoming gravitational wave detectors such as eLISA, advanced LIGO and BBO/DECIGO. The largest contribution is obtained from cosmic strings which is, for typical parameter values, at least eight orders of magnitude higher then the contribution from inflation. Finally, we study the possibility of realizing hybrid inflation in a superconformal framework. We find that superconformal D-term inflation is an interesting possibility generically leading to a two-field inflation model, but in its simplest version disfavoured by the recently published Planck data.

Zusammenfassung

Die kosmologische Realisierung der spontanen Brechung von $B-L$, der Differenz zwischen Baryon- und Leptonzahl, kann die Anfangsbedingungen für das frühe, heiße Universum schaffen. Insbesondere zeigen wir, dass Entropie, dunkle Materie und eine Materie-Antimaterie Asymmetrie in Übereinklang mit aktuellen Beobachtungen erzeugt werden können. Falls $B-L$ an der Skala der großen Vereinheitlichung gebrochen wird, kann F-Term Hybrid-Inflation im falschen Vakuum der ungebrochenen $B-L$ Symmetrie stattfinden. Der Phasenübergang am Ende von Inflation, getrieben durch tachyonisches Preheating, bricht die $U(1)_{B-L}$ Symmetrie spontan und legt die Anfangsbedingungen für die folgende, störungstheoretisch behandelbare Reheatingphase fest. Wir geben eine detaillierte, zeitaufgelöste Beschreibung des Ablaufs von Reheating. Das Wechselspiel von kosmischer Expansion und Entropieproduktion führt zu einer zwischenzeitlich konstanten Temperatur, die sowohl die erzeugte Leptonasymmetrie als auch die Menge der produzierten dunklen Materie kontrolliert. Somit können wir Beziehungen zwischen dem Neutrino- und Superteilchen-Massenspektrum herstellen, was ein Überprüfen dieses Mechanismus erlaubt. Darüber hinaus berechnen wir das vollständige Gravitationswellenspektrum für dieses Modell. Dies eröffnet die vielversprechende Möglichkeit, kosmologische $B-L$ Brechung mit zukünftigen Gravitationswellendetektoren wie eLISA, advanced LIGO und BBO/DECIGO zu testen. Der größte Beitrag stammt dabei von kosmischen Strings. Für typische Parameterwerte liegt dieser mindestens acht Größenordnungen über dem Beitrag der Inflation. Schließlich untersuchen wir die Möglichkeit, Hybrid-Inflation in einer superkonformen Theorie zu realisieren. Wir zeigen, dass superkonforme D-Term-Inflation eine interessante Möglichkeit darstellt, die generisch zu einem Zwei-Feld-Inflationsmodel führt. In seiner einfachsten Version ist superkonforme D-term-Inflation allerdings nicht sehr gut mit den kürzlich veröffentlichten Planck Daten verträglich.

Contents

List of Figures

Introduction

With the survey of the cosmic microwave background by the Planck satellite and with the Large Hadron Collider (LHC) up and running, we have entered new testing grounds to probe and distinguish different models, in cosmology as well as in particle physics. For example, the Planck mission is providing valuable input for models of inflation [1]. By searching for topological defects, which are relics of spontaneous symmetry breaking processes in the early universe, it is moreover probing the possibility of cosmological phase transitions [2]. In a totally complementary approach, the LHC is investigating spontaneous symmetry breaking by studying the mechanism of electroweak symmetry breaking in the Standard Model. Further exciting developments are expected from a new generation of upcoming gravitational wave detectors. These are expected to reach, for the first time, the sensitivity needed to detect gravitational waves from various astrophysical and cosmological sources [3]. This would open up a fascinating window to the very early universe, enabling us to probe time and energy scales far beyond the reach of cosmic microwave background observations.

In this situation, we study the consequences of a $U(1)$ phase transition which is well motivated from a particle physics point of view and at the same time addresses open questions in cosmology: Extending the minimal supersymmetric Standard Model by a gauged $U(1)$ symmetry with charge $B-L$, i.e. the difference between baryon and lepton number, which is spontaneously broken at the grand unification scale (GUT scale) can naturally explain the smallness of neutrino masses. Studying the cosmological realization of spontaneous $B-L$ breaking yields the following intriguing picture [4]: F-term Hybrid inflation [5] can be realized in a false vacuum which respects the $B-L$ symmetry. The phase transition at the end of inflation, governed by tachyonic preheating [6], spontaneously breaks $B-L$ and generates the initial conditions for the hot early universe, in particular a matter-antimatter asymmetry via leptogenesis [7] as well as dark matter in accordance with current observations [8].

We study the $B-L$ phase transition in the full supersymmetric Abelian Higgs model. For the subsequent reheating process, we give a time-resolved description of all particle abundances by employing Boltzmann equations. We find that a crucial player is the lightest of the heavy right-handed neutrinos. Moreover, the competition of cosmic expansion and entropy production leads to an intermediate period of constant reheating temperature, during which a $B-L$ asymmetry and a gravitino abundance are produced. Depending on the underlying

superparticle mass spectrum, the latter can either directly explain the observed dark matter abundance or can, in its decays, produce a nonthermal contribution to neutralino dark matter. Requiring consistency of hybrid inflation, leptogenesis and dark matter, the key role of the reheating temperature enables us to establish relations between the parameters of the neutrino sector and the superparticle mass spectrum. For gravitino dark matter, we find a lower bound of 10 GeV on the gravitino mass, assuming a gluino mass of 1 TeV. For neutralino dark matter, we find that, for instance, a mass of the lightest neutrino of 0.05 eV would require a gravitino mass of at least 10 TeV and for a higgsino-like lightest supersymmetric particle a mass below 900 GeV. A promising way of probing this model is by measuring the gravitational wave background [9]. We thus calculate the complete gravitational wave spectrum for this setup, i.e. from inflation, from preheating and from cosmic strings in the scaling regime. The largest contribution is expected from cosmic strings, for which, using the Abelian Higgs model of cosmic strings, we find a contribution of the same shape as the gravitational background from inflation, but an amplitude many orders of magnitude larger. For comparison, we also estimate the contribution from Nambu-Goto cosmic strings, in this way quantifying the large theoretical uncertainties involved in modelling cosmic strings. Future gravitational wave detectors such as eLISA [10], advanced LIGO [11] and BBO/DECIGO [12, 13] are expected to reach the necessary sensitivity to detect the cosmic string contribution. Finally, we turn to an interesting possibility of refining the inflationary sector of this model, based on a superconformal symmetry [14]. This setup is conceptually promising, featuring an amazingly simple structure in the Jordan frame based on symmetry principles while at the same exhibiting a rich phenomenology: we find a two-field D-term inflation model with a scalar spectral index which can be as low as $n_s \sim 0.96$ while the gauge coupling can take large values compatible with grand unification. However, taking into account the recent Planck data, we find a significant tension when simultaneously considering the constraints on the spectral index and on the cosmic string tension. These results are based on work partly published in Refs. [15–19].

This thesis is organized as follows. Chapter 1 sets the stage for this thesis, briefly reviewing several concepts and open questions in both particle physics and cosmology which will be addressed in the following chapters. In Chapters 2 and 3 we discuss the $B-L$ phase transition and the subsequent reheating process from a particle physics and from a cosmological point of view, respectively. Chapter 4 investigates the resulting phenomenology, i.e. the amount of baryon asymmetry and dark matter produced, the features in the gravitational wave spectrum and the low-energy neutrino properties. In Chapter 5 we turn to superconformal D-term inflation as an idea to improve the inflation model governing the early unbroken phase of $B-L$. We review the conceptually interesting features of superconformal models and calculate the predictions for the primordial power spectrum. Three appendices are dedicated to the CP-violation in the $2 \to 2$ scattering processes, the calculation of the scalar spectral index in the Jordan frame and the parameter dependence of the reheating process.

Chapter 1

The Pieces of the Puzzle

Over the last decades, there has been great progress in developing models which address open questions in elementary particle physics and cosmology. However, we are still lacking a complete and consistent elementary particle theory at high energies which incorporates all we have learned about the different stages of early universe cosmology. This thesis aims at taking a step towards filling this gap, discussing the cosmological implications of a well-motivated particle physics model. In this chapter, we briefly review the current status and recent developments in cosmology and particle physics which will be relevant in later chapters.

1.1 Symmetry as a guiding principle

A crucial step in understanding the laws of particle physics was the uncovering of the gauge symmetry structure of the elementary particles, $SU(3)_C \times SU(2)_L \times U(1)_Y$. This was a milestone in the discovery of the Standard Model (SM) [20–22] and is an excellent example of a simple and fundamental principle yielding a rich phenomenology in very good agreement with observations. This success encourages us to employ symmetry principles when searching for possible extensions of the SM.

Grand Unified Theories and $U(1)_{B-L}$

Grand Unified Theories (GUTs) extend the SM gauge group by embedding it in a larger simple Lie group. This group is then broken spontaneously down to the SM gauge group at the GUT scale of about 10^{16} GeV. This process is related to one or more cosmological phase transitions, which can have a significant impact on the evolution of the early universe. A particularly appealing example is unification in $SO(10)$ [23, 24]. In this case, after adding the right-handed neutrino, one generation of SM fermions exactly fills one spinor representation of the underlying Lie algebra. When breaking $SO(10)$ down to the standard model gauge group an extra $U(1)_X$ symmetry emerges. A linear combination of this and the SM hypercharge $U(1)_Y$ can be identified as a local $U(1)$ symmetry with the difference of baryon number B and lepton number L as gauge charge, i.e. as $U(1)_{B-L}$. This symmetry will play a key role in this

thesis. The dynamical mechanism of breaking $SO(10)$ down to the SM is still a question of current research. Throughout this thesis, we assume that the first stage of this spontaneous breaking occurred significantly before the end of inflation, so that we are effectively left with the SM gauge group augmented by a local $U(1)_{B-L}$ symmetry.

Alternatively, even without specifying a complete GUT, considering $U(1)_{B-L}$ can be motivated by a bottom-up approach: the corresponding global symmetry is already a symmetry of the SM Lagrangian. After adding three generations of right-handed neutrinos, it can be promoted to a local anomaly-free symmetry. Spontaneously broken at the GUT scale, it can naturally explain the observed small neutrino masses. In this sense it is a truly minimal extension of the SM. Note that this procedure is not possible for B or L separately, since the SM allows for vacuum-to-vacuum transitions which violate $B+L$ while conserving $B-L$ [25, 26]. An example for such transitions are so-called sphaleron processes [27], which play an important role in leptogenesis, cf. Sec. 1.2. As a consequence, the matter-antimatter asymmetry observed today can be traced back to a $B-L$ asymmetry in the early universe, making $U(1)_{B-L}$ a promising starting point for explaining this asymmetry.

Topological defects

Cosmological phase transitions can leave traces detectable today in the form of topological defects. These arise from a non-trivial topology of the vacuum manifold and, depending on their spatial dimension, can be classified as monopoles, cosmic strings or domain walls. Here, since we are considering the spontaneous breaking of a $U(1)$ symmetry, we will focus on cosmic strings [28]. The formation and evolution of the cosmic string network is a very complicated process, requiring numerical simulations. Due to the enormous range of scales involved, simplifying assumptions must be made. Two possibilities are the Abelian Higgs model [29–31] and the Nambu-Goto model [32–35]. They both yield similar results for the network of long strings, however, they differ quite significantly in their predictions for small cosmic string loops. Which one of these two models is closer to reality is currently an open question. At the same time, observations of the cosmic microwave background (CMB) [2] as well as searches for gravitational waves [36, 37] are starting to seriously probe GUT-scale cosmic strings, rendering the theoretical understanding of the cosmic string network and its possible signals even more important.

In this thesis, we consider the consequences of cosmic strings formed in a $U(1)_{B-L}$ phase transition in the early universe. In particular when calculating the expected gravitational wave background, we consider both the Abelian Higgs as well as the Nambu-Goto model. This direct comparison allows us to quantify the theoretical uncertainties arising from the simulation method.

Supersymmetry and beyond

An alternative way to extend the symmetry group of the SM is to enlarge its space-time symmetry, determined by the Poincaré group, by fermionic generators. This is the route

chosen in supersymmetry [38]. Among other consequences, this introduces superpartners for all SM particles, which can act as candidates for dark matter as well as for the scalar field required for inflation, cf. Secs. 1.2 and 1.3. As a further step, supersymmetry can be advanced to a gauge symmetry. This implies promoting the invariance under the global space-time transformations of supersymmetry to an invariance under general local space-time transformations, i.e. to the symmetry group of general relativity. The resulting symmetry is thus called supergravity. This framework allows for an effective description of the influence of gravity on particle physics below the Planck scale of about 10^{19} GeV, while at the same time introducing a particle physics description of the gravitational interaction in form of a spin-2 particle, the graviton. The spin-3/2 superpartner of the graviton, the gravitino, is a further promising candidate for dark matter.

Recently, a non-standard approach to supergravity has received a lot of interest. Starting from a larger symmetry group, the superconformal group, the usual formulation of supergravity can be recovered by gauge-fixing the additional degrees of freedom [14]. Hence, it might prove useful to employ this larger superconformal symmetry in (inflationary) model building. An example are the so-called canonical superconformal supergravity (CSS) models [39], which are characterized by their simple structure in the Jordan frame. They generically yield a non-minimal coupling of gravity to the scalar field driving inflation, a feature which has independently received a lot of interest from a phenomenological point of view in Higgs inflation [40–42].

Throughout this thesis, we work in a supersymmetric framework, with the gravitino and the neutralinos playing crucial roles as dark matter candidates. Supergravity effects become important at the high scales relevant for inflation. Here, Chapter 3 assumes a (nearly) canonical Kähler potential whereas in Chapter 5, we present a model with a Kähler potential motivated by a superconformal symmetry.

1.2 Cosmology at the very high energy frontier

In an expanding cooling universe, high energy scales correspond to early cosmological times. In this sense, a step to higher energies is at the same time a glance back into the history of our universe. With the LHC at CERN collider experiments have begun to probe the TeV energy regime. In the context of cosmic history this is, however, only a tiny fraction of the energy range our universe has experienced, corresponding to the dilution of radiation and matter in an expanding universe and the decoupling of weakly coupled particle species. Exploiting our knowledge of nuclear physics and of the weak interaction processes keeping neutrons and protons in chemical equilibrium in the early universe, we can push our understanding of the history of the universe a bit further: big bang nucleosynthesis (BBN) explains the generation of light elements in the early universe and agrees very well with today's measurements of

their abundances. This brings us up to an energy scale of about a 1 MeV and back to about one second after the 'big bang'. But when it comes to this second, and in particular to the first fractions of this second, corresponding to a vast range of energy scales, possibly up to the Planck scale, a substantial number of fundamental questions remain unresolved.

Inflation

Inflation [43–45], by now a well established concept in early universe cosmology, addresses the so-called horizon problem and the flatness problem. In short, the former is the question of why the CMB is so extremely isotropic even though, according to standard cosmology, it originated from many causally disconnected patches. The latter is the question of why the universe we observe today is to very good approximation flat although, without fine-tuning, standard cosmology would suggest a much larger curvature. Inflation solves these problems by a phase of exponential expansion in the very early universe, implying that the universe observable today was indeed in causal contact at some early point in time and at the same time dynamically enforcing a very small spatial curvature. Moreover, inflation also dilutes any monopoles formed in pre-inflationary phase transitions, which would otherwise come to dominate the energy density of the universe. Finally, inflation predicts small fluctuations in the spectrum of the CMB, a prediction which has spectacularly been confirmed by the Cosmic Background Explorer (COBE) [46] and more recently, too high accuracy, by the Wilkinson Microwave Anisotropy Probe (WMAP) [47] and the Planck satellite [1]. These small fluctuations are thought to be the 'seeds' of structure formation, responsible for the formation of galaxies and clusters in our universe.

In spite of this great success, there are still a number of open questions related to inflation. In its simplest version, inflation is driven by a slowly rolling scalar field, the so-called inflaton. However, it is neither known how this scalar field is accommodated in the particle spectrum of a particle physics theory nor how an appropriate scalar potential is generated from a fundamental theory. In this context, inflation is often referred to as 'a paradigm in lack of a model'.

A tempting explanation is to use the only scalar field of the SM, the Higgs field. Alas, without further modifications the scalar potential of the Higgs is too steep to support inflation in agreement with current data on the power spectrum of the scalar fluctuations [1]. A possibility which has recently received a lot of interest is the introduction of a non-minimal coupling of the Higgs field to gravity [40–42], which would allow for slow-roll inflation, however, at the price of introducing a dimensionless coupling of $\mathcal{O}(10^4)$. More possibilities arise once supersymmetry is employed, which introduces additional scalar fields. In this context an interesting idea is to exploit flat directions in the scalar potential of the minimal supersymmetric standard model (MSSM) [48] or, omitting the concept of gauging $B-L$, to identify the inflaton with a right-handed sneutrino, the superpartner of one of the heavy neutrinos involved in the seesaw mechanism. The latter has been realized in chaotic [49, 50] as well

as in hybrid inflation [51, 52]. However, as of today the situation remains inconclusive, with current experiments unable to distinguish between these and further ideas. Indeed, the recently published Planck data [1] severely constrains many models without nominating a clear favourite, see e.g. [53] for a recent discussion.

In this thesis, the approach to embed inflation in a particle physics theory will be the following: Extending the SM gauge group by a local $U(1)_{B-L}$ symmetry which is spontaneously broken at the GUT scale, the scalar fields responsible for the dynamical symmetry breaking can simultaneously generate the dynamics of F-term hybrid inflation [5, 54, 55]. In Chapter 5, we refine this idea and study a superconformal D-term inflation model [56, 57]. This leads to a non-minimal coupling of the inflaton field to gravity as is employed in Higgs inflation, but without the drawback of a huge coupling constant.

Reheating

At the end of inflation, the universe is super-cooled with any initial thermal bath strongly diluted during the exponential expansion process. In order to connect this picture to standard cosmology, the universe must 'reheat', i.e. the vacuum energy present during inflation must be transferred into a hot, thermal plasma. The latter then slowly cools down as the universe expands until today's CMB temperature of 2.7 Kelvin is reached.

The mechanism of this reheating process is a question under debate. Originally, it was thought that the vacuum energy of inflation is transferred to coherent oscillations of the inflaton field which then decay into lighter (SM) particles [58, 59]. However, it was then discovered that in some inflation models this perturbative description was insufficient due to a dominant fast nonperturbative process, referred to as 'preheating'. The latter can be realized in two different ways, as preheating via parametric resonance [60] or as tachyonic preheating [6]. Both cases lead to an explosive particle production just after the end of inflation. In the former case, this is due to oscillating mass terms induced by the oscillations of the inflaton field. In the latter case a tachyonic mass term for one of the scalar fields triggers an exponential growth of low momentum modes.

Hence, the question of how reheating proceeds has become a model-dependent question with very important consequences for the evolution of our universe. What is the temperature of the thermal bath produced in the reheating process, i.e. what is the highest temperature ever reached in the universe? This affects the formation of very weakly coupled particles such as gravitinos, which decouple from the thermal bath right after production. If the reheating temperature is very high, i.e. (model-dependent) above roughly 10^{10} GeV, this leads to a large gravitino abundance which can result in the so-called 'gravitino problem' [61–68]. A lower bound on the reheating temperature of a few MeV is obtained from the abundance of light elements [69–71]. This leaves a large range of possible reheating temperatures. A striking observation is that the reheating temperature required to generate gravitino dark matter in just the right abundance to explain the observed value, $T_{\rm RH} \sim 10^{10}$ GeV, matches the

typical values for the mass of the lightest right-handed neutrino and hence the leptogenesis temperature [72]. This might be pointing to a common origin for matter and dark matter, i.e. a reheating temperature governed by the lifetime of the right-handed neutrino instead of the inflaton lifetime. Pursuing this idea leads to a two-stage reheating process with many phenomenologically interesting aspects [4, 73].

In this thesis, we address these questions by giving a detailed, time-resolved description of all the processes relevant during preheating and reheating for the Abelian Higgs model describing the $B-L$ breaking phase transition. We numerically track the momentum distributions of all particle species in a realistic model throughout the process based on a set of coupled Boltzmann equations, with the initial conditions determined by tachyonic preheating. This work is based on earlier studies [4, 73], extending these by taking into account the effect of all supersymmetric degrees of freedom. Furthermore, we derive semi-analytical expressions for all the relevant outputs of the reheating process, capturing the parameter dependencies and allowing for future use of the results without a tedious numerical calculation. In particular, we discuss which aspects of the temperature evolution during the reheating process (and hence which model parameters) can be probed by different types of observations.

Baryogenesis

In today's universe, there is evidently a vast overabundance of matter compared to antimatter. However, starting from a hot thermal plasma, we would expect the same amount of matter and antimatter to have been produced, and to have mostly annihilated into photons. The asymmetry measured today is thus conveniently expressed as [47]

$$\eta_B = (n_B - n_{\bar{B}})/n_\gamma = (6.19 \pm 0.15) \times 10^{-10}\,, \tag{1.1}$$

i.e. as the net number density of baryons normalized to the number density of photons today. So how can we explain this tiny, but so crucial asymmetry? Baryogenesis is an answer to this question, generating an asymmetry dynamically in the early universe provided that $B-L$, C and CP are violated[1] and that there is a departure from thermal equilibrium [74]. Like inflation, this is a process which cannot be realized within the SM and calls for new physics. A particularly interesting mechanism is leptogenesis [7], a realization of baryogenesis in the lepton sector. Here typically the decay of right-handed neutrinos is the source of $B-L$, C- and CP-violation. The departure from thermal equilibrium can be realized during the reheating process and the asymmetry is transferred to the baryon sector through sphalerons. Due to the high energy scales involved, leptogenesis is difficult to probe experimentally. However, probing properties of the neutrino sector such as the light neutrino mass scale [1, 75] or neutrinoless double-β decay [76] as well as linking leptogenesis to other stages of early universe cosmology can help to constrain the possible parameter space.

[1] Here $C(P)$ denotes the charge(parity) operator.

The work presented here is closely related to previous studies of thermal leptogenesis [77, 78] and nonthermal leptogenesis via inflaton decay [79–82]. We consider nonthermal as well as thermal contributions to the lepton asymmetry. On the one hand, after preheating, the energy density of the universe is stored in $B-L$ Higgs bosons, which decay into right-handed neutrinos and sneutrinos, which in turn decay into particles of the thermal bath, thereby generating a lepton asymmetry. On the other hand, right-handed neutrinos and sneutrinos are also produced thermally, yielding a thermal contribution to the lepton asymmetry. We explicitly track both contributions throughout the reheating process.

1.3 The invisible universe

There are a number of particle species which we have not observed yet, but for which we have good reasons to believe they exist, either from indirect experimental evidence or from theoretical considerations or both. Some of these play an important role when studying the evolution of our universe, providing a further link between particle physics and cosmology.

Dark matter

Numerous observations on galactic to cosmological scales point to a non-baryonic component of the matter energy density of the universe [83]. We know that this new particle species, dubbed dark matter (DM), must interact at least gravitationally, but at most weakly. It must be stable or at least have a lifetime comparable to the age of the universe. And it must be 'cold' or at most 'warm', i.e. non-relativistic at the onset of structure formation.

The SM contains no such particle, but extending it to the MSSM introduces the neutralinos, formed from the superpartners of the neutral electroweak gauge bosons and of the Higgs bosons. If one of these is the lightest supersymmetric particle (LSP) in the spectrum and if R-parity is conserved, then this neutralino is a viable DM candidate [84, 85]. Charged under $SU(2)_L$, neutralinos are part of a larger class of candidates referred to as weakly interacting massive particles (WIMPs). Any locally supersymmetric theory additionally introduces the gravitino. In a gauge mediated supersymmetry breaking scenario, the gravitino is typically the LSP and hence a viable DM candidate [86]. Another well-motivated candidate is the QCD axion, originally introduced to solve the strong CP problem.

On the experimental side, the particle physics nature of dark matter is being probed by direct and indirect detection methods. At the time of writing, there is no clear evidence of a positive signal in any of these searches, though there have been some anomalies observed both in direct and in indirect detection channels, see e.g. Ref. [87] for a recent overview. Moreover, the LHC is probing the parameter space of WIMPs, and is in particular in the constrained MSSM severely pushing the 'WIMP miracle' arising for thermally-produced neutralino-only DM, see e.g. Ref. [88]. Hence, at the moment WIMPs respecting the current experimental constraints, gravitinos, which are notoriously hard to detect due to their very weak coupling,

as well as axions or axion-like particles (for bounds on the parameter space, see e.g. Ref. [89]) all remain viable, theoretically well-motivated candidates.

In the following, we will consider both the case of gravitino and of neutralino dark matter. If the gravitino is the LSP, gravitino dark matter can be thermally produced at a reheating temperature compatible with leptogenesis [72]. If the gravitino is the heaviest superparticle, as realized in anomaly mediated supersymmetry breaking [90, 91], dark matter can be formed as neutralino dark matter. This has been recently reconsidered in the case of wino [92], higgsino [93] and bino [94] LSP, motivated by the discovery of a Higgs-like scalar boson with a mass of about 126 GeV by the LHC experiments ATLAS and CMS [95, 96]. In this case, it has been pointed out that a gravitino mass above 10 TeV is consistent with BBN and leptogenesis [61, 97, 98]. In this thesis, we will discuss these two options in the context of the $U(1)_{B-L}$ phase transition. In particular, we will focus on constraints on the model parameters which can be derived by requiring the consistency of hybrid inflation, leptogenesis, BBN as well as the correct DM abundance.

Gravitational waves

Gravitational waves (GWs) are produced as fluctuations of the metric in cosmological processes as well as by astrophysical sources, for a review see e.g. Refs. [99, 100]. Since they only interact gravitationally, i.e. extremely weakly, with all other components of the universe, they decouple instantaneously and then travel freely ever since. A detection of a GW signal would thus yield direct information about its source as well as, due to the red-shift the GW experiences on its way to the detector, about the expansion history of our universe. This would open up a window to probe cosmological models up to the scale of inflation. This is similar to the way the CMB photons carry information on their last scattering surface, but due to the much weaker interactions of GWs compared to photons, significantly earlier times can be probed, when the universe was transparent for GWs but not for electromagnetic waves.

Many of the cosmological processes discussed above are expected to produce GWs. From inflation, we expect an almost scale-invariant stochastic background over a wide range of frequencies, with the amplitude depending mainly on the tensor-to-scalar ratio of the inflationary model [101, 102]. This scale invariance is slightly distorted if degrees of freedom decay, annihilate or decouple during the radiation-dominated era, which in principle allows to probe for example the scale of supersymmetry breaking [103]. At a frequency controlled by the reheating temperature, the scale-invariant behaviour ends and the amplitude becomes strongly suppressed [104]. From preheating, we expect additional features in the spectrum at high frequencies, both for preheating via parametric resonance [105] and for tachyonic preheating [106]. For the latter case, the spectrum has been determined numerically for certain parameter regimes of hybrid inflation [107, 108]. If the $U(1)$ symmetry broken at preheating is a gauge symmetry, there is an additional feature in the spectrum associated with the mass of the gauge boson [109]. Finally, a very interesting source of GWs, which is, however, plagued

with large theoretical uncertainties, is the cosmic string network [110]. In the $B-L$ breaking phase transition local cosmic strings are formed. The initial state of such a network can be simulated numerically, and recently the amplitude of the scale-invariant spectrum of GWs produced during the radiation-dominated epoch has been determined [111]. This analysis was performed for the Abelian Higgs model of cosmic strings, where it is usually assumed that strings lose their energy mostly via radiation of massive particles. On the contrary, in the Nambu-Goto model cosmic strings lose their energy by radiating GWs. The resulting spectrum was studied, for example, in Refs. [112–114].

On the experimental side, GWs can be probed directly by millisecond pulsar timing measurements as well as by ground- and space-based interferometers. The most recent constraints come from PPTA [115] and LIGO [116]. Future experiments such as eLISA [10], advanced LIGO [11] and BBO/DECIGO [12, 13] will reach the sensitivity necessary to probe a GUT-scale $U(1)$ phase transition.

In this situation, it is crucial to understand the GW signal of different astrophysical sources and cosmological models. To this end, we study the GW background expected from a $U(1)_{B-L}$ breaking phase transition in the early universe. In particular, we do not restrict ourselves to the signal generated at one particular step of the cosmological evolution, but calculate the entire spectrum for a consistent particle cosmology model of the early universe. Moreover, our discussion here can serve as a worked example of how to relate features in the GW spectrum to model parameters.

Summarizing, a variety of experiments is currently probing aspects of SM extensions and cosmological models. Indeed, well-motivated extensions of the SM more often than not have important consequences for cosmology and, vice versa, tackling open questions in cosmology very often involves extending the SM. Hence, it is crucial to combine our understanding of particle physics and of the different stages of early universe cosmology. Following this spirit, this thesis studies the cosmological implications of extending the MSSM by a gauged $U(1)_{B-L}$ symmetry which is dynamically broken close to the GUT scale.

Chapter 2

Spontaneous Breaking of $B-L$

The study presented here is based on promoting the global $U(1)_{B-L}$ symmetry present in the SM to a gauge symmetry which is dynamically broken at a high energy scale. This chapter is dedicated to introducing this framework in a supersymmetric setup. In Chapter 3 we will then study the implications of this model for cosmology, identifying the $B-L$ breaking phase transition with the phase transition at the end of inflation. The inflationary phase is then realized in the false vacuum of $B-L$ and the creation and decay of particles at and after the phase transition is responsible for the production of entropy, matter and dark matter. In this context, a crucial role is played by the right-handed neutrino, which is a key player in the reheating process and at the same time responsible for creating a matter asymmetry via leptogenesis.

In this chapter, we focus on the realization of the spontaneous breaking of $U(1)_{B-L}$ in a particle physics framework. In Sec. 2.1, we motivate and introduce the superpotential of our model. In Sec. 2.2, we focus on a crucial ingredient of our model, the supersymmetric Abelian Higgs mechanism. We derive the full Lagrangian for the spontaneous breaking of a $U(1)$ gauge symmetry, in particular during and after the phase transition. We discuss some issues related to the choice of gauge and give the resulting Lagrangian before gauge fixing as well as in unitary gauge, which will be the most useful gauge for our application. With this, we then proceed to discuss the actual process of symmetry breaking in Sec. 2.3, explaining the particle content before, during and after the phase transition. In Sec. 2.4 we combine the results derived so far to calculate the decay rates and branching ratios needed to quantify the outcome of the reheating process discussed in the next chapter. Finally, in Sec. 2.5, we introduce the flavour model used in this thesis to parametrize the couplings in the superpotential. This chapter is based on work partly published in Ref. [16], with a particular focus on the role of the gauge choice and the interpretation of the degrees of freedom of the Higgs and inflaton sector in the context of spontaneous symmetry breaking.

2.1 A promising superpotential

Our studies here are based on Ref. [73], where a model was presented which features a dynamically broken local $U(1)_{B-L}$ symmetry in a supersymmetric framework. Here, we give a review of this model, concentrating on aspects which are especially relevant for this thesis and introducing the notation we will use in the following.

Dynamical $B-L$ breaking is achieved by introducing three additional chiral superfields which spontaneously break the $U(1)_{B-L}$ by means of a supersymmetric version of the Abelian Higgs mechanism and simultaneously allow for a phase of hybrid inflation. Additionally, three generations of right-handed neutrino supermultiplets are added to the MSSM particle content, which take care of anomaly cancellation in the gauged $B-L$ symmetry while simultaneously generating light neutrino masses via the seesaw mechanism. Their $B-L$ violating mass term is induced after the spontaneous symmetry breaking by the vacuum expectation value (vev) the $B-L$ breaking Higgs field. The superpotential is given by

$$W = \frac{\sqrt{\lambda}}{2}\,\Phi\,(v_{B-L}^2 - 2\,S_1 S_2) + \frac{1}{\sqrt{2}} h_i^n n_i^c n_i^c S_1 + h_{ij}^{\nu} \mathbf{5}_i^* n_j^c H_u + W_{\text{MSSM}}\,, \tag{2.1}$$

where S_1 and S_2 are the chiral superfields containing the Higgs field responsible for breaking $B-L$ and the dynamics of the scalar component of Φ controls the transition from the $B-L$ conserving to the $B-L$ breaking vacuum. In Sec. 3.1, we will identify these fields as the waterfall and inflaton fields of hybrid inflation, respectively. n_i^c denote the superfields containing the charge conjugates of the right-handed neutrinos. In the following, we will refer to the components of S_1, S_2 and Φ as the symmetry breaking sector, whereas the components of n_i^c form the neutrino sector. v_{B-L} is the scale at which $B-L$ is broken. The $B-L$ charges are $q_S \coloneqq q_{S_2} = -q_{S_1} = 2$, $q_\Phi = 0$ and $q_{n_i^c} = +1$. h and λ denote coupling constants, which we will restrict by imposing a flavour symmetry in Sec. 2.5, and W_{MSSM} represents the MSSM superpotential,

$$W_{\text{MSSM}} = h_{ij}^u \mathbf{10}_i \mathbf{10}_j H_u + h_{ij}^d \mathbf{5}_i^* \mathbf{10}_j H_d\,. \tag{2.2}$$

All superfields have been arranged in $SU(5)$ multiplets, $\mathbf{10} = (q,\, u^c,\, e^c)$ and $\mathbf{5}^* = (d^c,\, l)$, and $i, j = 1, 2, 3$ are flavour indices. We assume that the colour triplet partners of the electroweak Higgs doublets H_u and H_d have been projected out. The vevs $v_u = \langle H_u \rangle$ and $v_d = \langle H_d \rangle$ break the electroweak symmetry. In the following we will assume large $\tan\beta = v_u/v_d$, implying $v_d \ll v_u \simeq v_{\text{EW}} = (v_u^2 + v_d^2)^{1/2}$. For notational convenience, we will refer to H_u as H in the following.

The superpotential (2.1) is the simplest renormalizable superpotential meeting our requirements. Note that the structure of the right-handed neutrino mass term[1] is determined

[1] Here, the term 'right-handed' also refers to the transformation behaviour under the SM gauge group $SU(2)_L$. In this sense, we will refer to these additional neutrinos as well as to their superpartners as 'right-handed' to distinguishing them from the MSSM (s)neutrinos.

by the symmetry structure and in particular the $B-L$ charge assignments. A coupling of the right-handed neutrinos to the other $B-L$ Higgs field S_2 is not possible, since the holomorphic structure of the superpotential only allows the use of the left-chiral Weyl spinors associated to the charge conjugates of the right-handed neutrinos, which carry the $B-L$ charge $q_{n_i^c} = 1$. This is similar to the distinct roles the two MSSM Higgs fields H_u and H_d play after electroweak symmetry breaking, giving mass to either up- or down-type fermions. However, the symmetries introduced so far would allow for additional terms involving the gauge singlet field Φ, i.e. a coupling to the MSSM Higgs fields $\Phi H_u H_d$ as well as Φ^2 and Φ^3 terms. In the following, we will stay with the simple expression in Eq. (2.1) and avoid obscuring the discussion with additional terms.[2] In an explicit model, these can be forbidden by introducing additional symmetries (e.g. discrete symmetries and interpreting v_{B-L} as the vev of an additional field or a $U(1)_R$ symmetry).

Note also that here and in the following, we will not explicitly be concerned about the mechanism of low energy supersymmetry breaking, and hence we omit a possible constant term governed by the gravitino mass as well as a possible $\mu H_u H_d$ term in Eq. (2.2), assuming that this term is absent at the GUT-scale but arises at the electro-weak scale. During inflation, supersymmetry is strongly broken and this plays a decisive role for the dynamics at this time. On the contrary, the scale of low energy supersymmetry breaking in the visible sector is expected to be much lower in order for supersymmetry to solve the hierarchy problem, and hence any effects on early universe cosmology can be expected to be small[3]. We will hence only come back to this topic in the context of identifying the LSP (and hence our DM candidate), whose properties depend on the underlying supersymmetry breaking mechanism. In the following we will assume exact, or nearly exact, R-parity conservation, rendering the LSP stable on cosmological time scales.

In addition to the chiral superfields mentioned above, the model contains the usual MSSM superfields as well as a vector supermultiplet V ensuring invariance under local $B-L$ transformations and the gravity supermultiplet, consisting of the graviton G and the gravitino $\widetilde{G}$.

2.2 The supersymmetric Abelian Higgs model

2.2.1 A suitable gauge

The superpotential (2.1) features a local $U(1)_{B-L}$ symmetry. Supplemented by a canonical Kähler potential,

$$K(\Phi, V) = \Phi_\alpha^* \, e^{p_\alpha V} \Phi_\alpha \,, \qquad p_\alpha = 2 g q_\alpha \,, \tag{2.3}$$

[2] See however Ref. [117] for an interesting discussion on how the $\Phi H_u H_d$-term can help circumvent bounds arising from the non-observation of cosmic strings.

[3] For a discussion of possible effects of a constant term in the superpotential, see e.g. Refs. [118, 119].

with Φ_α denoting the chiral superfields of the theory, q_α their $B-L$ charge, and g the $B-L$ gauge coupling, the resulting theory is invariant under the supersymmetric $U(1)$ gauge transformations

$$\Phi_\alpha \mapsto \Phi_\alpha \exp(2iq_\alpha \Lambda)\,, \qquad V \mapsto V - \frac{i}{g}\left(\Lambda - \Lambda^*\right)\,, \tag{2.4}$$

with Λ a chiral superfield. In the following, we study the dynamics of the spontaneous breaking of this symmetry. In the familiar non-supersymmetric Abelian Higgs mechanism, the choice of gauge plays a decisive role. In an appropriate gauge, in this case the unitary gauge, the unphysical Goldstone mode is gauged away, rendering the vector boson massive and thus making the physical degrees of freedom of the theory manifest. In this section, we derive an analogous procedure for a supersymmetric Abelian gauge theory, following the notation of Ref. [38].

A common approach in supersymmetric Abelian gauge theories is to use the Wess-Zumino gauge. This choice eliminates the real scalar C, the Weyl spinor χ and the auxiliary fields M and N in the general expansion of the gauge multiplet V in superspace,

$$\begin{aligned} V = {} & C + i\theta\chi - i\bar{\theta}\bar{\chi} + \frac{i}{2}\,\theta\theta\left(M + iN\right) - \frac{i}{2}\bar{\theta}\bar{\theta}\left(M - iN\right) - \theta\sigma^\mu\bar{\theta}A_\mu \\ & + i\theta\theta\bar{\theta}\left(\bar{\xi} + \frac{i}{2}\,\bar{\sigma}^\mu\partial_\mu\chi\right) - i\bar{\theta}\bar{\theta}\theta\left(\xi + \frac{i}{2}\,\sigma^\mu\partial_\mu\bar{\chi}\right) + \frac{1}{2}\,\theta\theta\bar{\theta}\bar{\theta}\left(D + \frac{1}{2}\,\Box C\right)\,, \end{aligned} \tag{2.5}$$

yielding the following expression in the Wess-Zumino gauge,

$$V_{WZ} = \theta\sigma^\mu\bar{\theta}A_\mu + i\theta\theta\bar{\theta}\bar{\xi} - i\bar{\theta}\bar{\theta}\theta\xi + \frac{1}{2}\,\theta\theta\bar{\theta}\bar{\theta}D\,. \tag{2.6}$$

The remaining degrees of freedom are the massless vector boson A_μ, the massless gaugino Weyl spinor ξ and the auxiliary field D. This corresponds to gauge fixing most of the original gauge degrees of freedom, leaving only the non-supersymmetric $U(1)$ gauge invariance manifest,

$$A_\mu \mapsto A_\mu + \partial_\mu\lambda\,, \tag{2.7}$$

with $\lambda(x)$ a real scalar. The remaining symmetry is then spontaneously broken by the usual non-supersymmetric Higgs mechanism. Imposing the unitary gauge, this eliminates a further degree of freedom, the would-be Goldstone boson.

However, when considering the spontaneous breaking of the $U(1)$ symmetry (2.4), there is a problem with this formalism. In the $B-L$ breaking vacuum, the Wess-Zumino gauge, which relies on an unbroken $U(1)$ symmetry, can no longer be applied in this way. For example, the Weyl spinor χ can no longer be set to zero, but must be gauged away in a way that simultaneously renders the gaugino massive. A hint on how to solve this problem can be found by counting the degrees of freedom involved in the mechanism above. We find that in all, two real scalar degrees of freedom, one Weyl spinor and two real auxiliary degrees of

freedom are eliminated by fixing the gauge - exactly the content of the chiral supermultiplet appearing in the gauge transformations (2.4) and exactly the particle content of a 'Goldstone chiral supermultiplet' which is necessary to render the entire gauge multiplet massive. With this is mind, it becomes clear that we are looking for a formalism which treats all entries of this supermultiplet on equal footing, i.e. a manifestly supersymmetric mechanism.

Recalling that the unitary gauge, which is so convenient for the non-supersymmetric Higgs mechanism, is closely related to the $U(1)$ symmetry of the problem, we shall here try a unitary gauge based on the supersymmetric transformation (2.4). We thus perform a special supersymmetric gauge transformation, which maps the two Higgs superfields S_1 and S_2 onto the same field S' in unitary gauge (thus reflecting the fact that one chiral supermultiplet is 'eaten' by the vector multiplet), while simultaneously mapping $V \mapsto Z$ as follows:

$$S_{1,2} = \frac{1}{\sqrt{2}} S' \exp(\pm 2 i q_S \Lambda) \,, \qquad V = Z - \frac{i}{g} \left(\Lambda - \Lambda^*\right) \,. \tag{2.8}$$

In this manifestly supersymmetric gauge, we can now calculate the Lagrangian and demonstrate that this yields a description in which the physical degrees of freedom involved in the symmetry breaking process become manifest. In the following chapters, we will come back to the mass terms as well as the decay and scattering processes resulting from the interactions of this Lagrangian. A reader mainly interested in the phenomenological consequences of this model may skip the derivation outlined in the following and directly turn to the final result for the Lagrangian in unitary gauge, cf. Eqs. (2.32) to (2.37).

2.2.2 The Lagrangian before gauge-fixing

In principle, the Lagrangian can be calculated in the standard way [38],

$$\mathcal{L} = \int d^4\theta \, K(\Phi, Z) + \int d^2\theta \, (W(\Phi) + h.c.) + \frac{1}{4} \int d^2\theta \, \left(\sum_a W_a W^a + h.c. \right) \,. \tag{2.9}$$

with $\int d^4\theta = \int d^2\theta \, d^2\bar{\theta}$ and $\int d^2\theta$ projecting out the $\theta\theta\bar{\theta}\bar{\theta}$ and $\theta\theta$ terms and W_a denoting the field strength chiral superfield.[4] Here, we have in mind that the Φ_α are the chiral superfields of Eq. (2.1) in unitary gauge, cf. Eq. (2.8), but the results obtained here hold beyond this. As far as this subsection is concerned, we are considering an arbitrary superpotential invariant under a $U(1)$ gauge symmetry, supplemented by a canonical Kähler potential, cf. Eq. (2.3), and without any gauge-fixing imposed. In particular, we explicitly keep all the degrees of freedom of the gauge supermultiplet. This enables us to use this formalism in a vacuum where the $U(1)$ symmetry is spontaneously broken and the vector multiplet is massive.

[4] Here, we have explicitly written out the spinor indices $a = \{1, 2\}$ in the last term, so as not to confuse the field strength superfield with the superpotential, both commonly denoted as W. In the rest of this thesis, the spinor indices are suppressed in spinor products, following the convention of e.g. Ref. [120].

The D-term of the Kähler potential

We now pay the price for abandoning the Wess-Zumino gauge. Without gauge fixing, in particular with $C \neq 0$ in Eq. (2.5), the calculation of the D-term of the Kähler potential is significantly more complicated, since the Taylor expansion of $\exp(Z)$ is not truncated at any finite power. The strategy is thus to proceed by calculating

$$\int d^4\theta\ \Phi_\alpha^*\, Z^n\, \Phi_\alpha\,, \qquad n = 0, 1, 2, \ldots \tag{2.10}$$

using the expansion of the vector superfield, cf. Eq. (2.5), and of the chiral superfield,

$$\Phi_\alpha = \ z_\alpha + i\theta\sigma^\mu\bar\theta\partial_\mu z_\alpha + \frac{1}{4}\,\theta\theta\bar\theta\bar\theta\,\partial^\mu\partial_\mu z_\alpha + \sqrt{2}\,\theta\psi_\alpha - \frac{i}{\sqrt{2}}\,\theta\theta\,\partial_\mu\psi_\alpha\sigma^\mu\bar\theta + \theta\theta F_\alpha\,, \tag{2.11}$$

and identifying all $\theta\theta\bar\theta\bar\theta$ terms. For any given n, there are only a finite number of such terms. Summing over n yields the D-term of the Kähler potential,

$$K(\Phi, Z)|_D = \sum_\alpha \sum_n \frac{p_\alpha^n}{n!} \int d^4\theta\ \Phi_\alpha^*\, Z^n\, \Phi_\alpha\,. \tag{2.12}$$

Using integration by parts and the identities for Weyl spinors,

$$\begin{aligned} (\theta\psi)(\theta\chi) &= -\frac{1}{2}\,(\theta\theta)(\psi\chi)\,, \qquad & (\bar\theta\bar\psi)(\bar\theta\bar\chi) &= -\frac{1}{2}\,(\bar\theta\bar\theta)(\bar\psi\bar\chi)\,, \\ \theta\sigma^\mu\bar\theta\,\theta\sigma^\nu\bar\theta &= -\frac{1}{2}\,\theta\theta\bar\theta\bar\theta\eta^{\mu\nu}\,, & \chi\sigma^\mu\bar\psi &= -\bar\psi\bar\sigma^\mu\chi\,, \end{aligned} \tag{2.13}$$

we find for the D-term of the Kähler potential

$$\int d^4\theta \sum_\alpha \Phi_\alpha^* \exp(p_\alpha Z)\,\Phi_\alpha = \sum_\alpha \left(\mathcal{L}^\alpha_{\text{coupl}} + \mathcal{L}^\alpha_{\text{kin}} + \mathcal{L}^\alpha_{\text{aux}}\,,\right) \tag{2.14}$$

with

$$\begin{aligned} \mathcal{L}^\alpha_{\text{coupl}} = e^{p_\alpha C}\Bigg\{ & -\frac{1}{4}\,p_\alpha^2\, z_\alpha^* z_\alpha\, A_\mu A^\mu - \frac{1}{2}\,p_\alpha\,\psi_\alpha\sigma^\mu\bar\psi_\alpha\,A_\mu - \frac{1}{4}\,p_\alpha^3\, z_\alpha^* z_\alpha\,\chi\sigma^\mu\bar\chi\,A_\mu \\ & + \frac{1}{16}\,p_\alpha^4\, z_\alpha^* z_\alpha\,\chi\chi\,\bar\chi\bar\chi + \frac{1}{2}\,p_\alpha^2\,\psi_\alpha\chi\,\bar\psi_\alpha\bar\chi \\ & + \Bigg[\Bigg(-\frac{1}{2}\,p_\alpha^2\, z_\alpha^* z_\alpha\,\bar\chi\bar\xi\ - \frac{i}{\sqrt{2}}\,p_\alpha z_\alpha\,\bar\psi_\alpha\bar\xi - \frac{i}{2\sqrt{2}}\,p_\alpha^2\, z_\alpha\,\chi\sigma^\mu\bar\psi_\alpha\,A_\mu + \frac{i}{2}\,p_\alpha z_\alpha^*\,A^\mu\,\partial_\mu z_\alpha \\ & + \frac{i}{4\sqrt{2}}\,p_\alpha^3\, z_\alpha\,\chi\chi\,\bar\chi\bar\psi_\alpha + \frac{i}{4}\,p_\alpha^2 z_\alpha^*\,\chi\sigma^\mu\bar\chi\,\partial_\mu z_\alpha\ - \frac{1}{2\sqrt{2}}\,p_\alpha\,\chi\sigma^\mu\bar\psi_\alpha\,\partial_\mu z_\alpha\Bigg) + h.c.\Bigg]\Bigg\}\,, \end{aligned} \tag{2.15}$$

$$\mathcal{L}^{\alpha}_{\text{kin}} = e^{p_\alpha C}\left\{\frac{1}{4}\,p_\alpha\, z^*_\alpha z_\alpha\,\partial_\mu\partial^\mu C - \partial_\mu z^*_\alpha\,\partial^\mu z_\alpha - i\bar\psi_\alpha\bar\sigma^\mu\partial_\mu\psi_\alpha - \frac{i}{2}\,p_\alpha\,\bar\psi_\alpha\bar\sigma^\mu\psi_\alpha\,\partial_\mu C \right.$$
$$+\left[\left(-\frac{1}{4}\,p_\alpha z^*_\alpha\,\partial_\mu C\,\partial^\mu z_\alpha\; - \frac{i}{4}\,p^2_\alpha\, z^*_\alpha z_\alpha\,\bar\chi\bar\sigma^\mu\partial_\mu\chi + \frac{1}{2\sqrt{2}}\,p_\alpha z_\alpha\,\bar\psi_\alpha\bar\sigma^\mu\partial_\mu\chi\right.\right.$$
$$\left.\left.+\;\frac{1}{2\sqrt{2}}\,p_\alpha z^*_\alpha\,\partial_\mu\psi\sigma^\mu\bar\chi\right) + h.c.\right]\Bigg\}\,, \tag{2.16}$$

$$\mathcal{L}^{\alpha}_{\text{aux}} = e^{p_\alpha C}\left\{F^*_\alpha F_\alpha + \frac{1}{4}\,p^2_\alpha\, z^*_\alpha z_\alpha\,(M+iN)(M-iN) + \frac{1}{2}\,p_\alpha\, z^*_\alpha z_\alpha\, D\right.$$
$$+\left[\left(-\frac{i}{\sqrt{2}}\,p_\alpha F^*_\alpha\,\chi\psi_\alpha\; + \frac{1}{4}\,p^2_\alpha\,F^*_\alpha z_\alpha\,\chi\chi + \frac{i}{2}\,z_\alpha p_\alpha F^*_\alpha\,(M+iN)\right.\right.$$
$$\left.\left.-\;\frac{1}{2\sqrt{2}}\,p^2_\alpha z_\alpha\,(M+iN)\,\bar\psi_\alpha\bar\chi\; + \frac{i}{8}\,p^3_\alpha z^*_\alpha z_\alpha\,(M+iN)\,\bar\chi\bar\chi\right) + h.c.\right]\Bigg\}\,. \tag{2.17}$$

Note that here C and χ do not have the right mass dimension to be directly interpreted as a scalar field and Weyl spinor, respectively. We will come back to the point of the correct normalization of these fields later. The other parts of the Lagrangian, cf. Eq. (2.9), can be calculated in the standard way, cf. Ref. [38],

$$\mathcal{L} = \int d^4\theta\, K(\Phi, Z) - \frac{1}{4}F^{\mu\nu}F_{\mu\nu} - i\bar\xi\bar\sigma^\mu\partial_\mu\xi + \frac{D^2}{2} + \left(\sum_\alpha W_\alpha F_\alpha - \sum_{\alpha,\beta}\frac{W_{\alpha\beta}}{2}\,\psi_\alpha\psi_\beta + h.c.\right), \tag{2.18}$$

with $W_\alpha = \partial W(z)/\partial z_\alpha$ and $W_{\alpha\beta} = \partial W_\alpha/\partial z_\beta$. Here we have introduced the superpotential as a function of the complex scalar fields instead of, as above, of the superfields. This allows for a more compact notation and we will exploit it in the following for both the superpotential and Kähler potential.

Eliminating the auxiliary fields

Having obtained an explicit expression for the Lagrangian, we now turn to eliminating the auxiliary fields. For each chiral supermultiplet Φ_α the Lagrangian contains an auxiliary field F_α, as well as the auxiliary fields $M + iN$ and D from the $U(1)$ gauge supermultiplet. The Euler-Lagrange formalism yields equations of motion (eoms) for all of these fields. Solving these and substituting the solution back into the Lagrangian eliminates the auxiliary fields. For n charged chiral superfields, this is a coupled system of $n + 2$ equations, involving quite complicated expressions, see e.g. Eq. (2.17). Here we introduce a shortcut to eliminate these auxiliary fields. The terms in the Lagrangian containing the auxiliary field D are

$$\mathcal{L}_D = \frac{1}{2}\,D^2 + \frac{1}{2}\sum_\alpha p_\alpha\, e^{p_\alpha C} z^*_\alpha z_\alpha\, D\,. \tag{2.19}$$

The eom $\partial\mathcal{L}/\partial D = 0$ is decoupled from the eoms for F_α and $M+iN$. Substituting its solution into Eq. (2.19), we find

$$\mathcal{L}_D = -\frac{1}{8}\sum_{\alpha\beta} p_\alpha p_\beta \, \exp\left[(p_\alpha + p_\beta)C\right] \, z_\alpha^* z_\alpha z_\beta^* z_\beta = -\frac{1}{2}D^2 =: -V_D \,. \tag{2.20}$$

The terms in the Lagrangian containing the auxiliary fields F_α can be rewritten as

$$\begin{aligned}\mathcal{L}_F^\alpha &= \left\{ W_\alpha F_\alpha + e^{p_\alpha C}\left[F_\alpha^* + \frac{i\,p_\alpha}{\sqrt{2}}\,\bar\psi_\alpha\bar\chi - \frac{i\,p_\alpha}{2} z_\alpha^*(M-iN) + \frac{p_\alpha^2}{4}\, z_\alpha^*\,\bar\chi\bar\chi\right] F_\alpha + h.c.\right\} \\ &\quad - e^{p_\alpha C} F_\alpha^* F_\alpha \\ &= \frac{\partial\mathcal{L}_F^\alpha}{\partial F_\alpha} F_\alpha + \frac{\partial\mathcal{L}_F^\alpha}{\partial F_\alpha^*} F_\alpha^* - e^{p_\alpha C} F_\alpha^* F_\alpha \;=\; -e^{p_\alpha C} F_\alpha^* F_\alpha \,, \end{aligned} \tag{2.21}$$

where in the last step we inserted the eom of F_α,

$$\partial\mathcal{L}_F^\alpha/\partial F_\alpha = 0 \,. \tag{2.22}$$

Writing Eq. (2.22) explicitly and solving for F_α^* yields

$$-F_\alpha^* = e^{-p_\alpha C} W_\alpha + \frac{i}{2}\, p_\alpha \left(\sqrt{2}\,\bar\psi_\alpha\bar\chi - z_\alpha^*(M-iN)\right) + \frac{1}{4}\, p_\alpha^2 z_\alpha^*\,\bar\chi\bar\chi \,. \tag{2.23}$$

Substituting this back into Eq. (2.21), and comparing the result with Eqs. (2.15) to (2.17) we find that lots of terms cancel. Taking into account that the term

$$-\sum_\alpha \left\{ \frac{i}{2}\, p_\alpha z_\alpha W_\alpha \,(M+iN) + h.c. \right\} \tag{2.24}$$

vanishes due to the gauge invariance of the superpotential,

$$0 = \delta W = \sum \frac{\partial W}{\partial z_\alpha}\,\delta z_\alpha \,, \qquad \delta z_\alpha \sim p_\alpha z_\alpha \,, \tag{2.25}$$

we are finally left with

$$\mathcal{L}_F^\alpha = \underbrace{e^{-p_\alpha C}\, W_\alpha^* W_\alpha}_{-V_F} - \left\{ W_\alpha \left(\frac{1}{4}\, p_\alpha^2 z_\alpha\, \chi\chi - \frac{i}{\sqrt{2}}\, p_\alpha\, \psi_\alpha\chi \right) + h.c. \right\} \tag{2.26}$$

and a reduced number of terms in Eqs. (2.15) to (2.17). In particular, all terms depending on M and N in (2.17) cancel and we have hence succeeded in eliminating all the auxiliary fields without explicitly solving the coupled system of eoms.

Canonical normalization

As noted above, the fields C and χ have the 'wrong' mass dimensions. As long as the $U(1)$ symmetry is unbroken, C and χ can be gauged away and are not physical degrees of freedom of the theory. However, once the symmetry is spontaneously broken, which corresponds to some 'Higgs' field obtaining a vev, C and χ become physical and we need to take care of the correct normalization. Defining a mass scale pv as

$$p^2 v^2 \coloneqq \sum_\alpha p_\alpha^2 \left\langle z_\alpha^* z_\alpha \right\rangle , \tag{2.27}$$

i.e. as the gauge invariant quantity which obtains a vev during spontaneous symmetry breaking, we see that we can obtain canonical normalized kinetic terms in Eq. (2.16) if we perform the following field redefinitions:

$$C \to \frac{pv}{\sqrt{2}} C , \qquad \chi \to \frac{pv}{\sqrt{2}} \chi . \tag{2.28}$$

In the following, we will promote v to a time dependent function, representing the homogeneous $B-L$ Higgs vev during and after the symmetry breaking process.

The resulting Lagrangian

Combining all the steps above we can now finally write down the full Lagrangian of a spontaneously broken $U(1)$ gauge symmetry:

$$\mathcal{L} = \mathcal{L}_{\text{WZ}}^{\text{kin}} + \mathcal{L}_{\text{WZ}}^{\text{gauge}} + \mathcal{L}_{\text{WZ}}^{\text{ferm}} - V_F - V_D + \mathcal{L}_{\text{non-WZ}} , \tag{2.29}$$

with

$$\begin{aligned}
\mathcal{L}_{\text{WZ}}^{\text{kin}} &= -\frac{1}{4} F_{\mu\nu} F^{\mu\nu} - i\bar{\xi}\bar{\sigma}^\mu \partial_\mu \xi - \sum_\alpha \exp\left(\frac{p_\alpha \sqrt{2} C}{pv}\right) \left(\partial_\mu z_\alpha^* \, \partial^\mu z_\alpha + i\bar{\psi}_\alpha \bar{\sigma}^\mu \partial_\mu \psi_\alpha\right) , \\
\mathcal{L}_{\text{WZ}}^{\text{gauge}} &= \sum_\alpha \exp\left(\frac{p_\alpha \sqrt{2} C}{pv}\right) \left[\frac{p_\alpha}{2} \left(i z_\alpha^* \partial^\mu z_\alpha - i z_\alpha \partial^\mu z_\alpha^* + \bar{\psi}_\alpha \bar{\sigma}^\mu \psi_\alpha\right) A_\mu - \frac{p_\alpha^2}{4} z_\alpha^* z_\alpha \, A_\mu A^\mu\right] , \\
\mathcal{L}_{\text{WZ}}^{\text{ferm}} &= \sum_\alpha \exp\left(\frac{p_\alpha \sqrt{2} C}{pv}\right) \frac{i p_\alpha}{\sqrt{2}} z_\alpha^* \, \psi_\alpha \xi - \frac{1}{2} \sum_{i,j} W_{\alpha\beta} \, \psi_\alpha \psi_\beta + h.c. , \\
V_F &= \sum_\alpha \exp\left(-\frac{p_\alpha \sqrt{2} C}{pv}\right) W_\alpha^* W_\alpha , \\
V_D &= \frac{1}{8} \sum_{\alpha\beta} p_\alpha p_\beta \exp\left(\frac{(p_\alpha + p_\beta)\sqrt{2} C}{pv}\right) z_\alpha^* z_\alpha z_\beta^* z_\beta ,
\end{aligned} \tag{2.30}$$

and

$$\begin{aligned}\mathcal{L}_{\text{non-WZ}} = \sum_\alpha \exp\left(\frac{p_\alpha\sqrt{2}C}{pv}\right)\Bigg[&\frac{p_\alpha}{2\sqrt{2}}\, z_\alpha^* z_\alpha \,\Box\frac{C}{pv} - \frac{ip_\alpha^2}{pv} z_\alpha^*\,\bar\chi\bar\sigma^\mu\partial_\mu\frac{z_\alpha\chi}{pv}\\ &+\frac{ip_\alpha}{\sqrt{2}}\left(\frac{i}{2}z_\alpha^*\partial_\mu z_\alpha + \frac{i}{2}z_\alpha\partial_\mu z_\alpha^* - \bar\psi_\alpha\bar\sigma_\mu\psi_\alpha - \frac{p_\alpha^2}{(pv)^2}z_\alpha^* z_\alpha\,\bar\chi\bar\sigma_\mu\chi\right)\partial^\mu\frac{C}{pv}\\ &+\left\{\frac{p_\alpha^2}{\sqrt{2}pv} z_\alpha^*\,\bar\chi\bar\sigma^\mu\psi_\alpha\,\partial_\mu\frac{C}{pv} + \frac{p_\alpha}{pv}z_\alpha^*\,\bar\chi\bar\sigma^\mu\partial_\mu\psi_\alpha + \frac{ip_\alpha^2}{2pv}z_\alpha^*\,\bar\chi\bar\sigma^\mu\psi_\alpha\,A_\mu + h.c.\right\}\\ &+\frac{p_\alpha^3}{2(pv)^2}z_\alpha^* z_\alpha\,\bar\chi\bar\sigma^\mu\chi\,A_\mu + \frac{p_\alpha^2}{\sqrt{2}pv}z_\alpha^* z_\alpha\left(\chi\xi+\bar\chi\bar\xi\right)\Bigg]\\ &-\sum_\alpha\left\{W_\alpha\left(\frac{p_\alpha^2}{2(pv)^2}z_\alpha\,\chi\chi + \frac{ip_\alpha}{pv}\,\psi_\alpha\chi\right) + h.c.\right\}\,. \end{aligned} \tag{2.31}$$

Evaluating the exponential functions in Eq. (2.30) to leading order in $p_\alpha\sqrt{2}C/(pv)$ yields the familiar Lagrangian in Wess-Zumino gauge. The terms collected in $\mathcal{L}_{\text{non-WZ}}$ represent additional terms involving the gauge degrees of freedom C and χ.

2.2.3 The supersymmetric Abelian Higgs model in unitary gauge

We are now ready to apply the general result (2.29) to the specific case we are interested in, the $B-L$ symmetry breaking sector introduced in Sec. 2.1. In unitary gauge, cf. Eq. (2.8), this involves the chiral fields $S_{1,2} = S'/\sqrt{2}$ and Φ, with $B-L$ charges $q_S \coloneqq q_{S_2} = -q_{S_1} = 2$ and $q_\Phi = 0$. Denoting $p \coloneqq p_s = 2gq_S$, $S' = (s,\tilde s)$, and $\Phi = (\phi,\tilde\phi)$, one now obtains[5]

$$\begin{aligned}\mathcal{L}_{\text{WZ}}^{\text{kin}} =& -\frac{1}{4}F_{\mu\nu}F^{\mu\nu} - i\bar\xi\bar\sigma^\mu\partial_\mu\xi - \partial_\mu\phi^*\,\partial^\mu\phi - i\bar{\tilde\phi}\bar\sigma^\mu\partial_\mu\tilde\phi\\ &-\cosh\left(\frac{\sqrt{2}C}{v}\right)\left(\partial_\mu s^*\,\partial^\mu s + i\bar{\tilde s}\bar\sigma^\mu\partial_\mu\tilde s\right)\,, \end{aligned}\tag{2.32}$$

$$\begin{aligned}\mathcal{L}_{\text{WZ}}^{\text{gauge}} =& \sinh\left(\frac{\sqrt{2}C}{v}\right)\left[\frac{p_s}{2}\left(is^*\,\partial^\mu s - is\,\partial^\mu s^* + \bar{\tilde s}\bar\sigma^\mu\tilde s\right)A_\mu\right]\\ &-\cosh\left(\frac{\sqrt{2}C}{v}\right)\frac{p_s^2}{4}s^* s\,A_\mu A^\mu\,, \end{aligned}\tag{2.33}$$

$$\mathcal{L}_{\text{WZ}}^{\text{ferm}} = \sinh\left(\frac{\sqrt{2}C}{v}\right)\frac{ip_s}{\sqrt{2}}s^*\,\tilde s\xi + \frac{1}{2}\sqrt{\lambda}\phi\,\tilde s\tilde s + \sqrt{\lambda}\,s\tilde\phi\tilde s + h.c.\,, \tag{2.34}$$

$$V_F = \frac{\lambda}{4}\left|v_{B-L}^2 - s^2\right|^2 + \cosh\left(\frac{\sqrt{2}C}{v}\right)\lambda\phi^*\phi\,s^* s\,, \tag{2.35}$$

$$V_D = \frac{1}{8}\,p_s^2\sinh^2\left(\frac{\sqrt{2}C}{v}\right)(s^*s)^2\,, \tag{2.36}$$

[5]For notational convenience, we have omitted the prime on the complex scalar Higgs boson s.

and

$$\begin{aligned}\mathcal{L}_{\text{non-WZ}} = &\sinh\left(\frac{\sqrt{2}C}{v}\right)\left[\frac{1}{2\sqrt{2}}\,s^*s\,\Box\frac{C}{v} + \frac{p_s}{2v^2}s^*s\,\bar\chi\bar\sigma^\mu\chi\,A_\mu + \left\{\frac{1}{v}s^*\,\bar\chi\bar\sigma^\mu\partial_\mu\tilde s + h.c.\right\}\right.\\ &\left. + \frac{i}{\sqrt{2}}\left(\frac{i}{2}s^*\,\partial_\mu s + \frac{i}{2}s\,\partial_\mu s^* - \bar{\tilde s}\bar\sigma_\mu\tilde s - \frac{1}{v^2}s^*s\,\bar\chi\bar\sigma_\mu\chi\right)\partial^\mu\frac{C}{v}\right]\\ &+ \cosh\left(\frac{\sqrt{2}C}{v}\right)\left[\left\{\frac{1}{\sqrt{2}v}s^*\,\bar\chi\bar\sigma^\mu\tilde s\,\partial_\mu\frac{C}{v} + \frac{ip_s}{2v}s^*\,\bar\chi\bar\sigma^\mu\tilde s\,A_\mu + h.c.\right\} - \frac{i}{v}s^*\,\bar\chi\bar\sigma^\mu\partial_\mu\frac{s\,\chi}{v}\right.\\ &\left. + \frac{p_s}{\sqrt{2}v}s^*s\left(\chi\xi + \bar\chi\bar\xi\right)\right] + \left\{\sqrt{\lambda}\,\phi s\frac{1}{2v^2}\,s\,\chi\chi + h.c.\right\}\ . \end{aligned} \tag{2.37}$$

The ground state of the theory corresponds to $|s|^2 = v_{B-L}^2$. Identifying the mass scale v with the time-dependent vacuum expectation value of the $B-L$ Higgs field in the broken phase, which approaches v_{B-L} at large times, the Lagrangian $\mathcal{L}_{\text{non-WZ}}$ yields kinetic terms for C and χ and a mass term for χ and ξ. The mass terms for A_μ and C are contained in Eqs. (2.33) and (2.36), respectively. As expected, in unitary gauge the vector field Z describes a massive vector multiplet. Shifting s around its expectation value, $s \to v(t) + \frac{1}{\sqrt{2}}(\sigma + i\tau)$, one reads off the masses for the particles of the gauge multiplet and the symmetry breaking sector. The real degree of freedom σ can be identified with the Higgs boson of the Abelian Higgs mechanism. The Goldstone boson, just like the other degrees of freedom of the 'Goldstone supermultiplet', does not appear in Eqs. (2.32) to (2.37), it has already been gauged away by choosing the unitary gauge. We have hence achieved our goal of formulating a Lagrangian which can describe the dynamics of the symmetry breaking process and which manifestly displays only the physical degrees of freedom.

Note that due to the time-dependence of v, the kinetic term for C in Eq. (2.37) yields a contribution to the mass m_C. In the following, we omit this term for two reasons. First, it is much smaller than the contribution to m_C obtained from Eq. (2.36) throughout the symmetry breaking process. Second, as discussed in detail in Sec. 4.5 of Ref. [16], our final results prove insensitive to the dynamics of the gauge sector and we can hence safely ignore this technically rather complicated contribution.

2.3 Spontaneous symmetry breaking

Making use of the results obtained in the previous section, we are now ready to give a physical interpretation of the processes involved in the $B-L$ phase transition. Before the spontaneous breaking of $B-L$, supersymmetry is broken by the vacuum energy density $\rho_0 = \frac{1}{4}\lambda v_{B-L}^4$, which drives inflation. During this time, the dynamics of the system is governed by the slowly rolling scalar component ϕ of the inflaton multiplet Φ. The scalar components of the Higgs superfields $S_{1,2}$ are stabilized at zero. The right-handed sneutrinos and the scalar

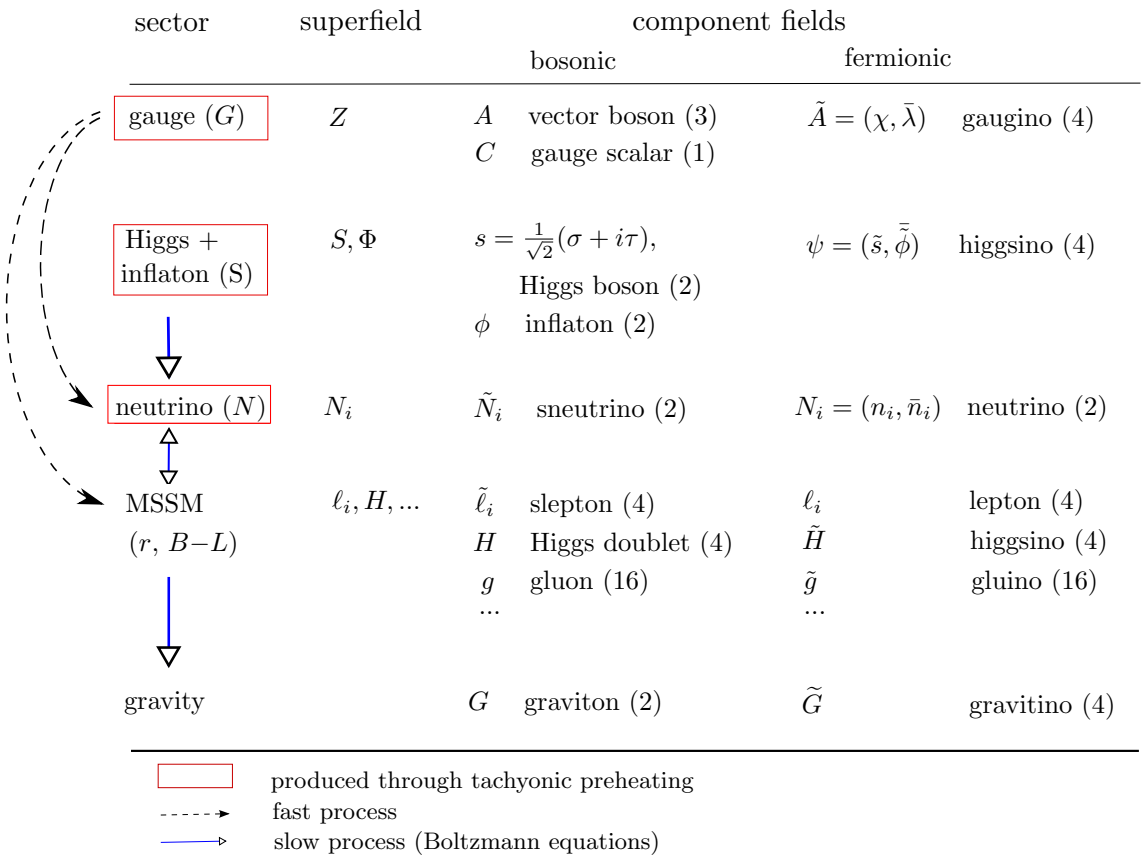

Figure 2.1: Nomenclature, production and decay processes after $B-L$ breaking. The Higgs field σ and particles coupled to it are produced during tachyonic preheating, as marked by the red boxes, cf. Sec. 3.2.1. The gauge degrees of freedom then decay nearly instantaneously (black, dashed arrows), whereas the decay and production of the other degrees of freedom can be described by Boltzmann equations (blue, solid arrows), cf. Sec. 3.4. The numbers in parentheses denote the respective internal degrees of freedom.

MSSM particles obtain their masses due to supergravity contributions. As the field value of the inflaton decreases, so do the effective masses in the Higgs sector, until a tachyonic direction develops in the effective scalar potential.

As shown in the previous section, the subsequent phase transition can best be treated in unitary gauge (2.8), in which the physical degrees of freedom are manifest. The supermultiplet associated with the $B-L$ Higgs boson in unitary gauge, S', contains two real scalar degrees of freedom, $s' = \frac{1}{\sqrt{2}}(\sigma' + i\tau)$, where τ remains massive throughout the phase transition and σ' is the actual symmetry-breaking Higgs field. It acquires a vacuum expectation value proportional to $v(t) = \frac{1}{\sqrt{2}}\langle\sigma'^2(t,\vec{x})\rangle_{\vec{x}}^{1/2}$ which approaches v_{B-L} at large times. In the Lagrangian, we account for symmetry breaking by making the replacement $\sigma' \to \sqrt{2}v(t) + \sigma$, where σ denotes the fluctuations around the homogeneous Higgs background.

The fermionic component $\tilde{s}$ of the supermultiplet S' pairs up with the fermionic component $\tilde{\phi}$ of the inflaton supermultiplet Φ to form a Dirac fermion ψ, the higgsino, which becomes

massive during the phase transition. Due to supersymmetry, the corresponding scalar fields (σ, τ and inflaton ϕ) end up having the same mass as the higgsino in the supersymmetric true vacuum. Likewise, the gauge supermultiplet Z (gauge boson A, real scalar C, Dirac gaugino $\tilde{A}$) and the (s)neutrinos N_i ($\tilde{N}_i$) acquire masses, cf. Sec. 2.2. Here N refers to the physical Majorana particle $N = (n, \bar{n})^T$ built from the two Weyl spinors contained in the superfields n^c and n. $\tilde{N}$ denotes the complex scalar superpartner of the left-chiral fermion n. For an overview of the particle spectrum, see Fig. 2.1.

At the end of the phase transition, supersymmetry is restored. From Eqs. (2.33) to (2.37), we can read off the mass eigenvalues during the phase transition:

$$\begin{aligned} m_\sigma^2 &= \frac{1}{2}\lambda\left(3v^2(t) - v_{B-L}^2\right), & m_\tau^2 &= \frac{1}{2}\lambda\left(v_{B-L}^2 + v^2(t)\right), \\ m_\phi^2 &= \lambda v^2(t), & m_\psi^2 &= \lambda v^2(t), \\ m_G^2 &= 8g^2 v^2(t), & & \\ M_i^2 &= (h_i^n)^2 v^2(t), & & \end{aligned} \tag{2.38}$$

with m_G and M_i denoting the common mass of the gauge and right-handed neutrino multiplets, respectively. Here we have ignored corrections which arise due to thermal effects and due to supersymmetry breaking before the end of inflation in some hidden sector, leading to a mass for the gravitino.

2.4 Decay rates and branching ratios

After the spontaneous breaking of $B-L$, we are left with the particle spectrum depicted in Fig. 2.1 and the corresponding masses given by Eq. (2.38) with $v(t) \to v_{B-L}$. Most of these particles are unstable, and their decay rates and branching ratios will play a crucial role when discussing the cosmology of this model in Chapter 3. With the full Lagrangian, cf. Eqs. (2.32) to (2.37), at hand, we thus use this section to list the total and partial vacuum decay rates which we will need in this thesis.

The total vacuum decay rates for the particles of the symmetry breaking, gauge and neutrino sectors are

$$\Gamma_S^0 \coloneqq \Gamma^0_{\sigma,\tau,\phi,\psi} = \frac{1}{32\pi}\,(h_1^n)^2\, m_S \left(1 - 4\,\frac{M_1^2}{m_S^2}\right)^{1/2}, \tag{2.39}$$

$$\Gamma_G^0 \coloneqq \Gamma^0_{A,\tilde{A},C} = \frac{1}{16\pi}\, g^2\, m_G \sum_\alpha q_\alpha^2 \left(1 - 4\,\frac{m_\alpha^2}{m_G^2}\right)^{1/2}, \tag{2.40}$$

$$\Gamma^0_{N_i,\tilde{N}_i} = \frac{1}{4\pi}\left[(h^\nu)^\dagger h^\nu\right]_{ii} M_i = \frac{1}{4\pi}\,\frac{\widetilde{m}_i M_i^2}{v_{\mathrm{EW}}^2}, \tag{2.41}$$

with $\widetilde{m}_i = [(h^\nu)^\dagger h^\nu]_{ii} v_{\mathrm{EW}}^2 / M_i$ and α labelling the superfields of the model carrying $B-L$

charges q_α. In Eq. (2.39) we have assumed that due to kinematic constraints, the particles of the symmetry breaking sector can only decay into the first generation of heavy (s)neutrinos, see also Sec. 2.5. The relevant partial decay rates at leading order are given by

$$\begin{aligned}
\Gamma^0_{\sigma\to\tilde{N}_1\tilde{N}_1} &= 4\,\frac{M_1^2}{m_S^2}\,\Gamma^0_S\,, \qquad \Gamma^0_{\sigma\to N_1 N_1} = \left(1-4\,\frac{M_1^2}{m_S^2}\right)\Gamma^0_S\,,\\
\Gamma^0_{\tau\to N_1 N_1} &= \Gamma^0_{\phi\to\tilde{N}_1\tilde{N}_1} = \Gamma^0_{\psi\to\tilde{N}_1^* N_1} = \Gamma^0_S\,,\\
\Gamma^0_{A\to z_\alpha z_\alpha} &= \frac{1}{2}\,\Gamma^0_{A\to\psi_\alpha\psi_\alpha} = \frac{1}{3}\,\Gamma^0_{C\to z_\alpha z_\alpha} = \frac{1}{3}\,\Gamma^0_{\tilde{A}\to z_\alpha\psi_\alpha} = \frac{q_\alpha^2\left(1-4\frac{m_\alpha^2}{m_S^2}\right)^{1/2}\Gamma^0_G}{3\sum_\alpha q_\alpha^2\left(1-4\frac{m_\alpha^2}{m_S^2}\right)^{1/2}}\,,
\end{aligned} \tag{2.42}$$

with z_α and ψ_α denoting the scalar and fermionic components of a superfield Φ_α.

2.5 Froggatt-Nielsen flavour model

So far, we have discussed the field content, masses, and decay rates of the symmetry breaking, the neutrino and the gauge sector during the $B-L$ phase transition. Now, we want to turn to the coupling constants appearing in Eq. (2.1). To this end, we will parametrize the flavour structure of the model by a Froggatt-Nielsen flavour model based on a global $U(1)_{\rm FN}$ group and compatible with the $SU(5)$ structure of Eqs. (2.1) and (2.2), following Refs. [121, 122]. According to this model, the couplings in the superpotential can be estimated up to $\mathcal{O}(1)$ factors as powers of a common hierarchy parameter η, with the exponent given by the sum of the flavour charges Q_i of the fields involved in the respective operators in the superpotential. Setting the charges of all Higgs fields to zero, this implies

$$h_{ij} \sim \eta^{Q_i+Q_j}\,, \quad \sqrt{\lambda} \sim \eta^{Q_\Phi}\,. \tag{2.43}$$

The numerical value of the parameter $\eta \simeq 1/\sqrt{300}$ is deduced from the quark and lepton mass hierarchies. This remarkably simple flavour model can reproduce the experimental data on SM masses and mixings, while at the same time remaining flexible enough to incorporate the phenomena beyond the SM mentioned above. Further details on the predictive power of this model can be found in Ref. [15], where we performed a Monte-Carlo study to examine the impact of the $\mathcal{O}(1)$ factors, cf. also Sec. 4.4 for a brief overview of the main results of this study.

In the following, we will restrict our analysis to the case of a hierarchical heavy (s)neutrino mass spectrum, $M_1 \ll M_2, M_3$, where $M_i = h_i^n\, v_{B-L}$. Furthermore we assume the heavier (s)neutrino masses to be of the same order of magnitude as the common mass m_S of the particles in the symmetry breaking sector, for definiteness we set $M_2 = M_3 = m_S$. With this, the Froggatt-Nielsen flavour charges are fixed as denoted in Tab. 2.1. Taking the $B-L$ gauge

ψ_i	$\mathbf{10}_3$	$\mathbf{10}_2$	$\mathbf{10}_1$	$\mathbf{5}^*_3$	$\mathbf{5}^*_2$	$\mathbf{5}^*_1$	n^c_3	n^c_2	n^c_1	H	$S_{1,2}$	Φ
Q_i	0	1	2	a	a	$a+1$	$d-1$	$d-1$	d	0	0	$2(d-1)$

Table 2.1: Froggatt-Nielsen flavour charge assignments.

coupling to be $g^2 = g^2_{\mathrm{GUT}} \simeq 1/2$, the model can now, up to $\mathcal{O}(1)$ factors, be parametrized by the $U(1)_{\mathrm{FN}}$ charges a and d. The $B-L$ breaking scale v_{B-L}, the mass of the lightest of the heavy (s)neutrinos M_1, and the effective light neutrino mass parameter $\widetilde{m}_1$ are related to these by

$$v_{B-L} \sim \eta^{2a}\,\frac{v^2_{\mathrm{EW}}}{\overline{m}_\nu}\,, \qquad M_1 \sim \eta^{2d}\,v_{B-L}\,, \qquad \widetilde{m}_1 = \frac{(m_D^\dagger m_D)_{11}}{M_1} \sim \eta^{2a}\,\frac{v^2_{\mathrm{EW}}}{v_{B-L}}\,. \tag{2.44}$$

Here, $\overline{m}_\nu = \sqrt{m_2 m_3}$, the geometric mean of the two light neutrino mass eigenvalues m_2 and m_3, characterizes the light neutrino mass scale, which, with the charge assignments above and the experimentally measured neutrino mass squared differences, can be fixed to 3×10^{-2} eV. To obtain this result, we exploited the seesaw formula $m_\nu = -m_D M^{-1} m_D^T$ with $m_D = h^\nu v_{\mathrm{EW}}$. Furthermore, it can be shown that $\widetilde{m}_1$ is bounded from below by the lightest neutrino mass m_1 [123].

In the following, we will study the model in terms of the more physical quantities v_{B-L} and M_1 instead of the two $U(1)_{\mathrm{FN}}$ charges. To partly account for the $\mathcal{O}(1)$ uncertainties in the neutrino mass matrices, we will additionally independently vary $\widetilde{m}_1$. Apart from this, we ignore any further uncertainties of the model and simply set the $\mathcal{O}(1)$ prefactors to one, i.e. promote the approximate relations in Eq. (2.44) to exact relations. Furthermore, when considering the production of dark matter in form of gravitinos or neutralinos, cf. Secs. 4.2.1 and 4.2.2 respectively, additional parameters from the superparticle mass spectrum enter the description. In the former case, these are the gravitino ($m_{\widetilde{G}}$) and the gluino ($m_{\tilde{g}}$) mass, in the latter case the gravitino mass and the mass of the lightest neutralino (m_χ).

In this chapter, we have discussed the $B-L$ phase transition from a particle physics point of view, i.e. considering the degrees of freedom, the masses and the couplings before, during and after the symmetry breaking. This sets the stage for the next chapter, in which we discuss this phase transition from a cosmological point of view.

Chapter 3

A Consistent Cosmological Picture

In Chapter 2 we studied the spontaneous breaking of a $U(1)_{B-L}$ symmetry. Now, we discuss the cosmological realization of this phase transition. At first, in the unbroken phase of $B-L$, the universe is governed by a large vacuum energy which drives inflation. We outline the resulting F-term hybrid inflation model in Sec. 3.1. At the end of inflation, the $U(1)_{B-L}$ is spontaneously broken. As explained in Sec. 3.2, this induces the nonperturbative processes of tachyonic preheating and cosmic string formation. These in turn set the initial conditions for the following perturbative processes which we turn to in Sec. 3.4. These govern the reheating of the universe and can be treated using Boltzmann equations. Finally, in Sec. 3.5 we give a time-resolved, quantitative description of the resulting reheating process for a representative choice of parameters.

This chapter is based on work partly published in Ref. [16], with a particular focus on the interpretation of the reheating process as a two-stage process, which will simplify the discussion in the next chapter. Additionally, we here review the current status and open questions related to cosmic strings, setting the stage for discussing the consequences of cosmic string formation throughout this thesis.

3.1 F-term hybrid inflation

Inflation is a phase of exponential expansion in the early universe, governed by a large, basically constant energy density. In its simplest version, the dynamics of inflation is controlled by a slowly rolling scalar field, the inflaton [124]. Calculating the predictions of inflation thus implies solving the eom of the inflaton in its scalar potential. Moreover, the quantum fluctuations of the inflaton field and the metric seed inhomogeneities in the CMB which can be observed today.

The scalar potential

The superpotential given in Eq. (2.1) allows for a phase of hybrid inflation [5]. For $|\phi| \gg v_{B-L}$, the $B-L$ Higgs fields are fixed at vanishing field value, $B-L$ is unbroken and the energy

density of the universe is dominated by the false vacuum energy, $\rho_0 \simeq (\lambda/4)\, v_{B-L}^4$, generated by the non-vanishing vev of the auxiliary field F_ϕ.

At these high energies, supergravity corrections[1] to the Lagrangian calculated in Sec. 2.2 become important, resulting in a tree-level scalar F- and D-term potential given by

$$V_{\rm SUGRA}^F = e^{K/M_P^2}\left[\sum_{\alpha\bar\beta} K^{\alpha\bar\beta}\,\mathcal{D}_\alpha W\,\mathcal{D}_{\bar\beta}W^* - 3\,\frac{|W|^2}{M_P^2}\right], \tag{3.1}$$

$$V_{\rm SUGRA}^D = \frac{1}{2}\,g^2\left(\sum_\alpha q_\alpha\, K_\alpha\, z_\alpha\right)^2, \tag{3.2}$$

where $\mathcal{D}_\alpha W = W_\alpha + K_\alpha W/M_P^2$, the subscript $\alpha, \beta, (\bar\alpha, \bar\beta)$ denotes the derivative with respect to the (complex conjugate of the) scalar component z_α of the superfield Φ_α, $K^{\alpha\bar\beta}$ is the inverse Kähler metric and $M_P = 2.435 \times 10^{18}$ GeV is the reduced Planck mass. Here, the superpotential W and the Kähler potential K are understood as functions of the complex scalar fields z_α. For a canonical Kähler potential[2],

$$K = \sum_\alpha |z_\alpha|^2\,, \tag{3.3}$$

the D-term scalar potential reduces to the expression familiar from global supersymmetry, cf. Eq. (2.19), but an important supergravity contribution arising from the F-term potential is

$$V_{\rm SUGRA}^F = \cdots + \sum_\alpha |z_\alpha|^2 \frac{\rho_0}{M_P^2} + \dots\,. \tag{3.4}$$

This yields large contributions to the masses of the scalar fields z_α of the theory. For the superpotential (2.1), this stabilizes the right-handed sneutrinos and the MSSM scalars at a vanishing field value. The $B-L$ Higgs boson masses also obtain supergravity contributions, however, these are suppressed by factors of $(v_{B-L}/M_P)^2$ or $(\phi/M_P)^2$ compared to the global supersymmetry contribution[3]. We can thus safely neglect them in the following, resorting to the expressions of global supersymmetry for the mass eigenvalues of the scalars and fermions, respectively:

$$(m_\pm^S)^2 = \frac{\lambda}{2}(\varphi^2 \pm v^2)\,, \qquad (m_f^S)^2 = \frac{\lambda}{2}\varphi^2\,. \tag{3.5}$$

Here we have introduced the radial component φ of ϕ, defined by $\phi = \frac{1}{\sqrt{2}}\varphi e^{i\alpha}$, which will play the role of the inflaton. Note that in this subsection we keep the four scalar and four fermionic degrees of freedom of the Higgs sector and do not employ the unitary gauge, since

[1] For a dedicated discussion of inflation in supergravity, see Chapter 5 of this thesis, in particular Sec. 5.1.1.

[2] Here we omit the gauge fields because for discussing inflation, we are merely interested in the scalar part of the Lagrangian. The auxiliary component D of the vector superfield which is responsible for a contribution to the scalar potential is kept explicitly in Eq. (3.2).

[3] Moreover, they do not change the zero point φ_c of $m_-^S(\varphi)$, cf. Eq. (3.5).

we are working in the unbroken phase of $B-L$.

Eq. (3.4) does not give a mass-term to the inflaton φ because after expanding e^{K/M_P^2} in Eq. (3.1), the term in question is cancelled by the corresponding term in $D_\phi W D_{\bar{\phi}} W^*$. Hence, we need to take the one-loop Coleman-Weinberg potential for the inflaton field into account, obtained by integrating out the heavy $B-L$ Higgs bosons,

$$V_{1l} = \frac{1}{64\pi^2}\,\mathrm{STr}\left[M^4\left(\ln\left(\frac{M^2}{Q^2}\right)-\frac{1}{2}\right)\right] \simeq \frac{\lambda^2 v_{B-L}^4}{64\pi^2}\left[\ln\left(\frac{\varphi^2}{v_{B-L}^2}\right)+\mathcal{O}\left(\frac{v_{B-L}^2}{\varphi^2}\right)\right], \qquad (3.6)$$

Here STr denotes the supertrace running over all degrees of freedom of S_1 and S_2. M is the corresponding mass matrix, cf. Eq. (3.5), and Q an appropriate renormalization scale, which we have set to $Q^2 = \lambda v_{B-L}^2/2$.

From the resulting scalar potential, $V = V_{\mathrm{SUGRA}}^{F+D} + V_{1l}$, we find the following picture: For $\varphi > v_{B-L}$, the Higgs fields $s_{1,2}$ are fixed at zero and the inflaton slowly rolls towards the origin. At $\varphi = v_{B-L}$, $(m_-^S)^2$ becomes negative, triggering a tachyonic instability. The Higgs field acquires a vev and $B-L$ is broken. Both the Higgs (which, now that $B-L$ is broken, is best parametrized in unitary gauge as σ', cf. Sec. 2.2) and the inflaton field then quickly fall into their true vacuum, $\varphi \to 0$ and $\sigma' \to \sqrt{2}\,v_{B-L}$, see also Eqs. (2.35) and (2.36), eliminating the vacuum energy contribution of the scalar potential and ending inflation.

Slow-roll inflation

Today, traces of this early inflationary phase can be observed in the CMB. These are calculated as follows. First we solve the slow-roll equation governing the evolution of the inflaton field during inflation,

$$3H\dot{\varphi} = -V'(\varphi)\,. \qquad (3.7)$$

where H denotes the Hubble parameter. Then we evaluate the scalar potential and its derivatives at $\varphi = \varphi_*$, the value of φ at $N_* \approx 50$ e-folds before the end of inflation, when the reference scale commonly used to describe the CMB fluctuations left the horizon. With φ_f denoting the value of the inflaton at the end of inflation[4], φ_* is given by

$$\varphi_*^2 = \varphi_f^2 + \frac{\lambda}{4\pi^2} M_P^2\, N_* \qquad (3.8)$$

Of particular interest in the following will be the predictions from F-term hybrid inflation for the amplitude of the scalar fluctuations A_s, the spectral index n_s and the tensor-to-scalar

[4]Here, φ_f is determined by either $m_-^S(\varphi_c) = 0$, cf. Eq. (3.5), or by the violation of the slow-roll condition $|\eta(\varphi_\eta)| = 1$, cf. Eq. (3.10), whatever occurs earlier: $\varphi_f = \max\{v_{B-L}, \sqrt{\lambda} M_P/(\sqrt{8}\pi)\}$.

ratio r:

$$\begin{aligned} A_s &= \left.\frac{H^2}{8\pi^2\epsilon M_P^2}\right|_{\varphi_*} \approx \frac{1}{3}\left(\frac{v_{B-L}}{M_P}\right)^4 N_*\,, \\ n_s &= 1-6\epsilon+2\eta|_{\varphi_*} \approx 1-\frac{1}{N_*}\,, \\ r &= \frac{A_t}{A_s} = 16\epsilon\Big|_{\varphi_*} \approx \frac{\lambda}{2\pi^2}\frac{1}{N_*}\,, \end{aligned} \tag{3.9}$$

where $A_t = 2H^2/(\pi^2 M_P^2)|_{\varphi^*}$ denotes the amplitude of the tensor fluctuations and ϵ and η are the so-called slow-roll parameters,

$$\epsilon = \frac{M_P^2}{2}\left(\frac{V'}{V}\right)^2\,, \qquad \eta = M_P^2\,\frac{V''}{V}\,. \tag{3.10}$$

Moreover, in Eq. (3.9) we have employed the the approximation[5] $\varphi_*^2 \gg \varphi_f^2$.

Another quantity which is relevant in the following is the velocity of the inflaton field when passing the critical point,

$$\dot{\varphi}_c = -\frac{\lambda^{3/2}}{16\sqrt{3}\pi^2}(v_{B-L}\,M_P)\,. \tag{3.11}$$

In fact, this is an upper bound on $|\dot{\varphi}_c|$, obtained by assuming that inflation ends at $\varphi = \varphi_c$. If instead inflation ends by violation of the slow-roll condition at $\varphi = \varphi_\eta$, then Eq. (3.11) is modified because the term $\ddot{\varphi}$ in Eq. (3.7) cannot be neglected towards the end of inflation.

Outlook

The analysis sketched here can be refined by considering deviations from a canonical Kähler potential and/or additional terms in the superpotential, see e.g. Ref.[118] for a recent analysis. This allows for a tuning of the spectral index to match the observed value [1] and yields bounds on the v_{B-L} and λ range allowed by requiring the correct normalization of A_s. We will come back to the resulting constraints on our parameter space in Sec. 3.2.2, after discussing further constraints imposed by the non-observation of cosmic strings.

In supersymmetric hybrid inflation the so-called 'η-problem', which refers to dangerous contribution to the inflaton mass induced by supergravity corrections as in Eq. (3.4), is solved by 'accidental' cancellation of two terms in the tree-level scalar potential, cf. comment above Eq. (3.6). This only works for a (nearly) canonical Kähler potential and it only works to leading order in $1/M_P^2$. Tuning the coefficients of the Kähler potential, one can avoid the η-problem while simultaneously reproducing the observed spectral index. But from a conceptual point of view, this is somewhat unsatisfactory. It would be more attractive to determine the

[5] In fact, this in not a very good approximation for small values of λ. Nevertheless, Eq. (3.9) gives a good impression of the predictions of supersymmetric F-term hybrid inflation. In the following, we will not use Eqs. (3.9), but the results of the refined analysis in Ref. [118].

form of the Kähler potential (and in particular the non-existence of terms which could cause an η-problem) by a symmetry principle. We will come back to this point in Chapter 5, in which we will discuss superconformal D-term inflation as an alternative scenario of hybrid inflation.

3.2 A cosmological phase transition

As discussed in the last section, the end of hybrid inflation features a negative squared mass term for the $B-L$ Higgs field σ'. This triggers the $U(1)_{B-L}$ breaking phase transition discussed in Sec. 2.3. The cosmological realization of this phase transition is accompanied by two important processes, tachyonic preheating and the formation of cosmic strings. To describe these, the notion of a complex $U(1)$ Higgs field with the radial component describing the physical Higgs field σ' and the phase describing the corresponding Goldstone boson, is crucial. Hence, for this section we explicitly reintroduce this notion, although absent in the unitary gauge discussed in Sec. 2.2.3.

3.2.1 Tachyonic preheating

Qualitative picture

Tachyonic preheating is a fast and nonperturbative process triggered by the tachyonic instability in the scalar potential in the direction of the Higgs field. As the inflaton field passes the critical point φ_c, the Higgs field acquires a negative effective squared mass $(m_\sigma^*)^2$, with the linearized equation of motion for σ' yielding $|m_\sigma^*| = (-\lambda v_{B-L}\dot{\varphi}_c)^{1/3}$. This causes an exponential growth of the quantum fluctuations of the Higgs field σ'_k with wave number $|\vec{k}| < k_* = |m_\sigma^*|$ [125], while the average value of the Higgs field remains zero. Once the amplitude of these fluctuations reaches $\langle|\sigma'|^2\rangle^{1/2} = \mathcal{O}(v_{B-L}/\sqrt{3})$, the effective squared mass becomes positive and the usual oscillating behaviour of the modes is re-established [6]. A direct consequence of the early phase of exponential growth are high occupation numbers in the low-momentum Higgs modes and hence a semi-classical situation with a large abundance of non-relativistic $B-L$ Higgs bosons.

A further result of this nonperturbative and (apart from very early times) non-linear process is the formation of 'bubble'-like inhomogeneities which randomly feature different phases of the complex Higgs field [126]. Their initial size is given by k_*^{-1}, since this is the smallest scale amplified during tachyonic preheating. These 'bubbles' expand at the speed of light, thereby colliding with each other. This phase of the preheating process is an important source of gravitational waves (GWs), cf. [106], a point to which we will return in Sec. 4.3. After this very turbulent phase the true Higgs vev is reached in almost the entire volume, with the regimes of false vacuum reduced to topologically stable cosmic strings, cf. Sec. 3.2.2, separated by the characteristic length scale k_*^{-1} [125].

Secondary Particle production

The mode equations for the particles coupled to the $B-L$ Higgs field, i.e. for the gauge, Higgs, inflaton and neutrino supermultiplets, are governed by the time-dependent masses proportional to $v(t)$ given by Eq. (2.38). The growth of $v^2(t) \propto \langle \sigma'^2 \rangle$ during tachyonic preheating induces a rapid change of their effective masses. According to Ref. [127], this leads to particle production with the energy and number densities for bosons and fermions after tachyonic preheating given by[6]

$$\begin{aligned} \rho_B/\rho_0 &\simeq 2 \times 10^{-3}\, g_\sigma\, \lambda\, f(x_1, 1.3)\,, & n_B(x_1) &\simeq 1 \times 10^{-3}\, g_\sigma\, m_S^3\, f(x_1, 1.3)/x_1\,, \\ \rho_F/\rho_0 &\simeq 1.5 \times 10^{-3}\, g_\sigma\, \lambda\, f(x_1, 0.8)\,, & n_F(x_1) &\simeq 3.6 \times 10^{-4}\, g_\sigma\, m_S^3\, f(x_1, 0.8)/x_1\,, \end{aligned} \tag{3.12}$$

with $f(x_1, x_2) = (x_1^2 + x_2^2)^{1/2} - x_2$ and $x_1 = m/m_S$, where m denotes the mass of the respective particle in the true vacuum and g_σ counts its spin degrees of freedom. Just like the Higgs bosons, these particles are produced with very low momentum, i.e. non-relativistically.

A deviation from this mechanism is found for the imaginary component τ of the complex field s', due to the constant contribution to its mass, cf. Eq. (2.38). Neglecting the expansion of the universe, the linearized mode equation for τ reads

$$\partial_t^2 \tau_k + (k^2 + m_\tau^2)\tau_k = 0\,. \tag{3.13}$$

We can absorb the constant mass contribution in the momentum k. In the language of Ref. [127], this is equivalent to a shift in the 'asymptotic *in* frequency' $\omega_-(k)$. To excite a given mode more energy is necessary, the production is thus less efficient.

Note that from Eq. (2.42) it is clear that the pseudoscalar τ decays exclusively into fermionic neutrinos, similar to its scalar partner σ, whose branching ratio into scalar neutrinos is suppressed by the mass ratio M_1/m_S. However, from Eqs. (3.12) and (3.13) we can see that the production of τ particles during tachyonic preheating is negligible compared to the production of σ particles. Hence we neglect the contribution from the pseudoscalar τ in the following.

3.2.2 Cosmic strings

Due to the non-trivial topology of its vacuum manifold, the Abelian Higgs model underlying the $B-L$ phase transition gives rise to solitonic field configurations, so-called cosmic strings (for a review, see e.g. [28, 129, 130]). These cosmic strings are formed during the process of tachyonic preheating, cf. Sec. 3.2.1, and are topologically stable. The evolution of the resulting network is governed by the intersection of the infinite strings, which leads to the formation of closed loops separated from the infinite string, as well as by the energy loss due

[6] Note that particle production can be significantly enhanced by quantum effects [128], which require further investigation.

to the emission of GWs and massive radiation. After a relaxation time τ_{string} the network reaches the scaling regime, i.e. the typical length scale of the cosmic string network remains constant relative to the size of the horizon. This implies that a constant fraction of the total energy density is stored in cosmic strings throughout the further evolution of the universe and that there is $\mathcal{O}(1)$ cosmic string per Hubble volume.

Observational prospects

So far, no experimental evidence for the existence of cosmic strings has been found. However, current and upcoming experiments are starting to seriously probe the cosmologically interesting regions of the parameter space. First, cosmic strings give rise to anisotropies in the CMB temperature map. Cosmic strings distort the surface of last scattering of the CMB photons, leaving an imprint on the spectrum observable today. Since the CMB photons observable today stem from roughly 10^5 Hubble patches during recombination, these observations are mainly sensitive to the effect of long (Hubble-sized) strings at recombination and not to small cosmic string loops. In contrast to the perturbations due to inflation, these anisotropies are not phase correlated across distant Hubble patches and hence the resulting multipole spectrum does not show the oscillations characteristic to inflation. Moreover, whereas the primordial power spectrum due to inflation is (nearly) scale-invariant, the anisotropies on the last scattering surface due to cosmic strings are governed by a characteristic scale. The resulting spectrum thus features a single broad peak associated with this scale. Due to the re-scattering of a fraction of the CMB photons at reionisation, the CMB spectrum is, to a lesser extent, also sensitive to the long cosmic strings present at reionisation. This leads to a second, smaller peak in the spectrum, in particular visible in the power spectrum of the B-mode polarization, see e.g. [131] for a recent analysis. The contribution from cosmic strings to the CMB temperature anisotropies is typically measured at the multipole $l = 10$ and is referred to as f_{10}. Recent analyses show that f_{10} can at most be a few percent, see Sec. 3.3.

Second, the gravitational field of cosmic strings gives rise to weak and strong lensing effects of (CMB) photons on their way from the surface of last scattering or from an astrophysical source to us. The non-observation of such effects puts a bound on the string tension μ, cf. Sec. 3.3. Again, this effect is mainly sensitive to long (Hubble-sized) strings.

Third, the energy emitted by cosmic strings in the scaling regime is at least partly emitted in form of GWs. Due to their extremely weak coupling, these can then propagate freely through the universe and are therefore in principle detectable today. We will come back to the resulting GW background and the discovery potential of current and upcoming GW experiments in detail in Sec. 4.3.

Finally, the Abelian Higgs cosmic string model (see below) entails the emission of massive radiation from cosmic strings. If this mechanism is still active at late times it could yield ultra high energetic cosmic rays and GeV-scale γ-rays, which have not been observed. This too, can be translated into a (model-dependent) bound on μ [132–136].

Currently the most stringent and model-independent bounds on the cosmic string tension come from CMB observations, and we shall mainly employ these in the following, cf. Sec. 3.3.

Numerical simulations

Quantitatively understanding the formation of cosmic strings, the dynamics of the cosmic string network and the energy loss mechanism during the scaling regime requires lattice simulations. Performing these is extremely challenging due to the huge range of scales involved in the problem [28]: the width of the string remains constant while the scales of the network are blown up as the universe expands. Or, in comoving coordinates, the comoving width of the string shrinks, until it becomes comparable with the lattice spacing and the simulation loses its validity. There have been different approaches to tackle this problem. Simulations based on solving the field theory equations for the Abelian Higgs (AH) model set the comoving width to a finite constant before it comes too close to the lattice spacing [29–31]. Simulations based on the Nambu-Goto (NG) string model assume cosmic strings to be infinitely thin, i.e. strictly one-dimensional objects, throughout the simulation [32–35]. The outcome of simulations based on these two models is dramatically different. The AH simulations show the formation of large, Hubble sized structures which lose their energy predominantly by emitting massive radiation, i.e. particles of the Higgs and gauge field forming the string configuration. The NG simulations on the other hand display the formation of small loops, which lose their energy into GWs. The size of these loops is thought to be controlled by gravitational backreaction, but is as yet undetermined [28]. Concerning the network of long strings, both simulations, however, yield a similar result [28]. Which of these two simulations methods is closer to reality is currently an open question.

In the following, we will work under the following hypothesis: For early times, while the comoving cosmic string width is large compared to the lattice spacing, the AH simulation describes the $U(1)$ phase transition very well. We will thus use the results from these simulations when discussing the formation and early evolution of cosmic strings. For late times, the AH simulations become questionable and the NG approximations of infinitely thin strings becomes viable. Hence for late times, in particular when discussing possible GW signatures from cosmic strings, cf. Sec. 4.3, we will discuss both the AH as well as the NG results.

Quantitative description

The cosmic string network in the AH model is characterized by the energy per unit length μ, the characteristic length scale separating two strings ξ and the cosmic string width m_G^{-1}. The energy per unit length is given by [137]

$$\mu = 2\pi B(\beta) v_{B-L}^2 \,, \tag{3.14}$$

where $\beta = (m_\sigma/m_G)^2 = \lambda/(8g^2)$ with m_σ the mass of the Higgs boson in the true vacuum, cf. Eq. (2.38), and $B(\beta)$ is a slowly varying function parametrizing the deviation from the

Bogomol'nyi bound,

$$B(\beta) \simeq \begin{cases} 1.04\,\beta^{0.195}, & \text{if } 10^{-2} < \beta \ll 1 \\ 2.4\,(\ln\frac{2}{\beta})^{-1}, & \text{if } \beta < 10^{-2} \end{cases} \tag{3.15}$$

For the special case of $\beta = 1$ the Bogomol'nyi bound is saturated and $B(1) = 1$ analytically [138]. Finally, from Sec. 3.2.1, we know that the characteristic length separating two strings at the time of their formation is

$$\xi = k_*^{-1} = (-\lambda v_{B-L}\dot{\varphi}_c)^{-1/3}\,. \tag{3.16}$$

This also determines the relaxation time of the cosmic string network, $\tau_{\text{string}} \sim \xi$ [31, 125].

3.3 Constraints on the parameter space

Experimental status

Measurements of the CMB put stringent bounds on the primordial perturbation spectrum from inflation, cf. Eq. (3.9), as well as on the cosmic string parameters. The most recent CMB data was obtained by the Planck satellite. In [1], the parameters of the primordial fluctuations based on 'standard cosmology' and on the Planck, WMAP polarization and high-l data sets are given as

$$\begin{aligned} A_s^0 &= (2.198 \pm 0.056) \times 10^{-9}\,, & dn_s/d\ln k &= -0.022 \pm 0.010 \quad , \\ n_s &= 0.959 \pm 0.007\,, & r &< 0.26\,, \end{aligned} \tag{3.17}$$

where for A_s^0, n_s and dn_s/dk the 68% confidence levels (CLs) and for r the 95% CL is denoted. Here, n_s is obtained assuming $dn_s/dk = 0$ and $r = 0$, however, it is not very sensitive to including non-vanishing running and tensor contributions, cf. Ref. [1] for details. The values for dn_s/dk and r quoted here were obtained allowing for $r \neq 0$ and $dn_s/dk \neq 0$, respectively. The Planck collaboration also studied a possible contribution from cosmic strings [2]. For the AH cosmic string model, they find

$$\begin{aligned} A_s^0 &= 2.18^{+0.05}_{-0.06} \times 10^{-9}\,, & G\mu &< 3.2 \times 10^{-7}\,, \\ n_s &= 0.963 \pm 0.008\,, & f_{10} &< 2.8\%\,, \end{aligned} \tag{3.18}$$

with the 68% (95%) CLs given for A_s^0 and n_s ($G\mu$ and f_{10}) and $G = 1/(8\pi M_P^2)$ denoting Newton's constant. Comparing Eq. (3.17) with Eq. (3.18) we note that the inclusion of cosmic strings allows for a larger value of the spectral index. However, the effect on the best-fit value is only $\Delta n_s = 0.004$, and is hence much less significant than it used to be based on older data sets [139].

The upper bound on the string tension has a considerable theoretical uncertainty. For

instance, the corresponding bounds on $G\mu$ and f_{10} obtained from NG simulations are roughly stricter by a factor of two, cf. Ref. [2]. Indeed, only the fact that the CMB is mainly sensitive to long cosmic strings ensures that the bounds derived in the AH and NG model are of the same order of magnitude. For GWs, which are also sensitive to the loop population, the uncertainty will be even larger, see Sec. 4.3. Note also that all simulations have been carried out for a bosonic AH model, whereas here we are considering a supersymmetric theory. Additional fermionic decay channels may further relax the cosmic string bound by a factor of $\mathcal{O}(1)$. Last but not least, one has to worry about initial conditions. Clearly, strings cannot form until the causal horizon is larger than their characteristic width [140], and one should remember that tachyonic preheating proceeds very fast. In fact, the expectation value $\langle|\sigma'|^2\rangle$ of the waterfall field grows with time faster than exponentially [141].

Constraints on the parameter space from hybrid inflation and cosmic strings
Applying the above results to our model we can determine bounds on the parameter space. From Eqs. (3.14), (3.15) and (3.18) we obtain an upper bound on v_{B-L}, which weakly depends on λ,

$$v_{B-L} \lesssim 7.3 \times 10^{-4} \left(\ln \frac{16\, g^2}{\lambda}\right)^{1/2} M_P \,. \tag{3.19}$$

In Ref. [118], the authors discuss hybrid inflation and cosmic string production in a setup very similar to ours.[7] Taking into account current experimental bounds inferred from the spectrum of fluctuations in the CMB [47] and from the non-observation of cosmic strings [145], they find viable inflation for

$$\begin{aligned} 3 \times 10^{15}\ \text{GeV} \ \lesssim v_{B-L} \lesssim\ 7 \times 10^{15}\ \text{GeV}\,, \\ 10^{-4} \ \lesssim \ \sqrt{\lambda} \ \lesssim \ 10^{-1}\,. \end{aligned} \tag{3.20}$$

This significantly constrains the allowed parameter space. Indeed, taking into account the recent Planck results (3.18), the upper bound on the $B-L$ breaking scale even comes down to about $v_{B-L} \lesssim 6 \times 10^{15}$, cf. Eq. (3.19). Thus, with the scale of $B-L$ breaking basically fixed, $v_{B-L} \approx 5 \times 10^{15}$ GeV, Eq. (2.44) implies $a = 0$ and a factor of proportionality of about 5. This is still consistent with the Froggatt-Nielsen model, since three $\mathcal{O}(1)$ factors enter in the calculation of v_{B-L}. The bounds on λ restrict the second free $U(1)_{\text{FN}}$ charge, $1.4 \lesssim d \lesssim 2.6$, cf. Eq. (2.43), and therefore M_1. In the following, we will consider the restricted parameter space

$$\begin{aligned} &v_{B-L} = 5 \times 10^{15}\ \text{GeV}\,, \\ &10^{9}\ \text{GeV} \leq M_1 \leq 3 \times 10^{12}\ \text{GeV}\,, \\ &10^{-5}\ \text{eV} \leq \widetilde{m}_1 \leq 1\ \text{eV}\,. \end{aligned} \tag{3.21}$$

[7] Cf. also the analyses in Refs. [119, 142–144].

Here, the variation of $\widetilde{m}_1$ accounts for the uncertainties of the Froggatt-Nielsen model. The chosen range easily covers the expected values for $\widetilde{m}_1$ in this setup, cf. Ref. [15] for a recent analysis.

Initial cosmic string production

The energy density stored in strings just after the end of the phase transition can be estimated as

$$\rho_{\text{string}} \simeq \frac{\mu}{\xi^2} \,. \tag{3.22}$$

Using Eqs. (3.11), (3.14) and (3.16), we find that the fraction of energy stored in cosmic strings directly after the phase transition increases strongly with the coupling parameter λ. This is due to the higher energy density per cosmic string as well as the shorter average distance between two strings. For instance, for $v_{B-L} = 5 \times 10^{15}$ GeV and $\lambda = 10^{-2}$, we find $(H\xi)^{-1} \simeq 400$ and $\rho_{\text{string}}/\rho_0 \simeq 60\,\%$. For $\lambda = 10^{-5}$, this is reduced to $(H\xi)^{-1} \simeq 40$ and $\rho_{\text{string}}/\rho_0 \simeq 0.2\,\%$. In principle, in particular for large values of λ, the production and decay of cosmic strings can have a large influence on the state of the universe just after the phase transition. However, as we will argue in the following, for our purposes it is not necessary to treat these processes in detail, as long as we restrict ourselves to the parameter space in Eq. (3.21).

For the maximal value of the coupling constant, $\lambda = 10^{-2}$, not only is the fraction of energy stored in the cosmic string network just after the phase transition particularly high, but also the relaxation time is particularly short, $\tau_{\text{string}} \simeq \mathcal{O}(10^{-3})H^{-1}$. Hence, the major component of this energy has been converted back into Higgs and gauge degrees of freedom before the processes which we describe by means of Boltzmann equations, cf. Sec. 3.4, become relevant. At the very most, cosmic strings will convert about half of the initial energy density of the Higgs bosons into particles of the Higgs and gauge multiplets. Due to supersymmetry, the extra higgsinos produced will decay into the same supermultiplets as the Higgs bosons would have, thus inducing no significant change in the following discussion. The extra gauge particles will decay predominantly into radiation, which is quickly diluted at this early stage of the matter-dominated phase governed by the non-relativistic Higgs bosons. Thus, it can be expected that our setup is insensitive to a modification of the initial conditions of the reheating phase due to a contribution from cosmic strings. We confirmed this in a numerical study. Considering the case of extremal string production, we shifted half of the energy initially stored in the Higgs bosons at the end of preheating into the gauge degrees of freedom and calculated the resulting entropy, baryon asymmetry and gravitino dark matter. We found no deviations above the percent level from the results obtained for the final outcome of the reheating process when neglecting this effect. We will thus omit the effect of cosmic strings on the reheating process in the remainder of this thesis.

3.4 Perturbative particle production and decay processes

Tachyonic preheating nonperturbatively generates a large abundance of non-relativistic $B-L$ Higgs bosons as well as, to a much lesser extent, non-relativistic abundances of the particles coupled to the Higgs boson, cf. Sec. 3.2.1. Among these are the particles of the $B-L$ gauge supermultiplet, which decay quickly due to their strong gauge interactions, cf. Eq. (2.40). This sets the initial conditions for the following slow, perturbative reheating process, depicted by the solid blue arrows in Fig. 2.1.

Due to our choice of a hierarchical right-handed (s)neutrino mass spectrum, the decay of particles from the symmetry breaking sector into the two heavier (s)neutrino generations is kinematically forbidden. These particles can hence only decay into particles of the N_1 supermultiplet. These (s)neutrinos, just as the (s)neutrinos produced through gauge particle decays and thermally produced (s)neutrinos, decay into MSSM particles, thereby generating the entropy of the thermal bath as well as a lepton asymmetry [146]. Note that these different production mechanisms yield (s)neutrinos with different energies, which, due to relativistic time-dilation, decay at different rates. Finally, the thermal bath produces a thermal gravitino abundance, which will turn out to be in the right ball-park to yield the observed dark matter abundance.

The main tool to obtain a time-resolved description of this reheating process are Boltzmann equations which describe the evolution of the phase space densities of the various particles species due to decay and scattering processes in an expanding universe. After introducing the general formalism of Boltzmann equations in Sec. 3.4.1, we will turn to the implications for the individual particle species in Sec. 3.4.2. This analysis is a supersymmetric extension of the study performed in [73], exploiting the techniques explained there in more detail.

3.4.1 The formalism of Boltzmann equations

The evolution of the phase space density $f_X(t,p)$ of a particle species X is determined by

$$\hat{\mathcal{L}} f_X(t,p) = \sum_{i'j'..} \sum_{ij..} C_X(Xi'j'.. \leftrightarrow ij..)\,, \tag{3.23}$$

with i, j, i', j' labelling other particle species, t and p referring physical time and momentum, $\hat{\mathcal{L}}$ denoting the Liouville operator describing the evolution of the phase space density in an expanding universe and the C_X containing the collision operators of all relevant processes

involving the particle X:

$$\begin{aligned}\hat{\mathcal{L}} f_X(t,p) =& \frac{d}{dt} f_X(t,p)\,,\\ C_X(Xi'j'..\leftrightarrow ij..) =& \frac{1}{2g_X E_X}\sum_{\text{dof}}\int d\Pi(X|i',j',..;i,j,..)(2\pi)^4\delta^{(4)}(P_{\text{out}}-P_{\text{in}})\\ &\times\left[f_i f_j..|\mathcal{M}(ij..\to Xi'j'..)|^2 - f_X f_{i'} f_{j'}..|\mathcal{M}(Xi'j'..\to ij..)|^2\right].\end{aligned} \tag{3.24}$$

Here, $\sum_{\text{dof}}$ denotes the sum over all internal degrees of freedom of the initial and final states, g_X and E_X are the number of degrees of freedom and the energy of a particle X, P_{out} and P_{in} refer to the total out- and ingoing momentum, $\mathcal{M}$ denotes the matrix element and the momentum space element $d\Pi$ is given by

$$d\Pi(X|i',j',..;i,j,..) = S(X,i',j',..;i,j,..)\,d\tilde{p}_{i'}d\tilde{p}_{j'}..d\tilde{p}_i d\tilde{p}_j..\,,\qquad d\tilde{p} = \frac{d^3p}{(2\pi)^3\,2E}\,. \tag{3.25}$$

$S(X,i',j',..;i,j,..)$ is a statistical factor to prevent double counting of identical particles. The quantum statistical factors due to Bose enhancement and Pauli blocking have been omitted, since they typically yield only minor corrections [147].

Some useful quantities

In the following, we will often work with integrated Boltzmann equations, which are obtained by integrating Eq. (3.23) over $g_X\,d^3p_X/(2\pi)^3$. In a Friedmann-Robertson-Walker (FRW) universe, the resulting equation can be simplified to

$$aH\frac{d}{da}N_X = \hat{\Gamma}_X N_X\,, \tag{3.26}$$

with a denoting the scale factor, $\hat{\Gamma}_X$ the effective production rate of X particles, and

$$N_X(t) = \left(\frac{a(t)}{\text{GeV}}\right)^3 n_X = \left(\frac{a(t)}{\text{GeV}}\right)^3 \frac{g_X}{(2\pi)^3}\int d^3p\, f_X(t,p)\,, \tag{3.27}$$

the comoving number density, i.e. the number of X particles in a volume $(a/\text{GeV})^3$. A rescaling of a in Eq. (3.26) leaves the physical number density n_X invariant. For convenience, we will thus set $a_{\text{PH}} \equiv 1$ at the end of preheating. Another useful quantity is the energy density ρ_X,

$$\rho_X = g_X\int\frac{d^3p}{(2\pi)^3}\,E_X(p)\,f_X(t,p)\,. \tag{3.28}$$

In the following, decay rates Γ, comoving number densities N and energy densities ρ will sometimes appear with upper and lower indices. In this case, the lower index refers to the particle species under consideration, while the upper index refers to its origin, e.g. its parent particle or 'PH' for preheating.

Evolution of the gravitational background

The time-dependence of the scale factor $a(t)$ is governed by the Friedmann equation. For a flat universe and a constant equation of state $\omega = \rho/p$ between some reference time t_0 and time t, the Friedmann equation yields

$$a(t) = a(t_0)\left[1 + \frac{3}{2}(1+\omega)\left(\frac{\rho_{\rm tot}(t_0)}{3M_P^2}\right)^{1/2}(t-t_0)\right]^{\frac{2}{3(1+\omega)}}. \tag{3.29}$$

After preheating the universe is dominated by non-relativistic Higgs bosons, i.e. $\omega = 0$. After the end of the reheating process the universe is radiation-dominated, $\omega = 1/3$. In the intermediate region the equation of state changes continuously. We approximate this by implementing a piecewise constant effective equation of state with coefficients ω_n in the intervals $(t_n, t_{n+1}]$ with $a^i_{\rm RH} \leq a(t_n) < a(t_{n+1}) \leq a^f_{\rm RH}$, where $a^i_{\rm RH}$ and $a^f_{\rm RH}$ denote the beginning and the end of the reheating process, respectively. The ω_n are determined iteratively by requiring self-consistency of the Friedmann equation,

$$\frac{\rho_{\rm tot}(t_n)}{\rho_{\rm tot}(t_{n+1})} = \left(\frac{a(t_{n+1})}{a(t_n)}\right)^{3(1+\omega_n)}. \tag{3.30}$$

In our numerical calculations we approximate the total energy density by its two dominant components, the energy density of the Higgs bosons and the energy density of the neutrinos produced in Higgs, higgsino and inflaton decays, $\rho_{\rm tot} \approx \rho_\sigma + \rho^S_{N_1}$, for which we will obtain analytical expressions below, cf. Eqs. (3.36) and (3.38). In the following we will calculate the Hubble rate $H = \dot{a}/a$ using Eq. (3.29). In Appendix B.2, we comment on how, in certain regions of the parameter space, this procedure can be improved, leading to slightly more precise numerical results and in particular clarifying the parameter dependence of the evolution of $a(t)$.

3.4.2 Boltzmann equations for individual particle species

Having introduced the general formalism of Boltzmann equations, we now apply this formalism to the various particle species involved in the $B-L$ phase transition. Consecutively, we will discuss the Boltzmann equations for the massive particle species, for the MSSM particles and for gravitinos. We will discuss analytical solutions wherever possible, before turning to the the numerical solution of the remaining coupled system of equations in Sec. 3.5.

Massive degrees of freedom

The Boltzmann equations describing the massive degrees of freedom introduced above are

$$\hat{\mathcal{L}} f_\sigma = -C_\sigma(\sigma \to N_1 N_1) - C_\sigma(\sigma \to \tilde{N}_1 \tilde{N}_1)\,, \tag{3.31}$$

$$\hat{\mathcal{L}} f_\phi = -C_\phi(\phi \to \tilde{N}_1 \tilde{N}_1)\,, \qquad \hat{\mathcal{L}} f_\psi = -C_\psi(\psi \to \tilde{N}_1^* N_1)\,, \tag{3.32}$$

$$\hat{\mathcal{L}} f_{N_{2,3}} = -C_{N_{2,3}}(N_{2,3} \to \text{MSSM}), \qquad \hat{\mathcal{L}} f_{\tilde{N}_{2,3}} = -C_{\tilde{N}_{2,3}}(\tilde{N}_{2,3} \to \text{MSSM}), \tag{3.33}$$

$$\hat{\mathcal{L}} f_{N_1} = 2\,C_{N_1}(\sigma \to N_1 N_1) + C_{N_1}(\psi \to \tilde{N}_1^* N_1) + C_{N_1}(N_1 \leftrightarrow \text{MSSM}), \tag{3.34}$$

$$\hat{\mathcal{L}} f_{\tilde{N}_1} = 2\,C_{\tilde{N}_1}(\sigma \to \tilde{N}_1 \tilde{N}_1) + 2\,C_{\tilde{N}_1}(\phi \to \tilde{N}_1 \tilde{N}_1) + C_{\tilde{N}_1}(\psi \to \tilde{N}_1^* N_1) + C_{\tilde{N}_1}(\tilde{N}_1 \leftrightarrow \text{MSSM}). \tag{3.35}$$

The particles of the symmetry breaking sector, σ, ϕ and ψ, are produced via tachyonic preheating only, hence their initial number densities are given by Eq. (3.12). Their initial phase space distributions are peaked at low momenta and can be taken to be proportional to $\delta(p)$. The collision operators on the right-hand side of Eqs. (3.31) and (3.32) describe the decay of these particles. The resulting ordinary differential equations are solved by

$$f_X(t,p) = \frac{2\pi^2}{g_X}\, N_X(t_{\text{PH}})\, \frac{\delta(ap)}{(ap)^2}\, \exp[-\Gamma_X^0\,(t - t_{\text{PH}})], \qquad X = \sigma,\, \phi,\, \psi, \tag{3.36}$$

with t_{PH} denoting the time at the end of preheating. We fix the origin of the time axis by setting $t_{\text{PH}} = 0$. Also the abundances of all heavy (s)neutrinos obtain contributions from tachyonic preheating. The corresponding phase space distribution functions are of the same form as f_X in Eq. (3.36).

The collision operators for the lightest (s)neutrinos are more involved. As in Ref. [73], they can be treated best by separating the phase space density into the contributions due to thermal (th) and nonthermal (nt) (s)neutrinos. Introducing $\mathcal{E}_X(E_0; t, t')$, the energy of a particle X at time t which was produced with energy E_0 at time t',

$$\mathcal{E}_X(E_0; t', t) \coloneqq E_0 \frac{a(t')}{a(t)} \left\{ 1 + \left[\left(\frac{a(t)}{a(t')} \right)^2 - 1 \right] \left(\frac{M_X}{E_0} \right)^2 \right\}^{1/2}, \tag{3.37}$$

we find for the comoving number densities of nonthermally produced (s)neutrinos governed by the respective integrated Boltzmann equation (3.26):

$$\begin{aligned} N_X^{\text{nt}}(t) &= N_X^S(t) + N_X^{\text{PH}}(t) + N_X^G(t) \\ &= \int_{t_{\text{PH}}}^{t} dt'\, a^3(t')\, \gamma_{S,X}(t')\, \exp\left[- \int_{t'}^{t} dt'' \frac{M_1\, \Gamma_{N_1}^0}{\mathcal{E}_X(m_S/2; t', t'')} \right] \\ &\quad + N_X^{\text{PH}}(t_{\text{PH}})\, e^{-\Gamma_{N_1}^0 (t - t_{\text{PH}})} + N_X^G(t_G)\, \exp\left[- \int_{t_G}^{t} dt' \frac{M_1\, \Gamma_{N_1}^0}{\mathcal{E}_X(m_G/2; t_G, t')} \right], \end{aligned} \tag{3.38}$$

with $X = N_1,\, \tilde{N}_1$ and

$$\begin{aligned} \gamma_{S,N_1}(t) &\coloneqq 2\, n_\sigma(t)\, \Gamma^0_{\sigma \to N_1 N_1} + n_\psi(t)\, \Gamma^0_\psi, \\ \gamma_{S,\tilde{N}_1}(t) &\coloneqq 2\, n_\sigma(t)\, \Gamma^0_{\sigma \to \tilde{N}_1 \tilde{N}_1} + 2\, n_\phi(t)\, \Gamma^0_\phi + n_\psi(t)\, \Gamma^0_\psi. \end{aligned} \tag{3.39}$$

Here $N_X^{\rm PH}$ denotes the X abundance from nonperturbative particle production during tachyonic preheating, whereas N_X^G refers to the X abundance from the decay of the gauge degrees of freedom. The time t_G denotes the lifetime of the gauge particles after preheating, $t_G = t_{\rm PH} + 1/\Gamma_G^0$, cf. Eq. (2.40), and corresponds to the value a_G of the scale factor, $a_G = a\,(t_G)$. Note that also the (s)neutrinos of the second and third generation are produced in the decays of gauge particles. The corresponding comoving number densities of these (s)neutrino species are of the same form as N_X^G in Eq. (3.38).

Unlike the two heavier (s)neutrino generations, (s)neutrinos of the first generation are also produced from the thermal bath. Assuming kinetic equilibrium, their comoving number densities are determined by the integrated Boltzmann equation

$$aH\frac{d}{da}N_X^{\rm th} = -\Gamma_X^{\rm th}\,(N_X^{\rm th} - N_X^{\rm eq})\;, \qquad X = N_1,\,\tilde{N}_1\,, \tag{3.40}$$

with $N_X^{\rm eq}$ denoting the comoving number density in thermal equilibrium and $\Gamma^{\rm x}_{X\to ij..}$ is the vacuum decay width weighted with the average inverse time dilation factor,

$$N_{N_1}^{\rm eq} = N_{\tilde{N}_1}^{\rm eq} = \left(\frac{a}{\rm GeV}\right)^3 g_{N_1}\frac{M_1^2\,T}{2\pi^2}\,K_2\left(\frac{M_1}{T}\right)\,, \tag{3.41}$$

$$\Gamma^{\rm x}_{N_1\to ij..} = \Gamma^{\rm x}_{\tilde{N}_1\to ij..} = \Gamma^0_{N_1\to ij..}\,\frac{g_{N_1}}{(2\pi)^3\,n^x_{N_1}}\int d^3p\,\frac{M_1}{E_{N_1}}\,f^{\rm x}_{N_1}\,. \tag{3.42}$$

In Eq. (3.40) we are interested in the total decay width of the thermally produced neutrinos, $\Gamma_{N_1}^{\rm th}$. In this case Eq. (3.42) can be evaluated to $\Gamma_{N_1}^{\rm th} = \Gamma_{N_1}^0\,K_1(M_1/T)/K_2(M_1/T)$, where K_n denotes the modified Bessel function of the second kind of order n. Note, however, that Eq. (3.42) is not restricted to this case but also allows the calculation of, for example, the effective decay width of the neutrinos produced by the decay of the Higgs bosons, $\Gamma_{N_i}^S$.

MSSM degrees of freedom

The Boltzmann equations governing the lepton number asymmetry and the abundance of MSSM particles in the thermal bath are

$$\hat{\mathcal{L}}f_L \;=\; C_\ell + C_{\tilde{\ell}} - C_{\ell^c} - C_{\tilde{\ell}^c}\,, \tag{3.43}$$

$$\hat{\mathcal{L}}f_r \;=\; \kappa\,(C_\ell + C_{\tilde{\ell}} + C_{\ell^c} + C_{\tilde{\ell}^c})\,, \tag{3.44}$$

with $C_{\ell,\tilde{\ell},..}$ denoting the collision operators responsible for the production, decay and scattering of (anti)(s)leptons and κ describing the number of radiation quanta produced in the respective processes.

A subtle but important point concerning the Boltzmann equation for the lepton asymmetry is the correct treatment of $2 \to 2$ scattering processes with heavy (s)neutrinos in the intermediate state. The collision operator for (s)neutrino decays and inverse decays takes care of the on-shell contributions to these processes, so we need to add the off-shell contributions.

The CP-conserving part of the off-shell contribution is negligible compared to the corresponding on-shell contribution, so we shall concentrate on the CP-violating off-shell part. This can be obtained by calculating the CP-violating contribution of the full $2 \to 2$ scattering process and then subtracting the on-shell CP-violating contribution. Exploiting unitarity and CPT invariance, we prove in Appendix A that the total CP-violating contribution of the $2 \to 2$ scattering process vanishes up to corrections of $\mathcal{O}((h^\nu)^4)$, so that we can replace the CP-violating off-shell contribution by the negative of the CP-violating on-shell contribution. With this, the integrated Boltzmann equation up to $\mathcal{O}((h^\nu)^2)$ obtained from Eq. (3.43) reads

$$aH\frac{d}{da}N_L = \hat{\Gamma}_L^{\mathrm{nt}} N_L^{\mathrm{nt}} + \hat{\Gamma}_L^{\mathrm{th}} N_L^{\mathrm{th}} - \hat{\Gamma}_W N_L \,, \tag{3.45}$$

with the wash-out rate $\hat{\Gamma}_W$ and the effective (non)thermal production rates for the lepton asymmetry $\hat{\Gamma}_L^{\mathrm{th,nt}}$ given by

$$\begin{aligned}
\hat{\Gamma}_W &\coloneqq \frac{N_{N_1}^{\mathrm{eq}}}{2N_\ell^{\mathrm{eq}}}\Gamma_{N_1}^{\mathrm{th}} \,, \\
\hat{\Gamma}_L^{\mathrm{nt}} &\coloneqq \left(N_L^{\mathrm{nt}}\right)^{-1} \sum_{i=1}^{3} \sum_{X=N_i,\tilde{N}_i} \epsilon_i \left(\Gamma_X^{\mathrm{PH}} N_X^{\mathrm{PH}} + \Gamma_X^G N_X^G + \Gamma_X^S N_X^S\right) \,, \\
\hat{\Gamma}_L^{\mathrm{th}} &\coloneqq \left(N_L^{\mathrm{th}}\right)^{-1} \epsilon_1 \, \Gamma_{N_1}^{\mathrm{th}} (N_{N_1}^{\mathrm{th}} + N_{\tilde{N}_1}^{\mathrm{th}} - 2N_{N_1}^{\mathrm{eq}}) \,.
\end{aligned} \tag{3.46}$$

In Eq. (3.45) we have introduced N_L^{nt} and N_L^{th} as the nonthermal and thermal contributions to the total lepton asymmetry $N_L = N_L^{\mathrm{nt}} + N_L^{\mathrm{th}}$, respectively. The decay rate of the thermally produced (s)neutrinos, $\Gamma_{N_1}^{\mathrm{th}}$, as well as the decay rates Γ_X^{PH}, Γ_X^G, and Γ_X^S for nonthermally produced (s)neutrinos, are given by Eq. (3.42). Note that Eq. (3.46) relates decay rates Γ and effective production rates $\hat{\Gamma}$. The latter describe the relative increase of the respective particle species due to a given production process and can directly be compared with the Hubble rate H in order to determine the efficiency of the respective process. ϵ_i parametrizes the CP asymmetry in the N_i and $\tilde{N}_i$ decays, which, in the Froggatt-Nielsen model, can be estimated as [148, 149]

$$\epsilon_i \lesssim 0.1 \, \frac{\overline{m}_\nu \, M_i}{v_{\mathrm{EW}}^2} \,. \tag{3.47}$$

In the following, we will set ϵ_i to its maximal value, thus obtaining an upper bound for the produced lepton asymmetry.

Analogously, this time neglecting terms of $\mathcal{O}(\epsilon_i)$, Eq. (3.44) yields the integrated Boltzmann equation for the relativistic degrees of freedom of the thermal bath,

$$aH\frac{d}{da}N_r = \hat{\Gamma}_r^{\mathrm{nt}} N_r^{\mathrm{nt}} + \hat{\Gamma}_r^{\mathrm{th}} N_r^{\mathrm{th}} \,, \tag{3.48}$$

with $\hat{\Gamma}_r^{\mathrm{th,nt}}$ denoting the effective rates of (non)thermal radiation production,

$$\begin{aligned}\hat{\Gamma}_r^{\mathrm{nt}} &\coloneqq \left(N_r^{\mathrm{nt}}\right)^{-1} \sum_i \sum_{X=N_i,\tilde{N}_i} \left(\kappa_X^{\mathrm{PH}} \Gamma_X^{\mathrm{PH}} N_X^{\mathrm{PH}} + \kappa_X^G \Gamma_X^G N_X^G + \kappa_X^S \Gamma_X^S N_X^S\right) , \\ \hat{\Gamma}_r^{\mathrm{th}} &\coloneqq \left(N_r^{\mathrm{th}}\right)^{-1} \sum_i \kappa_r^{\mathrm{th}} \, \Gamma_{N_i}^{\mathrm{th}} \left(N_{N_i}^{\mathrm{th}} + N_{\tilde{N}_i}^{\mathrm{th}} - 2N_{N_i}^{\mathrm{eq}}\right) .\end{aligned} \tag{3.49}$$

Here κ_X^{x} denotes the effective increase of radiation quanta in the thermal bath by adding a particle X stemming from the production mechanism x with energy $\varepsilon_X^{\mathrm{x}}$,

$$\kappa_X^{\mathrm{x}} = \frac{3\,\varepsilon_X^{\mathrm{x}}}{4\,\varepsilon_r} . \tag{3.50}$$

Another important quantity in this context is the total radiation production rate $\hat{\Gamma}_r$. It counts the radiation quanta produced per unit time and is obtained by dividing the right-hand side of the Boltzmann equation for radiation, Eq. (3.48), by N_r,

$$\hat{\Gamma}_r = aH \, \frac{dN_r}{da} \, N_r^{-1} = \frac{\dot{n}_r}{n_r} + 3H \simeq \kappa_r^{\mathrm{x}} \, \frac{N_{N_i}^{\mathrm{x}}}{N_r} \, \Gamma_{N_i}^{\mathrm{x}} . \tag{3.51}$$

Here in the last expression $N_{N_i}^{\mathrm{x}}$ denotes the number density of the dominant source for radiation production at a given time.

Solving Eq. (3.48) finally yields the temperature T of the thermal bath,

$$T = \left(\frac{\pi^2}{g_{*,n}\,\zeta(3)} \frac{N_r}{a^3}\right)^{1/3} , \tag{3.52}$$

with $g_{*,n}$ counting the effective relativistic degrees of freedom contributing to the number density of the thermal bath n_r. In the MSSM one finds $g_{*,n} = 427/2$.

Gravitinos

Gravitinos are predominantly[8] produced through supersymmetric QCD scattering processes in the thermal bath. The corresponding integrated Boltzmann equation is

$$aH \frac{d}{da} N_{\widetilde{G}} = \hat{\Gamma}_{\widetilde{G}} N_{\widetilde{G}} . \tag{3.53}$$

In QCD, at leading order in the strong gauge coupling g_s, the effective production rate $\hat{\Gamma}_{\widetilde{G}}$ is given by[9] [150]

$$\hat{\Gamma}_{\widetilde{G}}(T) = \frac{(a/\mathrm{GeV})^3}{N_{\widetilde{G}}} \left(1 + \frac{m_{\tilde{g}}^2(T)}{3m_{\widetilde{G}}^2}\right) \frac{54\zeta(3) g_s^2(T)}{\pi^2 M_P^2} \, T^6 \left[\ln\left(\frac{T^2}{m_g^2(T)}\right) + 0.8846\right] , \tag{3.54}$$

[8] Note that due to the high temperatures reached in this setup, we do not expect a significant contribution from nonthermal gravitino production [118].

[9] Here, the theoretical uncertainty of $\hat{\Gamma}_{\widetilde{G}}$ is at least a factor of 2.

with the energy dependent thermal gluino mass, gluon mass and strong coupling constant

$$\begin{aligned} m_{\tilde{g}}(T) &= \frac{g_s^2(T)}{g_s^2(\mu_0)} m_{\tilde{g}}(\mu_0)\,, \quad m_g(T) = \sqrt{3/2}\, g_s(T)\, T\,, \\ g_s(\mu(T)) &= g_s(\mu_0) \left[1 + \frac{3}{8\pi^2}\, g_s^2(\mu_0)\, \ln \frac{\mu(T)}{\mu_0}\right]^{-1/2} . \end{aligned} \tag{3.55}$$

The typical energy scale during reheating is estimated as the average energy per relativistic particle in the thermal bath, $\mu(T) \simeq \varepsilon_r \simeq 3T$. The gravitino mass $m_{\widetilde{G}}$ and the gluino mass at the electroweak scale $m_{\tilde{g}} \coloneqq m_{\tilde{g}}(\mu_0)$ remain as free parameters.

3.5 Birth of the hot early universe: an illustrative parameter example

Combining our initial conditions with the Boltzmann equations derived in the previous section poses an initial-value problem. Its solution allows us to give a time-resolved description of the reheating process, in particular of the generation of entropy, matter and dark matter. We have numerically solved this problem for all values of the input parameters within the ranges specified in Eq. (3.21). In this section we first illustrate our findings for a representative choice of parameter values, to gain an understanding of the different processes involved in the reheating of the universe. In Chapter 4 we will present the results for the entire parameter space.

Compared to Refs. [4, 73], we take into account all particles involved in the reheating process and consider a higher scale of $B-L$ breaking, $v_{B-L} = 5 \times 10^{15}\,\mathrm{GeV}$, which is compatible with hybrid inflation and cosmic strings, cf. Secs. 3.1 and 3.2.2. However, many of the techniques employed when solving the Boltzmann equations are very similar to those discussed in detail in Refs. [4, 73], and more details on the technical aspects of the procedure we use to solve the Boltzmann equations can be found there. Furthermore, in this section we will focus on the most relevant physical aspects of the reheating process, in particular those relevant for the following chapter. A more detailed discussion of this reheating process is given in Ref. [16].

The point in parameter space which we will focus on in this section is

$$M_1 = 5.4 \times 10^{10}\,\mathrm{GeV}\,, \quad \widetilde{m}_1 = 4.0 \times 10^{-2}\,\mathrm{eV}\,, \quad m_{\widetilde{G}} = 100\,\mathrm{GeV}\,, \quad m_{\tilde{g}} = 1\,\mathrm{TeV}\,, \tag{3.56}$$

which is a typical parameter point in the sense that qualitatively, the effects discussed in this section are present in most of the parameter space. An overview of the resulting comoving number and energy densities during the reheating process, obtained by numerically solving the Boltzmann equations (cf. Sec. 3.4) with the initial conditions imposed by tachyonic preheating (cf. Sec. 3.2.1) and the subsequent decay of the gauge degrees of freedom is shown in Fig. 3.1.

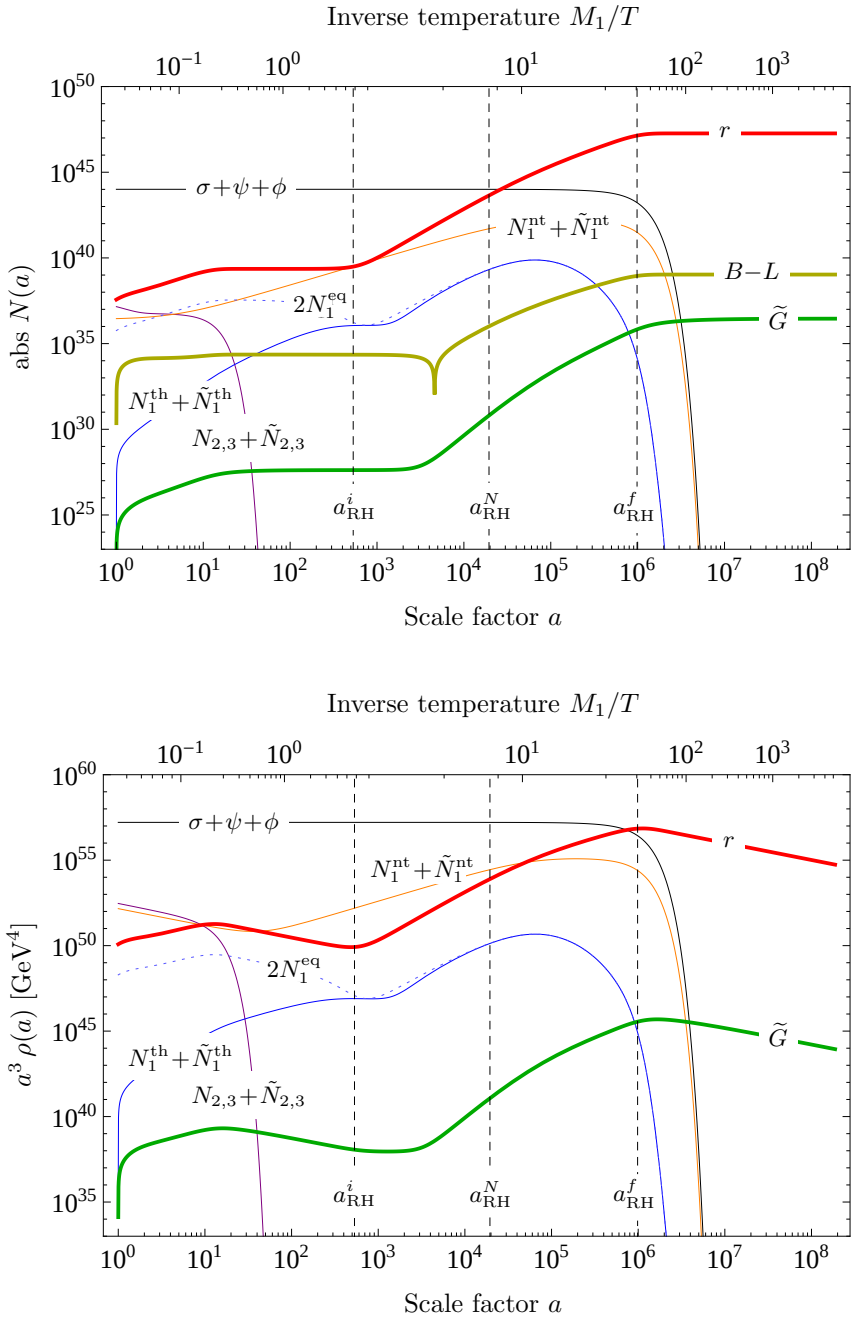

Figure 3.1: Comoving number densities (upper panel) and comoving energy densities (lower panel) for particles from the symmetry breaking sector (Higgs σ + higgsinos ψ + inflatons ϕ), (non)thermally produced (s)neutrinos of the first generation ($N_1^{\rm th}+\tilde{N}_1^{\rm th}$, $N_1^{\rm nt}+\tilde{N}_1^{\rm nt}$), thermal equilibrium abundance of (s)neutrinos of the first generation for comparison ($2N_1^{\rm eq}$), (s)neutrinos of the second and third generation ($N_{2,3}+\tilde{N}_{2,3}$), the MSSM radiation (r), the lepton asymmetry ($B-L$) and gravitinos ($\widetilde{G}$) as functions of the scale factor a. The vertical lines labelled $a^i_{\rm RH}$, $a^N_{\rm RH}$ and $a^f_{\rm RH}$ mark the beginning, the middle and the end of the reheating process, cf. Sec. 3.5.2. The corresponding values for the input parameters are given in Eq. (3.56).

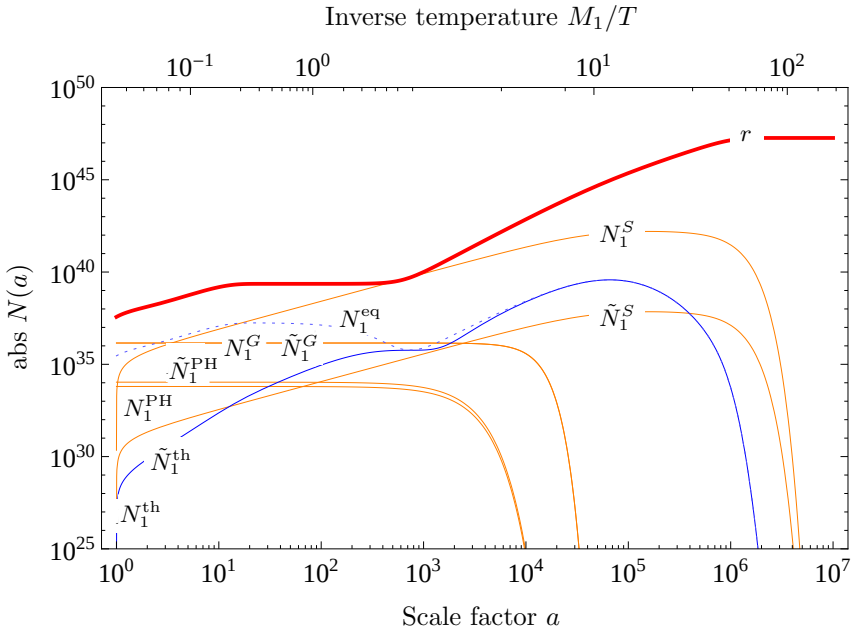

Figure 3.2: Breakdown of the comoving number densities shown in the upper panel of Fig. 3.1. The (s)neutrinos of the first generation ($N_1^{\rm nt}+\tilde{N}_1^{\rm nt}$, $N_1^{\rm th}+\tilde{N}_1^{\rm th}$) split into (s)neutrinos produced during preheating ($N_1^{\rm PH}$, $\tilde{N}_1^{\rm PH}$), in the decay of the gauge degrees of freedom (N_1^G, $\tilde{N}_1^G$), in the decay of the particles from the symmetry breaking sector (N_1^S, $\tilde{N}_1^S$), and from the thermal bath ($N_1^{\rm th}$, $\tilde{N}_1^{\rm th}$).

Specific steps of the reheating process are resolved in more detail in Figs. 3.2 to 3.4. In the following, we discuss the reheating process step by step, starting with the decay of the massive particles, proceeding with a discussion of the thermal bath and in particular the reheating temperature, before finally turning to the small departures from thermal equilibrium responsible for the generation of matter and dark matter.

3.5.1 Decay of massive particles

Among all the particles present after the end of tachyonic preheating and after the decay of the $B-L$ gauge degrees of freedom, the heavy (s)neutrinos of the second and third generation have the shortest lifetime. They decay into particles of the MSSM, thereby generating a contribution to the thermal bath and causing a first stage of reheating, which we will refer to as $N_{2,3}$-reheating. This corresponds to the first rise of the thick red curve marking the MSSM radiation in Figs. 3.1 and 3.2.

The remaining massive degrees of freedom are now the members of the N_1 multiplet and the symmetry breaking sector, with the Higgs boson as clearly dominant component. Due to the kinematic constraints introduced in Sec. 2.5, the particles of the symmetry breaking sector decay exclusively into neutrinos and sneutrinos of the first generation, with the decay rate Γ_S^0 given in Eq. (2.39). Hereby, the decay into sneutrinos is suppressed compared to

the decay into their fermionic superpartners, cf. Eq. (2.42). The first generation (s)neutrino population thus consists of non-relativistic (s)neutrinos which are produced during preheating ($N_1^{\rm PH}$, $\tilde{N}_1^{\rm PH}$), relativistic (s)neutrinos from gauge boson decay (N_1^G, $\tilde{N}_1^G$) and from the decay of symmetry breaking sector (N_1^S, $\tilde{N}_1^S$) as well as thermally produced (s)neutrinos ($N_1^{\rm th}$, $\tilde{N}_1^{\rm th}$). They all decay into MSSM particles, thereby producing the lion's share of the hot thermal bath during what we will refer to as (N_1-) reheating. Their different kinetic energies entail different relativistic time dilation factors and hence different decay rates, cf. Eq. (3.42). The resulting evolution of their abundances is shown in Fig. 3.2. The N_1-reheating phase is responsible for the second rise visible in the thick red curve marking the MSSM radiation.

The dominant component of the first generation (s)neutrino population is formed by the neutrinos N_1^S produced by the decay of the Higgs boson, and hence the time-scale governing the neutrino decay is $1/\Gamma_{N_1}^S$, cf. Eq. (3.42),

$$\Gamma_{N_1}^S(a) = \gamma^{-1}(a)\,\Gamma_{N_1}^0\,, \qquad \gamma^{-1}(a) = \left\langle \frac{M_1}{E_{N_1}} \right\rangle_a^{(S)}\,, \tag{3.57}$$

evaluated at $a = a_{\rm RH}^N$ when the decay of these neutrinos starts to become effective, i.e. $\Gamma_{N_1}^S(a_{\rm RH}^N) = H(a_{\rm RH}^N)$. Here γ, accounting for the time-dilation in the decay of the relativistic neutrinos, is numerically found to be large in the entire parameter space considered, e.g. $\gamma(a_{\rm RH}^N) \simeq 85$ for the parameter point (3.56), indicating that the N_1^S neutrinos remain ultra-relativistic throughout their lifetime. In the following, we shall employ the short notation $\Gamma_{N_1}^S := \Gamma_{N_1}^S(a_{\rm RH}^N)$ when comparing characteristic decay rates. For the parameter example (3.56) we find $\Gamma_S^0 \ll \Gamma_{N_1}^S$, hence $1/\Gamma_S^0$ sets the overall time-scale of N_1-reheating. As we will see in Sec. 4.1, $\Gamma_S^0 \ll \Gamma_{N_1}^S$ holds in most of the viable parameter space. If the situation is reversed, then qualitatively we find a very similar picture, however with the roles of $\Gamma_{N_1}^S$ and Γ_S^0 exchanged, see also the parameter example discussed in Ref. [73].

3.5.2 Reheating and the temperature of the thermal bath

The main part of the thermal bath is produced during N_1-reheating, with $N_{2,3}$-reheating and the decay of the gauge particles adding only small contributions. Solving the Boltzmann equation for radiation, Eq. (3.48), we obtain the temperature of the thermal bath throughout the reheating process, cf. Eq. (3.52). The result is depicted by the solid thick red curve in Fig. 3.3. A striking feature and one of the key results of this subsection is the basically constant temperature during N_1-reheating.

A temperature plateau

To quantify this result, note that both reheating phases are characterized by $\hat{\Gamma}_r \geq H$, with $\hat{\Gamma}_r$ the total radiation production rate, cf. Eq. (3.51). For N_1-reheating we use this to define $a_{\rm RH}^i$ and $a_{\rm RH}^f$, the values of the scale factor marking the beginning and the end of the reheating

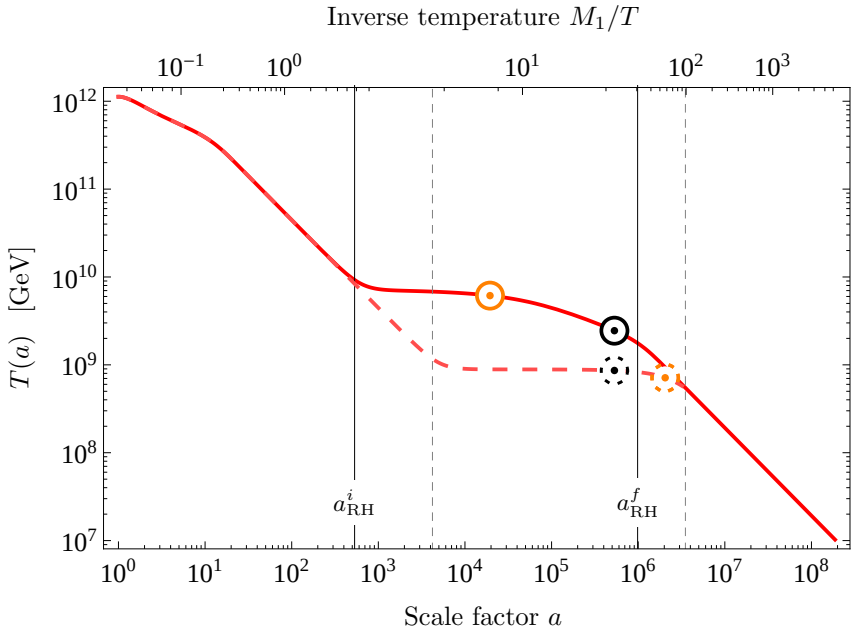

Figure 3.3: Temperature of the thermal bath T for two different parameter examples. The solid curve shows the result for the parameter point (3.56), for which $\Gamma_S^0 \ll \Gamma_N^S$. For comparison, the dashed quantities are obtained for $\widetilde{m}_1 = 10^{-5}$ eV and M_1 unchanged, implying $\Gamma_S^0 \gg \Gamma_N^S$. The orange (black) markers denote the respective values of $T_{\rm RH}^N$ ($T_{\rm RH}^\sigma$), the vertical lines mark the beginning and the end of the reheating process.

process, i.e. at which $\hat{\Gamma}_r = H$. As shown in Fig. 3.3, the temperature of the thermal bath changes less than an order of magnitude between $a^i_{\rm RH}$ and $a^f_{\rm RH}$. The reason for this is the continuous production of N_1^S neutrinos during reheating. As long as the N_1 neutrinos are produced much faster than they decay, their comoving number density grows linearly in time, $N^S_{N_1} \propto \int_{t_{\rm PH}}^t dt'$, cf. Eq. (3.38). Taking into account that as long as $\Gamma_S^0 < H$ the expansion of the universe is driven by the energy stored in the Higgs bosons, i.e. non-relativistic matter, this translates into $N^S_{N_1} \propto a^{3/2}$. The N_1^S number density in turn controls the scaling behaviour on the right-hand side of the Boltzmann equation for radiation during N_1-reheating, cf. Eq. (3.48). Using $H \propto a^{-3/2}$, we find

$$a^i_{\rm RH} \lesssim a \lesssim a^f_{\rm RH} : \quad aH\frac{d}{da}N_r \propto N^S_{N_1} \propto a^{3/2}\,, \quad N_r \propto a^3\,, \quad T \approx \text{const.}\,, \tag{3.58}$$

Here, we used $\Gamma_S^0 \ll \Gamma^S_{N_1}$, as is the case for the parameter example (3.56). What happens in the reverse case? For $H(a^i_{\rm RH}) > H(a) > \Gamma_S^0$, the situation is analogous as described above Eq. (3.58), resulting in a nearly constant temperature. For $\Gamma_S^0 > H(a) > \Gamma^S_{N_1}$, the Hubble rate on the left-hand side of the Boltzmann equation for radiation begins to drop faster, since ultra-relativistic N_1^S neutrinos take over as the dominant component of the energy density. At the same time, the growth of the comoving number density $N^S_{N_1}$ on the right-hand side of

this equation begins to slow down as its source is depleted. In summary, even after $H \sim \Gamma_S^0$, the temperature remains approximately constant until at $H \sim \Gamma_{N_1}^S$ the neutrino abundance rapidly decreases. For comparison, this is shown in Fig. 3.3 by the dashed red curve for $\widetilde{m}_1 = 10^{-5}$ eV and $M_1 = 5.4 \times 10^{10}$ GeV.

The reheating temperature(s)

In Fig. 3.3, we depict the evolution of the temperature throughout the reheating process. In order to define a characteristic temperature for this process, the existence of a temperature plateau during the reheating process is a great advantage. It implies that for any of the possible definitions of the 'reheating temperature' introduced below, the resulting value of the temperature will not vary by more than an order of magnitude. Beyond that, there are two temperatures which will be of interest in the following. First, the temperature $T_{\rm RH}^\sigma$ is the temperature at which the Hubble rate is equal to the decay rate of the Higgs bosons,

$$T_{\rm RH}^\sigma = T\left[H(a_{\rm RH}^\sigma) = \Gamma_\sigma^0\right] , \tag{3.59}$$

marked by the black circles in Fig. 3.3. Second, the temperature $T_{\rm RH}^N$ is the temperature at which the Hubble rate drops below the effective decay rate of the first generation neutrinos produced in the decay of the Higgs bosons,

$$T_{\rm RH}^N = T\left[H(a_{\rm RH}^N) = \Gamma_{N_1}^S\right] , \tag{3.60}$$

marked by the orange circles in Fig. 3.3. These temperatures mark characteristic points in the evolution of the temperature of the thermal bath during N_1-reheating. The appearance of two distinct temperatures is a characteristic feature of the two-stage reheating process found in this model, with the energy budget during reheating successively dominated by two different nonthermal species, namely non-relativistic Higgs bosons and relativistic neutrinos. The physical interpretation of these temperatures depends on which of the decay rates Γ_σ^0 and $\Gamma_{N_1}^S$ is the larger one. Note that since this differs for the solid and the dashed curve in Fig. 3.3, the order of $a_{\rm RH}^N$ and $a_{\rm RH}^\sigma$ is reversed.

On the one hand, $\max\{T_{\rm RH}^\sigma, T_{\rm RH}^N\}$, corresponding to a scale factor of $a_{pl} = \min\{a_{\rm RH}^\sigma, a_{\rm RH}^N\}$, can be interpreted as typical value for the temperature on the plateau. Moreover, it picks up an interesting physical feature. For $a_{\rm RH}^i < a < a_{pl}$ the temperature is constant to high accuracy. At a_{pl} the decay of either the Higgs bosons or the neutrinos becomes effective, leading in both cases to the decrease of one of the components in the supply chain of the thermal bath. This results in a slight decrease of the temperature for $a_{pl} < a < a_{\rm RH}^f$, cf. Fig. 3.3. On the other hand, $\min\{T_{\rm RH}^\sigma, T_{\rm RH}^N\}$ marks a characteristic value of the temperature at the end of the reheating process, when the abundance of N_1^S-neutrinos drops rapidly. This marks the point in time when the energy density stored in MSSM radiation takes over as the dominant component. Finally, independent of the hierarchy of Γ_σ^0 and $\Gamma_{N_1}^S$, $T_{\rm RH}^\sigma$ can be to

good approximation identified as the temperature when the expansion history of the universe switches from $H \propto a^{-3/2}$ (non-relativistic matter) to $H \propto a^{-2}$ (radiation). For $\Gamma^S_{N_1} > \Gamma^0_S$ the MSSM radiation takes over directly at this point, for $\Gamma^S_{N_1} < \Gamma^0_S$, there is an intermediate stage dominated by relativistic N_1^S neutrinos.

Which temperature one refers to as 'the reheating temperature' thus depends on what physical feature is relevant for the question under consideration. In the analysis of the parameter space in the context of leptogenesis and DM production in Secs. 4.1 and 4.2, $T^N_{\rm RH}$ will prove to be a convenient choice. When studying the expansion history of our universe in the course of determining the gravitational wave spectrum in Sec. 4.3, $T^\sigma_{\rm RH}$ will be a good starting point. A more detailed discussion of the different temperatures, their interpretation and their parameter dependencies is given in Appendix B.

3.5.3 Small departures from thermal equilibrium

In the last two subsections, we discussed the decay of the heavy particles of the neutrino and symmetry breaking sector and the resulting formation of the thermal bath. As we shall see in this subsection, these processes are accompanied by departures from thermal equilibrium which are crucial for the generation of a matter asymmetry as well as for the production of dark matter.

Leptogenesis

First, let us return to the first generation neutrino population. We can safely assume the thermally produced (s)neutrinos to be in kinetic equilibrium. However, departures from thermal equilibrium can occur throughout the reheating process. The comoving thermal equilibrium abundance is depicted by the dashed blue curve in Fig. 3.4. After an initial increase it decreases due to Boltzmann suppression when the thermal (s)neutrinos become non-relativistic. The onset of N_1-reheating, accompanied by a basically constant temperature, leads to a second increase of the comoving equilibrium number density until at the end of the reheating phase a rapidly dropping temperature reinforces the Boltzmann suppression factor, leading to an exponential decrease. The actual thermal (s)neutrino number density, depicted by the solid blue curve in Fig. 3.4, is initially significantly lower than the equilibrium number density, but is steadily driven towards the equilibrium curve. At the end of the reheating phase the situation is reversed, and the actual thermal (s)neutrino abundance, driven by a continuous production from the thermal bath, overshoots the equilibrium abundance. Although this overshooting is too small to be visible in the double-logarithmic scaling of Fig. 3.4, we will see in a moment that it is nonetheless very relevant for leptogenesis.

We are now ready to turn to the generation of the $B-L$ asymmetry. Solving the integrated Boltzmann equation (3.45) for the parameter point (3.56) yields the thermal and nonthermal contribution to the asymmetry depicted in Fig. 3.4. The nonthermal lepton asymmetry receives a first contribution from the decay of the heavy (s)neutrinos of the second and third

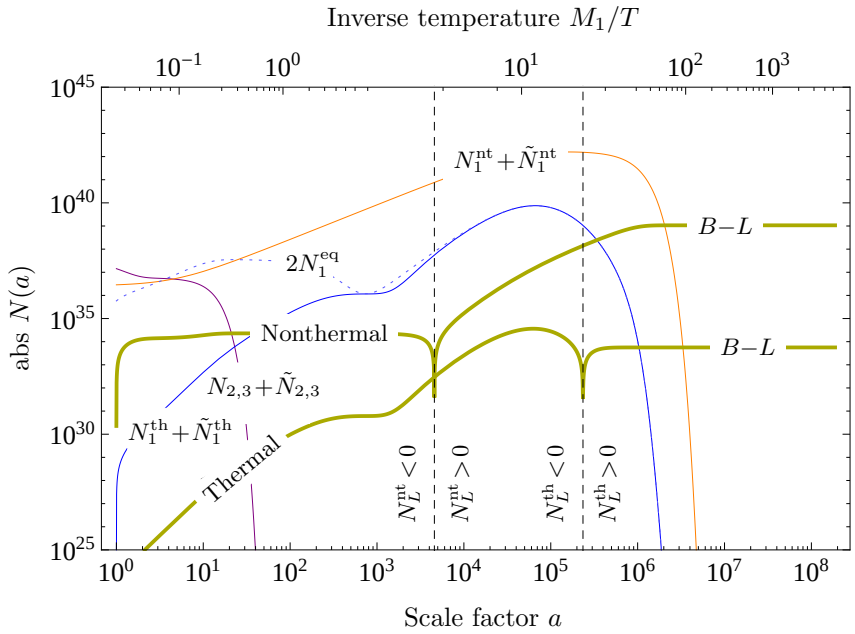

Figure 3.4: Comoving number densities for the nonthermal ($N_L^{\rm nt}$) and thermal ($N_L^{\rm th}$) contributions to the total lepton asymmetry as well as all (s)neutrino species ($N_1^{\rm nt}+\tilde{N}_1^{\rm nt}$, $N_1^{\rm th}+\tilde{N}_1^{\rm th}$, $2N_1^{\rm eq}$ for comparison and $N_{2,3}+\tilde{N}_{2,3}$) as functions of the scale factor a. The vertical lines mark the changes in the signs of the two components of the lepton asymmetry.

generation. To clearly distinguish this contribution from the main contribution arising during N_1-reheating, we have assigned opposite signs to $\epsilon_{2,3}$ and ϵ_1 in $\hat{\Gamma}_L^{\rm nt}$, cf. Eq. (3.46). This entails the change of sign visible at $a \simeq 4.6\times10^3$ in Fig. 3.4, when N_1-reheating becomes efficient and the main part of the nonthermal asymmetry is produced by the decay of the N_1^S-neutrinos. Wash-out effects are negligibly small throughout this process and hence, once the production of the nonthermal asymmetry becomes inefficient, $\hat{\Gamma}_L^{\rm nt} < H$, the asymmetry freezes out.

The production of the thermal asymmetry is driven by the deviation of the thermal (s)neutrino abundance from the equilibrium value, cf. Eq. (3.46). This leads to an initially negative asymmetry with a rapidly increasing absolute value. This increase slows down as the thermal (s)neutrino abundance approaches the equilibrium value. At around $a \simeq 6.3\times10^4$ wash-out processes start to play a role, leading to a decrease of the asymmetry. The situation rapidly changes when the thermal (s)neutrino abundance overshoots the equilibrium abundance at the end of N_1-reheating. This generates an asymmetry with an opposite sign, which overcompensates the asymmetry generated so far. Shortly after, both $\hat{\Gamma}_W$ and $\Gamma_L^{\rm th}$ drop significantly below the Hubble rate and the asymmetry freezes out.

The final values of $N_L^{\rm nt}$ and $N_L^{\rm th}$ allow us to infer the present baryon asymmetry η_B as

well as its composition in terms of a nonthermal ($\eta_B^{\rm nt}$) and a thermal ($\eta_B^{\rm th}$) contribution,

$$\eta_B = \frac{n_B^0}{n_\gamma^0} = \eta_B^{\rm nt} + \eta_B^{\rm th}\,, \quad \eta_B^{\rm nt,th} = C_{\rm sph}\frac{g_{*,s}^0}{g_{*,s}^{\rm RH}}\,\frac{N_L^{\rm nt,th}}{N_\gamma}\bigg|_{a_f}\,. \tag{3.61}$$

Here, $C_{\rm sph} = 8/23$ denotes the sphaleron conversion factor, $g_{*,s}^{\rm RH} = 915/4$ and $g_{*,s}^0 = 43/11$ are the effective numbers of relativistic degrees of freedom in the MSSM that enter the entropy density s of the thermal bath in the high- and low-temperature regime, respectively, and $N_\gamma = g_\gamma/g_{*,n}\,N_r$ is the comoving number density of photons. As final value for the scale factor we use $a_f \simeq 1.9\times 10^8$ which is the maximal value depicted in Fig. 3.1. For our parameter example we find

$$\eta_B \simeq 3.7\times 10^{-9}\,, \quad \eta_B^{\rm nt} \simeq 3.7\times 10^{-9}\,, \quad \eta_B^{\rm th} \simeq 1.9\times 10^{-14}\,. \tag{3.62}$$

Note that to obtain these values, we have set ϵ_1 to the maximal value allowed by Eq. (3.47). Hence η_B in Eq. (3.62) yields an upper bound on the baryon asymmetry produced in this setup and is thus perfectly compatible with the observed value, $\eta_B^{\rm obs} \simeq 6.2\times 10^{-10}$ [47]. In fact, the Froggatt-Nielsen model typically predicts a value for ϵ_1 that is smaller than the maximal possible value by roughly a factor of $\mathcal{O}(10)$, cf. Ref. [15], implying excellent agreement between prediction and observation for this parameter example, $\eta_B \simeq \eta_B^{\rm obs}$.

To summarize, let us highlight the points which are somewhat special in the leptogenesis mechanism presented here. First, we explicitly trace both the thermal as well as the nonthermal contributions to the asymmetry. For the parameter example presented here the nonthermal component is clearly dominant. This will indeed prove to be the case for most of the parameter space, although the reversed situation is also possible, cf. Sec. 4.1.2. Note that omitting the nonthermal production channel and resorting to standard thermal leptogenesis would yield $\eta_B^{\rm st} \sim 10^{-10}$ for this parameter point, cf. [78], which is almost an order of magnitude below the observed value. Second, our result for the final thermal asymmetry is significantly lower than the result obtained from standard thermal leptogenesis. This is mainly due to two effects. The decays of the nonthermal neutrinos entail a continuous production of entropy, thus leading to a dilution of the produced asymmetry which does not occur in standard thermal leptogenesis. Furthermore, in consequence of the specific reheating mechanism at work the generation of the thermal asymmetry is delayed in time, so that it takes place at a lower temperature than in the standard case. This implies a correspondingly smaller abundance of thermal (s)neutrinos, rendering our thermal mechanism for the generation of an asymmetry less efficient.

Gravitino production

Finally, let us consider the production of gravitinos, cf. the dark green curves in Fig. 3.1. Gravitino production is efficient as long as $\hat{\Gamma}_{\widetilde{G}} > H$, cf. Eq. (3.53). This leads to two produc-

tion phases, one during $N_{2,3}$-reheating and then a more important one during N_1-reheating. Due to their very weak interactions, gravitinos decouple from the thermal bath as soon as they are produced, and hence their comoving abundance remains constant after the end of N_1-reheating. Note that the existence of a temperature plateau has an interesting effect on the Boltzmann equation governing the gravitino production. From Eq. (3.54) it is evident that for a constant temperature the effective gravitino production rate grows as the physical volume, $\hat{\Gamma}_{\widetilde{G}} \propto a^3$, entailing a constant space-time density of gravitino production. In other words, the production of radiation just compensates the expansion of the universe and gravitinos are produced as in a static universe.

Assuming that the gravitino is the LSP, we can deduce today's gravitino dark matter abundance $\Omega_{\widetilde{G}}h^2$ from the final value of $N_{\widetilde{G}}$:

$$\Omega_{\widetilde{G}}h^2 = \frac{\rho^0_{\widetilde{G}}}{\rho_c/h^2} = \frac{m_{\widetilde{G}}\, n^0_\gamma}{\rho_c/h^2}\frac{g^0_{*,s}}{g^{\mathrm{RH}}_{*,s}}\left.\frac{N_{\widetilde{G}}}{N_\gamma}\right|_{a_f}, \tag{3.63}$$

where $\rho_c = 3H^2/(8\pi G) = 1.052 \times 10^{-5}\, h^2\,\mathrm{GeV\,cm^{-3}}$ denotes the critical energy density of the universe, h the Hubble rate in the units $H = h \times 100\,\mathrm{km\,s^{-1}\,Mpc^{-1}}$ and $n^0_\gamma = 410\,\mathrm{cm^{-3}}$ the number density of the CMB photons. For our parameter example we find $\Omega_{\widetilde{G}}h^2 \simeq 0.11$, matching the observed amount of dark matter $\Omega^{\mathrm{obs}}_{\mathrm{DM}}h^2 \simeq 0.11$ [47][10]. Note that in the choice of the parameter example, cf. Eq. (3.56), $M_1 = 5.4\times10^{11}$ GeV was tuned to obtain this result. This demonstrates that it is possible, within the setup discussed here, to obtain the correct abundance of gravitino DM while simultaneously generating enough baryon asymmetry. We will return to the question of how easily this can be achieved in other parts of the parameter space in Sec. 4.2.1. An alternative to gravitino DM in this setup is to assume that the LSP is a neutralino, which is then produced nonthermally from gravitino decays as well as through thermal freeze-out. We will come back to this option in Sec. 4.2.2.

Robustness against theory uncertainties

After having discussed the reheating mechanism present in our model in some detail, an interesting question is the robustness of this process against possible theory uncertainties. For example, there are still considerable uncertainties connected to the production and decay of cosmic strings, cf. Sec. 3.2.2. This could have a significant influence on the initial conditions of the reheating process. A detailed study of this question can be found in Ref. [16]. The bottom line is that the time-resolved evolution of the various number densities, cf. Fig. (3.1), can vary significantly whereas the final outcome of the reheating process, i.e. the resulting abundances of entropy and dark matter as well as the generated lepton asymmetry, is remarkably insensitive to even quite dramatic changes of the initial conditions as well as to omitting entire particle species, e.g. the degrees of freedom of the gauge multiplet. This shows that

[10]The recently published Planck data yields a slightly larger value, $\Omega^{\mathrm{obs}}_{\mathrm{DM}}h^2 = 0.12$ [1]. The effect of this change on the work presented here is marginal, and in the following we will stay with the value quoted above.

the mechanism presented here is extremely robust against possible theory uncertainties.

In this chapter, we studied the cosmological processes accompanying the spontaneous breaking of $B-L$ in the early universe. In particular, we discussed the phase of hybrid inflation in the false vacuum of $B-L$, the nonperturbative processes of tachyonic preheating and cosmic string formation which accompany the actual phase transition as well as the subsequent perturbative reheating process governed by the Boltzmann equations. In particular the last step, yielding a time-resolved picture of the reheating process, was discussed for a single representative parameter point. In the following chapter, we will investigate the phenomenology of this model, thereby extending the discussions of this chapter to the entire parameter space.

Chapter 4

Phenomenology

In Chapters 2 and 3 we discussed the process of spontaneous symmetry breaking in the Abelian Higgs model and the processes accompanying the cosmological realization of this phase transition. In this chapter we turn to the resulting phenomenology. In Sec. 4.1 we present the results of a parameter scan for the reheating temperature and the baryon asymmetry. In particular, we give semi-analytical formulas for both quantities in terms of the neutrino parameters M_1 and $\widetilde{m}_1$ and determine in which part of the parameter space leptogenesis and entropy production can be realized in accordance with the experimental data. In Sec. 4.2 we additionally require a dark matter abundance in agreement with observations. We consider both the possibility of gravitino as well as neutralino dark matter, and in both cases find relations between the neutrino parameters and superparticle masses. Another possibility to search for signatures of a $B-L$ phase transition in the early universe is the gravitational wave spectrum. This is the topic of Sec. 4.3, where we discuss possible signatures of the cosmological process introduced in Chapter 3 in the gravitational wave background, in particular of inflation, (p)reheating and cosmic strings. Finally in Sec. 4.4 we very briefly comment on possible implications for low-energy neutrino physics. This chapter is based on work partly published in Refs. [15–17, 19].

4.1 Reheating temperature and baryon asymmetry

In Sec. 3.5 we discussed the reheating process for a representative parameter example. We now turn to the investigation of the entire parameter space. We will present our main results for the reheating temperature and the baryon asymmetry, cf. Ref. [16] for a more detailed discussion. The relevant model parameters for this section are the scale of $B-L$ breaking v_{B-L}, the heavy neutrino mass M_1 and the effective light neutrino mass $\widetilde{m}_1$, constrained by Eq. (3.21).

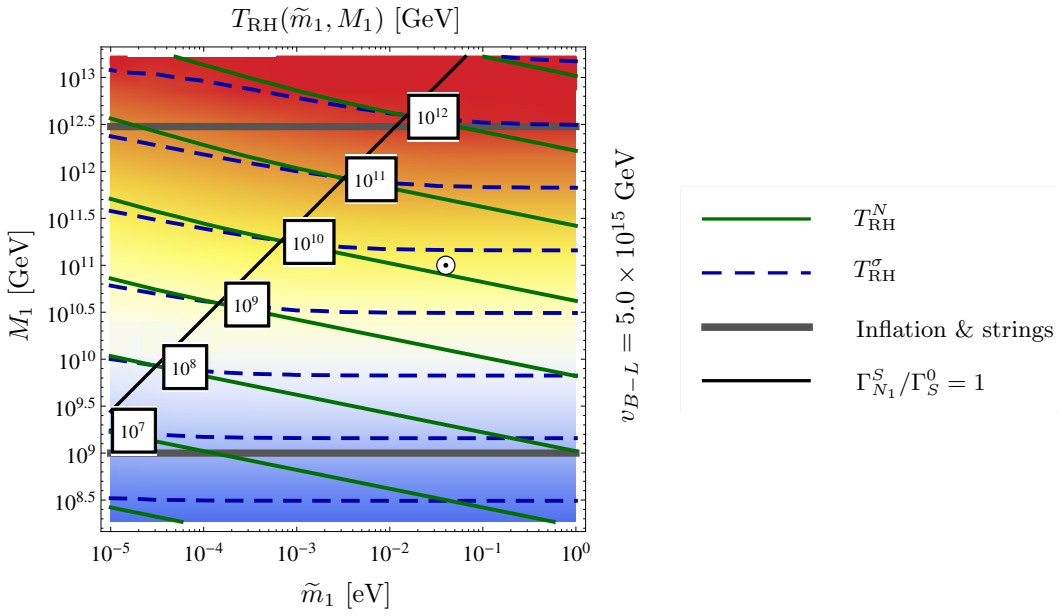

Figure 4.1: Contour plot of the 'reheating temperatures' $T^N_{\rm RH}$ and $T^\sigma_{\rm RH}$, cf. Sec. 3.5.2, as a function of the effective neutrino mass $\widetilde{m}_1$ and the heavy neutrino mass M_1. The thick horizontal grey lines represent the lower and the upper bound on M_1, respectively, which arise from requiring consistency with F-term hybrid inflation and the bound on the cosmic string tension, cf. Eq. (3.21). The small white circle marks the position of the parameter point discussed in Sec. 3.5.

4.1.1 Reheating temperature

Figure 4.1 shows the result of the parameter scan in the $(\widetilde{m}_1, M_1)$ - plane for the two characteristic temperatures $T^N_{\rm RH}$ and $T^\sigma_{\rm RH}$ of the reheating process introduced in Sec. 3.5.2. The black line denotes $\Gamma^S_{N_1} = \Gamma^0_S$, with $\Gamma^S_{N_1} > \Gamma^0_S$ on the right-hand side, and the thick horizontal grey lines limit the allowed values of M_1 according to Eq. (3.21). The resulting values for the reheating temperature range from about 10^7 GeV for small $(\widetilde{m}_1, M_1)$ to 10^{12} GeV for large $(\widetilde{m}_1, M_1)$. As anticipated in Sec. 3.5.2, the two definitions of the reheating temperature differ at most by about one order of magnitude.

The contour lines of $T^N_{\rm RH}$ and $T^\sigma_{\rm RH}$ in Fig. 4.1 are very well described by

$$T^N_{\rm RH} \simeq \begin{cases} T^{N\,(-)}_{\rm RH} = 9.4 \times 10^9 \text{ GeV} \left(\dfrac{M_1}{10^{11} \text{ GeV}}\right)^{1.25} \left(\dfrac{\widetilde{m}_1}{10^{-2} \text{ eV}}\right)^{0.25} & \text{for } x \gtrsim 36 \\ T^{N\,(+)}_{\rm RH} = 2.9 \times 10^9 \text{ GeV} \left(\dfrac{M_1}{10^{11} \text{ GeV}}\right)^{1.2} \left(\dfrac{\widetilde{m}_1}{10^{-4} \text{ eV}}\right)^{0.3} & \text{for } x \lesssim 36 \end{cases}, \tag{4.1}$$

$$T^\sigma_{\rm RH} \simeq \begin{cases} T^{\sigma\,(-)}_{\rm RH} = 5.6 \times 10^9 \text{ GeV} \left(\dfrac{M_1}{10^{11} \text{ GeV}}\right)^{1.5} & \text{for } x \gtrsim 300 \\ T^{\sigma\,(+)}_{\rm RH} = 3.1 \times 10^9 \text{ GeV} \left(\dfrac{M_1}{10^{11} \text{ GeV}}\right)^{1.3} \left(\dfrac{\widetilde{m}_1}{10^{-4} \text{ eV}}\right)^{0.2} & \text{for } x \lesssim 300 \end{cases}, \tag{4.2}$$

with

$$x = \frac{\Gamma^0_{N_1}}{\Gamma^0_S} \simeq 2200 \left(\frac{\widetilde{m}_1}{10^{-2}\ \mathrm{eV}}\right)\left(\frac{10^{11}\ \mathrm{GeV}}{M_1}\right), \tag{4.3}$$

serving as discriminator between the two regimes $\Gamma^S_{N_1} \gg \Gamma^0_S$ and $\Gamma^S_{N_1} \ll \Gamma^0_S$, reflecting our expectation of the different roles of T^N_{RH} and T^σ_{RH} in the two regimes, cf. Sec. 3.5.2. The semi-analytical formulas (4.1) and (4.2) can be understood from the Friedmann equation,

$$3H^2 M_P^2 = \rho_{\mathrm{tot}}\,, \qquad \rho_{\mathrm{tot}} = \alpha\,\rho_r = \frac{\alpha\,\pi^2}{30}\,g_* T^4\,, \tag{4.4}$$

after substituting H with the respective (effective) decay rate and taking into account that only a fraction $1/\alpha$ of the total energy density is stored in thermal radiation at a^N_{RH} or a^σ_{RH}. Here g_* counts the degrees of freedom with $g_* = 915/4$ for the MSSM at high energies. α and if needed the relativistic time-dilation factor γ for the N^S_1 neutrinos have to be determined numerically by solving the Boltzmann equations. For example, $T^{\sigma\,(-)}_{\mathrm{RH}}$ is directly obtained by inserting $H = \Gamma^0_S$ and $\alpha(a^\sigma_{\mathrm{RH}}) = 0.3$. Since in this case the $B-L$ Higgs bosons decay quasi directly into MSSM radiation, the process does not depend on the neutrino parameter $\widetilde{m}_1$. On the other hand, for $\Gamma^0_S \gg \Gamma^S_{N_1}$ there is an intermediate state when relativistic neutrinos dominate the energy density, leading to an $\widetilde{m}_1$ dependence of $\alpha(a^\sigma_{\mathrm{RH}})$ and consequently of the temperature $T^{\sigma\,(+)}_{\mathrm{RH}}$.

4.1.2 Baryon asymmetry

The parameters determining η_B are the neutrino parameters $\widetilde{m}_1$ and M_1 and the temperature of the thermal bath, which is itself a function of $\widetilde{m}_1$ and M_1, cf. Eqs. (4.1) and (4.2). Fig. 4.2 shows the results of the parameter scan, thereby differentiating between regions in which the nonthermal asymmetry alone is sufficient to explain the observed value (light green), regions in which the thermal asymmetry alone is sufficient (grey green) and regions which must be excluded because the produced asymmetry is too low (red). We observe that in most of the parameter space the nonthermal production (i.e. via neutrinos from Higgs boson decays) is significantly more important, as was the case for the parameter example discussed in Sec. 3.5. Furthermore, note that in most of the parameter space where the nonthermal production is dominant, the dependence on $\widetilde{m}_1$ is negligible. This directly corresponds to negligible wash-out in this regime. However, wash-out is important in the regime where thermal production is significant, entailing a strong $\widetilde{m}_1$ dependence for large $(\widetilde{m}_1, M_1)$.

Separating the weak wash-out regime from the strong wash-out regime, we can derive semi-analytical estimates for the two components of the baryon asymmetry valid within the respective regimes. On the one hand, in the weak wash-out regime, the nonthermal production channel is dominant. Assuming that all N^S_1 neutrinos decay instantaneously into radiation

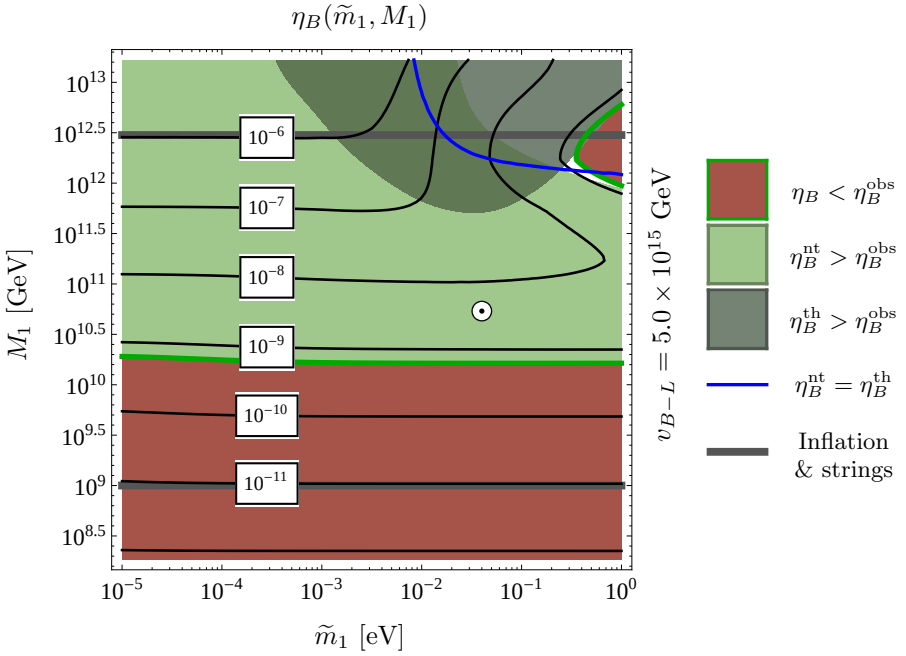

Figure 4.2: Contour plot of the baryon asymmetry η_B as a function of the effective neutrino mass $\widetilde{m}_1$ and the heavy neutrino mass M_1. The baryon asymmetry is calculated according to Eq. (3.61) after solving the Boltzmann equations. In the light green (grey green) region the nonthermal (thermal) asymmetry is consistent with the observed asymmetry. In the red region the total asymmetry falls short of the observational bound. Below (above) the thin blue line the nonthermal (thermal) asymmetry dominates over the thermal (nonthermal) asymmetry. The thick horizontal grey lines represent the lower and the upper bound on M_1, respectively, which arise from requiring consistency with F-term hybrid inflation and the bound on the cosmic string tension, cf. Eq. (3.21). The small white circle marks the position of the parameter point discussed in Sec. 3.5.

we can estimate the total asymmetry in this regime as

$$\eta_B \simeq \eta_B^{\rm nt} \simeq 6.7 \times 10^{-9} \left(\frac{M_1}{10^{11}\,\text{GeV}} \right)^{1.5} . \tag{4.5}$$

On the other hand, in the regime where the total asymmetry is governed by the thermal contribution, i.e. in the region above the blue curve in Fig. 4.2, wash-out is important. In this case, the expectation from standard thermal leptogenesis reproduces our result well and we find for the total asymmetry

$$\eta_B \simeq \eta_B^{\rm th} \simeq 7.0 \times 10^{-10} \left(\frac{0.1\,\text{eV}}{\widetilde{m}_1} \right)^{1.1} \left(\frac{M_1}{10^{12}\,\text{GeV}} \right) . \tag{4.6}$$

In their respective regimes, Eq. (4.5) and Eq. (4.6) reproduce the results obtained by numerically solving the Boltzmann equations up to a factor of two. The intermediate regime interpolates between these two results. The requirement to generate a sufficient amount of baryon asymmetry to explain the value observed today yields a lower bound on M_1, cf.

Fig. 4.2,

$$\eta_B \geq \eta_B^{\text{obs}} \simeq 6.2 \times 10^{-10} \quad \longrightarrow \quad M_1 \gtrsim 1.7 \times 10^{10}\,\text{GeV}\,. \tag{4.7}$$

4.2 Dark matter

Depending on the hierarchy of the superparticle mass spectrum, our model has different viable DM candidates. If the gravitino is the LSP, as is typically the case if supersymmetry breaking is gauge-mediated, the gravitino abundance produced during the reheating process, cf. Sec. 3.5.3, can directly yield today's DM abundance in form of gravitino DM. Alternatively, if a neutralino is the LSP, as occurs in anomaly mediation, we find a WIMP DM scenario. However, it differs from the vanilla WIMP thermal freeze-out scenario due to additional non-thermal neutralino production from gravitino decays. We will discuss both options, gravitino DM in Sec. 4.2.1 and neutralino DM in Sec. 4.2.2. In both cases imposing the constraint of reproducing the correct DM abundance today will yield relations between the neutrino parameters and superparticle masses. This section is based on work partly published in Ref. [16] and Ref. [17], respectively.

4.2.1 Gravitino dark matter

In this section we shall assume that the gravitino is the LSP, and hence we require the gravitino abundance obtained at the end of the reheating process to directly translate to today's DM abundance. The final abundance of gravitinos $\Omega_{\widetilde{G}}h^2$, governed by the Boltzmann equation (3.53), depends on three parameters: the temperature of the thermal bath as well as the two superparticle masses $m_{\widetilde{G}}$ and $m_{\tilde{g}}$. Keeping the gluino mass fixed[1] at 1 TeV and taking into account that the temperature of the thermal bath is controlled by $\widetilde{m}_1$ and M_1, the gravitino abundance becomes a function of $\widetilde{m}_1$, M_1 and $m_{\widetilde{G}}$. Imposing the constraint

$$\Omega_{\widetilde{G}}h^2 = 0.11\,, \tag{4.8}$$

allows us to eliminate one free parameter. The upper panel of Fig. 4.3 shows the value of M_1 in the $(\widetilde{m}_1, m_{\widetilde{G}})$ - plane, obtained after imposing the constraint (4.8). With this, for a given point in the $(\widetilde{m}_1, m_{\widetilde{G}})$ - plane all parameters are fixed and we can calculate the quantities we are interested in, e.g. η_B and the temperature of the thermal bath, by solving the Boltzmann equations for this point in parameter space. This allows us to include the $\eta_B = \eta_B^{\text{obs}}$ contour line in the upper panel of Fig. 4.3, separating the region excluded due to an insufficient production of baryon asymmetry (red) and the viable region (green). Due to

[1] The results presented in the following can easily be generalized to other gluino masses, cf. App. D of Ref. [73]. Varying $m_{\tilde{g}}$ can be compensated by rescaling $m_{\widetilde{G}} \to m'_{\widetilde{G}}(m_{\tilde{g}})$, so that the gravitino abundance remains unchanged.

the procedure described above, the green region now does not only account for a sufficient baryon asymmetry but additionally yields the correct DM abundance.

The lower panel of Fig. 4.3 shows the resulting reheating temperature T_{RH}^{N} after imposing the constraint (4.8). As in the upper panel, the regions excluded due to insufficient baryon asymmetry are marked red. Given the values of M_1 in the upper panel, we find $x \gtrsim \mathcal{O}(1)$ (cf. Eq. (4.3)) in the entire parameter space constrained by Eq. (3.21) and compatible with gravitino dark matter. Moreover, we find $x > 36$ everywhere except for in the very top left corner of the depicted $(\widetilde{m}_1, m_{\widetilde{G}})$ - plane. Thus to very good approximation, the temperature curves depicted in the lower panel of Fig. 4.3 are determined by $T_{\mathrm{RH}}^{N} \simeq T_{\mathrm{RH}}^{N\,(-)}$, cf. Eq. (4.1). Furthermore, transferring the black line marking $\Gamma_{N_1}^{S}/\Gamma_{S}^{0} = 1$ in Fig. 4.1 into the upper panel of Fig. 4.3, we find $\Gamma_{S}^{0} < \Gamma_{N_1}^{S}$ for $\widetilde{m}_1 \gtrsim 10^{-4}$ eV and thus in most of the viable parameter space T_{RH}^{N} corresponds to the plateau temperature, cf. Sec. 3.5.2.

With this, we can parametrize our results in the $(\widetilde{m}_1, m_{\widetilde{G}})$ - plane semi-analytically, cf. Ref. [16] for a more detailed derivation. For the final gravitino abundance $\Omega_{\widetilde{G}}h^2$ we find

$$\Omega_{\widetilde{G}}h^2 = \frac{m_{\widetilde{G}}\,\eta_{\widetilde{G}}\,n_{\gamma}^{0}}{\rho_c/h^2} \simeq 0.26\,\varepsilon\left(\frac{T_{\mathrm{RH}}^{N}}{10^{10}\,\mathrm{GeV}}\right)\left[0.13\left(\frac{m_{\widetilde{G}}}{100\,\mathrm{GeV}}\right) + \left(\frac{100\,\mathrm{GeV}}{m_{\widetilde{G}}}\right)\left(\frac{m_{\tilde{g}}}{1\,\mathrm{TeV}}\right)^2\right]. \quad (4.9)$$

Neglecting the production of entropy and gravitinos after a_{RH}^{N}, $\eta_{\widetilde{G}} \coloneqq n_{\widetilde{G}}^{0}/n_{\gamma}^{0}$ can readily be expressed in terms of $\hat{\Gamma}_{\widetilde{G}}$ and T_{RH}^{N}. The factor ε parametrizes the effect of entropy and gravitino production after a_{RH}^{N}. Solving the Boltzmann equations numerically, we find that it is mainly controlled by $\widetilde{m}_1$,

$$\varepsilon\left(\widetilde{m}_1\right) \simeq 1.2\left(\frac{10^{-3}\,\mathrm{eV}}{\widetilde{m}_1}\right)^{c}, \qquad \text{with} \quad c = \begin{cases} -0.01 & \text{for } \widetilde{m}_1 \lesssim 10^{-3}\ \mathrm{eV} \\ 0.21 & \text{for } \widetilde{m}_1 \gtrsim 10^{-3}\ \mathrm{eV} \end{cases}. \quad (4.10)$$

Inserting $T_{\mathrm{RH}}^{N} \simeq T_{\mathrm{RH}}^{N\,(-)}$, cf. Eq. (4.1) and the discussion above Eq. (4.9), fixing the gluino mass $m_{\tilde{g}} = 1$ TeV and solving for M_1, Eq. (4.9) yields

$$M_1 \simeq 7.2 \times 10^{10}\,\mathrm{GeV}\left(\frac{\widetilde{m}_1}{10^{-3}\,\mathrm{eV}}\right)^{d}\left[0.13\left(\frac{m_{\widetilde{G}}}{100\,\mathrm{GeV}}\right) + \left(\frac{100\,\mathrm{GeV}}{m_{\widetilde{G}}}\right)\right]^{-0.8}, \quad (4.11)$$

with the exponent $d = 0.8\,c - 0.2$. This reproduces the contours in the upper panel of Fig. 4.3 to an accuracy of about 10%. Inserting the lower bound on M_1 from Eq. (4.7), this yields a lower bound on the gravitino mass $m_{\widetilde{G}}$ in terms of the effective light neutrino mass $\widetilde{m}_1$, cf. Fig. 4.3,

$$m_{\widetilde{G}} \geq 16\,\mathrm{GeV}\left(\frac{\widetilde{m}_1}{10^{-3}\,\mathrm{eV}}\right)^{0.25-c}. \quad (4.12)$$

Physically, this bound can be understood as follows. For gravitino masses below $\mathcal{O}\,(10)$ GeV,

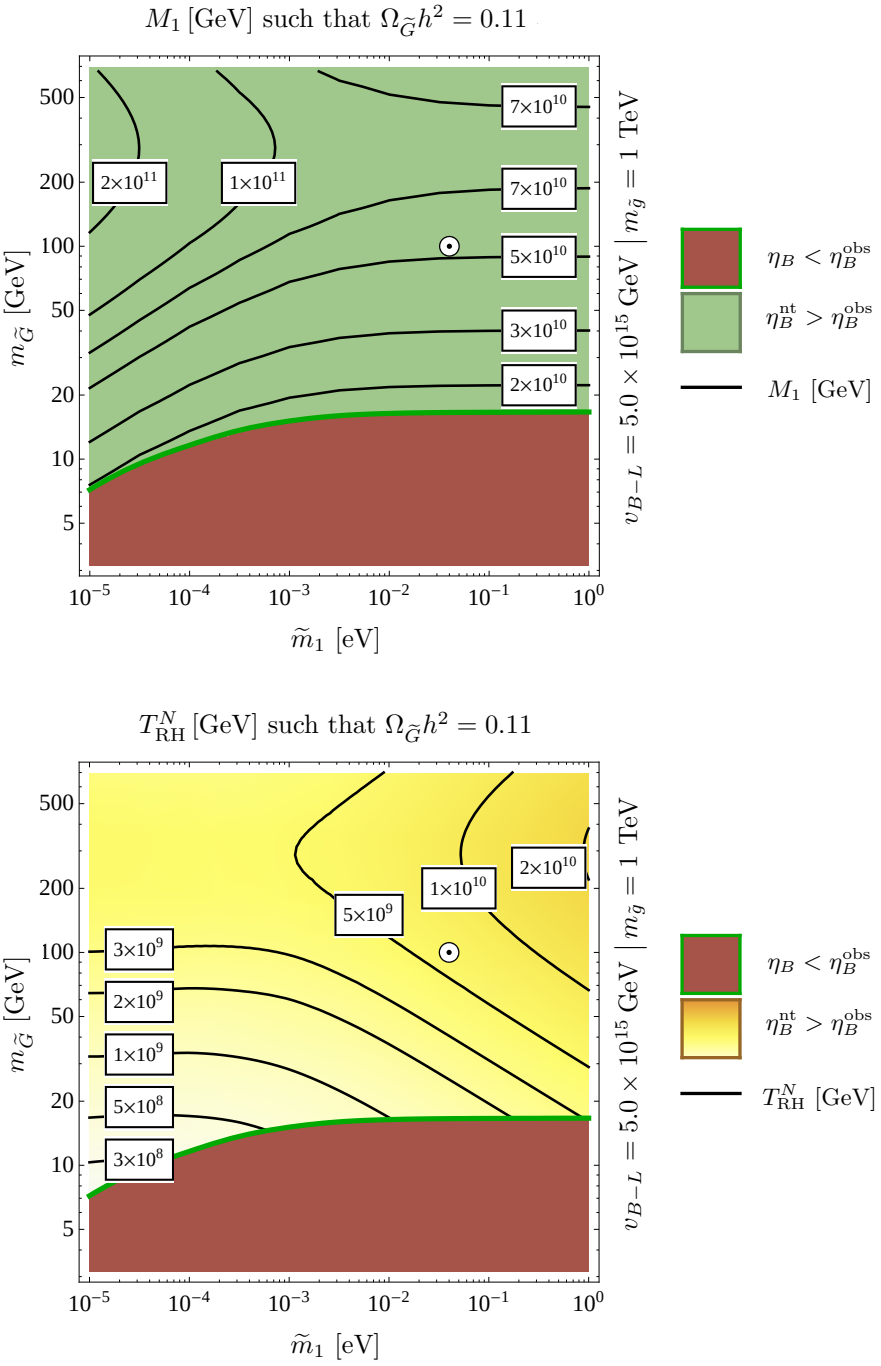

Figure 4.3: Contour plots of the heavy neutrino mass M_1 (upper panel) and the reheating temperature $T^N_{\rm RH}$ (lower panel) as functions of the effective neutrino mass $\widetilde{m}_1$ and the gravitino mass $m_{\widetilde{G}}$ such that the relic density of dark matter is accounted for by gravitinos, cf. Eq. (4.8). In the red region the lepton asymmetry generated by leptogenesis is smaller than the observed one, providing a lower bound on the gravitino mass dependent on $\widetilde{m}_1$. The colour code is the same as in Figs. 4.1 and 4.2, respectively. The small white circle marks the position of the parameter point discussed in Sec. 3.5.

a reheating temperature $T_{\rm RH}^N \lesssim \mathcal{O}\left(10^8 - 10^9\right)$ GeV is required to avoid overproduction of gravitinos. According to our reheating mechanism such low reheating temperatures are associated with relatively small values of the neutrino mass, $M_1 \lesssim \mathcal{O}\left(10^{10}\right)$ GeV. The low temperature and low mass then entail a small abundance of (s)neutrinos at the time the asymmetry is generated and a small CP parameter ϵ_1. Both effects combine and result in an insufficient lepton asymmetry, rendering dark matter made of gravitinos with a mass below $\mathcal{O}\left(10\right)$ GeV inconsistent with leptogenesis.

In conclusion, we find that our scenario of reheating can be easily realized in a large fraction of the parameter space. The two conditions of successful leptogenesis and gravitino dark matter, linked by the reheating temperature, allow us to interconnect parameters of the neutrino and supergravity sector. In particular, we are able to determine the right-handed neutrino mass scale M_1 and the temperature of the thermal bath as functions of the effective light neutrino mass $\widetilde{m}_1$ and the gravitino mass $m_{\widetilde{G}}$. Furthermore, the consistency of inflation, cosmic strings, matter and dark matter generation imposes constraints on the parameter space. In particular, we find M_1 values around 10^{11} GeV and $T_{\rm RH}^N$ values around 3×10^9 GeV, as well as a lower bound on the gravitino mass of roughly 10 GeV.

4.2.2 WIMP dark matter

We now turn to an alternative scenario, in which the LSP is not the gravitino but a neutralino, labelled as χ in this section. This introduces the additional parameter m_χ, the mass of the lightest neutralino. Motivated by the recent discovery of a Higgs-like scalar boson at the LHC with a mass of about 126 GeV [95, 96], we will focus on a hierarchical superparticle mass spectrum,

$$m_\chi \ll m_{\text{squark, slepton}} \ll m_{\widetilde{G}}\,, \tag{4.13}$$

as is found in anomaly mediation [92–94]. Due to this hierarchy the LSP is typically a 'pure' gaugino or higgsino [151]. Generically, the thermal abundance of a bino LSP is too large. We therefore focus on the possibility of a wino or higgsino LSP. Since a pure neutral wino or higgsino is almost mass degenerate with a chargino belonging to the same $SU(2)$ multiplet [151], the current lower bound on chargino masses [8] also applies to the LSP in this case. There are two relevant production channels for the neutralino: thermal production, accompanied by the standard thermal freeze-out mechanism for WIMPs, and nonthermal production, as a decay product of the gravitinos produced during the reheating process.

Thermal and nonthermal production

The thermal abundance of a pure wino ($\widetilde{w}$) or higgsino ($\widetilde{h}$) LSP becomes significant only for masses above 1 TeV where it is well approximated by [152]

$$\Omega_\chi^{\rm th} h^2 = c_\chi \left(\frac{m_\chi}{1\ \text{TeV}}\right)^2\,, \qquad c_{\widetilde{w}} = 0.014\,, \quad c_{\widetilde{h}} = 0.10\,, \tag{4.14}$$

for winos[2] and higgsinos, respectively. The nonthermal abundance is governed by the abundance of gravitinos produced during reheating. The decay of a heavy gravitino produces approximately one LSP. Denoting the 'would-be' gravitino abundance today if the gravitino were stable by $\Omega_{\widetilde{G}}h^2$, the nonthermally produced DM abundance today is given by

$$\Omega_\chi^{\widetilde{G}}h^2 = \left(\frac{m_\chi}{m_{\widetilde{G}}}\right)\Omega_{\widetilde{G}}h^2\,. \tag{4.15}$$

For gravitino masses in the range from 10 TeV to 10^3 TeV as suggested by anomaly mediation, we can neglect the second summand in Eq. (4.9), and thus $\Omega_\chi^{\widetilde{G}}h^2$ is given by

$$\Omega_\chi^{\widetilde{G}}h^2 \simeq 2.7\times10^{-2}\left(\frac{m_\chi}{100\text{ GeV}}\right)\left(\frac{T_{\rm RH}^N(M_1,\widetilde{m}_1)}{10^{10}\text{ GeV}}\right)\,, \tag{4.16}$$

where for simplicity[3], we have averaged over the weak $\widetilde{m}_1$ dependence of ε, cf. Eq. (4.10). As in Sec. 4.2.1, we will impose the condition that the total DM abundance matches the observed abundance today,

$$\Omega_\chi h^2 = \Omega_\chi^{\widetilde{G}}h^2 + \Omega_\chi^{\rm th}h^2 \stackrel{!}{=} 0.11\,. \tag{4.17}$$

Inserting Eqs. (4.14) and (4.16) into Eq. (4.17) we find that for higgsino (wino) LSP masses below 0.6 TeV (1.6 TeV), the total DM abundance is governed by the contribution from gravitino decay.

Gravitino problem and structure formation

The decay of the large abundance of gravitinos produced during reheating into lighter MSSM particles induces an increase of the entropy of the thermal bath and thus a dilution of the baryon asymmetry η_B, cf. Eq. (3.61). If this occurs after primordial nucleosynthesis (BBN), η_B must have been much higher at BBN than now to compensate for this effect. This, however, spoils the very successful predictions of BBN and is referred to as the gravitino problem for unstable gravitinos, see e.g. [155]. The gravitino lifetime is given by

$$\tau_{\widetilde{G}} = \Gamma_{\widetilde{G}}^{-1} = \left(\frac{1}{32\pi}\left(n_v+\frac{n_m}{12}\right)\frac{m_{\widetilde{G}}^3}{M_{\rm P}^2}\right)^{-1} = 24\left(\frac{10\text{ TeV}}{m_{\widetilde{G}}}\right)^3\text{ sec}\,, \tag{4.18}$$

where $n_v = 12$ and $n_m = 49$ are the number of vector and chiral matter multiplets, respectively. Exploiting Eq. (4.4) with $\alpha = 1$ well after the end of reheating, the temperature of

[2] Compared to Ref. [152] we have reduced the abundance by 30% to account for the Sommerfeld enhancement effect [153, 154].

[3] Keeping the $\widetilde{m}_1$ dependence would yield a weak $\widetilde{m}_1$ dependence for the upper bound for $T_{\rm RH}^N$ marked by the dark grey region in Fig. 4.4. However, this bound does not enter into the following discussion, in particular it does not appear in Figs. 4.5 and 4.6. Hence, omitting the $\widetilde{m}_1$ dependence here has no effect on the final results of this section.

the thermal bath when the gravitinos decay is

$$T_{\widetilde{G}} = \left(\frac{90\,\Gamma_{\widetilde{G}}^2 M_{\rm P}^2}{\pi^2\, g_*(T_{\widetilde{G}})}\right)^{1/4} = 0.24\,\left(\frac{10.75}{g_*(T_{\widetilde{G}})}\right)^{1/4}\left(\frac{m_{\widetilde{G}}}{10\ \text{TeV}}\right)^{3/2}\text{MeV}\,. \tag{4.19}$$

For gravitino masses between 10 TeV and 10^3 TeV the decay temperature $T_{\widetilde{G}}$ varies between 0.2 MeV and 200 MeV, i.e. roughly between the temperatures of nucleosynthesis and the QCD phase transition, thus avoiding the gravitino problem. Note that in this temperature range the entropy increase due to gravitino decays and hence the corresponding dilution of the baryon asymmetry are negligible, and the results obtained in Sec. 4.1.2 remain valid.

Another important point to check is the effect of the neutralinos from gravitino decay on structure formation. Since they are produced relativistically, they form warm dark matter which can affect structure formation on small scales. The decisive quantity here is the free-streaming length, which roughly gives the scale below which primordial perturbations are erased,

$$\lambda_{FS} = \int_{\tau_{\widetilde{G}}}^{t_0} dt\,\frac{v_\chi}{a} \simeq \left(\frac{3}{4}\right)^{2/3}\frac{m_{\widetilde{G}}}{2\,m_\chi}\,\left(\tau_{\widetilde{G}}\,t_{\rm eq}\right)^{1/2}\left(\frac{t_0}{t_{\rm eq}}\right)^{2/3}\left(\ln\frac{16\,t_{\rm eq}\,m_\chi^2}{\tau_{\widetilde{G}}\,m_{\widetilde{G}}^2}+4\right)\,, \tag{4.20}$$

where $v_\chi = (p/m_\chi)(a(\tau_{\widetilde{G}})/a(t))$ refers to the velocity of the LSP and $t_{\rm eq}$ and t_0 denote the time of radiation-matter-equality and the age of the universe, respectively. For the gravitino and LSP masses considered in this section, one finds $\lambda_{FS} \lesssim 0.1$ Mpc, which is below the scales relevant for structure formation [156].

Investigating the parameter space

An important factor governing the nonthermal production is the reheating temperature. The allowed temperature range is constrained by three effects, cf. Fig. 4.4. First, taking into account that the neutralino mass is bounded from below by the chargino bound, $m_\chi \geq 94$ GeV, the DM abundance (governed by the nonthermal contribution for small neutralino masses) exceeds the observed value for $T_{\rm RH}^N \gtrsim 4.3\times 10^{10}$ GeV, cf. Eq. (4.16). This is depicted by the dark grey region in Fig. 4.4. Second, the reheating temperature is bounded from below by the lower bound on M_1 from F-term hybrid inflation, cf. Fig. 4.1, with the value of this bound depending on $\widetilde{m}_1$. This excludes the light grey regions in Fig. 4.4. In principle, also the upper bound on M_1 from successful hybrid inflation translates into an upper bound on $T_{\rm RH}^N$. However, the bound arising from the chargino bound is more restrictive. Third, for gravitino masses below 40 TeV BBN provides stringent upper bounds on the reheating temperature [157], marked by the medium grey region in Fig. 4.4.

Fixing the DM abundance to the value observed today yields a one-to-one correspondence between the reheating temperature and the mass of the lightest neutralino m_χ, as can be seen by combining Eqs. (4.14), (4.16) and (4.17). Fig. 4.5 shows the result obtained by translating

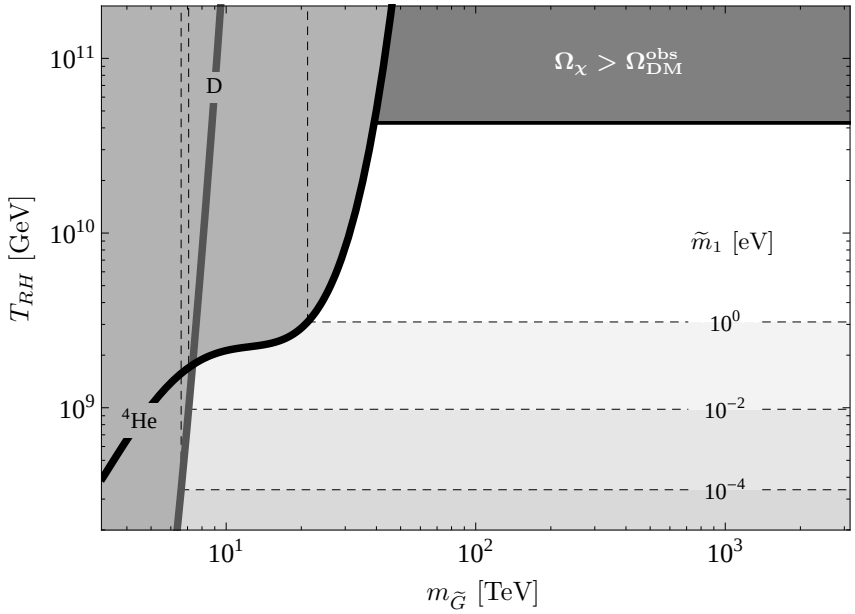

Figure 4.4: Upper and lower bounds on the reheating temperature as functions of the gravitino mass. The horizontal dashed lines denote lower bounds imposed by successful leptogenesis for different values of the effective neutrino mass $\widetilde{m}_1$, cf. Fig. 4.1 after imposing the bound in Eq. (4.7). The curves labelled ^{4}He and D denote upper bounds originating from the primordial helium-4 and deuterium abundances created during BBN, which are taken from [157] (case 2, which gives the most conservative bounds). The vertical dashed lines represent the absolute lower bounds on the gravitino mass for fixed effective neutrino mass $\widetilde{m}_1$ and minimal reheating temperature. The shaded region marked $\Omega_\chi > \Omega_{\rm DM}^{\rm obs}$ is excluded as it corresponds to overproduction of dark matter, taking into account that the neutralino mass is bounded from below, $m_\chi \geq 94$ GeV.

the bounds on the reheating temperature shown in Fig. 4.4 into bounds on the LSP mass for the higgsino (left panel) and the wino (right panel) case. In addition to the upper bounds on the LSP mass imposed by the lower bound on $T_{\rm RH}^N$ (dashed horizontal lines), we also show an absolute, $T_{\rm RH}^N$- and hence $\widetilde{m}_1$-independent, upper bound on the LSP mass which indicates the thermal overproduction of dark matter, $\Omega_\chi^{\rm th} > \Omega_{\rm DM}^{\rm obs}$ (upper dark grey region).

As can be seen from Fig. 4.5, the absolute upper bound on the neutralino LSP mass (for any $m_{\widetilde{G}}$), as well as the absolute lower bound on $m_{\widetilde{G}}$ (for any m_χ) depends on $\widetilde{m}_1$. In Fig. 4.5 this is indicated by the dashed lines denoting the respective bounds for three example values of $\widetilde{m}_1$. In Fig. 4.6 we go beyond this and explicitly depict the $\widetilde{m}_1$ dependence of the absolute upper bound for the higgsino and wino LSP masses (solid curves) as well as the absolute lower bound for the gravitino mass (dashed curve).

Fig. 4.6 conveys two remarkable points. First, we find that also in the case of a neutralino LSP, the spontaneous breaking of $B-L$ in the early universe can successfully generate not only a sufficient baryon asymmetry but also the correct abundance of dark matter, as long as the bounds depicted in Fig. 4.6 are satisfied. Second, in the quest of identifying the viable

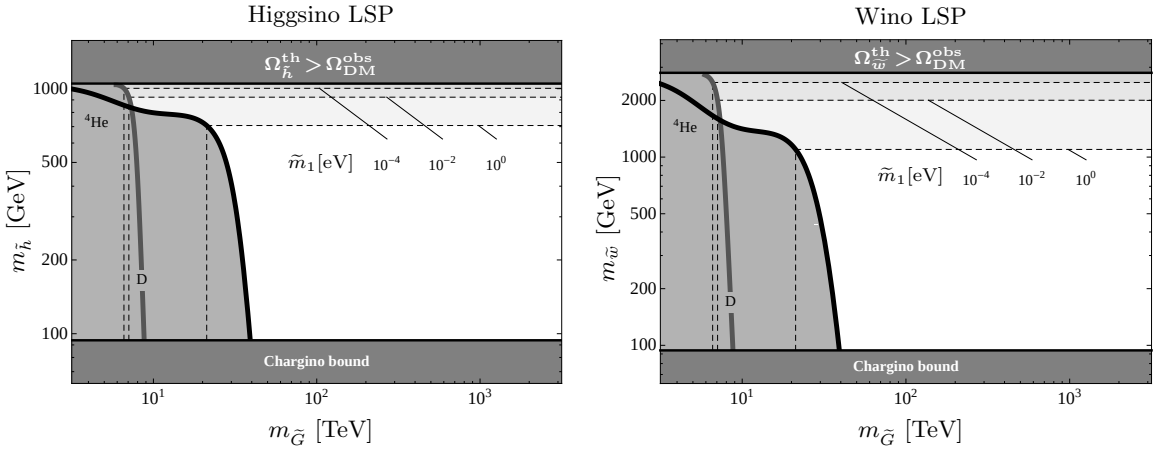

Figure 4.5: Upper and lower bounds on the LSP mass in the higgsino and wino case, respectively, and lower bounds on the gravitino mass. These bounds are in one-to-one correspondence to the bounds on the reheating temperature and the gravitino mass in Fig. 4.4. The horizontal dashed lines denote the upper bounds on the LSP mass imposed by successful leptogenesis for different values of the effective neutrino mass $\widetilde{m}_1$. The curves labelled ^{4}He and D denote lower bounds on the LSP as well as on the gravitino mass originating from the primordial helium-4 and deuterium abundances created during BBN. The vertical dashed lines represent the absolute lower bounds on the gravitino mass for fixed effective neutrino mass $\widetilde{m}_1$ and maximal LSP mass. The dark shaded regions on the upper edge of the plots correspond to thermal overproduction of dark matter and are hence excluded. We do not consider LSP masses below 94 GeV due to the present lower bound on the chargino mass.

parameter space, we find correlations between the neutrino physics parameter $\widetilde{m}_1$ on the one hand and superparticle masses ($m_{\widetilde{G}}$, m_χ) on the other hand. The reason for this is the crucial role the reheating temperature plays in the generation of the DM abundance in the setup presented here, while at the same time, the dynamics of our reheating process ensure that the reheating temperature itself is a function of the neutrino parameters.

Prospects for direct detection and collider experiments

For pure wino and higgsino LSPs, the exchange of the lightest Higgs boson yields for the spin-independent elastic scattering cross section at tree level [158],

$$\sigma^{\widetilde{w}}_{\rm SI} \simeq 2\times 10^{-43}\ {\rm cm}^2 \left(\frac{125\ {\rm GeV}}{m_{h^0}}\right)^4 \left(\frac{100\ {\rm GeV}}{m_{\widetilde{h}}}\right)^2 \left(\sin 2\beta + \frac{m_{\widetilde{w}}}{m_{\widetilde{h}}}\right)^2 , \tag{4.21}$$

$$\sigma^{\widetilde{h}}_{\rm SI} \simeq 7\times 10^{-44}\ {\rm cm}^2 \left(\frac{125\ {\rm GeV}}{m_{h^0}}\right)^4 \left(\frac{100\ {\rm GeV}}{m_{\widetilde{w}}}\right)^2 , \tag{4.22}$$

where m_{h^0} is the mass of the lightest Higgs boson. For the hierarchical mass spectrum of Eq. (4.13) one has $r_{\widetilde{w}} = m_{\widetilde{w}}/m_{\widetilde{h}} \ll 1$ for wino LSP and $r_{\widetilde{h}} = m_{\widetilde{h}}/m_{\widetilde{w}} \ll 1$ for higgsino LSP, respectively [151]. Hence, the spin-independent scattering cross sections in the viable mass range, $m_\chi \sim 100\ {\rm GeV} - \mathcal{O}(1)$ TeV, are significantly below the present experimental sensitivity of currently about $10^{-45} - 10^{-44}$ cm^2, see e.g. [159].

For the considered hierarchy of superparticle masses, gluinos and squarks are heavy.

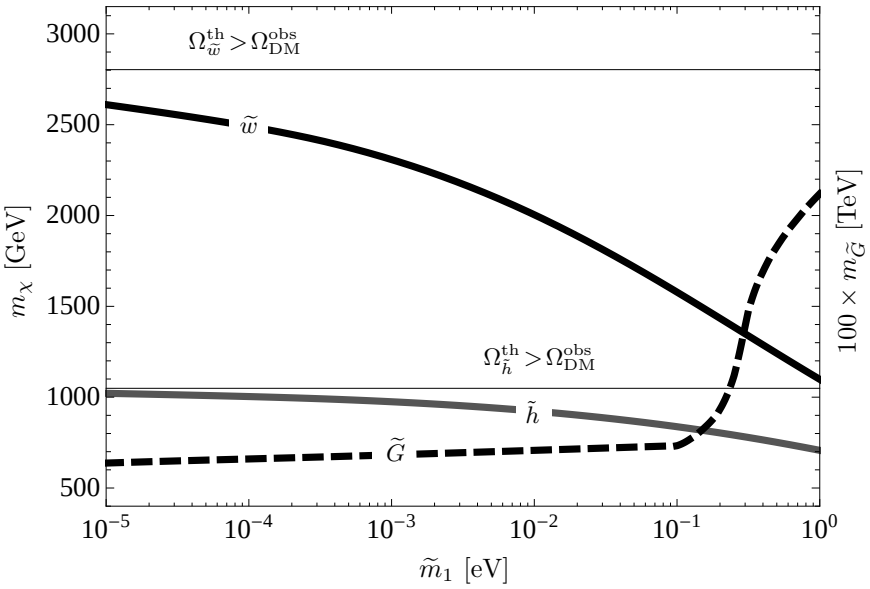

Figure 4.6: Upper bounds on wino ($\widetilde{w}$) and higgsino ($\widetilde{h}$) LSP masses imposed by successful leptogenesis as well as absolute lower bound on the gravitino mass according to BBN as functions of the effective neutrino mass $\widetilde{m}_1$. Note that in Fig. 4.5 these bounds are indicated by horizontal and vertical dashed lines, respectively, for different values of $\widetilde{m}_1$. Wino masses larger than 2.8 TeV and higgsino masses larger than 1.0 TeV result in thermal overproduction of DM.

Hence, the characteristic missing energy signature of events with LSPs in the final state may be absent and the discovery of winos or higgsinos therefore very challenging, for recent discussions see e.g. [160–162]. In both cases the neutral LSP is almost mass degenerate with a chargino, which increases the discovery potential. One may hope for macroscopic charged tracks of the produced charginos. A generic prediction is also the occurrence of monojets caused by the Drell-Yan production of higgsino/wino pairs associated by initial state gluon radiation. In this case, the upper bound on the wino LSP mass implies a lower bound on the respective cross section, cf. [162] for a recent analysis.

4.3 Gravitational wave spectrum

In this section, we turn to a complementary way of probing a $B-L$ phase transition in the early universe: by measuring the gravitational wave (GW) background. GWs are generated whenever strong gravitational fields occur, decouple immediately and to very good approximation propagate freely ever since. Hence, GWs can carry information on the very early universe.

In Chapters 2 and 3, we derived a time-resolved, quantitative description of the symmetry breaking process and the subsequent reheating phase. After introducing some basic notation

and formulas in Sec. 4.3.1, we will in Sec. 4.3.2 quantify the expected GW signal from the different phases of this process, i.e. from inflation, from preheating and from cosmic strings in the scaling regime. As we will show in Sec. 4.3.3, the resulting spectrum indeed has very interesting features which can be probed with future GW detectors. In Sec. 4.3.4 we explain how detecting these features would turn the relations found in Secs. 4.1 and 4.2 into testable predictions. This section is based on work partly published in Ref. [19].

4.3.1 Cosmic gravitational wave background

Gravitational waves are perturbations of the homogeneous background metric. In a flat FRW background, these perturbations can be parametrized as [99]

$$ds^2 = a^2(\tau)\,(\eta_{\mu\nu} + h_{\mu\nu}) dx^\mu dx^\nu\,. \tag{4.23}$$

Here $\eta_{\mu\nu} = \mathrm{diag}(-1,1,1,1)$, a is the scale factor, and x^μ are conformal coordinates with x^i, $i = 1..3$, denoting the comoving spacial coordinates and $\tau = x^0$ the conformal time. These are related to the physical coordinates and the cosmic time as $\boldsymbol{x}_{\rm phys} = a(\tau)\,\boldsymbol{x}$ and $dt = a(\tau)\,d\tau$, respectively[4]. Introducing

$$\bar{h}_{\mu\nu} = h_{\mu\nu} - \frac{1}{2}\,\eta_{\mu\nu}\,h^\rho_\rho\,, \tag{4.24}$$

the linearized Einstein equation describing the generation and propagation of GWs reads

$$\bar{h}''_{\mu\nu}(\boldsymbol{x},\tau) + 2\,\frac{a'}{a}\,\bar{h}'_{\mu\nu}(\boldsymbol{x},\tau) - \nabla^2_{\boldsymbol{x}}\,\bar{h}_{\mu\nu}(\boldsymbol{x},\tau) = 16\pi\,G\,T_{\mu\nu}(\boldsymbol{x},\tau)\,, \tag{4.25}$$

with a prime referring to the derivative with respect to conformal time and $T_{\mu\nu}$ denoting the anisotropic part of the stress energy tensor of the source. The total stress energy tensor is the sum of $T_{\mu\nu}$ and an isotropic part which determines the background metric. Outside the source, we can choose the transverse traceless (TT) gauge for the GW, i.e. $h^{0\mu} = 0$, $h^i_i = 0$, $\partial^j h_{ij} = 0$, which implies $\bar{h}_{\mu\nu} = h_{\mu\nu}$. The mode equation which describes the generation and propagation of these degrees of freedom can be obtained by using an appropriate projection operator [99] on the Fourier transform[5] of Eq. (4.25),

$$\tilde{h}''_{ij}(\boldsymbol{k},\tau) + \left(k^2 - \frac{a''}{a}\right)\tilde{h}_{ij}(\boldsymbol{k},\tau) = 16\pi\,G\,a\,\Pi_{ij}(\boldsymbol{k},\tau)\,, \tag{4.26}$$

where $\tilde{h}_{ij} = a h_{ij}$, Π_{ij} denotes the Fourier transform of the TT part of the anisotropic stress tensor $T_{\mu\nu}$, $k = |\boldsymbol{k}|$, and $\boldsymbol{k}$ is the comoving wavenumber, related to the physical wave number through $\boldsymbol{k}_{\rm phys} = \boldsymbol{k}/a$.

[4] Here, bold letters indicate 3-vectors.

[5] Our convention for the Fourier transformation is $h_{ij}(\boldsymbol{x},\tau) = \int \frac{d^3k}{(2\pi)^3}\; h_{ij}(\boldsymbol{k},\tau)\exp(i\boldsymbol{k}\boldsymbol{x})$.

A useful plane wave expansion of GWs is given by

$$h_{ij}\left(\boldsymbol{x},\tau\right)=\sum_{P=+,\times}\int_{-\infty}^{+\infty}\frac{dk}{2\pi}\int d^2\hat{\boldsymbol{k}}\;h_P\left(\boldsymbol{k}\right)\,T_k(\tau)\;e_{ij}^P\big(\hat{k}\big)\,e^{-ik\left(\tau-\hat{\boldsymbol{k}}\boldsymbol{x}\right)}\,. \tag{4.27}$$

Here, $\hat{\boldsymbol{k}}=\boldsymbol{k}/k$, $P=+,\times$ labels the two possible polarization states of a GW in the TT gauge and $e_{ij}^{+,\times}$ are the two corresponding polarization tensors satisfying the normalization condition $e_{ij}^P e^{ij\,Q}=2\delta^{PQ}$. $h_P(\boldsymbol{k})$ denote the coefficients of the expansion after factorizing out the red-shift due to the expansion of the universe, with the latter captured in the so-called transfer function $T_k(\tau)$.

An analytical expression for T_k can be obtained by studying the homogeneous, i.e. source-free, version of Eq. (4.26). Using the Friedmann equations, we find $a''/a\sim a^2H^2$. The mode equation describes two distinct regimes. On sub-horizon scales, $k\gg aH$, we can neglect the a''/a term. The solution is thus simply $\tilde{h}_{ij}\sim\cos(\omega\tau)$ and hence $h_{ij}\sim\cos(\omega\tau)/a$, i.e. the amplitude decreases as $1/a$ inside the horizon. On the other hand, on super-horizon scales, $k\ll aH$, we can neglect the k^2 term. This yields $2a'h_{ij}'+ah_{ij}''=0$, with the solution

$$h_{ij}(\tau)=A+B\int^{\tau}\frac{d\tau'}{a^2(\tau')}\,, \tag{4.28}$$

with A and B constants of integration. This solution is a constant plus a decaying mode which can be neglected. Hence, on super-horizon scales the amplitude of the mode remains constant, the mode is 'frozen'. Identifying the transfer function T_k capturing the effects due to the expansion of the universe as

$$T_k(\tau_*,\tau)=\frac{h_{ij}^E(\boldsymbol{k},\tau)}{h_{ij}^E(\boldsymbol{k},\tau_*)}\,, \tag{4.29}$$

with $h_{ij}^E(\boldsymbol{k},\tau)$ denoting the envelope of the oscillating function $h_{ij}(\boldsymbol{k},\tau)$, we can employ the approximation[6] (see e.g. [163])

$$T_k(\tau_*,\tau_0)\approx\frac{a(\tau_*)}{a(\tau_0)}\qquad\text{with }\tau_*=\begin{cases}\tau_i\text{ for sub-horizon sources}\\ \tau_k\text{ for super-horizon sources}\end{cases}\,. \tag{4.30}$$

Here, τ_i marks the time when the GW was generated and τ_k denotes the time when a given mode with wavenumber k entered the horizon,

$$k=a(\tau_k)\,H(\tau_k)\,. \tag{4.31}$$

[6] In Chapter 3, we set $a_{\rm PH}=1$. Another convention used frequently is $a_0=1$, with a_0 referring to the value of the scale factor today. In this section, we explicitly keep a_0 without specifying a convention. In the end, the dependence on a_0 must drop out of the observables, which must be independent of the choice of convention.

In Eq. (4.30), we assume for super-horizon sources that the amplitude is constant until $\tau = \tau_k$ and then drops as $1/a$ immediately afterwards. The actual solution to the mode equation yields corrections to both of these assumptions. However, as a numerical check reveals, the effects roughly compensate each other so that Eq. (4.30) reproduces the full result very well. For super-horizon sources we will use the more compact notation $T_k(\tau) = T_k(\tau_k, \tau)$ in the following.

The GW background is a superposition of GWs propagating with all frequencies in all directions. An important observable characterizing the GW background is the ensemble average of the energy density [99], which is expected to be isotropic,

$$\rho_{\mathrm{GW}}(\tau) = \frac{1}{32\pi G}\left\langle \dot{h}_{ij}\left(\boldsymbol{x},\tau\right)\dot{h}^{ij}\left(\boldsymbol{x},\tau\right)\right\rangle = \int_{-\infty}^{\infty} d\ln k\ \frac{\partial\rho_{\mathrm{GW}}(k,\tau)}{\partial\ln k}\ , \tag{4.32}$$

with the angular brackets denoting the ensemble average and the dot referring to the derivative with respect to cosmic time. Alternatively, one uses the ratio of the differential energy density to the critical density,

$$\Omega_{\mathrm{GW}}(k,\tau) = \frac{1}{\rho_c}\frac{\partial\rho_{\mathrm{GW}}(k,\tau)}{\partial\ln k}\ . \tag{4.33}$$

In the model considered in this thesis, the energy density has a part of quantum origin and a part of classical origin,

$$\rho_{\mathrm{GW}}(\tau) = \rho^{\mathrm{qu}}_{\mathrm{GW}}(\tau) + \rho^{\mathrm{cl}}_{\mathrm{GW}}(\tau)\ . \tag{4.34}$$

The former part is due to inflation and is therefore stochastic, whereas the latter part is determined by the contributions to the stress energy tensor from cosmic strings and from tachyonic preheating,

$$\rho^{\mathrm{cl}}_{\mathrm{GW}}(\tau) = \rho^{\mathrm{CS}}_{\mathrm{GW}} + \rho^{\mathrm{TP}}_{\mathrm{GW}}(\tau)\ . \tag{4.35}$$

For a stochastic GW background the Fourier modes $h_A\left(\boldsymbol{k}\right)$ are random variables and their ensemble average is determined by a time-independent spectral density $S_h(k)$ [99],

$$\left\langle h_P\left(\boldsymbol{k}\right)h^*_Q\left(\boldsymbol{k}'\right)\right\rangle = 2\pi\,\delta\left(k-k'\right)\frac{1}{4\pi}\,\delta^{(2)}\big(\hat{\boldsymbol{k}}-\hat{\boldsymbol{k}}'\big)\,\delta_{PQ}\,\frac{1}{2}\,S_h(k)\ . \tag{4.36}$$

This relation reflects the fact that different modes are uncorrelated and that the background is isotropic. On sub-horizon scales, $k \gg aH$, Eqs. (4.27), (4.30) and (4.36) yield

$$\left\langle h_{ij}\left(\boldsymbol{x},\tau\right)h^{ij}\left(\boldsymbol{x},\tau\right)\right\rangle = \frac{1}{\pi}\int_{-\infty}^{\infty} dk\ S_h(k)\,\frac{a^2(\tau_*)}{a^2(\tau)}\ , \tag{4.37}$$

and

$$\left\langle \dot{h}_{ij}\left(\boldsymbol{x},\tau\right)\dot{h}^{ij}\left(\boldsymbol{x},\tau\right)\right\rangle = \frac{1}{\pi a^2(\tau)}\int_{-\infty}^{\infty} dk\ k^2\ S_h(k)\,\frac{a^2(\tau_*)}{a^2(\tau)}\ . \tag{4.38}$$

Comparing this with Eq. (4.32) yields an expression for the differential energy density in

terms of the spectral density,

$$\frac{\partial \rho_{\rm GW}\,(k,\tau)}{\partial \ln k} = \frac{a^2(\tau_*)}{16\pi^2\, G\, a^4(\tau)}\, k^3\, S_h(k)\,. \tag{4.39}$$

The classical contribution to the GW energy density is obtained by integrating Eq. (4.26) from the initial time τ_i of GW production until today,

$$h_{ij}(\boldsymbol{k},\tau) = 16\pi G\, \frac{1}{a(\tau)} \int_{\tau_i}^{\tau} d\tau'\; a(\tau')\, \mathcal{G}(k,\tau,\tau')\, \Pi_{ij}(\boldsymbol{k},\tau')\,, \tag{4.40}$$

where $\mathcal{G}(k,\tau,\tau')$ is the retarded Green's function of the differential operator on the left-hand side of Eq. (4.26). For sub-horizon modes, i.e. $k\tau \gg 1$, one has $\mathcal{G}(k,\tau,\tau') = \sin(k(\tau-\tau'))/k$. With this, one can evaluate the ensemble average $\langle \dot{h}^2 \rangle$ in terms of $\langle \Pi^2 \rangle$ by calculating the derivative of Eq. (4.40) on sub-horizon scales. Assuming translation invariance and isotropy of the source,

$$\left\langle \Pi_{ij}(\boldsymbol{k},\tau) \Pi^{ij}(\boldsymbol{k}',\tau') \right\rangle = (2\pi)^3\, \Pi^2(k,\tau,\tau')\, \delta(\boldsymbol{k}+\boldsymbol{k}')\,, \tag{4.41}$$

the resulting differential energy density simplifies to

$$\frac{\partial \rho_{\rm GW}\,(k,\tau)}{\partial \ln k} = \frac{2G}{\pi}\, \frac{k^3}{a^4(\tau)} \int_{\tau_i}^{\tau} d\tau_1 \int_{\tau_i}^{\tau} d\tau_2\; a(\tau_1)\, a(\tau_2)\, \cos(k(\tau_1-\tau_2))\, \Pi^2(k,\tau_1,\tau_2)\,, \tag{4.42}$$

Here, in order to perform the ensemble average, we have also averaged the integrand over a period $\Delta\tau = 2\pi/k$, assuming ergodicity.

4.3.2 Gravitational waves from a $B-L$ phase transition

The cosmological setup discussed in Chapter 3 contains several sources for gravitational waves. In this section, we will in turn discuss the resulting GW background from inflation, from tachyonic preheating and from cosmic strings in the scaling regime. An overview of the resulting contributions is shown in Fig. 4.7. In the analysis of this section we will employ the temperature $\hat{T}^{\sigma}_{\rm RH}$ defined as the temperature at the time when half of the energy of the $B-L$ Higgs bosons has been shifted to relativistic degrees of freedom (relativistic neutrinos and/or MSSM degrees of freedom),

$$\rho_{\rm tot}(\hat{a}^{\sigma}_{\rm RH}) = 2\rho_S(\hat{a}^{\sigma}_{\rm RH}) = 2\left[\rho_r(\hat{a}^{\sigma}_{\rm RH}) + \rho_N(\hat{a}^{\sigma}_{\rm RH}) + \rho_{\tilde{N}}(\hat{a}^{\sigma}_{\rm RH})\right], \qquad \hat{T}^{\sigma}_{\rm RH} = T(\hat{a}^{\sigma}_{\rm RH})\,. \tag{4.43}$$

This temperature is naturally closely related to the Higgs decay temperature $T^{\sigma}_{\rm RH}$, which marks the point in time when the Higgs boson abundance has decrease to a fraction $1/e$ of its original abundance. Here $a^{\sigma}_{\rm RH}$, marking the time-scale over which the Higgs abundance is significantly reduced, is characteristic for describing the Higgs boson decay in the context of the time-resolved picture of the reheating process developed in Sec. 3.5. The quantity $\hat{a}^{\sigma}_{\rm RH}$ is

slightly better adapted to answer the question which we will be interested in here, namely of whether non-relativistic or relativistic particles are dominant, i.e. make up more than 50% of the energy budget of the universe. This determines the evolution of the scale factor and hence, cf. Eq. (4.30), the transfer function. Performing an analysis analogous to the one described in Sec. 4.1.1, but for $\hat{T}^{\sigma}_{\mathrm{RH}}$ instead of T^{σ}_{RH}, we find that as expected, T^{σ}_{RH} and $\hat{T}^{\sigma}_{\mathrm{RH}}$ are very similar, exhibiting the same parameter dependencies with $\hat{T}^{\sigma}_{\mathrm{RH}} \simeq 0.86\, T^{\sigma}_{\mathrm{RH}}$ ($\hat{T}^{\sigma}_{\mathrm{RH}} \simeq 0.97\, T^{\sigma}_{\mathrm{RH}}$) well inside the the '-' ('+') regime of Eq. (4.2):

$$\hat{T}^{\sigma}_{\mathrm{RH}} \simeq \begin{cases} \hat{T}^{\sigma\,(-)}_{\mathrm{RH}} = 4.8 \times 10^{9}\ \mathrm{GeV} \left(\dfrac{M_1}{10^{11}\ \mathrm{GeV}}\right)^{1.5} & \text{for } x \gtrsim 170 \\ \hat{T}^{\sigma\,(+)}_{\mathrm{RH}} = 3.0 \times 10^{9}\ \mathrm{GeV} \left(\dfrac{M_1}{10^{11}\ \mathrm{GeV}}\right)^{1.3} \left(\dfrac{\widetilde{m}_1}{10^{-4}\ \mathrm{eV}}\right)^{0.2} & \text{for } x \lesssim 170 \end{cases} . \tag{4.44}$$

In the remainder of this chapter we will thus work with the quantity $\hat{T}^{\sigma}_{\mathrm{RH}}$, denoting it as $T_{\mathrm{RH}} \coloneqq \hat{T}^{\sigma}_{\mathrm{RH}}$ and all letters with the index 'RH' will refer to this quantity. Of course, using instead T^{σ}_{RH} would lead to the same final results, only the auxiliary quantities used to describe the effects which quantify the discrepancies between the analytical approximations and the full solution of the Boltzmann equations would have slightly different numerical values.

One goal of this section will be to pinpoint which model parameters are related to which features in the GW spectrum, and might therefore be probed by a measurement of the GW background. We will therefore in the remainder of this section keep both the neutrino and $B-L$ Higgs boson masses, M_1 and m_S, as independent parameters and will not employ the relation $M_1 = \eta^2\, m_S$, cf. Sec. 2.5, unless stated explicitly otherwise.

Gravitational waves from inflation

During inflation quantum fluctuations of the metric are stretched to ever larger physical scales so that they eventually cross the Hubble horizon. Outside the horizon, the amplitudes of these metric perturbations remain preserved and they only begin to evolve again once they re-enter the Hubble horizon after the end of inflation. Inflation hence gives rise to a stochastic background of gravitational waves with a spectrum which is directly related to the properties of the primordial quantum metric fluctuations, and which is characterized by the spectral density $S_h(k)$. Expanding the tensor perturbations h_{ij} into Fourier modes yields

$$h_{ij}\left(\boldsymbol{x}, \tau\right) = \sum_{P=+,\times} \int \frac{d^3k}{\left(2\pi\right)^3}\ \varphi^{P}_{k}(\tau)\ e^{P}_{ij}\ e^{i\boldsymbol{k}\boldsymbol{x}} . \tag{4.45}$$

For each wavenumber k we thus have two modes φ^{+}_{k} and $\varphi^{\times}_{k}$. After rescaling these fields in order to render them canonically normalized, the two-point function for the modes which have not yet re-entered the horizon is given by the usual expression for free scalar fields in an

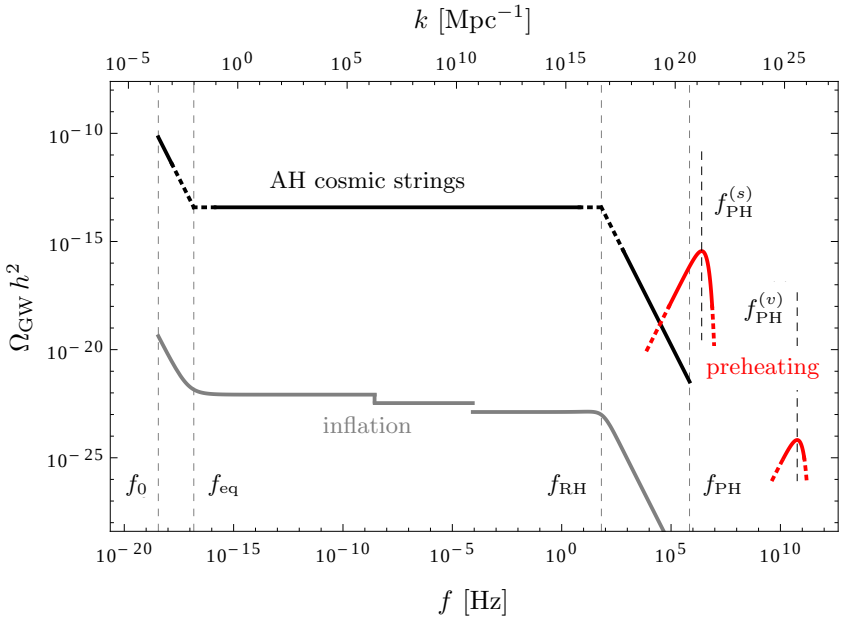

Figure 4.7: Predicted GW spectrum due to inflation (grey), preheating (red) and AH cosmic strings (black) for $M_1 = 5.4 \times 10^{10}$ GeV, $v_{B-L} = 5 \times 10^{15}$ GeV and $m_S = 3 \times 10^{13}$ GeV, as in Eq. (3.56). f_0, $f_{\rm eq}$, $f_{\rm RH}$ and $f_{\rm PH}$ denote the frequencies associated with a horizon sized wave today, at matter-radiation equality, at reheating and at preheating, respectively. $f_{\rm PH}^{(s)}$ and $f_{\rm PH}^{(v)}$ denote the positions of the peaks in the GW spectrum associated with the scalar and the vector boson present at preheating. The dashed segments indicate the uncertainties due to the breakdown of the analytical approximations. The GW spectrum from inflation is based on an analytical calculation, cf. Eq. (4.66), augmented by a numerical determination of the auxiliary transfer functions (4.69) and and (4.70); the 'steps' in the plateau are determined by the change in the degrees of freedom at the QCD scale and at a supersymmetry scale of 1 TeV. The GW spectrum from preheating is given by Eqs. (4.81) and (4.82), with $c_{\rm PH} = 0.05$. The GW spectrum from AH cosmic strings is determined by Eqs. (4.88) and (4.89), with $F^r = F^r_{\rm FHU}$.

inflationary background [164],

$$\phi_k^P(\tau) = \frac{M_P}{\sqrt{2}\,(2\pi)^{3/2}}\,\varphi_k^P(\tau)\,, \quad \left\langle \phi_k^P(\tau)\,\phi_{k'}^Q(\tau)\right\rangle = \frac{H_{\rm inf}^2}{2k^3}\,\delta^{PQ}\,\delta^{(3)}\left(\boldsymbol{k}+\boldsymbol{k}'\right)\,, \quad k \ll aH\,, \tag{4.46}$$

with $H_{\rm inf}$ denoting the value of the Hubble parameter during inflation. The evolution of the modes ϕ_k^P after the end of inflation is accounted for by the transfer function T_k (cf. Eq. (4.29)). This enables us to write down an expression for the two-point function valid for all k,

$$\left\langle \phi_k^P(\tau)\,\phi_{k'}^Q(\tau)\right\rangle = \frac{H_{\rm inf}^2}{2k^3}\,T_k^2(\tau)\,\delta^{PQ}\,\delta^{(3)}\left(\boldsymbol{k}+\boldsymbol{k}'\right)\,. \tag{4.47}$$

The correlation function of the tensor perturbations h_{ij} is correspondingly given by

$$\left\langle h_{ij}\left(\boldsymbol{x},\tau\right)\,h^{ij}\left(\boldsymbol{x},\tau\right)\right\rangle = \int_{-\infty}^{+\infty} dk\,\frac{H_{\rm inf}^2}{\pi^2 k M_P^2}\,T_k^2(\tau) = \frac{1}{\pi}\int_{-\infty}^{+\infty} dk\,S_h(k)\,T_k^2(\tau)\,, \tag{4.48}$$

from which we can read off the spectral density S_h, cf. Eq. (4.37),

$$S_h(k) = \frac{H_{\rm inf}^2}{\pi k M_P^2}\,. \tag{4.49}$$

With Eqs. Eq. (4.33) and (4.39), we hence obtain for today's spectrum of GWs from inflation

$$\Omega_{\rm GW}(k,\tau) = \frac{k^3}{6a_0^2H_0^2}\,\frac{H_{\rm inf}^2}{\pi^2 k M_P^2}\,T_k^2(\tau) = \frac{A_t}{12}\,\frac{k^2}{a_0^2H_0^2}\,T_k^2(\tau)\,, \tag{4.50}$$

where we have introduced the amplitude A_t of the tensor perturbations due to inflation, cf. Eq. (3.9).

It is instructive to compute the transfer function T_k and thus the amplitude $\Omega_{\rm GW}$ of the GW spectrum analytically for the three relevant intervals of k values,

$$k \;\in\; [k_0, k_{\rm eq}),\;\; [k_{\rm eq}, k_{\rm RH}),\;\; [k_{\rm RH}, k_{\rm PH})\,, \qquad\qquad k_n = a_n H(a_n)\,, \tag{4.51}$$

where the subscript $n = 0, {\rm eq}, {\rm RH}, {\rm PH}$ labels the boundaries of the three eras between preheating and today.[7] $k_{\rm eq}$ and $k_{\rm RH}$ stand for the wavenumbers of the modes that re-enter the Hubble horizon at the time of radiation-matter equality at a redshift of roughly 3300 and close to the end of reheating, when half of the non-relativistic $B-L$ Higgs bosons and its superpartners have decayed, respectively. $k_{\rm PH}$ is the wavenumber of the mode that has just grown to the size of the Hubble horizon by the end of inflation and which begins to move inside the horizon once the expansion of the universe becomes matter-dominated in the course of preheating. Metric fluctuations with $k > k_{\rm PH}$ are never stretched to horizon-size scales and thus always remain at the quantum level.

$k_{\rm eq}, k_{\rm RH}$ and $k_{\rm PH}$: As a preparation for our computation of T_k, let us now determine $k_{\rm eq}$, $k_{\rm RH}$ and $k_{\rm PH}$. After the end of reheating the reheating process, the comoving entropy density of radiation is conserved, $a^3 s = $ const., so that the Friedmann equation takes the following form,

$$H(a(\tau)) = H_0\left[\Omega_\Lambda + \Omega_m\left(\frac{a_0}{a(\tau)}\right)^3 + \frac{g_*(\tau)}{g_*^0}\left(\frac{g_{*,s}^0}{g_{*,s}(\tau)}\right)^{4/3}\Omega_r\left(\frac{a_0}{a(\tau)}\right)^4\right]^{1/2}\,. \tag{4.52}$$

Here, Ω_Λ, Ω_m and Ω_r denote the ratios of the vacuum, matter and radiation energy densities to the critical energy density today, respectively. The boundary wavenumber $k_{\rm eq}$ can now be

[7] As a consequence of the late-time acceleration of the universe, perturbation modes only re-enter the Hubble horizon until $a_{k_{\rm min}} \simeq (\Omega_m/(2\Omega_\Lambda))^{1/3}\,a_0$. At later times, the physical wavelengths of the modes grow faster than the Hubble horizon, similarly as during inflation, so that they cross outside the Hubble horizon again. The smallest wavenumber that ever crosses inside the Hubble horizon after inflation consequently corresponds to $k_{\rm min} \simeq (3/2)^{1/2}\,(2\Omega_\Lambda)^{1/6}\,(\Omega_m)^{1/3} k_0 \simeq 0.86\,k_0$. By comparison, the mode with wavenumber k_0 re-enters the Hubble horizon slightly earlier at $a \simeq \Omega_m a_0$.

calculated by means of Eqs. (4.52) and (4.31). Taking into account the dominant contributions at $a_{\rm eq}$, i.e. the second and third term in Eq. (4.52), yields

$$k_{\rm eq} = \left(\frac{g_{*,s}^{\rm eq}}{g_{*,s}^{0}}\right)^{2/3} \left(\frac{2g_{*}^{0}}{g_{*}^{\rm eq}}\right)^{1/2} \frac{\Omega_m}{{\Omega_r}^{1/2}}\, k_0 = 7.33 \times 10^{-2}\, a_0\, \Omega_m h^2\ {\rm Mpc}^{-1}\,, \tag{4.53}$$

with $g_{*,s}^{\rm eq} = g_{*,s}^{0}$ as introduced below Eq. (3.61) and g_* referring to the effective number of degrees of freedom in the radiation energy density. In particular, $g_*^{\rm RH} = g_{*,s}^{\rm RH}$, $g_*^{\rm eq} = 3.36$ and the present value of g_* is sensitive to the mass spectrum of the light SM neutrinos. If all neutrinos are non-relativistic at present, we have $g_*^0 = 2$. However, if the lightest neutrino has not yet turned non-relativistic, g_*^0 is slightly larger, $g_*^0 = 2.45$. Note that the numerical value of $k_{\rm eq}$ is, however, not affected by this subtlety as it only depends on the ratio Ω_r/g_*^0, which is directly obtained from the actually measured quantity T_γ^0, the temperature of the CMB photons today:

$$\frac{\Omega_r h^2/g_*^0}{1.237 \times 10^{-5}} = \left(\frac{T_\gamma^0}{2.725\ {\rm K}}\right)^4 . \tag{4.54}$$

Compared to $k_{\rm eq}$, the computation of $k_{\rm RH}$ is complicated by two effects. First, at $T_{\rm RH}$, the energy density of the non-relativistic $B-L$ Higgs bosons and its superpartners at $a = a_{\rm RH}$ is balanced by MSSM radiation and the heavy, relativistic but nonthermal (s)neutrinos together, see Eq. (4.43). We shall quantify the contribution of the thermal bath to the total energy density at $a = a_{\rm RH}$ by the factor $\alpha_{\rm RH} = \rho_{\rm tot}\left(a_{\rm RH}\right)/\rho_r\left(a_{\rm RH}\right) \geq 2$. Second, the comoving radiation entropy density $a^3 s$ is only conserved once all non-relativistic particles and heavy (s)neutrinos have decayed, i.e. only for sufficiently late times after $a = a_{\rm RH}$. In order to quantify the amount of entropy production after $a = a_{\rm RH}$, we introduce the dilution factor

$$\Delta = \frac{\left(a^3 s\right)_{a \gg a_{\rm RH}}}{\left(a^3 s\right)_{a = a_{\rm RH}}} \geq 1\,. \tag{4.55}$$

Based on Δ, we may also define two further useful quantities: the would-be reheating temperature $\tilde{T}_{\rm RH}$ and the would-be radiation energy density at reheating $\tilde{\rho}_r^{\rm RH}$,

$$\tilde{T}_{\rm RH} = \Delta^{1/3}\, T_{\rm RH}\,, \qquad \tilde{\rho}_r^{\rm RH} = \Delta^{4/3}\, \rho_r\left(a_{\rm RH}\right)\,, \tag{4.56}$$

which represent the temperature and the energy density the thermal bath would have had at $a = a_{\rm RH}$ if, extrapolating back in time from the present epoch, no entropy production took place as long as $a > a_{\rm RH}$. Both $\alpha_{\rm RH}$ and Δ need to be determined by solving the Boltzmann equations introduced in Sec. 3.4.2 and depend on the parameters of our model, cf. Appendix B. For now, we simply state that, taking both effects quantified by the two factors

$\alpha_{\rm RH}$ and Δ into account, one finds the following expression for $k_{\rm RH}$,

$$k_{\rm RH} = \left(\frac{\alpha_{\rm RH}}{2}\right)^{1/2} \Delta^{-1/3} \left(\frac{g^0_{*,s}}{g^{\rm RH}_{*,s}}\right)^{1/3} \left(\frac{2\, g^{\rm RH}_*}{g^0_*}\right)^{1/2} {\Omega_r}^{1/2}\, \frac{T_{\rm RH}}{T^0_\gamma}\, k_0\,. \tag{4.57}$$

The above relations imply

$$\frac{\alpha_{\rm RH}}{2} = R\,\Delta^{4/3}\,, \qquad \text{with } R = \frac{\rho_S\,(a_{\rm RH})}{\tilde\rho^{\rm RH}_r}\,. \tag{4.58}$$

The ratio R can be shown to take a constant value across the entire parameter space, $R \simeq 0.41$, cf. Appendix B. Physically, $1/R$ corresponds to the increase of $(a/a_{\rm PH})^4(\rho_r + \rho_N + \rho_{\tilde N})$ after $a = a_{\rm RH}$ due to the decay of the remaining $B{-}L$ Higgs bosons. Because R is a constant, it is possible to rewrite Eq. (4.57) in terms of the would-be reheating temperature $\tilde T_{\rm RH}$ or, equivalently, in terms of the effective temperature $T_* = R^{1/2}\,\tilde T_{\rm RH} \simeq 0.64\,\tilde T_{\rm RH}$,

$$\begin{aligned} k_{\rm RH} &= R^{1/2} \left(\frac{g^0_{*,s}}{g^{\rm RH}_{*,s}}\right)^{1/3} \left(\frac{2g^{\rm RH}_*}{g^0_*}\right)^{1/2} {\Omega_r}^{1/2}\, \frac{\tilde T_{\rm RH}}{T^0_\gamma}\, k_0 \\ &= \left(\frac{g^0_{*,s}}{g^{\rm RH}_{*,s}}\right)^{1/3} \left(\frac{2g^{\rm RH}_*}{g^0_*}\right)^{1/2} {\Omega_r}^{1/2}\, \frac{T_*}{T^0_\gamma}\, k_0 = 2.75\times 10^{14}\, a_0\,{\rm Mpc}^{-1} \left(\frac{T_*}{10^7\,{\rm GeV}}\right). \end{aligned} \tag{4.59}$$

Here, T_* is defined such that it appears in our final expression for $k_{\rm RH}$ in exactly the same way as the actual reheating temperature $T_{\rm RH}$ would appear in $k_{\rm RH}$ if one were to perform a more naive calculation, neglecting the two correction factors $\alpha_{\rm RH}$ and Δ. Put differently, if one tried to deduce the reheating temperature from a measurement of $k_{\rm RH}$ making use of the standard formula for $k_{\rm RH}$, i.e. Eq. (4.57) with $\alpha_{\rm RH} = 2$ and $\Delta = 1$, the temperature one obtain would be the effective temperature T_*. As we will see shortly, the GW spectrum exhibits a kink just at $k = k_{\rm RH}$. This is why we shall refer to T_* as the 'effective kink temperature'. Finally, we emphasize that the distinction between $T_{\rm RH}$ and T_* is crucial since the reheating temperature $T_{\rm RH}$ turns is sensitive to the properties of the Higgs sector as well as of the neutrino sector, cf. Eq. (4.44), while the effective kink temperature T_* is solely determined by the $B{-}L$ Higgs decay rate Γ^0_S and the vacuum energy during inflation ρ_0, cf. Appendix B.

Next, we turn to $k_{\rm PH}$. The total energy density at the end of preheating is approximately given by $\rho_0 = \lambda v^4_{B-L}/4$, implying

$$\begin{aligned} \frac{k_{\rm PH}}{k_{\rm RH}} &= C_{\rm RH} \left(\frac{\rho_0}{\rho^{\rm RH}_{\rm tot}}\right)^{1/6} = \frac{C_{\rm RH}}{\alpha^{1/6}_{\rm RH}} \left(\frac{30\lambda}{4\pi^2 g^{\rm RH}_*}\right)^{1/6} \left(\frac{v_{B-L}}{T_{\rm RH}}\right)^{2/3} \\ &= \frac{C_{\rm RH}}{R^{1/6}} \left(\frac{15\lambda}{4\pi^2 g^{\rm RH}_*}\right)^{1/6} \left(\frac{v_{B-L}}{\tilde T_{\rm RH}}\right)^{2/3} = C_{\rm RH} R^{1/6} \left(\frac{15\lambda}{4\pi^2 g^{\rm RH}_*}\right)^{1/6} \left(\frac{v_{B-L}}{T_*}\right)^{2/3}. \end{aligned} \tag{4.60}$$

Here, we have introduced $C_{\rm RH} = \left(a_{\rm PH} H_{\rm PH}^{2/3}\right) / \left(a_{\rm RH} H_{\rm RH}^{2/3}\right)$ in order to account for the complicated evolution of the Hubble parameter during reheating. Making the simplifying assumption that the universe is strictly matter-dominated throughout the entire reheating process, one has $C_{\rm RH} = 1$. Hence, the actual value of $C_{\rm RH}$ ought to be larger than 1. In fact, as demonstrated in Appendix B, $C_{\rm RH}$ takes a constant value in the entire parameter space, $C_{\rm RH} \simeq 1.13$. All of the four wavenumbers k_0, $k_{\rm eq}$, $k_{\rm RH}$ and $k_{\rm PH}$ can be translated into frequencies $f = k/\left(2\pi a_0\right)$ at which GW experiments could observe the corresponding modes,

$$f_0 = 3.58 \times 10^{-19}\,{\rm Hz} \left(\frac{h}{0.70}\right) , \tag{4.61}$$

$$f_{\rm eq} = 1.57 \times 10^{-17}\,{\rm Hz} \left(\frac{\Omega_m h^2}{0.14}\right) , \tag{4.62}$$

$$f_{\rm RH} = 4.25 \times 10^{-1}\,{\rm Hz} \left(\frac{T_*}{10^7\,{\rm GeV}}\right) , \tag{4.63}$$

$$f_{\rm PH} = 1.93 \times 10^{4}\,{\rm Hz} \left(\frac{\lambda}{10^{-4}}\right)^{1/6} \left(\frac{10^{-15}\, v_{B-L}}{5\,{\rm GeV}}\right)^{2/3} \left(\frac{T_*}{10^7\,{\rm GeV}}\right)^{1/3} , \tag{4.64}$$

where in Eq. (4.64), we have set $C_{\rm RH} = 1.13$ and $R = 0.41$.

Transfer function: For modes with wavenumbers well inside one of the three intervals in Eq. (4.51), the transfer function T_k can be computed analytically.

$$T_k \simeq {\Omega_r}^{1/2} \left(\frac{g_*^k}{g_*^0}\right)^{1/2} \left(\frac{g_{*,s}^0}{g_{*,s}^k}\right)^{2/3} \frac{k_0}{k} \times \begin{cases} \frac{1}{\sqrt{2}}\, k_{\rm eq}/k\,, & k_0 \ll k \ll k_{\rm eq} \\ 1\,, & k_{\rm eq} \ll k \ll k_{\rm RH} \\ \sqrt{2}\, R^{1/2}\, C_{\rm RH}^3\, k_{\rm RH}/k\,, & k_{\rm RH} \ll k \ll k_{\rm PH} \end{cases} . \tag{4.65}$$

To obtain this result, we have approximated T_k by the ratio $a\left(\tau_k\right)/a_0$, cf. Eq. (4.30), and have made use of the Friedmann equation as well as the conservation of the comoving entropy density for $a \gg a_{\rm RH}$. As long as a mode with wavenumber k re-enters the Hubble horizon during radiation domination, g_*^k and $g_{*,s}^k$ denote the usual values of $g_*(\tau)$ and $g_{*,s}(\tau)$ at time τ_k. On the other hand, during reheating and matter domination g_*^k and $g_{*,s}^k$ correspond to $g_*^{\rm RH}$ and $g_{*,s}^{\rm RH}$ as well as to $g_*^{\rm eq}$ and $g_{*,s}^{\rm eq}$, respectively. Inserting our result for T_k in Eq. (4.65) into Eq. (4.50), we arrive at the following expression for the energy spectrum of the GWs from inflation,

$$\Omega_{\rm GW}(k) = \frac{A_t^2}{12}\, \Omega_r\, \frac{g_*^k}{g_*^0} \left(\frac{g_{*,s}^0}{g_{*,s}^k}\right)^{4/3} \times \begin{cases} \frac{1}{2}\, \left(k_{\rm eq}/k\right)^2\,, & k_0 \ll k \ll k_{\rm eq} \\ 1\,, & k_{\rm eq} \ll k \ll k_{\rm RH} \\ 2\, R\, C_{\rm RH}^6\, \left(k_{\rm RH}/k\right)^2\,, & k_{\rm RH} \ll k \ll k_{\rm PH} \end{cases} . \tag{4.66}$$

Evidently, the energy spectrum $\Omega_{\rm GW}$ decreases like k^{-2} at its edges and features a plateau in

its centre. In the context of cosmological $B-L$ breaking, the height of the plateau is controlled by the coupling λ, which determines the self-interaction of the $B-L$ breaking Higgs field, as well as by the $B-L$ breaking scale, cf. Eq. (3.9),

$$\begin{aligned}\Omega_{\rm GW}^{\rm pl}h^2 &= \frac{\lambda}{72\pi^2}\left(\frac{v_{B-L}}{M_P}\right)^4 \Omega_r h^2 \left(\frac{g_*^k}{g_*^0}\right)\left(\frac{g_{*,s}^0}{g_{*,s}^k}\right)^{4/3} \\ &= 3.28\times 10^{-22}\left(\frac{\lambda}{10^{-4}}\right)\left(\frac{v_{B-L}}{5\times 10^{15}\ \text{GeV}}\right)^4\left(\frac{\Omega_r}{8.5\times 10^{-5}}\right)\bar{g}^k\ , \end{aligned} \tag{4.67}$$

where $\bar{g}^k = (4g_*^k/427)(427/(4g_{*,s}^k))^{4/3}$ is a ratio of energy and entropy degrees of freedom. Note that a further effect modifying the GW spectrum to a similar extent as the change of the degrees of freedom during radiation domination is a contribution to the stress energy tensor due to freely streaming neutrinos, cf. Ref. [165]. Since this effect is only relevant for frequencies below 10^{-10} Hz, i.e. outside the range accessible in near-future experiments, we omit it in this thesis.

In order to describe the two kinks in the energy spectrum at wavenumbers around $k_{\rm eq}$ and $k_{\rm RH}$ more accurately, let us rewrite the transfer function in Eq. (4.65) as

$$T_k = \Omega_m\left(\frac{g_*^k}{g_*^{\rm eq}}\right)^{1/2}\left(\frac{g_{*,s}^{\rm eq}}{g_{*,s}^k}\right)^{2/3}\left(\frac{k_0}{k}\right)^2 T_1\left(k/k_{\rm eq}\right)\, T_2\left(k/k_{\rm RH}\right)\ , \tag{4.68}$$

where T_1 and T_2 denote two auxiliary transfer functions accounting for the transition from matter to radiation domination and from radiation domination to reheating, respectively. We have determined both functions numerically by solving the equation of motion for the Fourier modes φ_k^P in appropriate k ranges. Our numerical results are reasonably well described by the two fit functions

$$T_1(x) \simeq c_1^{(0)}\left(1 + c_1^{(1)}x + c_1^{(2)}x^2\right)^{+1/2}\ , \qquad c_1^{(0)} \simeq 0.73\,,\ c_1^{(1)} \simeq \ \ 1.64\,,\ c_1^{(2)} \simeq 3.87\,, \tag{4.69}$$

$$T_2(x) \simeq \qquad \left(1 + c_2^{(1)}x + c_2^{(2)}x^2\right)^{-1/2}\ , \qquad\qquad\quad c_2^{(1)} \simeq -0.38\,,\ c_2^{(2)} \simeq 1.04\,. \tag{4.70}$$

The resulting spectrum for the parameter example discussed in Sec. 3.5 is depicted by the grey curve in Fig. 4.7.

These results are consistent with earlier approaches in the literature[8], see e.g. [104]. In particular, the coefficients of T_2 are very similar to the ones found in Ref. [104] for the case of reheating through inflaton decay. This implies that the kink in the GW spectrum at $k = k_{\rm RH}$ turns out to have the same shape, regardless of whether reheating proceeds as in our case or

[8]Note that in the expression for T_k usually given in the literature (see e.g. Ref. [104]), g_*^k and $g_{*,s}^k$ are divided by g_*^0 and $g_{*,s}^0$, while we find a division by $g_*^{\rm eq}$ and $g_{*,s}^{\rm eq}$ in Eq. (4.68). Our result thus coincides with the one in the literature in the case of massless neutrinos and is smaller than the standard result by a factor of $\left(g_*^0/g_*^{\rm eq}\right)^{1/2} \simeq 0.85$ in the case of three non-relativistic neutrino species in the present epoch.

as in the standard scenario. The reason for this insensitivity can be easily understood: the shape of the GW spectrum from inflation is solely controlled by the evolution of the scale factor $a(t)$, which in turn remains qualitatively unaffected when reheating via the decay of non-relativistic inflaton particles into arbitrary relativistic degrees of freedom is traded for reheating via the decay of non-relativistic $B-L$ Higgs bosons into relativistic (s)neutrinos, cf. Appendix B. As discussed below Eq. (4.59), it is rather the position of the kink and its dependence on the reheating temperature that distinguishes between reheating via inflaton decay and reheating after cosmological $B-L$ breaking. In Appendix B we will explore the connection between the position $f_{\rm RH}$ of the kink and the model parameters in more detail. The main result is that $f_{\rm RH}$ is determined by Γ_S^0 and ρ_0, and hence, in the the context of our Froggatt-Nielsen flavour model, is directly related to the Higgs boson mass m_S or equivalently to the neutrino mass M_1,

$$m_S \simeq 2.1 \times 10^{13}\ \text{GeV} \left(\frac{f_{\rm RH}}{100\ \text{Hz}}\right)^{0.67}, \qquad M_1 \simeq 7.1 \times 10^{10}\ \text{GeV} \left(\frac{f_{\rm RH}}{100\ \text{Hz}}\right)^{0.67}. \quad (4.71)$$

Gravitational waves from tachyonic preheating

As discussed in Sec. 3.2.1, the phase transition at the end of hybrid inflation is accompanied by tachyonic preheating. The process of tachyonic preheating forms a classical, sub-horizon source for GWs which is active only for a short time. The resulting GW spectrum can be obtained by calculating the solution to the mode equation, Eq. (4.40), and inserting it into Eq. (4.32)[9]. The anisotropic stress tensor Π_{ij} entering Eq. (4.40) is determined by the dynamics of preheating and vanishes after the end of preheating, allowing the GWs to propagate freely for $\tau \gg \tau_{\rm PH}$. The remaining challenge is thus to calculate Π_{ij} during preheating. This task can be performed numerically, see e.g. Ref. [107] for a detailed description of the method and an application to preheating after chaotic inflation, as well as Ref. [108] for an application to tachyonic preheating after hybrid inflation. The following discussion will be based on analytical estimates supported by the results of these simulations [106–108, 166].

GWs from tachyonic preheating are expected to yield a spectrum which is strongly peaked at a typical (physical) scale $d_{\rm PH}$ associated with the preheating process. The corresponding comoving wave number describing the position of this peak in today's spectrum is readily obtained by redshifting this scale,

$$k_{\rm PH} = a_{\rm PH}\, d_{\rm PH}^{-1} = \frac{a_{\rm PH}}{a_{\rm RH}} \frac{a_{\rm RH}}{a_0}\, d_{\rm PH}^{-1}\, a_0 = \frac{a_{\rm PH}}{a_{\rm RH}}\, \Delta^{-1/3} \left(\frac{g_{*,s}^0}{g_{*,s}^{\rm RH}}\right)^{1/3} \frac{T_\gamma^0}{T_{\rm RH}}\, d_{\rm PH}^{-1}\, a_0\,, \quad (4.72)$$

with Δ accounting for the deviation from an adiabatic expansion after $a = a_{\rm RH}$, see Eq. (4.55). The corresponding amplitude of the GW spectrum can be estimated by using the picture of

[9] Note that Eq. (4.41) cannot be employed here because translational invariance does not hold for the scales we are interested in during the preheating phase governed by bubble collisions.

bubble collisions, which implies that the fraction of energy converted into GWs at preheating is given by $\rho_{\rm GW}/\rho_c \sim (d_{\rm PH}H_{\rm PH})^2$ [107]. This quantity corresponds to the integrated GW wave spectrum (cf. Eq. (4.33)),

$$\int_{-\infty}^{\infty} d\ln k \;\; \Omega_{\rm GW}(k,\tau) = \frac{\rho_{\rm GW}(\tau)}{\rho_c(\tau)} \,. \tag{4.73}$$

Hence, for a strongly peaked spectrum we can estimate the amplitude of this peak at $\tau = \tau_{PH}$ as

$$\Omega_{\rm GW}^{\rm PH}(k_{\rm PH}) \simeq \;\; c_{\rm PH}\,(d_{\rm PH}H_{\rm PH})^2 \,. \tag{4.74}$$

Here $c_{\rm PH}$ is a model-dependent numerical factor, e.g. $c_{\rm PH} = 0.05$ for the model considered in Ref. [106]. Analogous to the stochastic GW background from inflation, this result can be redshifted to today, cf. Eqs. (4.50) and (4.65), yielding

$$\begin{aligned}\Omega_{\rm GW}(k_{\rm PH})\,h^2 \;&\simeq\; c_{\rm PH}\,(d_{\rm PH}H_{\rm PH})^2 \;\frac{a_{\rm PH}}{a_{\rm RH}}\;\Omega_r h^2 \;\frac{g_*^{\rm RH}}{g_*^0}\left(\frac{g_{*,s}^0}{g_{*,s}^{\rm RH}}\right)^{4/3} \left(2\,C_{\rm RH}^3 R\right) \\ &\simeq\; 1.5\times 10^{-5}\; c_{\rm PH}\;(d_{\rm PH}H_{\rm PH})^2\;\frac{a_{\rm PH}}{a_{\rm RH}}\left(\frac{\Omega_r h^2/g_*^0}{1.237\times 10^{-5}}\right) \,. \end{aligned} \tag{4.75}$$

Estimating $H_{\rm PH}$, $d_{\rm PH}$ and $a_{\rm PH}/a_{\rm RH}$ in the context of our model, Eqs. (4.72) and (4.75) enable us to predict the characteristic features of the GW spectrum due to preheating.

Tachyonic preheating is a very rapid process, and we can therefore to very good approximation express $H_{\rm PH}$ as the Hubble parameter at the end of inflation,

$$H_{\rm PH} \simeq H_{\rm inf} = \left(\frac{\lambda}{12}\right)^{1/2} \frac{v_{B-L}^2}{M_P} \,. \tag{4.76}$$

An estimate of $d_{\rm PH}$ can be obtained by studying the preheating process. For tachyonic preheating associated with the breaking of a local $U(1)$ symmetry, there are two typical scales, one associated with the dynamics of the scalar field, cf. Ref. [108], and the other associated with the presence of the gauge field, cf. Ref. [109]. For the former, there are two distinct possibilities, depending on what triggers the onset of tachyonic preheating: the inflaton crossing the critical point with a significant velocity or quantum diffusion triggered by the growth of quantum fluctuations around the critical point of the scalar potential [108]. For the range of model parameters of interest here, cf. Sec. 3.3, the inflaton velocity is the parameter governing the onset of preheating and hence with Eq. (3.11) we find [108],

$$\left(d_{\rm PH}^{(s)}\right)^{-1} = (\lambda\, v_{B-L}\,|\dot{\varphi}_c|)^{1/3} = 0.15\,\lambda^{5/6}\, v_{B-L}^{2/3}\, M_P^{1/3} \,. \tag{4.77}$$

The typical scale associated with the gauge field is given by the mass m_G of the gauge

boson [109],

$$\left(d_{\rm PH}^{(v)}\right)^{-1} \sim m_G = 2\sqrt{2}\, g\, v_{B-L}\,. \tag{4.78}$$

We now exploit the equation of state of the universe during reheating, which implies

$$\frac{a_{\rm PH}}{a_{\rm RH}} = C_{\rm RH}\, \left(\frac{H_{\rm RH}}{H_{\rm PH}}\right)^{2/3}\,, \tag{4.79}$$

with $H_{\rm PH}$ given by Eq. (4.76), $C_{\rm RH}$ as introduced below Eq. (4.60) and $H_{\rm RH} \simeq 0.58\,\Gamma_S^0$, cf. Eq. (2.39) and Appendix B. For the parameter point (3.56), this implies $a_{\rm PH}/a_{\rm RH} \simeq 10^{-6}$. Using $T_{\rm RH} \simeq \hat{T}_{\rm RH}^{\sigma\,(-)}$, cf. Eq. (4.44), which holds in most of the parameter space of interest, and reintroducing the explicit dependence on m_S and v_{B-L},

$$\hat{T}_{\rm RH}^{\sigma\,(-)} = 4.8\times 10^9\ {\rm GeV}\, \left(\frac{M_1}{10^{11}\ {\rm GeV}}\right) \left(\frac{5\times 10^{15}\ {\rm GeV}}{v_{B-L}}\right) \left(\frac{m_S}{3\times 10^{13}\ {\rm GeV}}\right)^{1/2}\,, \tag{4.80}$$

the positions and amplitudes of the peaks in the GW spectrum associated with preheating are given by

$$\begin{aligned}
f_{\rm PH}^{(s)} &\simeq 6.3\times 10^6\ {\rm Hz}\, \left(\frac{M_1}{10^{11}\ {\rm GeV}}\right)^{1/3} \left(\frac{5\times 10^{15}\ {\rm GeV}}{v_{B-L}}\right)^{2} \left(\frac{m_S}{3\times 10^{13}\ {\rm GeV}}\right)^{7/6}\,,\\
\Omega_{\rm GW}^{(s,{\rm max})}h^2 &\simeq 3.6\times 10^{-16}\, \frac{c_{\rm PH}}{0.05} \left(\frac{M_1}{10^{11}\ {\rm GeV}}\right)^{\frac{4}{3}} \left(\frac{5\times 10^{15}\ {\rm GeV}}{v_{B-L}}\right)^{-2} \left(\frac{m_S}{3\times 10^{13}\ {\rm GeV}}\right)^{-\frac{4}{3}}\,,\\
f_{\rm PH}^{(v)} &\simeq 7.5\times 10^{10}\ {\rm Hz}\, g \left(\frac{M_1}{10^{11}\ {\rm GeV}}\right)^{1/3} \left(\frac{m_S}{3\times 10^{13}\ {\rm GeV}}\right)^{-1/2}\,,\\
\Omega_{\rm GW}^{(v,{\rm max})}h^2 &\simeq 2.6\times 10^{-24}\, \frac{1}{g^2}\, \frac{c_{\rm PH}}{0.05} \left(\frac{M_1}{10^{11}\ {\rm GeV}}\right)^{\frac{4}{3}} \left(\frac{5\times 10^{15}\ {\rm GeV}}{v_{B-L}}\right)^{2} \left(\frac{m_S}{3\times 10^{13}\ {\rm GeV}}\right)^{2},
\end{aligned} \tag{4.81}$$

where we have used $C_{\rm RH} = 1.13$ and $R = 0.41$, as well as set $\Delta = 2$, as obtained numerically in this parameter region by solving the Boltzmann equations, cf. Appendix B. Note that $f_{\rm PH}^{(s)}$ and $f_{\rm PH}^{(v)}$ are related to microscopic quantities of the preheating process and are therefore much larger than the highest frequency relevant for inflation, $f_{\rm PH}$ (cf. Eq. (4.64)), which is determined by the Hubble parameter at preheating.[10]

Fig. 4.7 shows the peaks of the GW spectrum due to preheating (in red) for $c_{\rm PH} = 0.05$ and the parameter point (3.56). The frequencies and corresponding amplitudes of the two peaks are given in Eq. (4.81). The shape of the peaks in Fig. 4.7 is parametrized by

$$\Omega_{\rm GW}^{(i)}h^2 = \Omega_{\rm GW}^{(i,{\rm max})} \times \left(\frac{f}{f_{\rm PH}^{(i)}}\right)^2 {\rm Exp}\left[1 - \left(f/f_{\rm PH}^{(i)}\right)^2\right]\,, \tag{4.82}$$

[10] Moreover, $f_{\rm RH}^{(v)}$ is associated with the width of the Abelian Higgs string at preheating and hence represents the smallest scale (highest frequency) possible for GWs from this phase transition.

with $i = s, v$; motivated by the results found in Ref. [106] for the scalar peak. We do stress, however, that for the purpose of this thesis, we are mainly interested in the position and amplitude of the peaks. A precise quantitative description of the shape of the spectrum at these frequencies, in particular for the peak corresponding to the vector boson, requires a more detailed study.

GWs from cosmic strings

So far, we have discussed the GW spectrum due to inflation and due to the turbulent processes accompanying tachyonic preheating. We now discuss a third source, namely cosmic strings in the scaling regime, cf. Sec. 3.2.2. In this section, we review the calculation of the resulting GW background in the Abelian Higgs model following Ref. [111]. In Ref. [19], we additionally discuss an alternative approach based on the Nambu-Goto model of cosmic strings. In this thesis, we will merely give the final result of the latter calculation in order to quantify the theoretical uncertainties involved.

Starting point of this discussion is Eq. (4.42), which, for a classical, sub-horizon source, connects the GW spectrum to the unequal time correlator of the source. For a scaling network of cosmic strings in the Abelian Higgs model, we can now proceed and evaluate this expression by exploiting general properties of the unequal time correlator of a scaling source discussed in Ref. [167]. Introducing the dimensionless variable $x = k\tau$, one can express $\Pi^2(k, \tau, \tau')$ as

$$\Pi^2(k, \tau, \tau') = \frac{4v_{B-L}^4}{\sqrt{\tau\tau'}}\, C^T(x, x') \,, \tag{4.83}$$

where $C^T(x, x')$ is essentially local in time [167],

$$C^T(x, x') \sim \delta(x - x')\, \widetilde{C}(x) \,, \tag{4.84}$$

with $\widetilde{C}$ some function that falls off rapidly for $x \gg 1$, i.e. for modes well inside the horizon. Inserting Eqs. (4.83) and (4.84) into Eq. (4.42) yields

$$\Omega_{\mathrm{GW}}(k) = \frac{k^2}{3\pi^2 H_0^2 a_0^2} \left(\frac{v_{B-L}}{M_{\mathrm{Pl}}}\right)^4 \int_{x_i}^{x_0} dx\, \frac{a^2(x/k)}{a_0^2\, x}\, \widetilde{C}(x) \,. \tag{4.85}$$

As a result of the rapid decrease of $\widetilde{C}(x)$ for $x \gg 1$, this integral is dominated by its lower boundary and basically insensitive to the upper boundary for $x_0 \gg x_i \gtrsim 1$,

$$\int_{x_i}^{x_0} dx\, \frac{a^2(x/k)}{a_0^2\, x}\, \widetilde{C}(x) \simeq \int_{x_i}^{\infty} dx\, \frac{a^2(x/k)}{a_0^2\, x}\, \widetilde{C}(x) \,. \tag{4.86}$$

For scales which entered the Hubble horizon after the $B-L$ phase transition, $x_i = k\,\tau_k$ is an $\mathcal{O}(1)$ constant. Hence, the k-dependence of Eq. (4.86) can be traced back to $a(x/k)$. For radiation domination, we have $a(\tau) \simeq \sqrt{\Omega_r} H_0 \tau a_0^2$, where we have neglected the change in the

effective number of degrees of freedom. This yields

$$\int_{x_i}^{\infty} dx \, \frac{a^2(x/k)}{a_0^2 \, x} \, \widetilde{C}(x) \simeq \frac{\Omega_r \, H_0^2 \, a_0^2}{2 \, k^2} \, F^r \ , \tag{4.87}$$

where F^r is a constant, and therefore a flat spectrum, $\Omega_{\rm GW} \propto k^0$. For matter domination, one has $a(x/k) \propto k^{-2}$, which yields $\Omega_{\rm GW} \propto k^{-2}$.

For scales which entered the horizon at very early times before the cosmic string network reached its scaling regime, the lower boundary in Eq. (4.86) refers to the onset of scaling rather than horizon crossing, thus taking a larger value, $x_i > \mathcal{O}(1)$. Note that x_i is now also k-dependent. The qualitative effect of this is a suppression of the spectrum at these frequencies. However, in the model we are discussing here we expect scaling to set in well before the end of reheating, and hence this effect only influences the spectrum at very large frequencies which are currently experimentally inaccessible. We will thus omit it in the following discussion.

In summary, we can express today's spectrum of GWs from a scaling network of cosmic strings as[11]

$$\Omega_{\rm GW}(k) \simeq \Omega_{\rm GW}^{\rm pl} \times \begin{cases} (k_{\rm eq}/k)^2, & k_0 \ll k \ll k_{\rm eq} \\ 1, & k_{\rm eq} \ll k \ll k_{\rm RH} \\ (k_{\rm RH}/k)^2, & k_{\rm RH} \ll k \ll k_{\rm PH} \end{cases} \ . \tag{4.88}$$

Here, $k_{\rm eq}$, $k_{\rm RH}$ and $k_{\rm PH}$ are given by Eqs. (4.53), (4.57) and (4.64), and the height of the plateau $\Omega_{\rm GW}^{\rm pl}$ can be estimated using the result of the numerical simulations in Ref. [111],

$$\begin{aligned} \Omega_{\rm GW}^{\rm pl} h^2 &= \frac{1}{6\pi^2} \, F^r \left(\frac{v_{B-L}}{M_{\rm Pl}} \right)^4 \Omega_r h^2 \\ &= 4.0 \times 10^{-14} \, \frac{F^r}{F^r_{\rm FHU}} \left(\frac{v_{B-L}}{5 \times 10^{15} {\rm GeV}} \right)^4 \left(\frac{\Omega_r h^2}{4.2 \times 10^{-5}} \right) \ , \end{aligned} \tag{4.89}$$

where $F^r_{\rm FHU} = 4.0 \times 10^3$ is the numerical constant determined in Ref. [111] for global cosmic strings. The corresponding constant for local strings is expected to have the same order of magnitude [168].

Eq. (4.88) strikingly resembles the result found for the stochastic GW background from inflation, cf. Eq. (4.66), up to an overall normalization factor, cf. Fig. 4.7. Note, however, that the origin is quite different. On the one hand, in the case of inflation, the GWs can be traced back to vacuum fluctuations of the metric which remain 'frozen' outside the horizon. After horizon re-entry, they propagate according to the source-free wave equation in FRW space.

[11] Note that in Eq. (4.88), the normalization of the '$1/k^2$-flanks' was obtained by matching to the plateau value for $k = k_{\rm RH}$ and $k = k_{\rm eq}$, respectively. However, since close to these points the dominant component of the energy density is not much larger than the other components, a more detailed knowledge of $\widetilde{C}(x)$ is necessary to evaluate Eq. (4.86) at these points. This could lead to a slight shift in the normalization of the 'flanks', see also Eq. (4.66).

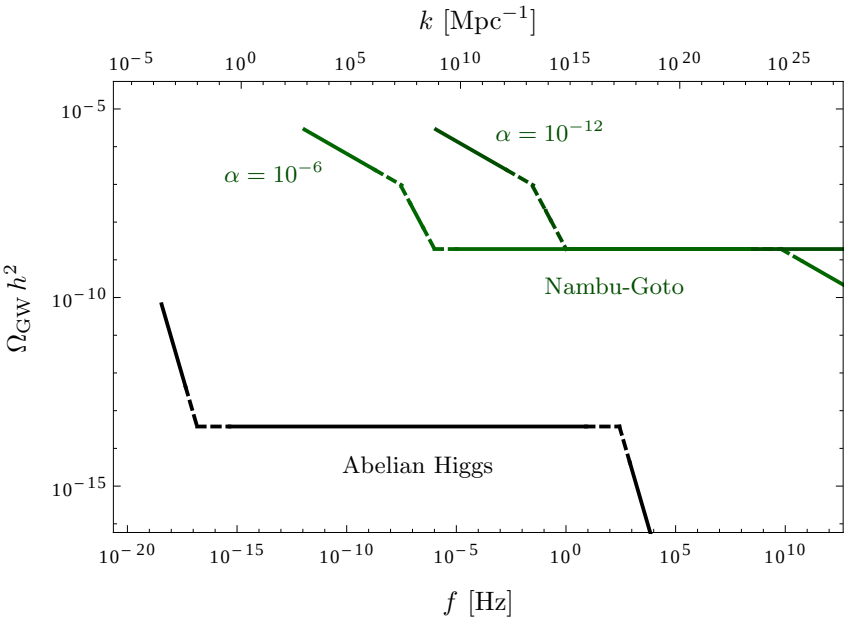

Figure 4.8: Comparison of the GW spectra predicted by AH strings and NG strings for two values of α (which governs the cosmic string loop size in the NG model). The AH curve is obtained as in Fig. 4.7, for the NG curve see Ref. [19] with $G\mu = 2 \times 10^{-7}$, as obtained e.g. by the parameter choice in Eq. (3.56).

The amplitude of the resulting stochastic GW background today is determined by the redshift of these modes after entering the horizon. On the other hand, the GWs from cosmic strings stem from a classical source, which is active until today. Only the nature of the unequal time correlator, with its rapid decrease for $x \gg 1$, effectively removes the impact of the source when the corresponding mode is well within the horizon. In more physical terms, this implies that the dominant source for GWs from cosmic strings are Hubble-sized structures of the cosmic string network. This explains why the wavenumbers associated with the horizon at $a_{\rm RH}$ and $a_{\rm eq}$ play crucial roles in the GW spectrum from AH cosmic strings, although the GW modes associated with cosmic strings never actually 'cross' the horizon. For cosmic strings the height of the plateau is enhanced by a very large numerical factor F^r. On the contrary, GWs from inflation are suppressed by the small Yukawa coupling λ. This explains the enormous difference in amplitude between GWs from inflation and cosmic strings.

Note that, contrary to inflation, the height of the plateau for the GW background from cosmic strings does not directly translate to the tensor contribution of the CMB scalar power spectrum. This can be traced back to the very different mechanism responsible for generating GWs in inflation and from cosmic strings, in particular concerning correlation properties on super-horizon scales. Determining the effect of GWs from cosmic strings on the CMB requires a specific numerical simulation [2, 28].

The calculation presented here, resulting in Eq. (4.88), was based on the Abelian Higgs

(AH) cosmic string model. For comparison, Fig. 4.8 shows the result obtained in the Nambu-Goto (NG) model, cf. Ref. [19]. In both approaches the radiation-dominated epoch leads to a plateau for intermediate frequencies. Compared to the AH result, the boundaries in the NG case are shifted to higher frequencies by a factor $1/\alpha$, where α denotes the size at which cosmic string loops are formed relative to the respective horizon size.[12] This shift in frequency is directly related to the maximal loop size which is determined by H^{-1} in the AH case but by αH^{-1} in the NG case. Furthermore, the frequency dependence for small and large frequencies differs, which is a consequence of the different mechanisms of gravitational radiation: in the AH model the dominant contribution to the GW background comes from Hubble-sized structures, in the NG model the dominant contribution is due to 'cusps' in small cosmic string loops, which are formed when waves moving in opposite directions on the loop collide. Most striking is the difference in normalization by five orders of magnitude. This can be traced back to the different assumptions on how the string network loses energy and stays in the scaling regime. While the energy loss of AH strings is mainly due to massive radiation, NG strings deposit all their energy into GWs. Hence, these two cases provide lower and upper bounds on the gravitational background produced by cosmic strings, and it is conceivable that the true answer corresponds to some intermediate value. Assuming a transition between the AH model at early times and the NG model at later times sometime during radiation domination, a notable point is that, due to the shift of the GW spectrum of NG strings to higher frequencies, the GWs generated at later times in the NG regime might cover up the GWs generated at earlier times in the AH regime. To address this important question of how to correctly describe the evolution of cosmic strings is clearly a theoretical challenge.

4.3.3 Observational prospects

In Sec. 4.3.2, we discussed the GW background produced during the different stages of a $B-L$ phase transition in the early universe, namely during inflation, during tachyonic preheating and from cosmic strings in the scaling regime. Fig. 4.9 summarizes the resulting GW spectrum of all these different sources for the parameter point (3.56), and for $\alpha = 10^{-12}$. Additionally, we show current bounds and the expected sensitivity of upcoming GW experiments, depicted by the solid and dashed blue curves, respectively. These experiments can be grouped into three categories, see e.g. Ref. [3] for a review: millisecond pulsar timing measurements (e.g. EPTA [115], PPTA [37] and SKA [169, 170]) sensitive to GWs with a frequency of about 10^{-9} Hz, space-based interferometers (e.g. BBO/DECIGO [12, 13] and eLISA [10]) sensitive at about 10^{-1} Hz and ground-based interferometers (e.g. (advanced) LIGO [11, 36], ET [171], and KAGRA [172]) which are most sensitive at about 10^2 Hz. It should be noted that in

[12] Note that α cannot take arbitrarily small values. A lower bound is given by the requirement that, in the area of application of the NG model, the loop size should be larger than the string width obtained in the AH model (controlled by m_S^{-1}, m_G^{-1}) or at the very least larger than M_P^{-1}.

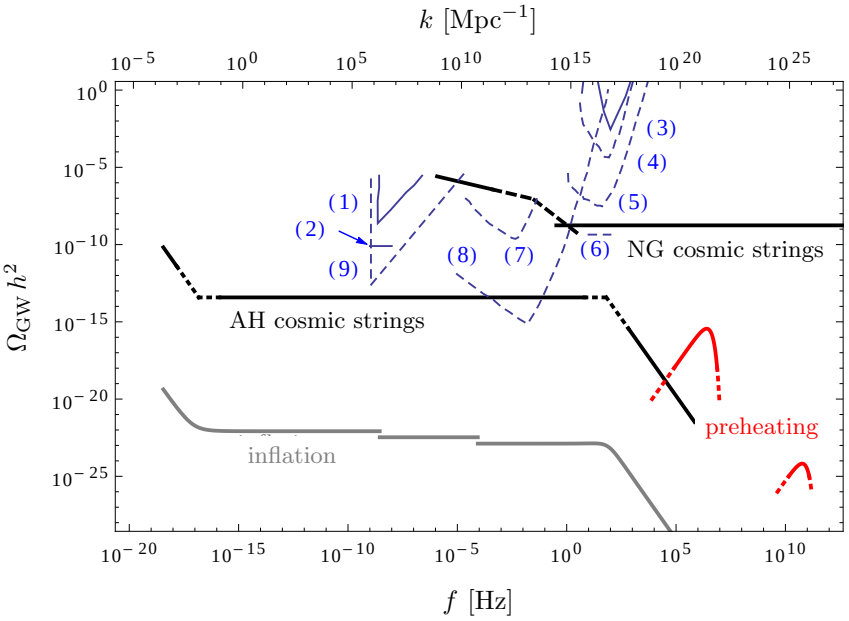

Figure 4.9: Predicted GW spectrum and the (expected) sensitivity of current and upcoming experiments. The GW spectrum due to inflation (grey), preheating (red) as well as AH and NG cosmic strings (black) is shown for the same parameters an in Figs. 4.7 and 4.8 with $\alpha = 10^{-12}$. The corresponding effective kink temperature is $T_* = 1.5 \times 10^9$ Gev, which, for $\widetilde{m}_1 = 0.04$ eV, yields a reheating temperature of $T_{\rm RH} = 1.9 \times 10^9$ GeV. The current bounds on the GW spectrum from (1) millisecond pulsar timing (taken from [163], with (2) marking the update from EPTA [115]) and (3) LIGO [116] are marked by solid blue lines. The dashed blue lines mark the expected sensitivity of some planned experiments: (4) KAGRA [175], (5) ET [171], (6) advanced LIGO [11], (7) eLISA [10], (8) BBO/DECIGO [176] and (9) SKA [169].

particular for the ground-based detectors the sensitivity is typically given in terms of the strain $\tilde{h}_f$ which is related to the amplitude $\Omega_{\rm GW}$ as [3]

$$\Omega_{\rm GW} h^2 = \frac{\rm SNR}{F} \frac{4\pi^2 f^3}{3(H_0/h)^2} \tilde{h}_f^2 \,, \tag{4.90}$$

with the sensitivity factor $F = 2/5$ for the ground-based interferometers and in Fig. 4.9, we have required a signal-to-noise ratio of SNR $= 1$. Moreover, constraints on the effective number of relativistic degrees of freedom from BBN and from the CMB yield an upper bound of $\Omega_{\rm GW} h^2 \lesssim 10^{-5}$ for $k > k_{\rm eq}$, with a weak dependence on the origin of the GW background, cf. Refs. [173, 174]. For further ideas of how to possibly probe the parameter space of Fig. 4.9 in the future, see Ref. [3] and references therein.

A clear message of Fig. 4.9 is that GWs from a GUT-scale $U(1)$ phase transition will be seriously probed by a number of upcoming experiments. Here, the dominant contribution originates from cosmic strings in the scaling regime, depicted by the black curves in Fig. 4.9. However, at the same time, this is the contribution with the largest theoretical uncertainty. In spite of the quite dramatic differences between the AH and NG predictions, it is worth

noting that in both cases upcoming experiments are expected to reach the sensitivity to probe the 'plateau value' for GUT-scale cosmic strings. Moreover, in both cases it seems possible to measure a very interesting feature of the spectrum. In the case of NG strings, the bend-over marking the transition from radiation to matter domination is within reach of planned satellite-based experiments, depending on the parameter α. In the case of AH strings, the transition between an early matter-dominated reheating phase and radiation domination at f_{RH} has the right frequency to possibly be within reach of future ground-based GW detectors. Assuming that the actual signal from cosmic strings lies somewhere between the AH and the NG prediction (or maybe can even be obtained by interpolating between the AH model at early times and the NG model at late times), it seems possible that future experiments will be able to probe one, or maybe even both, of these features.

The GW background from inflation, depicted in grey in Fig. 4.9, is probably the best understood cosmological source. However, as Fig. 4.9 shows, it is clearly subdominant compared to the GW background from cosmic strings in hybrid inflation models, which typically feature a very small tensor-to-scalar ratio, cf. Eq. (3.9). Nevertheless, a precise understanding of the GW background from inflation is crucial for two reasons: First, although their origin is very different, both the AH string and the inflationary GW spectrum are governed by the respective Hubble-sized modes throughout the expansion history. Hence, the kink marking the transition between an early matter-dominated reheating phase and radiation domination occurs at the same frequency in both spectra. Thus, although the shape of this kink is modified in the case of the signal from AH cosmic strings due to the precise shape of $\widetilde{C}$, cf. Eq. (4.85) and the footnote on page 87, any conclusion we can draw from measuring the position of the kink in the inflationary spectrum holds also for the corresponding kink in the AH cosmic string spectrum. In particular, measuring this kink would determine T_*, cf. Eq. (4.63), and probe the model parameters M_1 and m_S, cf. Eq. (4.71). Second, the prediction for the GW background from cosmic strings is plagued with large uncertainties. The discrepancy between the AH and the NG prediction is one, but there are also other mechanisms which might reduce or even eliminate the cosmic string contribution. For example, a coupling between the GUT and SM Higgs bosons can effectively reduce the string tension [117] or several e-folds of inflation occurring after the $U(1)$ phase transition could dilute the cosmic string loops in the NG model, thereby reducing the GW background, see e.g. Refs. [177–181]. Further theoretical uncertainties related to cosmic strings are mentioned below Eq. (3.18). It is thus crucial to take into account the second largest contribution, and over a wide range of frequencies, this is inflation.

Finally, the red curves in Fig. 4.9 depict the signals expected from tachyonic preheating. These are clearly at too high frequencies to be detectable in the near future. Consulting Eq. (4.81) it becomes clear that this is generically true for GUT-scale parameters. However, these signals show a distinctly different behaviour compared to the contributions from inflation

and cosmic strings. It would thus be very interesting to probe such frequencies, since it would enable us to break parameter degeneracies and distinguish different models describing the preheating and reheating phase.

4.3.4 Combining observations

The possibility of measuring $f_{\rm RH}$, the position of the kink associated with reheating in the GW spectrum from inflation and from AH cosmic strings, is a fascinating prospect. Measuring this feature of the GW spectrum would provide a unique possibility to probe the reheating process and in particular the reheating temperature, cf. Eq. (4.63), a quantity so far barely constrained by observations. In the context of our Froggatt-Nielsen model, a measurement of $f_{\rm RH}$ would determine the neutrino mass M_1, cf. Eq. (4.71). Now, we want to combine this with our results obtained in Secs. 4.1 and 4.2 to determine how a possible future measurement of $f_{\rm RH}$ would effect the parameter space of cosmological $B-L$ breaking.

Considering the generated baryon asymmetry, Eq. (4.5) demonstrates that η_B does not depend on $\widetilde{m}_1$ in the weak-washout regime, cf. Fig. 4.2. Now reading off the allowed M_1 values from the upper panel of Fig. 4.3, we find that η_B does not depend on $\widetilde{m}_1$ in the entire part of the considered parameter space which is consistent with gravitino dark matter. Hence in this setup, measuring $f_{\rm RH}$ would fix the maximally possible baryon asymmetry, obtained by assuming the maximal value for ϵ_1, cf. Eq. (3.47),

$$\eta_B \simeq 4.0 \times 10^{-9} \left(\frac{f_{\rm RH}}{100 \text{ Hz}} \right) . \tag{4.91}$$

Moreover, in the case of gravitino dark matter, fixing M_1 in Eq. (4.11) implies direct relations between $\widetilde{m}_1$ and $m_{\widetilde{G}}$ along the contour lines of the upper panel of Fig. 4.3. For example, for $M_1 = 10^{11}$ GeV and a gluino mass of $m_{\tilde{g}} = 1$ TeV, a light neutrino mass scale of $\widetilde{m}_1 = 2 \times 10^{-4}$ would predict $m_{\widetilde{G}} = 130$ GeV or $m_{\widetilde{G}} = 660$ GeV for the gravitino mass. For large values of $\widetilde{m}_1$, $m_{\widetilde{G}}$ becomes approximately independent of $\widetilde{m}_1$. This can also be seen from Eq. (4.11) with the exponent of $\widetilde{m}_1$, $d \simeq -0.03$ for $\widetilde{m}_1 > 10^{-3}$, determined by Eq. (4.10). Hence assuming $\widetilde{m}_1 \gtrsim 10^{-2}$, a measurement of $f_{\rm RH}$ would determine the gravitino mass as a function of the gluino mass,

$$\left[0.13 \left(\frac{m_{\widetilde{G}}}{100 \text{ GeV}} \right) + \left(\frac{100 \text{ GeV}}{m_{\widetilde{G}}} \right) \left(\frac{m_{\tilde{g}}}{1 \text{ TeV}} \right)^2 \right]^{-0.8} \simeq 0.99 \left(\frac{f_{\rm RH}}{100 \text{ Hz}} \right)^{0.67} , \tag{4.92}$$

up to a choice of the lower or upper branch in Fig. 4.3.

Turning to the case of neutralino dark matter, fixing M_1 by measuring $f_{\rm RH}$ yields m_χ as a function of $\widetilde{m}_1$ and vice versa, cf. Eqs. (4.14), (4.16) and (4.17). In particular for $x \gtrsim 36$,

cf. Eqs (4.2) and (4.3), we find

$$0.17\left(\frac{m_\chi}{1\text{ TeV}}\right)\left(\frac{f_{\rm RH}}{100\text{ Hz}}\right)^{0.83}\left(\frac{\widetilde{m}_1}{10^{-2}\text{ eV}}\right)^{0.25}+c_\chi\left(\frac{m_\chi}{1\text{ TeV}}\right)^2=0.11\,. \tag{4.93}$$

For example, a measurement of $f_{\rm RH}=100$ Hz would imply for the wino LSP case that for $\widetilde{m}_1=10^{-2}$ eV the wino mass must be $m_{\widetilde{w}}\simeq 600$ GeV in order to produce the correct DM abundance.

Summarizing, in the major part of the parameter space, a measurement of the kink in the GW spectrum associated with reheating would turn the relations found in Secs. 4.1 and 4.2 into interesting and testable predictions. However, two comments are in order. First, note that throughout this subsection we have assumed the Froggatt-Nielsen relation $M_1=\eta^2 m_S$. Dropping this assumption introduces an additional parameter into the game, which qualitatively will not change the reheating process discussed in Sec. 3.5 much, but which will introduce an additional adjustable parameter into Eqs. (4.91) to (4.93). Second, a measurement of $f_{\rm RH}$ is a very challenging task. Not only is the kink in the GW spectrum from AH cosmic strings probably out of reach of current and planned GW detectors for the high reheating temperatures expected in our model, but there is also a conceptual issue related to the uncertainties involved in the description of cosmic strings, cf. comment at the end of section 4.3.2. Even if the AH cosmic string model gives an accurate description of the strings during the reheating process, a transition to NG strings sometime during radiation domination would lead to the emittance of GWs in a frequency range around $f_{\rm RH}$. Due to the much larger amplitude expected from the GW background from NG strings, this would make a detection of the AH feature at $f_{\rm RH}$ nearly impossible. Again, this stresses the importance of a better theoretical understanding of the evolution of the cosmic string network.

As a final remark, note that if we could indeed one day measure the peaks in the GW spectrum due to preheating, this would yield independent measurements of M_1, m_S and $\widetilde{m}_1$, permitting to test the model presented here even after dropping the assumption $M_1=\eta^2 m_S$.

4.4 Low-energy neutrino phenomenology

In Sec. 2.5, we introduced the Froggatt-Nielsen model as an effective way to parametrize the flavour structure of our model. It can naturally reconcile the large quark and charged lepton mass hierarchies and the small quark mixing angles with the observed small neutrino mass hierarchy and their large mixing angles. Moreover, it is flexible enough to incorporate the new physics of spontaneous $B-L$ breaking. And finally, as we show in Ref. [15], this flavour structure, together with the measured neutrino mass squared differences and mixing angles, strongly constrains yet undetermined parameters of the neutrino sector. Treating the unknown $\mathcal{O}(1)$ factors of the model as random variables, we obtain surprisingly accurate

predictions for the smallest mixing angle θ_{13}, the smallest neutrino mass m_1 and one Majorana phase α_{21}:

$$\begin{aligned} \sin^2 2\theta_{13} &= 0.07^{+0.11}_{-0.05}\,, \\ m_1 &= 2.2^{+1.7}_{-1.4}\ \text{eV}\,, \\ \alpha_{21}/\pi &= 1.0^{+0.2}_{-0.2}\,, \end{aligned} \tag{4.94}$$

with a confidence level of 68%. The prediction for θ_{13} is remarkable, in particular in view of the recent measurements of the smallest mixing angle by different collaborations, for example, $\sin^2 2\theta_{13} = 0.089 \pm 0.010(\text{stat}) \pm 0.005(\text{syst})$ by Daya Bay [182]. In this sense, low-energy neutrino phenomenology can be used to probe the flavour structure of the model presented here.

In this chapter, we discussed various phenomenological aspects of a $B-L$ phase transition in the early universe. We found that in a substantial part of the parameter space, spontaneous $B-L$ breaking can generate lepton asymmetry, entropy and dark matter in accordance with observations. Moreover, we found no unique 'smoking-gun' signal, but instead many complementary channels of searching for traces of such a phase transition. Combining these different phenomenological aspects will help to probe this idea experimentally in the near future. In particular, we discussed connections between the neutrino parameters and the superparticle mass spectrum, induced by the key role of the reheating temperature. Furthermore, we found interesting features in the GW spectrum which might be detected by upcoming GW detectors. Finally, we pointed out how low-energy neutrino phenomenology is capable of probing the high-energy flavour structure.

Chapter 5

Superconformal D-term Inflation

In Chapter 3, we sketched an inflation model based on F-term hybrid inflation with a (nearly) canonical Kähler potential. We demonstrated that this fits very well with the concept of a $B-L$ breaking phase transition in the early universe. However, it also has several shortcomings. Obtaining a spectral index in accordance with current experimental data requires some degree of fine-tuning in the coefficients of the Kähler potential. Moreover, the choice of a canonical Kähler potential has no fundamental theoretical motivation. This is in particular critical in the context of D-term hybrid inflation, which typically implies values for the inflaton field of $\mathcal{O}(M_P)$, rendering higher-dimensional Planck-suppressed operators important. In summary, this leads us to the following question: Can we write down a supergravity inflation model which features a $U(1)$ phase transition, which is conceptually better motivated and which simultaneously is compatible with the experimental data on the CMB fluctuations?

To address this question, we will start by reviewing a class of models referred to as canonical superconformal supergravity models [39] in Sec. 5.1. These, pursuing the principle of using symmetries as a guideline for particle physics model building, are based on exploiting the underlying superconformal symmetry of supergravity. In Sec. 5.2 we will discuss two examples in this context, F-term and D-term hybrid inflation. The latter is particularly promising, and we will spend the remainder of the chapter working out the predictions for the primordial power spectrum in this case. At first, in Sec 5.3, we focus on the special case of single-field inflation and derive analytical expressions for the predictions. Then in Sec. 5.4 we extend the discussion to the general two-field case and present the results of our numerical studies.

This chapter is based on work partly published in Ref. [18]. Additionally we show here that the equivalence of the calculation in the Einstein and in the Jordan frame. We also comment on the impact of the recently published Planck data [1, 2].

5.1 Superconformal models of inflation

In this section, based on Ref. [39], we review an interesting class of supergravity inflation models based on a superconformal symmetry. These models feature an amazingly simple structure, with many expressions very similar to the familiar expressions in global supersymmetry, however only when treated in a suitable 'frame'. To understand this, we first recall the formulation of supergravity in the Einstein and in the Jordan frame in Sec. 5.1.1. In Sec. 5.1.2, we then introduce superconformal symmetry, focussing on the local conformal symmetry relevant for discussing inflation. Using a simple toy model, we demonstrate some of the key features of a special class of superconformal supergravity models which are discussed in full in Sec. 5.1.3. Finally, in Sec. 5.1.4 we discuss different mechanisms of superconformal symmetry breaking.

5.1.1 Supergravity in the Einstein and the Jordan frame

At scales well below the Planck scale, the supergravity corrections to global supersymmetry are suppressed by the weak gravitational interaction and hence negligible. During inflation however, when the vacuum energy density comes within a few orders of magnitude of the Planck scale and very large values for the scalar fields are possible, gravity must be taken into account.

In Sec. 3.1 we already came across a 'minimal' version of a supergravity embedding. We used a canonical Kähler potential, which leaves the kinetic terms and the D-term scalar potential unaffected, cf. Eq. (3.2), and hence all supergravity effects were contained in the scalar F-term potential (3.1). Here, we want to dig a bit deeper into the structure of supergravity. To this end, this section is dedicated to giving a brief review of the relevant formulas and relations which we will need in the remainder of this chapter. For inflation, the relevant parts of the Lagrangian are the scalar and gravity terms, and we will focus on these here. In particular, we will study these terms in two different frames, in the Einstein frame as well as in the Jordan frame. Switching between these two frames and exploiting the advantages of both frames will allow us to identify an interesting class of models in Sec. 5.1.3.

Einstein frame

The Einstein frame is the most common frame to study supergravity, see e.g. Refs. [38, 120] for an introduction. The Lagrangian contains an Einstein-Hilbert term for gravity,

$$\mathcal{L}_E^{\text{grav}} = \sqrt{-g_E}\,\frac{1}{2}\,R(g_E)\,M_P^2\,, \tag{5.1}$$

and no direct coupling between the Ricci scalar R and the scalars of the matter supermultiplets. Here $\sqrt{-g_E} = \sqrt{-\det(g_{E\,\mu\nu})}$, with $g_{E\,\mu\nu}$ denoting the metric in the Einstein frame. This is the frame we implicitly used in Sec. 3.1, taking $g_{E\,\mu\nu}$ to be the FRW metric, and which is in particular used when deriving the expressions (3.9) for the inflationary observables.

The scalar part of $\mathcal{L}_E$ consists of the kinetic terms for the scalars and the scalar potential,

$$\mathcal{L}_E^{\text{scal}} = \sqrt{-g_E}\left[g_E^{\mu\nu} K_{\alpha\bar{\beta}}(\partial_\mu z^\alpha)(\partial_\nu \bar{z}^{\bar{\beta}}) - (V_E^F + V_E^D)\right] . \tag{5.2}$$

Here the z^α denote the complex scalar fields of the theory, $\bar{z}^{\bar{\alpha}}$ their complex conjugates, and $K_{\alpha\bar{\beta}} = \partial_\alpha \partial_{\bar{\beta}} K(z, \bar{z})$, with $\partial_\alpha = \partial/\partial z^\alpha$, is the Kähler metric of the field space. In this chapter, we will need a compact notation to deal with a series of lengthy supergravity expressions. Hence contrary to Chapter 2, we will make use of the Einstein summation convention in field space. This implies the implicit summation over all indices which appear in pairs of sub- and superscripts, and raising and lowering the indices implies a multiplication with the corresponding metric. Moreover, we shall denote all complex conjugate quantities with overbars. In general, the space-time derivatives ∂_μ in Eq. (5.2) should be understood as the gauge covariant derivatives $\partial_\mu - igA_\mu^B T^B$ when considering a gauge field theory with the gauge fields A_μ^B. However, since for inflation we are only interested in the pure scalar-gravity part of the Lagrangian, we will omit these contributions here. V_E^F and V_E^D are the F- and D-term scalar potential, respectively:

$$\begin{aligned} V_E^F &= e^{K/M_P^2}\left[K^{\alpha\bar{\beta}}\mathcal{D}_\alpha W \mathcal{D}_{\bar{\beta}}\overline{W} - 3\,\frac{|W|^2}{M_P^2}\right] , \\ V_E^D &= \frac{1}{2}\left(\frac{1}{\text{Re}(f)}\right)^{AB} D_A D_B \, , \end{aligned} \tag{5.3}$$

with the Kähler covariant derivatives $\mathcal{D}$ defined as below Eq. (3.2). D_A denotes the auxiliary component of the vector super-field. As in global supersymmetry, cf. Eq. (2.6), they can be eliminated by exploiting their equation of motion, here

$$D_A = g\,(\partial_\alpha K)(T_A\, z)^\alpha \, , \tag{5.4}$$

with T_A denoting the generators of the gauge group. Finally, f is the so-called gauge kinetic function. Note that V_E^F is just the scalar potential we employed in Sec. 3.1 and for a minimal gauge kinetic function, $f_{AB} = \delta_{AB}$, and a canonical Kähler potential, V_E^D reduces to the expression found in global supersymmetry, cf. Eq. (2.20).

In the Einstein frame, the theory is thus fully defined by the superpotential W, the Kähler potential K and the gauge kinetic function f_{AB}. Eqs. (5.2) and (5.3) determine the dynamics of the scalar field and inflationary predictions can be calculated as outlined in Sec. 3.1.

Jordan frame

The Jordan frame has recently received a lot interest in the context of Higgs inflation [40–42], where introducing a non-minimal coupling of the Higgs field to gravity, i.e. more precisely to the Ricci scalar, can render the Higgs potential flat enough to achieve slow-roll inflation. Contrary to the Einstein frame, the gravitational part of the Jordan frame Lagrangian in

general contains couplings between the Ricci scalar and the scalar fields,

$$\mathcal{L}_J^{\text{grav}} = -\sqrt{-g_J}\,\frac{1}{6}\,\Phi(z,\bar{z})\,R(g_J)\,. \tag{5.5}$$

The real, field-dependent coefficient function $\Phi(z,\bar{z})$ of the Ricci scalar is called frame function and defines the Jordan frame. Note that there is only one single Einstein frame description for a given theory, but many possible Jordan frames, given by different choices of Φ. The transformation from the Einstein frame to a Jordan frame is achieved by rescaling the metric,

$$g_{J\,\mu\nu} = -\,\frac{3M_P^2}{\Phi(z,\bar{z})}\,g_{E\,\mu\nu}\,. \tag{5.6}$$

With this, the scalar part of the Jordan frame Lagrangian is given by[1]

$$\begin{aligned}\mathcal{L}_J^{\text{scal}} = \sqrt{-g_J}\,\Bigg[&-\Phi\mathcal{A}_\mu^2(z,\bar{z}) + i\mathcal{A}_\mu\left((\partial_{\bar{\alpha}}\Phi)\partial^\mu\bar{z}^{\bar{\alpha}} - (\partial_\alpha\Phi)\partial_\mu z^\alpha\right)\\ &+\left(\frac{\Phi\,K_{\alpha\bar{\beta}}}{3M_P^2} - \frac{(\partial_\alpha\Phi)(\partial_{\bar{\beta}}\Phi)}{\Phi}\right)g_J^{\mu\nu}(\partial_\mu z^\alpha)(\partial_\nu\bar{z}^{\bar{\beta}}) - V_J\Bigg]\end{aligned} \tag{5.7}$$

$$= \sqrt{-g_J}\left[\Phi\mathcal{A}_\mu^2(z,\bar{z}) + \left(\frac{\Phi\,K_{\alpha\bar{\beta}}}{3M_P^2} - \frac{(\partial_\alpha\Phi)(\partial_{\bar{\beta}}\Phi)}{\Phi}\right)g_J^{\mu\nu}(\partial_\mu z^\alpha)(\partial_\nu\bar{z}^{\bar{\beta}}) - V_J\right]\,, \tag{5.8}$$

with

$$V_J = \frac{\Phi^2}{9M_P^4}\,(V_E^F + V_E^D)\,, \tag{5.9}$$

and $\mathcal{A}_\mu$ denoting the purely bosonic part of the auxiliary field of the supergravity Weyl multiplet, which, just like the auxiliary fields appearing in global supersymmetry, can be replaced by its on-shell solution,

$$\mathcal{A}_\mu = -\,\frac{i}{2\Phi}\left[(\partial_\mu z^\alpha)\partial_\alpha\Phi - (\partial_\mu\bar{z})\partial_{\bar{\alpha}}\Phi\right]\,. \tag{5.10}$$

Exploiting this solution, we can rewrite Eq. (5.7) as Eq. (5.8).

To define a theory in a Jordan frame, one thus needs to specify W, K and f (as in the Einstein frame) as well as the frame function Φ. Comparing Eq. (5.8) with Eq. (5.2), switching to the Jordan frame looks like a significant complication, the benefit of which is not yet obvious. However, as we will see in a moment, enforcing superconformal symmetry (cf. Sec. 5.1.2), will allow us to identify a class of models (cf. Sec. 5.1.3) whose description in the Jordan frame is amazingly simple, while indeed the description in the Einstein frame is the more complicated one.

[1] $\mathcal{L}_J^{\text{scal}}$ can in principle be obtained by acting with Eq. (5.6) on the full Einstein frame Lagrangian and then extracting the scalar part. A more elegant derivation of the Jordan frame Lagrangian by exploiting the underlying superconformal symmetry of supergravity is given in Ref. [41].

5.1.2 Superconformal symmetry

Extending the Poincaré symmetry by fermionic generators yields supersymmetry, which as a local symmetry leads to supergravity. A further extension of the Poincaré symmetry is possible for scale-free field theories. We can then require conformal invariance, which imposes in particular the invariance under the simultaneous rescaling of the metric and the fields. Allowing this rescaling factor to vary locally, then leads to a local conformal symmetry. Imposing all of these symmetry requirements together leads to an action with a local $SU(2,1|1)$ superconformal symmetry. This encompasses invariance under local dilatation, special conformal symmetry, special supersymmetry and local $U(1)$ $\mathcal{R}$ symmetry, as well as invariance under supergravity transformations. Among all of these, the local conformal transformations

$$g_{\mu\nu} \mapsto g'_{\mu\nu} = e^{-2\alpha(x)} g_{\mu\nu}\,, \quad z \mapsto z' = e^{\alpha(x)} z\,, \quad \bar{z} \mapsto \bar{z}' = e^{\alpha(x)} \bar{z}\,, \tag{5.11}$$

are of particular importance for the scalar-gravity part of the Lagrangian which we are interested in in the context of inflation.

Starting from a fully superconformal action, the authors of Ref. [41] arrive at the supergravity Lagrangian in an arbitrary Jordan frame by gauge-fixing all the additional degrees of freedom present in the superconformal theory.[2] In particular, the so-called compensator field z^0 is fixed to the Planck scale, introducing the scale M_P into the formerly scale-free theory.

A toy model

With this in mind, one might try to preserve as much of the larger superconformal symmetry as possible. Let us first demonstrate this idea with a toy model, cf. Ref [39]. Consider the non-supersymmetric, conformally invariant Lagrangian

$$\frac{\mathcal{L}_{\text{toy}}}{\sqrt{-g}} = \frac{1}{2}\, g^{\mu\nu}(\partial_\mu \phi)(\partial_\nu \phi) + \frac{1}{12}\, \phi^2 R(g) - \frac{1}{2}\, g^{\mu\nu}(\partial_\mu h)(\partial_\nu h) - \frac{1}{12}\, h^2 R(g) - \frac{\lambda}{4}\, h^2\,, \tag{5.12}$$

for the real scalars h and ϕ. The Lagrangian exhibits a conformal coupling of the scalars to the Ricci scalar $R(g)$ and is invariant under the transformation (5.11). This can be checked explicitly exploiting the transformation behavior of R [183],

$$R \mapsto e^{2\alpha(x)} \left(R - 6\, e^{\alpha(x)} \frac{1}{\sqrt{-g}}\, \partial_\mu \left[g^{\mu\nu} \sqrt{-g}\, \partial_\nu e^{-\alpha(x)} \right] \right)\,. \tag{5.13}$$

The kinetic term of ϕ has the wrong sign. This does, however, not matter since ϕ is identified with the compensator field which is not associated with any physical degrees of freedom.

[2] This for itself interesting observation does neither answer the question of the role of the superconformal symmetry in an underlying quantum gravity theory nor if/how it might be dynamically broken in a way that yields models of the type introduced in Sec. 5.1.3 as an effective field theory. Addressing this challenging question is beyond the scope of this thesis.

Gauge-fixing $\phi = \sqrt{6}M_P$, we obtain

$$\mathcal{L}_{toy}^{\phi=\sqrt{6}M_P} = \sqrt{-g}\frac{M_P^2}{2}R(g) - \sqrt{-g}\left[\frac{1}{2}g^{\mu\nu}(\partial_\mu h)(\partial_\nu h) + \frac{1}{12}h^2 R(g) + \frac{\lambda}{4}h^2\right], \tag{5.14}$$

i.e. an Einstein Hilbert term $\sqrt{-g}\frac{M_P^2}{2}R(g)$, which is not conformally invariant, and the conformally invariant theory for the scalar field h, coupled non-minimally to gravity. Note that the conformal coupling of the scalar fields to gravity automatically leads us to a Jordan frame. Of course, we could now convert the Lagrangian (5.14) into the Einstein frame. However, we then lose the simple structure of the matter part of the Lagrangian, and the conformal symmetry present in the matter sector of the theory becomes well hidden.

5.1.3 A special class of models

In a next step, let us now generalize the toy model (5.12) to a supergravity model with n physical scalar fields. Introducing the $SU(1,n)$ invariant coefficient function of the Ricci scalar

$$\Xi = -|z^0|^2 + |z|^2, \tag{5.15}$$

with $|z|^2 = \delta_{\alpha\bar{\beta}}z^\alpha \bar{z}^{\bar{\beta}}$ and $\alpha, \bar{\beta} = \{1..n\}$, reproduces the structure found in the kinetic terms and frame function of Eq. (5.12). Gauge-fixing the complex compensator field $z^0 = \sqrt{3}M_P$ in order to reproduce the Einstein Hilbert term yields

$$\Xi|_{z^0\to\sqrt{3}M_P} = \Phi(z,\bar{z}) = -3M_P^2 + |z|^2. \tag{5.16}$$

In the toy model above, we started with a scale-free scalar potential for h. Similarly, we will restrict ourselves here to renormalizable superpotentials which are trilinear, i.e. which do not introduce an explicit mass scale. Furthermore, Eq. (5.14) exhibits canonical kinetic terms for the scalar fields in the Jordan frame. We can achieve the same feature in the more general case presented here by employing a Kähler potential constructed from the frame function Φ,

$$K = -3M_P^2 \ln\left(-\frac{1}{3M_P^2}\Phi(z,\bar{z})\right). \tag{5.17}$$

Inserting this into Eq. (5.8) yields $\frac{1}{3M_P^2}\Phi K_{\alpha\bar{\beta}} - (\partial_\alpha\Phi)(\partial_{\bar{\beta}}\Phi)/\Phi = -\partial_\alpha\partial_{\bar{\beta}}\Phi$. Together with the frame function (5.16), this implies canonical kinetic terms for the scalar fields up to Planck-suppressed corrections from the $\mathcal{A}_\mu$ term.[3] Furthermore, we shall restrict ourselves to the situation where the gauge kinetic function is given by $f_{AB} = \delta_{AB}$. This leads us to the so-called canonical superconformal supergravity (CSS) models, cf. Ref [39].

Before proceeding, let us summarize the interesting features of this class of models. In

[3]Note that $\mathcal{A}_\mu = 0$ on inflationary trajectories along the purely real or imaginary part of z, cf. Eq. (5.10).

the Jordan frame, the Lagrangian can be split into two parts: A pure supergravity part and an explicitly superconformal matter sector,

$$\frac{1}{\sqrt{-g_J}}\mathcal{L}_J = \underbrace{\frac{1}{2}M_P^2\left(R(g_J)+6\mathcal{A}_\mu^2\right)}_{\text{pure supergravity}} - \underbrace{\frac{1}{6}R(g_J)|z|^2 - \delta_{\alpha\bar\beta}\,g_J^{\mu\nu}\,(\widetilde\nabla_\mu z^\alpha)(\widetilde\nabla_\nu \bar z^{\bar\beta}) - V_J}_{\text{superconformal matter}}\,, \tag{5.18}$$

with $\widetilde\nabla_\mu z^\alpha = \partial_\mu z^\alpha - i\mathcal{A}_\mu z^\alpha$. For vanishing $\mathcal{A}_\mu$, the kinetic terms of the scalars are canonical with respect to the Jordan frame metric. The scalar potential can be calculated from Eqs. (5.3) and (5.9). From Eqs. (5.17) and for a frame function satisfying $\partial_\alpha\partial_{\bar\beta}\Phi = \delta_{\alpha\bar\beta}$ one obtains the Kähler metric

$$K_{\alpha\bar\beta} = -\frac{3M_P^2}{\Phi}\left(\delta_{\alpha\bar\beta} - \frac{1}{\Phi}\,(\partial_\alpha\Phi)(\partial_{\bar\beta}\Phi)\right). \tag{5.19}$$

One easily verifies that the inverse Kähler metric is given by

$$K^{\alpha\bar\beta} = -\frac{\Phi}{3M_P^2}\left(\delta^{\alpha\bar\beta} + \frac{1}{\Delta_K}\,\delta^{\alpha\bar\gamma}(\partial_{\bar\gamma}\Phi)\,\delta^{\gamma\bar\beta}(\partial_\gamma\Phi)\right), \tag{5.20}$$

where

$$\Delta_K = \Phi - \delta^{\alpha\bar\beta}(\partial_\alpha\Phi)(\partial_{\bar\beta}\Phi)\,. \tag{5.21}$$

Inserting Eq. (5.20) into the expression (5.2), we find the following compact expression for the F-term scalar potential in the Jordan frame[4]

$$V_J^F = \left(\delta^{\alpha\bar\beta}W_\alpha\overline{W}_{\bar\beta} + \frac{1}{\Delta_K}|\delta^{\alpha\bar\beta}W_\alpha\partial_{\bar\beta}\Phi - 3W|^2\right), \tag{5.22}$$

with $W_\alpha = \partial_\alpha W$. For the frame function (5.16) and a trilinear superpotential, this implies that the scalar F-term potential V_J^F in Eq. (5.18) is actually the globally supersymmetric scalar potential, cf. Sec. 2,

$$V_J^F = \delta^{\alpha\bar\beta}W_\alpha\overline{W}_{\bar\beta}\,. \tag{5.23}$$

Next, consider the D-term potential, which is readily calculated from Eqs. (5.3), (5.4) and (5.9). For the Kähler potential (5.17), the solution to the D-term equation of motion (5.4) simplifies to

$$D_A = g\left(-\frac{3M_P^2}{\Phi}\right)\Phi_\alpha(T_A\,z)^\alpha\,, \tag{5.24}$$

yielding the D-term scalar potential in the Jordan frame

$$V_J^D = \frac{1}{2}\,g^2\,(\Phi_\alpha(T_A\,z)^\alpha)^2\,. \tag{5.25}$$

[4]The same expression was derived independently in Ref. [184].

For the frame function (5.16) and $f_{AB} = \delta_{AB}$, this yields the D-term potential

$$V_J^D = \frac{1}{2}\, g^2 \left(\bar{z}^{\bar{\alpha}} T^A_{\bar{\alpha}\beta} z^\beta \right)^2 , \tag{5.26}$$

which again, is just the familiar expression from global supersymmetry!

Hence in the Jordan frame, the structure of these models is remarkably simple. To embed a globally supersymmetric model into supergravity in this framework, the Lagrangian in the Jordan frame is constructed by simply adding the pure supergravity part and the superconformal matter part. For vanishing $\mathcal{A}_\mu$, the superconformal matter part is given by canonical kinetic terms, a conformal coupling to the Ricci scalar and the globally supersymmetric scalar potential.

In the Einstein frame, the model is defined by the superpotential and the Kähler potential (5.17). Exploiting Eqs. (5.19), (5.3) and (5.23), the Einstein frame Lagrangian (5.2) is readily calculated. The scalar potential is the globally supersymmetric potential up to a rescaling $\Phi^2/(9M_P^4)$. The kinetic terms are no longer canonical, but are determined by the Kähler metric (5.19). Performing a field redefinition to achieve canonical kinetic terms induces modifications of the scalar potential, leading in general to quite unpleasant expressions. The simple structure found in a particular Jordan frame is well hidden in the Einstein frame.

5.1.4 Breaking the superconformal symmetry

In Sec. 5.1.3 we discussed a class of models in which the superconformal symmetry was broken only by the pure supergravity part of the action after gauge-fixing the conformal compensator, as well as by the superconformal anomaly[5]. We now extend the discussion to allow for other mechanisms which 'mildly' break the the superconformal invariance, i.e. mechanisms in which the effects of this symmetry breaking are suppressed at low energies. In particular, our goal is to preserve the appealing features of the models discussed above. To this end, we study a modification of the frame function as suggested in [41] as well as the introduction of an Fayet-Iliopoulos term.

A modification of the frame function

As suggested in [39, 41], given the gauge-invariant expression $\chi_{\alpha\beta} z^\alpha z^\beta$ with $\chi_{\alpha\beta}$ dimensionless, superconformal symmetry can be explicitly broken by using instead of (5.15) the real function

$$\Xi(z^0, \bar{z}^0; z, \bar{z}) = -|z^0|^2 + |z|^2 + \left(\chi_{\alpha\beta}\, \frac{z^\alpha z^\beta \bar{z}^0}{z^0} + h.c. \right) . \tag{5.27}$$

[5] The conformal anomaly is due to the non-vanishing vev of the trace of the energy momentum tensor, see e.g. Ref. [185] for an introduction.

After gauge fixing the compensator field as above, one obtains the modified frame function

$$\Phi(z,\bar{z}) = -3M_P^2 + |z|^2 + J(z) + \bar{J}(\bar{z}) \ , \quad J(z) = \chi_{\alpha\beta}\, z^\alpha z^\beta \, . \tag{5.28}$$

In the following analysis the symmetry breaking term $J(z)$ will play an important role. As we shall see, it will turn the single-field D-term inflation model into a two-field inflation model.

Returning to the interesting features observed in Sec. 5.1.3, we note that both the canonical kinetic terms for vanishing $\mathcal{A}_\mu$ and the structure of the Jordan frame potential displayed in Eq. (5.22) only require the frame function to fulfil $\partial_\alpha \partial_{\bar{\beta}} \Phi = \delta_{\alpha\bar{\beta}}$, and hence remain valid for the modified frame function (5.28). Furthermore, from Eq. (5.22), we can directly read off the effect this modification of the frame function on the Jordan frame F-term potential: Assuming a trilinear superpotential, the second term in Eq. (5.22) vanishes for $J(z) = 0$ yielding the globally supersymmetric potential (5.23). However, for non-vanishing $J(z)$ there is an additional term $|\delta^{\alpha\bar{\beta}} W_\alpha \partial_{\bar{\beta}} \bar{J}(\bar{z})|^2/\Delta_K$ in the Jordan frame F-term potential. With Δ_K as defined in Eq. (5.21) containing a contribution $(-3M_P^2)$, we see that for field values smaller than the Planck scale, the corrections due the breaking of the superconformal symmetry in Eq. (5.28) are suppressed. Similarly, the D-term scalar potential obtains corrections due to an additional term $\partial_\alpha J(z)$ arising from $\partial_\alpha \Phi$ in Eq. (5.24).

In the Einstein frame, after inserting the modified frame function (5.28) into the Kähler potential (5.17), terms proportional to $\chi_{\alpha\beta}$ appear in the scalar potential as well as in the kinetic terms.

Fayet-Iliopoulos term

In the context of D-term inflation, we are particularly interested in adding a Fayet-Iliopoulos (FI) - term for a $U(1)$ gauge symmetry to the Lagrangian (5.18). The standard procedure is the following [38]: Since the D-term of a $U(1)$ vector supermultiplet is gauge invariant (up to total derivatives), we can add a term proportional to $g\xi D$ to the Lagrangian, with $\sqrt{\xi}$ denoting a mass scale. This can be implemented by the substitution $D \mapsto D + g\xi$. Starting from the superconformal D-term scalar potential (5.25) for a $U(1)$ symmetry,

$$V_J^D = \frac{1}{2}\, g^2 \left[(\partial_\alpha \Phi) Q z^\alpha\right]^2 =: \frac{1}{2}\, D'^2 \tag{5.29}$$

where Q is the charge generator and $D' = D \times \Phi/(-3M_P^2)$, one might naively attempt to introduce an FI-term in the Jordan frame by substituting $D' \mapsto D' + g\xi$. This, however, would introduce another explicit breaking of the superconformal symmetry, since ξ is a constant of mass dimension two and moreover, this does not reproduce the familiar procedure $D \mapsto D + g\xi$ in the Einstein frame.

In the Jordan frame Lagrangian (5.18) as well as in the modified frame function (5.28), superconformal symmetry breaking only arises from $\Xi(z^0, \bar{z}^0; z, \bar{z})$ after gauge fixing. This

suggests to add to Eq. (5.18) a term with dimensionless constant $\hat{\xi} = \xi/(-3M_P^2)$,

$$\frac{\Delta\mathcal{L}_J^\xi}{\sqrt{-g_J}} = g\hat{\xi}D'\Xi(z^0,\bar{z}^0;z,\bar{z})\big|_{z^0=\sqrt{3}M_P} = -g\left(\frac{\Phi}{3M_P^2}\right)\xi D' \,, \tag{5.30}$$

Note that this implies a field-dependent FI-term in the Jordan frame. Eliminating the auxiliary field D by solving the resulting modified eom and using Eq. (5.9), one then immediately obtains for the D-term scalar potential in the Einstein frame,

$$V_E^D = -\frac{g^2}{2}\left(\left(\frac{-3M_P^2}{\Phi}\right)(\partial_\alpha\Phi)Qz^\alpha + \xi\right)^2 = \frac{g^2}{2}\left((\partial_\alpha K)Qz^\alpha + \xi\right)^2 \,, \tag{5.31}$$

which is the standard supergravity expression [38].

Note that the first expression in Eq. (5.30) can be interpreted as a quartic contribution to the scalar potential of the Jordan frame, i.e. of the type present in the toy model (5.12). So in this sense, the conformal symmetry breaking in the FI-term can be traced back to familiar symmetry breaking mechanisms, i.e. the gauge fixing of the compensator field and the modification of the frame function.

Finally, note that there are, of course, other possibilities to break the superconformal symmetry apart from those listed above. For example, one could drop the requirement of a trilinear superpotential. We will return to this possibility briefly in Sec. 5.2.1, where we discuss F-term hybrid inflation in this framework. Or, one could further modify the frame function and/or the Kähler potential, dropping the requirement of canonical kinetic terms in the Jordan frame. However, one then loses just those features, which made this class of models interesting in the first place. We will therefore in the following stay with the symmetry breaking terms listed above.

5.2 Hybrid inflation

In this section, we shall apply the framework introduced above to two examples, F-term and D-term hybrid inflation. In both cases, we will take the Einstein frame metric to be the FRW metric, and we will introduce a non-minimal coupling of the inflaton field ϕ to gravity while the waterfall fields $S_\pm$ remain minimally coupled, i.e. $J(z) = \frac{\chi}{2}\phi^2$. The frame function is thus given by

$$\Phi = -3M_P^2 + |\phi|^2 + |S_+|^2 + |S_-|^2 + \frac{\chi}{2}(\phi^2 + \bar{\phi}^2) \,, \tag{5.32}$$

with χ chosen to be real, implying the transformation between Jordan and Einstein frame metric

$$g_{J\mu\nu} = \Omega^2 g_{\mu\nu} \,, \quad \text{with } \Omega^2 = -\frac{3M_P^2}{\Phi} \,. \tag{5.33}$$

We will calculate the resulting scalar potentials in the Einstein frame. In Appendix C, using the example of D-term hybrid inflation, we demonstrate that a calculation in the Jordan frame leads to the same results.

5.2.1 F-term inflation

The expression (5.22) holds for all superpotentials and it is instructive to apply it to the superpotential of F-term hybrid inflation [8, 54, 55, 118],

$$W = \lambda\phi\left(S_+S_- - v^2\right) \ . \tag{5.34}$$

Here v is a mass parameter and the coupling λ is chosen to be real.

F-term hybrid inflation typically yields a scalar spectral index which is too large compared to observations, see Eq. (3.9). One may hope to improve the situation by a suitable choice of the χ-parameter of the frame function (5.32). From Eq. (5.22) one obtains for the scalar potential in the Einstein frame

$$V_E^F = \Omega^4\lambda^2\left(|\phi|^2\left(|S_+|^2+|S_-|^2\right)+|S_+S_- - v^2|^2 - \frac{\left|2\,v^2\phi+\chi\left(S_+S_- - v^2\right)\bar{\phi}\right|^2}{3M_P^2+\frac{\chi}{2}(\phi^2+\bar{\phi}^2)+\chi^2|\phi|^2}\right). \tag{5.35}$$

Along the expected inflationary trajectory, i.e. for $S_\pm = 0$, one has

$$V_E^F = \Omega^4\lambda^2v^4 - \frac{\Omega^4\lambda^2v^4\ \left|2\phi-\chi\bar{\phi}\right|^2}{3M_P^2+\frac{\chi}{2}(\phi^2+\bar{\phi}^2)+\chi^2|\phi|^2} \ . \tag{5.36}$$

Unfortunately, this potential exhibits a large tachyonic mass for ϕ and is therefore not phenomenologically viable. This holds for the not canonically normalized parameter ϕ describing the inflationary trajectory as well as for the canonically normalized inflaton $\hat{\phi}$, since for $\phi \ll M_P$, $\hat{\phi} \approx \phi$. This result can be anticipated from Eq. (5.22), where the second term cancels for a scale-invariant, trilinear superpotential but not for a superpotential containing a term linear in the superfields as Eq. (5.34). A notable exception are superpotentials which vanish along the inflationary trajectory.[6] Note that the large tachyonic mass for ϕ could be remedied by adding an $|\phi|^4$ term to the frame function [41, 187]. However, this introduces an additional breaking of the superconformal symmetry and we will not pursue this option here.

5.2.2 D-term inflation

Let us now consider D-term hybrid inflation. It has the attractive feature that in string compactifications an FI-term of GUT-scale size naturally arises, which is welcome for hybrid

[6] In this context, it would be interesting to consider a superconformal version of 'tribrid'-inflation [52, 186], a variant of supersymmetric F-term hybrid inflation which features $W = 0$ along the inflationary trajectory.

inflation. The superpotential reads

$$W = \lambda \phi S_+ S_- \,, \tag{5.37}$$

and for the frame function we again use Eq. (5.32). The corresponding F-term scalar potential in the Einstein frame reads

$$V_E^F = \Omega^4 \lambda^2 \left(|\phi|^2 (|S_+|^2 + |S_-|^2) + |S_+ S_-|^2 - \frac{\chi^2 |S_+|^2 |S_-|^2 |\phi|^2}{3M_P^2 + \frac{1}{2}\chi(\phi^2 + \bar{\phi}^2) + \chi^2 |\phi|^2} \right) . \tag{5.38}$$

This expression agrees with the potential (5.35) in the case $v = 0$. For field values below the Planck mass the potential (5.38) is well behaved. It vanishes identically for $S_\pm = 0$, which corresponds to the inflationary trajectory.

The potential (5.38) is supplemented by a D-term scalar potential of a $U(1)$ symmetry under which the chiral superfields ϕ and $S_\pm$ have charge ρ_0 and $\pm q$, respectively.

$$V_E^D = \frac{g^2}{2} \left(q\, \Omega^2 \left(|S_+|^2 - |S_-|^2 \right) - \xi \right)^2 , \tag{5.39}$$

where g is the gauge coupling. For $S_\pm = 0$, the FI-term provides the vacuum energy density $\rho_0 = g^2 \xi^2 / 2$ which drives inflation.

The slope of the inflaton potential is generated by quantum corrections, cf. Eq. (3.6). Along the inflationary trajectory the Weyl rescaling factor reads

$$\Omega_0 = \Omega\big|_{S_\pm = 0} = \left(1 - \frac{1}{3M_P^2} \left(|\phi|^2 + \frac{\chi}{2} \left(\phi^2 + \bar{\phi}^2 \right) \right) \right)^{-1/2} . \tag{5.40}$$

From Eqs. (5.9), (5.23), (5.25) and (5.19) one then obtains for the part of the Lagrangian quadratic in $S_\pm$,

$$\mathcal{L}_{S_\pm}^{\text{quadr}} = \Omega_0^2\, \partial_\mu S_\pm^* \partial^\mu S_\pm - \left(\Omega_0^4\, \lambda^2\, |\phi|^2 \mp \Omega_0^2\, q g^2 \xi \right) |S_\pm|^2 \,, \tag{5.41}$$

from which one reads off the scalar masses

$$m_\pm^2 = \Omega_0^2\, \lambda^2\, |\phi|^2 \mp q g^2 \xi \,. \tag{5.42}$$

For $|\phi|$ larger than a critical value ϕ_c, both S_+ and S_- have positive mass terms and are stabilized at zero, thus allowing inflation to proceed in the ϕ direction. At $|\phi| = \phi_c$, m_+^2 turns negative, triggering a phase transition which gives an expectation value to S_+ and ends inflation. The critical value ϕ_c is determined by the relation

$$\Omega^2(\phi_c)\, \phi_c^2 = \frac{q g^2 \xi}{\lambda^2} \,. \tag{5.43}$$

According to the mass sum rule, the Dirac fermion associated with $S_\pm$ has mass

$$m_f^2 = \lambda^2 \, \Omega_0^2 \, |\phi|^2 \ . \tag{5.44}$$

Inserting Eqs. (5.42) and (5.44) into the expression for the one-loop potential (3.6) and setting the renormalization scale to $Q^2 = g^2 q \xi$, one obtains for the one-loop potential,

$$\begin{aligned} V_E^{1l} &= \frac{g^4 q^2 \xi^2}{32\pi^2} \left((x-1)^2 \ln(x-1) + (x+1)^2 \ln(x+1) - 2x^2 \ln x - 1 \right) \\ &= \frac{g^4 q^2 \xi^2}{16\pi^2} \left(1 + \ln x + \mathcal{O}\left(\frac{1}{x}\right) \right) \ , \end{aligned} \tag{5.45}$$

where

$$x = \frac{\lambda^2 \, \Omega_0^2 \, |\phi|^2}{q g^2 \xi} = \frac{\Omega_0^2(\phi) \, |\phi|^2}{\Omega_0^2(\phi_c) \, \phi_c^2} \ . \tag{5.46}$$

The total potential for the inflaton field ϕ along the inflationary trajectory is given by, cf. Eqs. (5.38) and (5.45),

$$\begin{aligned} V_E &= (V_E^F + V_E^D + V_E^{1l})\big|_{\phi_\pm = 0} \\ &= \frac{g^2}{2} \xi^2 \left(1 + \frac{g^2 q^2}{8\pi^2} \left[1 + \ln x + \mathcal{O}\left(\frac{1}{x}\right) \right] \right) \ . \end{aligned} \tag{5.47}$$

Note that on the inflationary trajectory one has $|\phi| > \phi_c$ and $x > 1$. Contrary to the scalar potential found for F-term hybrid inflation in Sec. 5.2.1, the potential (5.47) for D-term hybrid inflation looks promising for realizing slow-roll inflation, and we shall thus focus on this scenario in the following.

In this section, we calculated the one-loop correction to the scalar potential in the Einstein frame for the Minkowski metric, $g_{\mu\nu} = \eta_{\mu\nu}$. A calculation in the Jordan frame would have led to the same result, as is demonstrated in Appendix C.

5.3 Single-field inflation

Having determined the scalar potentials of F- and D-term hybrid inflation in CSS models, this section is dedicated to calculating the predictions of superconformal D-term hybrid inflation. Since these predictions are most commonly expressed in terms of the slow-roll parameters in the Einstein frame, cf. Eqs. (3.9) and (3.10), we will stay in the Einstein frame for the remainder of this chapter. The corresponding calculation in the Jordan frame (for the single-field case) is given in Appendix C.

5.3.1 Slow-roll equation of motion

We are now ready to tackle the slow-roll equation of motion for the field ϕ. In the Einstein frame the inflaton field ϕ is not canonically normalized, leading to a modification of the standard slow-roll equations. Expressing the Lagrangian for the field ϕ in terms of real and imaginary components, $\phi = (\varphi + i\kappa)/\sqrt{2}$,

$$\frac{1}{\sqrt{-g}}\mathcal{L} = \frac{1}{2}\, K_{\phi\bar{\phi}}(\varphi,\kappa)\, (\partial_\mu\varphi\, \partial^\mu\varphi + \partial_\mu\kappa\, \partial^\mu\kappa) - V(\varphi,\kappa)\ , \tag{5.48}$$

one obtains the slow-roll equations for the homogeneous fields φ and κ,

$$3K_{\phi\bar{\phi}} H\dot{\varphi} = -\frac{dV_{1l}}{d\varphi}\ , \quad 3K_{\phi\bar{\phi}} H\dot{\kappa} = -\frac{dV_{1l}}{d\kappa}\ , \tag{5.49}$$

where now we have set $M_P = 1$ for convenience. These equations can be written as the standard slow-roll equations, cf. Eq. (3.7), for an effective potential defined by

$$\frac{dV_{\rm eff}}{d\varphi} = \frac{1}{K_{\phi\bar{\phi}}}\frac{dV_{1l}}{d\varphi}\ , \qquad \frac{dV_{\rm eff}}{d\kappa} = \frac{1}{K_{\phi\bar{\phi}}}\frac{dV_{1l}}{d\kappa}\ . \tag{5.50}$$

Calculating the second derivatives of the potential $V_{\rm eff}$ with respect to φ and κ, one finds that for $\chi < 0$, the trajectory $\varphi \neq 0, \kappa = 0$ yields a viable inflationary trajectory along which $d^2V_{\rm eff}/d\kappa^2$ is positive. Hence this trajectory is an attractor for a sufficiently long phase of inflation before the onset of the final 50 e-folds. For $\chi > 0$, the situation is reversed and an equivalent inflationary trajectory corresponds to $\varphi = 0, \kappa \neq 0$. For $\chi = 0$, the Lagrangian is independent of the phase of ϕ and the inflaton can be identified as the absolute value of ϕ. In the following we choose $\chi \leq 0$.

In this section we will restrict ourselves to the standard case of 'one-field' inflation along the ϕ-axis as described above, postponing the discussion of possible two-field inflation to Sec. 5.4. Inserting the Kähler metric

$$K_{\phi\bar{\phi}}\big|_{\phi_\pm,\kappa=0} = \frac{1}{1-\frac{1}{6}(1+\chi)\varphi^2}\left(1 + \frac{(1+\chi)^2\varphi^2}{6\left[1-\frac{1}{6}(1+\chi)\varphi^2\right]}\right)\ , \tag{5.51}$$

and the one-loop potential (5.45) into the slow-roll equation (5.49), one obtains after integrating from φ_* to φ_f,

$$3\ln\left(\frac{1-\frac{1}{6}(1+\chi)\varphi_*^2}{1-\frac{1}{6}(1+\chi)\varphi_f^2}\right) - \frac{\chi}{2}\left(-\varphi_*^2+\varphi_f^2\right) \simeq -\frac{g^2q^2}{4\pi^2}\, N_*\ . \tag{5.52}$$

Here φ_f denotes the value of φ at the end of inflation and φ_* is the value of φ N_* e-folds earlier. Inflation ends when either m_+^2 turns negative ($\varphi_f = \varphi_c$) or when the slow-roll conditions are

violated ($\varphi_f = \varphi_\eta$). From Eq. (5.43) and Eq. (5.57) with $|\eta| = 1$, one finds

$$\varphi_c^2 = \frac{6g^2q\xi}{3\lambda^2 + (1+\chi)g^2q\xi} \ , \qquad \varphi_\eta^2 \approx \frac{g^2q^2}{4\pi^2} \ . \tag{5.53}$$

For small field values, satisfying $|1+\chi|\varphi_*^2/6 \ll 1$, Eq. (5.52) can be solved analytically, leading to

$$\varphi_*^2 \simeq \varphi_f^2 + \frac{g^2q^2}{2\pi^2} N_* \ . \tag{5.54}$$

However, for most of the parameter space this is not a particularly good approximation, and one has to solve Eq. (5.52) numerically.

5.3.2 Slow-roll parameters

In order to calculate the spectral index and other observables, we need to evaluate the slow-roll parameters (3.10) obtained from the derivatives of the scalar potential with respect to the canonically normalized inflaton $\hat{\varphi}$. The latter is determined by (cf. Eq. (5.48))

$$\frac{d\varphi}{d\hat{\varphi}} = \frac{1}{\sqrt{K_{\phi\bar{\phi}}}} \ . \tag{5.55}$$

On the inflationary trajectory the derivatives of the scalar potential with respect to $\hat{\varphi}$ can be written as

$$\begin{aligned} V'(\hat{\varphi}) &= \frac{dV_{1l}}{d\hat{\varphi}} = \frac{dV_{1l}}{d\varphi}\frac{d\varphi}{d\hat{\varphi}} \ , \\ V''(\hat{\varphi}) &= \frac{d^2V_{1l}}{d\hat{\varphi}^2} = \frac{d\varphi}{d\hat{\varphi}}\frac{d}{d\varphi}\left(\frac{dV_{1l}}{d\hat{\varphi}}\right) \ , \end{aligned} \tag{5.56}$$

from which one obtains the slow-roll parameters

$$\begin{aligned} \epsilon &\simeq 2\left(\frac{g^2q^2}{8\pi^2}\right)^2 \frac{1}{\varphi^2}\frac{1}{1+\frac{1}{6}\chi(1+\chi)\varphi^2} \ , \\ \eta &\simeq -\frac{g^2q^2}{4\pi^2}\frac{1}{\varphi^2}\frac{\left[1-\frac{1}{6}(1+\chi)\varphi^2\right]\left[1+\frac{1}{3}\chi(1+\chi)\varphi^2\right]}{\left[1+\frac{1}{6}\chi(1+\chi)\varphi^2\right]^2} \ . \end{aligned} \tag{5.57}$$

Note that for $\chi = -1$, one obtains the results for D-term inflation in global supersymmetry.

5.3.3 Results and discussion

Normalization of the scalar power spectrum and cosmic strings

The normalization condition for the amplitude of the primordial power spectrum and the cosmic string bound represent observational constraints which have to be fulfilled by a viable model, cf. Sec. 3.3. Using Eq. (5.45) the amplitude of the primordial scalar contribution to the

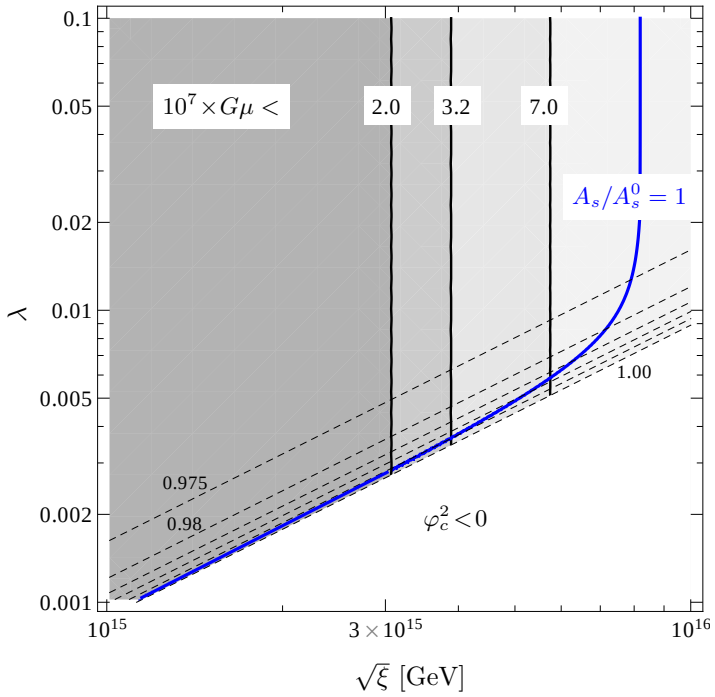

Figure 5.1: Normalization condition and cosmic string bound for $\chi = -15$, $q = 2$, $g^2 = 1/2$ and $N_* = 50$. The blue line shows the relationship between ξ and λ imposed by the correct normalization of the amplitude of the primordial fluctuations. The vertical black lines denote a cosmic string tension of $10^7\, G\mu = 2, 3.2$ and 7, respectively; the darker shaded regions to the left are in agreement with the respective constraint. The dashed lines show contours of constant scalar spectral index. The white region to the bottom right must be excluded since there is no positive solution to $m_+^2(\varphi_c^2) = 0$.

power spectrum of the temperature anisotropies in the CMB, cf. Eq. (3.9), can be expressed as

$$A_{\rm s} \simeq \frac{2\pi^2}{3}\,\frac{\xi^2\varphi_*^2}{g^2q^4}\left[1 + \frac{1}{6}\chi(1+\chi)\varphi_*^2\right] . \tag{5.58}$$

Comparing this to the observed value A_s^0, cf. Eq. (3.18), one obtains a relation between ξ and λ for given values of χ, q and g. As an example, we choose $q = 2$ and $g = 1/\sqrt{2}$ in the following, which is motivated by identifying the spontaneously broken $U(1)$ symmetry with $U(1)_{B-L}$, cf. Chapter 2. For $\chi = -15$, the resulting relation between ξ and λ is depicted by the blue line in Fig. 5.1.

Concerning the cosmic string bound (3.9), we find

$$G\mu = 5.3 \times 10^{-7}\left(\frac{2}{q}\,\frac{\xi}{(5\times 10^{15}\ \text{GeV})^2}\right) . \tag{5.59}$$

where we have inserted the vacuum expectation value of the waterfall field, $\langle S_+\rangle = (\xi/q)^{1/2}$, as well as $m_G^2 = m_\varphi^2 = 2g^2q\xi$ into Eq. (3.14). The solid black lines in Fig. 5.1 correspond to the string tensions $G\mu = (2, 3.2, 7)\times 10^{-7}$. The brighter region to the right of a given line is

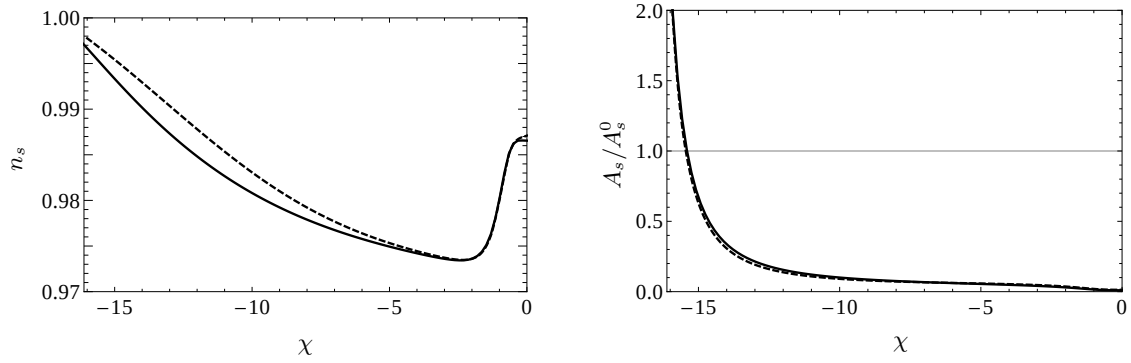

(a) (b)

Figure 5.2: Spectral index and amplitude of the scalar power spectrum for $\sqrt{\xi} = 4.0\times10^{15}$ GeV, $\lambda = 3.8\times10^{-3}$, $q = 2$, $g^2 = 1/2$, $N_* = 50$. The solid lines show the numerical results, the dashed lines the analytical ones. The values of ξ and λ are chosen such as to be compatible with the cosmic string bound as well as the normalization constraint, cf. (3.18), for $\chi = -15$ (cf. Fig. 5.1).

excluded, whereas the darker region to the left is in agreement with the respective bound. In particular, $G\mu = 3.2 \times 10^{-7}$ corresponds to the maximal string tension allowed by the Planck data at 95% CL, cf. Eq. (3.18). Note however that the upper bounds on the string tension come with a considerable theoretical uncertainty, cf. Sec. 3.2.2.

Spectral index

With the slow-roll parameters from Eqs. (5.57) and the value of φ evaluated N_* e-folds before the end of inflation, cf. Eq. (5.52), at hand, we can now easily calculate the spectral index, cf. Eq. (3.9). Fig. 5.2(a) shows the resulting χ dependence for a (ξ, λ) pair compatible with the cosmic string bound and the normalization condition (3.18) at $\chi = -15$ (cf. Fig. 5.1). For reference, Fig. 5.2(b) shows the corresponding χ-dependence of the amplitude of scalar power spectrum. Both curves are shown over the entire range of allowed χ-values for this choice of ξ and λ, which is bounded from below by the condition that φ_c^2 in Eq. (5.53) is positive.

The dashed lines show the results obtained by using the analytical formulas (3.9) and (5.57) with φ_* determined by Eq. (5.52), the solid lines show the full numerical results. The deviation visible in Fig. 5.2(a) is due to the approximation of the one-loop potential, which enters in the derivation of Eq. (5.52) and in the expressions for the slow-roll parameters ϵ and η. To obtain the numerical result, we do not use this approximation, but proceed with the full expression given in the first line of Eq. (5.45). Note, however, that these corrections only influence the result for the spectral index at the per mille level, proving that the analytical expressions derived above do indeed give a good description of the full numerical results.

Throughout the parameter region compatible with the normalization condition and the cosmic string bound, the spectral index is rather high, $n_s \simeq 0.99 - 1.0$, compared to the recently published results from the Planck collaboration, cf. Eq. (3.18). A spectral index of

$n_s = 1$ is compatible with the Planck data within the 5σ range, however, there is clearly a significant tension building up here. For comparison, note that based on data sets available before the publication of the Planck data, a spectral index of $n_s = 1$ was compatible with the data at 2.4σ when allowing for a cosmic string contribution [188].

Discussion

The qualitative behaviour of the relation between the coupling λ and the inflationary energy scale $\sqrt{\xi}$, displayed in Fig. 5.1, can be easily understood. In the case of small coupling, $\lambda \lesssim 0.01$, one has $\varphi_*^2 \simeq \varphi_c^2$ (cf. Eq.(5.53)). The correct fluctuation amplitude is then obtained for small values of $\sqrt{\xi}$ and the cosmic string bound can be satisfied. However, the field value φ_* is large, and one therefore obtains a large spectral index, $n_s \simeq 1$. On the other hand, for large couplings λ, one has $\varphi_f^2 \ll 1$. For large values of $(-\chi)$, Eq. (5.52) then implies for the field value φ_* at N_* e-folds,

$$\varphi_*^2 \simeq -\frac{g^2 q^2 N_*}{2\pi^2 \chi} \ . \tag{5.60}$$

Interestingly, the amplitude of scalar fluctuations is then only determined by the energy density during inflation, $\rho_0 = g^2\xi^2/2$ (cf. Eq. (5.58)),

$$A_s \simeq \frac{\rho_0}{18\pi^2} N_*^2 \ . \tag{5.61}$$

For the spectral index one finds[7]

$$n_s \simeq (1 - 2\eta)\big|_{\varphi_*} \simeq 1 - \frac{2}{N_*} \simeq 0.96 \ . \tag{5.62}$$

Contrary to the amplitude of scalar fluctuations, the string tension additionally depends on the coupling strength gq (cf. Eq. (5.59)),

$$G\mu = 5.3 \times 10^{-7} \left(\frac{2\sqrt{2}}{gq} \frac{\rho_0^{1/2}}{(5 \times 10^{15} \text{ GeV})^2} \right) \ . \tag{5.63}$$

Hence, for large values of $(-\chi)$ and λ, it is always possible to satisfy the cosmic string bound by increasing gq while at the same time keeping n_s small. This is in contrast to the case where $|1+\chi|\varphi_*^2/6 \ll 1$ and $\varphi_c^2 \ll \varphi_*^2$, with φ_* given by Eq. (5.54). In this case the amplitude is given by $A_s \simeq 2\epsilon N_*/(3g^2q^2)$ and thus also fixes the string tension. However, increasing gq by too much one moves to a regime of strong coupling and the theoretical consistency of the model becomes questionable. In this thesis, we will not pursue this option.

For the other CMB observables, i.e., the tilt of the spectral index $dn_s/d\ln k$ and the tensor-to-scalar ratio r, we find small values, well within the experimental bounds [1]. For

[7] Note the difference to D-term inflation in global supersymmetry, where one has $n_s \simeq 1 - \frac{1}{N_*} \simeq 0.98$, see Ref. [189].

instance, for the parameter point discussed above, $\sqrt{\xi} = 4.0 \times 10^{15}$ GeV, $\lambda = 3.8 \times 10^{-3}$, $q = 2$, $g^2 = 1/2$, $\chi = -15$ and $N_* = 50$, one obtains

$$\begin{aligned} dn_s/d\ln k &= 16\,\epsilon\,\eta - 24\,\epsilon^2 - 2\,\frac{V'V'''}{V^2}\Big|_{\varphi=\varphi_*} = -1.7 \times 10^{-4}\,, \\ r &= 16\epsilon\,\Big|_{\varphi=\varphi_*} = 8.9 \times 10^{-6}\,. \end{aligned} \tag{5.64}$$

In conclusion, Fig. 5.1 shows that there is a considerable region in parameter space which is compatible with the normalization condition as well as the cosmic string bound. However, for generic gauge coupling strengths gq, this implies a rather large value for the spectral index. Vice versa, in the region of parameter space which yields a spectral index close to the best-fit value $n_s \simeq 0.963$, we find a cosmic string tension exceeding the cosmic string bound. In the intermediate region of parameter space in between these two limiting cases, we thus find a high contribution of cosmic strings close to the current bounds as well as a value for the spectral index which is slightly larger than the measured value, both within the 3-sigma error bands of the respective best-fit values. Clearly, upcoming experiments will provide further stringent tests of superconformal D-term hybrid inflation.

It is worth stressing that the discussed parameter region allows for large values of the gauge coupling constant g, compatible with grand unification. In this respect, the model presented here differs significantly from D-term inflation with canonical Kähler potential. In the latter case, the masses entering the one-loop potential carry $\exp(|\phi|^2)$ factors, leading to problems for the super-Planckian values of $|\phi|$ typically obtained in D-term inflation. Avoiding this forces the gauge coupling g to be small, $g \lesssim 2 \times 10^{-2}$, as found e.g. in Ref. [190].

5.4 Two-field inflation

5.4.1 Two-field versus single-field inflation

In the previous section, we focused on the situation where one of the two real degrees of freedom of the complex scalar field ϕ plays the role of the inflaton, whereas the value of the other degree of freedom is fixed at zero. This is the case if either the second degree of freedom has a mass of order of the Hubble scale or if inflation before the onset of the final 50 e-folds lasted sufficiently long, so that the inflationary trajectory in the direction of the smallest curvature has become an attractor. However, with the mass difference between φ and κ governed by the symmetry breaking parameter χ, typically both masses are below the Hubble scale, resulting in a two-field inflation model. This section is hence dedicated to investigating alternative possible trajectories in (φ, κ) field space.

In single-field hybrid inflation, inflation ends at the critical value of the inflaton field, φ_f, determined by the zero point of the mass of the waterfall field, $m_+(\varphi_f) = 0$.[8] The

[8] Here and in the following, we assume that the slow-roll conditions hold until the inflaton field reaches its

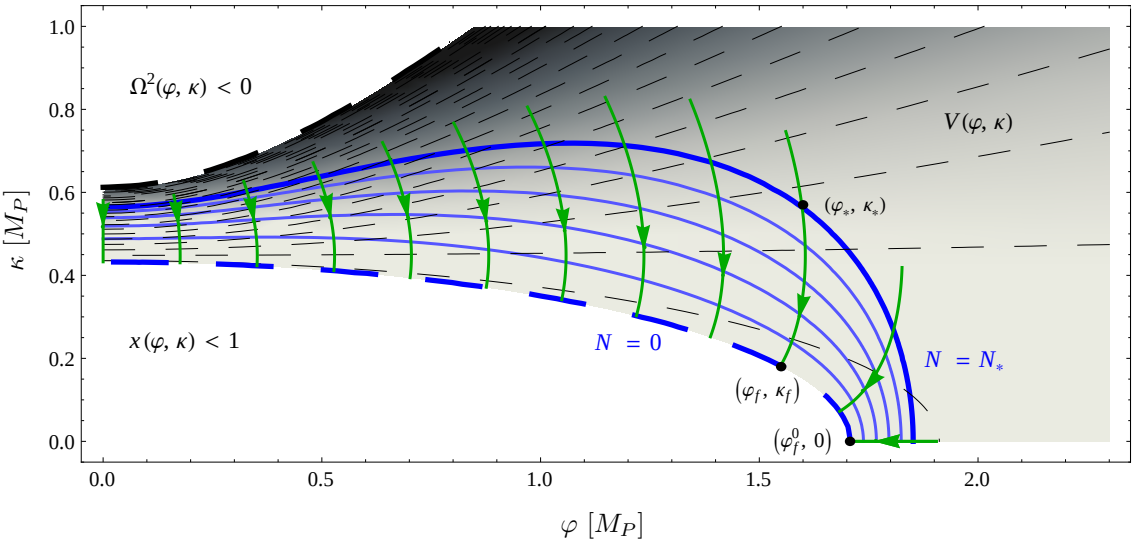

Figure 5.3: Inflationary trajectories in (φ, κ) field space for $\chi = -15$, $\lambda = 3.8 \times 10^{-3}$, $\sqrt{\xi} = 4.0 \times 10^{15}$ GeV, $g^2 = 1/2$ and $q = 2$. Contour lines of the scalar potential are denoted by dashed lines. The dashed blue line marks the $m_+ = 0$ condition, the green solid lines show several examples of inflationary trajectories. The blue lines show contours of the number of e-folds N, from $N = 0$ to $N = N_* = 50$. The single field case discussed in Sec. 5.3 corresponds to the trajectory coinciding with the φ-axis.

starting point φ_* of the inflationary trajectory is determined by solving the slow-roll equation. In two-field inflation, the condition $m_+(\varphi_f, \kappa_f) = 0$ defines a line in (φ, κ) field space. From each point on this line $(\varphi_f, \kappa_f(\varphi_f))$, a classical inflationary trajectory can be uniquely determined by solving the set of slow-roll equations (5.49). The resulting trajectory ends at $(\varphi_*(\varphi_f), \kappa_*(\varphi_f))$. The single-field case discussed in Sec. 5.3 is reproduced for $(\varphi_f, \kappa_f) = (\varphi_f^0, 0)$, where φ_f^0 is given by Eq. (5.53). Hence in two-field inflation, as opposed to single-field inflation, the inflationary predictions are not uniquely determined by the parameters of the Lagrangian, but depend on an additional parameter which labels the various possible trajectories. In the notation above, this additional parameter is φ_f. This is illustrated in Fig. 5.3.

A generalization of the usual single-field formulas for the amplitude of the scalar fluctuations and the spectral index to the case of multi-field inflation with a non-trivial metric in field space can be found in Ref. [191]. Starting from the action

$$S = \int d^4x \, \sqrt{-g} \left[\frac{1}{2} \, h_{ab} \, g^{\mu\nu} \partial_\mu \phi^a \partial_\nu \phi^b - V(\phi) \right] , \tag{5.65}$$

with $g_{\mu\nu}$ denoting the spacetime metric, h_{ab} the metric on the real scalar field space and ϕ^a the real scalar fields of the theory, the slow-roll conditions read

$$(\partial^a V)(\partial_a V) \ll V^2 \quad \text{and} \quad \sqrt{(\nabla^b \partial^a V)(\nabla_b \partial_a V)} \ll V \, . \tag{5.66}$$

critical value.

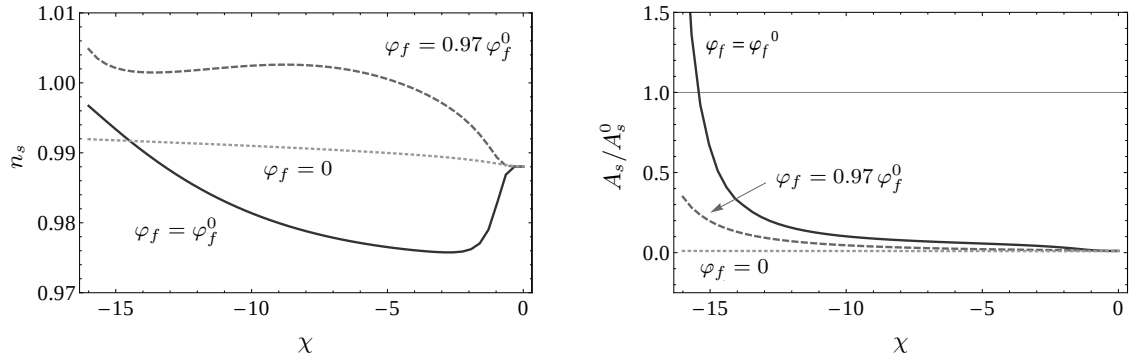

(a) (b)

Figure 5.4: Spectral index and amplitude of the scalar fluctuations resulting from different inflationary trajectories for the same values of model parameters as in the single-field case depicted in Fig. 5.2, i.e. $\sqrt{\xi} = 4.0 \times 10^{15}$ GeV, $\lambda = 3.8 \times 10^{-3}$, $q = 2$, $g^2 = 1/2$ and $N_* = 50$.

Here the usual partial and covariant derivatives in scalar field space are denoted by $\partial_a = \partial/\partial\phi^a$ and $\nabla_a X^b = \partial_a X^b + \Gamma^b{}_{ca} X^c$, with the Christoffel symbols $\Gamma^a{}_{bc} = \frac{1}{2} h^{ad}(\partial_c h_{db} + \partial_b h_{dc} - \partial_d h_{bc})$ As usual, the metric h_{ab} can be used to raise or lower indices. For inflationary trajectories satisfying these conditions, the authors of Ref. [191] obtain the following expressions for the amplitude of the primordial power spectrum and the spectral index:

$$\begin{aligned} A_s &= \left(\frac{H^2}{2\pi}\right)^2 h^{ab}(\partial_a N)(\partial_b N)\,, \\ n_s - 1 &= \frac{\left[2\,\nabla_b \partial^a \ln V + \left(\frac{2}{3} R^a{}_{cbd} - h^a{}_b h_{cd}\right)(\partial^c \ln V)(\partial^d \ln V)\right](\partial_a N)(\partial^b N)}{(\partial_e N)(\partial^e N)}\,, \end{aligned} \tag{5.67}$$

with N denoting the number of e-folds, h^{ab} the inverse metric, $h^a{}_b = \delta^a_b$ and $R^a{}_{bcd}$ the scalar field space curvature tensor, $R^a{}_{bcd} = \partial_c \Gamma^a{}_{bd} - \partial_d \Gamma^a{}_{bc} + \Gamma^a{}_{ce}\Gamma^e{}_{db} - \Gamma^a{}_{de}\Gamma^e{}_{cb}$.

The number of e-folds N as a function of the scalar fields ϕ^a is determined by integrating along all possible classical trajectories. Each point in field space lies on exactly one classical trajectory. Integrating along this trajectory yields the value of N at this point in field space, which is illustrated by the solid blue contour lines in Fig. 5.3.

5.4.2 Two-field results

Fig. 5.4 shows the spectral index and the amplitude of the scalar power spectrum corresponding to different inflationary trajectories. The solid lines represent the results for the trajectory along the φ-axis, i.e. for $\varphi_f = \varphi_f^0$, hence reproducing the single-field results depicted in Fig. 5.2. The dotted lines correspond to the other extremal case in which the inflationary trajectory runs along the κ-axis, i.e. in which $\varphi_f = 0$. Finally, the dashed lines show the results for an intermediate trajectory with non-trivial evolution in both φ- and κ-direction.

As illustrated in Fig. 5.4(b), the amplitude of the scalar power spectrum becomes smaller the more the inflationary trajectory deviates from the φ-axis. This can be understood by consulting the single-field expression for A_s in Eq. (5.58). Interpreting V' appearing in this expression as the derivative of the scalar potential along the respective inflationary trajectory, the single-field expression for A_s may serve as a lowest-order approximation of the full multi-field expression in Eq. (5.67). From Eq. (5.58) it is then apparent that a steeper potential, i.e. a larger V', entails a smaller amplitude. Since for negative χ the scalar potential indeed becomes steeper the further one moves along the $N = N_*$ contour towards the κ-axis, cf. Fig. 5.3, this explains our observation in Fig. 5.4(b).

Concerning n_s, we find that the minimal value of n_s as a function of χ is typically enhanced when considering trajectories involving a motion in the κ-direction. In the limit $\chi \to 0$, the three curves for the scalar spectral index as well as the amplitude in Fig. 5.4 respectively converge to common values. This reflects the fact that for $\chi = 0$ the phase of the complex inflaton field ϕ becomes unphysical, rendering all possible trajectories equivalent to each other.

For fixed values of the parameters ξ and λ, the normalization condition, cf. Eq. (3.18), can be used to eliminate the parameter φ_f, which we introduced to distinguish between the different inflationary trajectories. According to Fig. 5.4, with $\sqrt{\xi} = 4.0 \times 10^{15}\,\text{GeV}$ and $\lambda = 3.8 \times 10^{-3}$, it is for instance possible to find for each χ value below $\chi \simeq -15.4$ one particular φ_f, i.e. one inflationary trajectory such that $A_s = A_s^0$. It is important to note that it is only these sets of parameter values, which are compatible with the normalization condition, that we are allowed to consider when asking for the range of viable n_s values predicted by our model.

In order to determine this range of admissible n_s values, we perform a numerical scan of the parameter space and record n_s for all values of the parameters ξ, λ, χ and φ_f that yield an amplitude A_s within the 3-sigma range of the best-fit value A_s^0, cf. Eq. (3.18). Fig. 5.5 presents the results of this analysis for three representative values of the coupling constant, $\lambda = (5, 10, 20) \times 10^{-3}$, while keeping $g^2 = 1/2$ and $q = 2$. For each λ value, we vary χ between -30 and 0 and φ_f between 0 and φ_f^0, where φ_f^0 is a function of χ, cf. Eq. (5.53). Furthermore, for each λ value, we vary ξ within a small interval, so that we cover the entire region in parameter space where the amplitude comes out within 3 sigma of the best-fit value A_s^0. The lower boundaries of these intervals roughly coincide with the respective ξ values one would need in the case of single-field inflation to obtain the correct amplitude, i.e. they lie on the solid blue curve in the equivalent of Fig. 5.1 for $\chi = -30$. This is due to the decrease in the amplitude with decreasing $|\chi|$ as well as with decreasing φ_f/φ_f^0, cf. Fig. 5.4(b). In order to compensate for this decrease one has to employ ξ values in the two-field case that are a bit larger than in the single-field case. The resulting range of n_s values obtained for a given value of λ is marked by the shaded regions bounded by curves with a given stroke style in Fig. 5.5. Additionally, the solid-dashed curve marks the (pre-)Planck bound on the

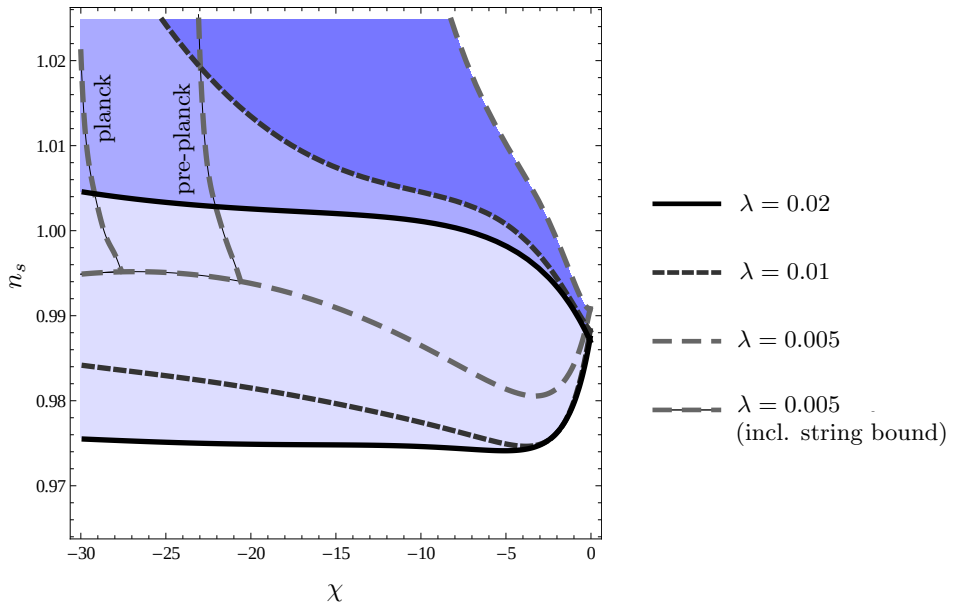

Figure 5.5: Possible values of the spectral index n_s as a function of χ. The shaded region bounded by a curve with a given stroke style shows the range of possible n_s values achieved by varying the inflationary trajectory for a given value of λ, while constraining the corresponding values of the amplitude to the 3-sigma range of the observed value A_s^0. For $\lambda = 0.005$, the region to the top left, bounded by the grey solid-dashed curve, is in accordance with the cosmic string bound $G\mu < 3.2 \times 10^{-7}$ [2], left) and $G\mu < 4.2 \times 10^{-7}$ [188], right), respectively.

cosmic string tension $G\mu = 3.2\,(4.2) \times 10^{-7}$ for $\lambda = 5 \times 10^{-3}$, with the region to the left of this curve in agreement with the bound. We clearly see the effect of the new Planck data on the model: whereas combining pre-Planck data sets [188], a significant region of the $\lambda = 5 \times 10^{-3}$ parameter space shown was still viable, the new bounds [2] restrict the viable region to $\chi < -27$. Of course, χ values smaller than shown in Fig. 5.5 are also still possible. For the two larger values of λ, the cosmic string bound is violated in the entire depicted χ-range.

The general trend in Fig. 5.5 is the same as in the case of single-field inflation, cf. Fig. 5.1: small λ values yield a large spectral index, while larger λ values give smaller n_s values. For instance, for $\lambda = 2 \times 10^{-2}$, we are able to reach n_s values below 0.98 for nearly the entire range of χ values. This illustrates that our model is in principle capable of generating a spectral index of the right magnitude, while simultaneously providing the correct amplitude of the scalar power spectrum. An obvious problem, however, is that in order to reproduce the observed amplitude A_s^0, we require quite large ξ values, such that the cosmic string tension becomes unpleasantly large. Considering trajectories different from the φ-axis, i.e. different from the trajectory studied in Sec. 5.3, increases the tension imposed by the cosmic string bound, since the decrease in the amplitude due to the motion in the κ-direction forces us to go to even larger values of ξ and hence larger values of $G\mu$. Moreover, we note that

among the viable values for n_s for a given value of λ and χ, the spectral index comes out smaller for inflationary trajectories closer to the φ-axis. In a universe undergoing a sufficiently long period of inflation, it may, however, not require much fine-tuning to end up with an inflationary trajectory running close to the φ-axis during the last N_* e-folds of inflation, cf. the comment below Eq. (5.50).

In this chapter, we derived an alternative scenario of hybrid inflation to the one employed in Chapter 3. Starting from a class of models which feature a conformal symmetry of the matter sector and an amazingly simple structure in the Jordan frame, we worked out the predictions for the simplest realization of D-term inflation in this setup. An interesting next step would be to extend the model described here to a more complete setup containing additional fields, possibly identifying the phase transition at the end of inflation with the $B-L$ phase transition as in Chapter 3. This might also alleviate the current tension of the minimal model presented here with the recent Planck data [2].

Conclusion and Outlook

The cosmological realization of spontaneous $U(1)_{B-L}$ breaking can account for inflation as well as for the production of matter and dark matter in accordance with all experimental bounds. In particular, the false vacuum of $B-L$ drives F-term hybrid inflation, ending in a $B-L$ breaking phase transition governed by tachyonic preheating. At the end of this non-perturbative process, the universe is dominated by non-relativistic $B-L$ Higgs bosons and cosmic strings. This sets the initial conditions for the following perturbative reheating phase. Here, the most important process is the decay of the $B-L$ Higgs bosons into relativistic, nonthermal right-handed neutrinos, which in turn decay into the MSSM degrees of freedom forming the thermal bath. Consequently, the parameters governing this process are the effective neutrino and Higgs decay rates. Remarkably, this reheating process does not only generate the entropy of the thermal bath but simultaneously generates a lepton asymmetry via the decay of thermally and nonthermally produced right-handed neutrinos and moreover, generates a gravitino abundance which can account for the dark matter abundance observed today. In summary, we find that spontaneous $B-L$ breaking can account for the origin of the hot early universe, with all cosmological processes determined by the parameters of a fundamental Lagrangian, i.e. the masses and couplings of elementary particles.

This is particularly true for the reheating temperature, which, in our model, is no longer an input parameter, but is determined by the parameters of the neutrino and $B-L$ Higgs sector. A characteristic feature is an epoch of approximately constant temperature, during which the expansion of the universe is just balanced by entropy production. During this epoch, the main part of the lepton asymmetry and the gravitino abundance is produced. This explains why the reheating temperature establishes a connection between the resulting matter-antimatter asymmetry and dark matter abundance, thus enabling us to derive relations between the neutrino parameters and the superparticle mass spectrum. Moreover, the existence of a plateau in the temperature evolution simplifies the analytical description of the process and allowed us to derive semi-analytical formulas for the output of the reheating process. In view of the prospect of possibly probing the reheating temperature by a measurement of the gravitational wave background, these semi-analytical expressions are particularly useful to determine which fundamental parameters of the theory could be constrained by such a measurement.

Considering the generation of matter and dark matter, our model features a rich phenomenology. The matter asymmetry is produced via leptogenesis with a thermal and a nonthermal contribution. The former is generated by right-handed neutrinos and sneutrinos originating from the thermal bath, whereas the latter is predominantly due to nonthermal neutrinos produced in $B-L$ Higgs boson decays. We tracked both contributions explicitly throughout the reheating process, identifying the regions in parameter space where they are important, respectively. For dark matter we considered two possibilities, depending on the hierarchy of the superparticle mass spectrum. If the gravitino is the LSP, then gravitino dark matter can be thermally produced during the reheating process in just the right amount to explain today's dark matter abundance. This places constraints on the parameter space. For example, for a gluino mass of 1 TeV, we found a lower bound on the gravitino mass of about 10 GeV. The order of magnitude of M_1, the mass of the lightest of the heavy neutrinos, is 10^{11} GeV. For a wide range of light neutrino masses this results in a reheating temperature of order $10^9 - 10^{10}$ GeV. If, on the contrary, the gravitino is the heaviest particle of the spectrum and the LSP is a neutralino, then the latter is produced nonthermally in the decay of gravitinos generated during reheating, as well as thermally, invoking the usual freeze-out mechanism. Also in this case we found relations between the parameters of the neutrino sector and the superparticle mass spectrum. For instance, if the LSP is a higgsino, a mass of the lightest neutrino of 0.05 eV would require a higgsino mass below 900 GeV and a gravitino mass of at least 10 TeV.

Turning to inflation, supersymmetric F-term hybrid inflation can naturally be accommodated in the superpotential describing the $B-L$ phase transition. The inflaton field is part of a gauge singlet supermultiplet governing the dynamical transition from the $B-L$ conserving phase to the true vacuum, where $B-L$ is broken. The $B-L$ Higgs fields can be identified as the waterfall fields of hybrid inflation. Requiring the correct normalization of the primordial power spectrum and consistency with bounds on the cosmic string tension, the scale of $B-L$ breaking is fixed to roughly $v_{B-L} \simeq 5 \times 10^{15}$ GeV. Supersymmetric F-term hybrid inflation generically yields a value for the scalar spectral index n_s which is somewhat larger than the observed value. This can be remedied by adding additional higher-dimensional terms to the Kähler potential and tuning their coefficients to reproduce $n_s \sim 0.96$.

In the attempt of avoiding such a tuning in the coefficients of the Kähler potential, we investigated a second inflation model, dubbed superconformal D-term inflation. This is an example of a larger class of models referred to as canonical superconformal supergravity models in [39]. These exhibit an amazingly simple structure in the Jordan frame. For example, the matter sector respects the superconformal symmetry and features canonical kinetic terms as well as a scalar potential which closely resembles the scalar potential of global supersymmetry. We find that in such a setup, supersymmetric F-term hybrid inflation cannot be realized, but implementing D-term hybrid inflation leads to an interesting and predictive model. We

generically find a two-field D-term inflation model with the trajectory along the real part of the inflaton field as an attractor. For this attractor, we analytically calculated the predictions for the primordial power spectrum, both in the Einstein and in the Jordan frame, thus demonstrating that both methods lead to the same result. This might prove useful for future work in this field, since the calculation in the Jordan frame, although less familiar, turns out to be significantly simpler. For the general two-field situation, we determined the outcome of inflation numerically. We find that large values of the $U(1)$ gauge coupling g, compatible with grand unification, are possible, and that a spectral index as low as $n_s \sim 0.96$ can be achieved. However, simultaneously requiring a small spectral index and a low cosmic string tension in accordance with the recent findings of the Planck satellite [2] disfavours this simplest model of superconformal D-term inflation at about 3σ. Nevertheless, this model can serve as a promising starting point for future work. A number of questions remain to be addressed. Can the $U(1)$ symmetry broken at the end of D-term inflation be related to $U(1)_{B-L}$? Moreover, the MSSM field content needs to be included into the model, with particular focus on possible flat directions during inflation. In both the F- and D-term model considered, it would be interesting to investigate a possible embedding into an (orbifold) GUT setup.

A promising possibility of testing early universe models is by a measurement of the gravitational wave background. We therefore calculated the entire GW spectrum associated with the $B-L$ phase transition. The contribution from Abelian Higgs cosmic strings has a very similar shape to the spectrum stemming from inflation but with an amplitude which is roughly eight orders of magnitude larger for typical parameter values. This opens up the possibility to probe the reheating temperature with future gravitational wave detectors such as BBO or DECIGO, even for models in which the GW background from inflation is suppressed by a small tensor-to-scalar ratio. Combining this with the results obtained from requiring the correct dark matter abundance and a sufficient baryon asymmetry, we found testable relations between f_{RH}, the frequency associated with a kink in the GW spectrum due to reheating, and parameters of the neutrino and superparticle mass spectrum. However, the prediction for the GW spectrum from cosmic strings is plagued with large theoretical uncertainties due to the technical problem of performing simulations over vast ranges of scales and to the physical question of how cosmic strings primarily lose energy. As a result, the predictions of the Abelian Higgs and the Nambu-Goto model differ not only in the shape of the spectrum, but also the normalization in the NG model is found to be five orders of magnitude larger than in the AH model. Consequently, in this case the resulting GW spectrum could already by discovered with eLISA or advanced LIGO. Clearly, these theoretical uncertainties require further study. In particular, including the effect of gravitational backreaction into the NG simulations (which is thought to determine the size of the cosmic string loops, an otherwise free parameter) and increasing the simulation length of AH simulations might shed light on the question of if, when and how these models converge [28]. Another challenging task is

the measurement of the GW background in the high frequency range relevant for preheating. These frequencies are currently out of reach for existing and planned GW detectors. However, there are some (rather speculative) ideas on how to tackle this task in the future, see Ref. [3] and references therein. In the context of our model, such a measurement would yield independent determinations of the model parameters M_1, m_S and $\tilde{m}_1$, allowing to test our predictions.

Throughout this thesis, we assumed a $B-L$ breaking scale of $v_{B-L} = 10^{15}$ GeV, motivated by the analysis in Ref. [118], requiring consistency between F-term hybrid inflation and bounds on the cosmic string tension. However, as was recently pointed out in Ref. [119], this might also be achieved for smaller values of $v_{B-L} \simeq (0.7 - 1.6) \times 10^{15}$ GeV. Significantly reducing the scale of $B-L$ breaking would open up a parameter region in which the nonthermal right-handed neutrinos produced in Higgs boson decays live long enough to become non-relativistic, cf. Appendix C of Ref. [73]. The energy density of the universe during reheating would hence successively be governed by nonthermal non-relativistic Higgs bosons, nonthermal relativistic neutrinos, nonthermal non-relativistic neutrinos and thermal relativistic MSSM degrees of freedom. If this additional epoch governed by non-relativistic neutrinos is long enough, it could lead to an additional feature in the GW spectrum, clearly distinguishing such a scenario from the standard reheating process driven by inflaton decay. The precise predictions for the GW spectrum for this case remain to be investigated.

Finally, assembling the pieces of the puzzle, we find that key features of our model can be tested in upcoming experiments. First, consider the concept of a local $B-L$ symmetry, spontaneously broken at the GUT scale. This is the starting point of our model, beautifully linking GUTs, leptogenesis, the observed small neutrino masses and hybrid inflation. A clear prediction of this concept is the formation of cosmic strings, with a string tension governed by the GUT scale. Already, the cosmic string bound deduced from the scalar power spectrum of the CMB fluctuations measured by the Planck satellite is approaching this regime [2]. With further data and analyses from the Planck mission expected next year, and ongoing searches for other cosmic string signals such as massive radiation and gravitational waves, probing this prediction is within reach.

A second important building block of our model is local supersymmetry, leading to the gravitino and the neutralinos as dark matter candidates, with their abundance governed by the reheating temperature of the early universe. Here, supersymmetry searches at colliders as well as dark matter searches might soon probe this idea. For example, if dark matter searches found WIMP dark matter with an annihilation cross section compatible with the pure thermal freeze-out model or axion dark matter in a sufficient amount to explain the observed dark matter abundance, this would rule out the model presented here. On the contrary, if dark matter searches discovered WIMPs with an annihilation cross-section too large to explain the observed abundance by thermal freeze-out only, this would support our

setup since the nonthermal WIMP contribution could explain the difference between a too small thermal abundance and the observed value. Alternatively, if the LHC found hints for supersymmetry with a gravitino LSP (cf. e.g. Ref. [192]), this would support our gravitino dark matter model. Note that in the model presented here, it is not possible to tune the produced gravitino abundance to arbitrary small values and to thus render the corresponding dark matter component (gravitinos or nonthermally produced neutralinos) subdominant to an arbitrary different dark matter component. The reason is that the gravitino abundance and the produced lepton asymmetry are linked by the reheating temperature, and reducing the former by more than about one order of magnitude would render leptogenesis incapable of explaining the observed baryon asymmetry.

Third, a measurement of the gravitational wave spectrum would yield direct information about early universe cosmology, probing inflation, preheating and the existence and energy loss mechanism of cosmic strings. Such a measurement could rule out or yield direct evidence for our model. And although a precise measurement of the entire spectrum is still a dream of the future, upcoming gravitational wave detectors such as eLISA, advanced LIGO and BBO/DECIGO might well yield the first detection of the gravitational wave background in frequency bands which are of great interest for probing our model.

Appendix A

CP Violation in $2 \to 2$ Scattering Processes

To calculate the lepton asymmetry consistently to first order in the CP violation parameter ϵ, $2 \to 2$ scattering processes involving an (anti-)(s)lepton in the initial and final state must be considered. Scatterings with an on-shell neutrino in the intermediate state are already included in decay and inverse decay processes. We are hence left with the task to calculate the off-shell contribution of these processes. For the non-supersymmetric case, this was discussed in Refs. [149] and [193]. Here we explain the supersymmetric case. We first study the CP-violating contribution of the full $2 \to 2$ scattering processes and will see that this vanishes to $\mathcal{O}((h^\nu)^4)$. Hence to this order in the Yukawa coupling, the CP-violating off-shell contributions can be added by subtracting the corresponding on-shell contributions.

The right-hand side of the integrated Boltzmann equation is given by the interaction density $\gamma = g_X (2\pi)^{-3} \int d^3p\, C_X$, cf. Eqs (3.23) and (3.26). For distinct final and initial states, this is related to the corresponding S-matrix elements

$$\sum_{i,f} \gamma(i \to f) = \sum_{I,F} |S_{FI}|^2 f_I \,, \tag{A.1}$$

where the summation over the lower case letters on the left-hand side runs over different particle species and the summation over capital letters on the right-hand side additionally includes the summation over all internal degrees of freedom as well as the phase space integrals for all initial and final state particles. For the case of $2 \to 2$ scatterings in the Boltzmann equation for the lepton asymmetry, the initial and final states of interest are $\{i, f\} \in \{\ell H, \tilde{\ell}\tilde{H}, \tilde{\ell}H, \ell\tilde{H}\}$. The internal degrees of freedom are helicity, weak isospin and flavour. f_I denotes the phase space distribution function of the particle species i.

Using this notation, we now consider the CP-violating contributions of the full $2 \to 2$

scattering processes,

$$\begin{aligned}\sum_{i,f}\left[\gamma(i\to\bar{f})-\gamma(\bar{i}\to f)\right] &= \sum_{I,F}\left[|S_{\bar{F}I}|^2 f_I - |S_{F\bar{I}}|^2 f_{\bar{I}}\right] \\ &= \sum_{I,F}\left[|S_{\bar{F}I}|^2 + |S_{FI}|^2 - |S_{F\bar{I}}|^2 - |S_{\bar{F}\bar{I}}|^2\right] f_I \\ &= \sum_{I}\left[1-1\right] f_I + \mathcal{O}((h^\nu)^4) = \mathcal{O}((h^\nu)^4)\,.\end{aligned} \tag{A.2}$$

The bar indicates CP conjugation and $f_I = f_{\bar{I}}$ are the phase space distributions of the light MSSM (anti-)particles in thermal equilibrium. Here in the second line of Eq. (A.2), we extended the summation over the final states to include the lepton number conserving processes. These can be grouped in pairs of CPT conjugates and hence, due to CPT invariance, yield a vanishing contribution in total. In the third line, we exploit the unitarity of the S matrix, i.e. that the summation over all possible final states yields 1. Since, however, in Eq. (A.2) the sum runs only over all possible two-particle final states, we obtain corrections caused by neglecting multi-particle final states. For off-shell intermediate states these corrections are of $\mathcal{O}((h^\nu)^8)$ [193], however close to the resonance pole they are enhanced to $\mathcal{O}((h^\nu)^4)$ [78, 148].

Concluding, we find that the CP-violating contributions of the $2 \to 2$ scattering processes involved in the production of the lepton asymmetry vanish, with corrections of $\mathcal{O}((h^\nu)^4)$. Hence the on- and off-shell contributions cancel each other and we can use the usual 'recipe' of replacing the CP-violating contributions of the off-shell (s)neutrino decays by the negative of the respective on-shell contributions, i.e.

$$\sum_f \sum_\alpha \gamma(N_\alpha^{\text{off}} \to f) = -\sum_f \sum_\alpha \gamma(N_\alpha^{\text{on}} \to f) + \mathcal{O}((h^\nu)^4)\,, \tag{A.3}$$

where α is a flavour index. Note that looking at this line of argument closely, this argument holds separately for neutrinos and sneutrinos because of distinct sets of initial and final states, but the summation over flavour and lepton/slepton is unavoidable.

Appendix B

Parameter Dependence of the Reheating Process

In view of the different 'reheating temperatures' which turned out to be relevant in different parts of this thesis, this appendix addresses the parameter dependence of the reheating process and in particular of the different characteristic temperatures. An important aspect will the parameter dependence of the kink in the GW spectrum at $f_{\rm RH}$ associated with reheating. Here, the influence of reheating on the GW spectrum has so far been discussed for the standard scenario of reheating via inflaton decay, see e.g. Refs. [104, 194], but not for a two-stage reheating process involving two different nonthermal particle species (here the $B-L$ Higgs boson σ and the right-handed neutrino N_1). We will thus discuss how this effects the predictions for the position and shape of kink compared to the standard situation. We expect that our results hold beyond the specific setup of our model for any two-stage reheating process.

This appendix is organized as follows. Sec. B.1 recalls the different characteristic temperatures employed to describe the reheating process, explaining their physical meaning and the parameter dependencies. Sec. B.2 deals with the evolution of the scale factor during reheating, a crucial ingredient in understanding the parameter dependencies of the reheating process and in particular the differences and similarities of one- and two-stage reheating. Finally, in Sec. B.3 we summarize by pinpointing which parameters can be constrained from measurements of the GW background. For simplicity, we shall employ the Froggatt-Nielsen relation $m_S = \eta^{-2} M_1$, cf. Sec. 2.5, throughout the discussion. For more details, see also [19].

B.1 Characteristic temperatures of the reheating process

The reheating process exhibits several characteristic temperatures. With a time-resolved description of the process at hand, obtained by numerically solving the respective Boltzmann equations, cf. Sec. 3.5, we can directly read off the temperature of the thermal bath at the different times of interest. The resulting temperatures, together with the evolution of the

dominant components of the energy density are visualized in Fig. B.1 for three different points in parameter space, $\widetilde{m}_1 = 10^{-5}$, 10^{-3} and 10^{-1} eV, corresponding to different values of the ratio Γ_N^S/Γ_S^0.

The neutrino and Higgs decay temperatures

The two-stage reheating process described in Sec. 3.5 is governed by the interplay of the two decay (effective) widths Γ_S^0 and $\Gamma_{N_1}^S$, which determine the time-scale of the decay of the $B-L$ Higgs bosons and neutrinos, respectively. The corresponding decay temperatures were introduced in Eqs. (3.59) and (3.60) as

$$T_{\mathrm{RH}}^{\sigma} = T\left[H(a_{\mathrm{RH}}^{\sigma}) = \Gamma_{\sigma}^{0}\right] , \qquad T_{\mathrm{RH}}^{N} = T\left[H(a_{\mathrm{RH}}^{N}) = \Gamma_{N_1}^{S}\right] .$$

After solving the Boltzmann equations governing the reheating process numerically, we were able to give semi-analytical formulas for these quantities, cf. Eqs. (4.1) and (4.2).

Transition from non-relativistic to relativistic degrees of freedom

In Sec. 4.3 we introduced the $\hat{T}_{\mathrm{RH}}^{\sigma}$ which marks the transition from a universe dominated by non-relativistic particles ($B-L$ Higgs bosons) to an universe dominated by relativistic particles (N_1 neutrinos and/or MSSM particles),

$$\hat{T}_{\mathrm{RH}}^{\sigma} = T\left[\rho_S(\hat{a}_{\mathrm{RH}}^{\sigma}) = \frac{1}{2}\rho_{\mathrm{tot}}(\hat{a}_{\mathrm{RH}}^{\sigma})\right] .$$

This temperature characterizes the point in time when the evolution of the Hubble parameter switches from $H^2 \propto a^{-3}$ to $H^2 \propto a^{-4}$. Consequently, this temperature is directly linked to the kink in the GW spectrum marking the change in the equation of state after reheating, and we refer to it as T_{RH} in Sec. 4.3. It is per definition closely related to the Higgs decay temperature and hence its parameter dependencies, given in Eq. (4.44), are identical to those of T_{RH}^{σ}.

Transition from nonthermal to thermal degrees of freedom

In our two-stage reheating scenario the transition from non-relativistic to relativistic particles dominating the energy density does not necessarily coincide with the transition from nonthermal to thermal degrees of freedom. The reason is that the right-handed neutrinos produced in the Higgs boson decay are relativistic (and remain so until they decay) but nonthermal. Hence another interesting temperature is the 'radiation domination temperature' T_R, marking the point in time when the thermal degrees of freedom, i.e. the MSSM particles, take over as the dominant contribution of the energy density,

$$T_R = T\left[\rho_r(a_R) = \frac{1}{2}\rho_{\mathrm{tot}}\right] . \tag{B.1}$$

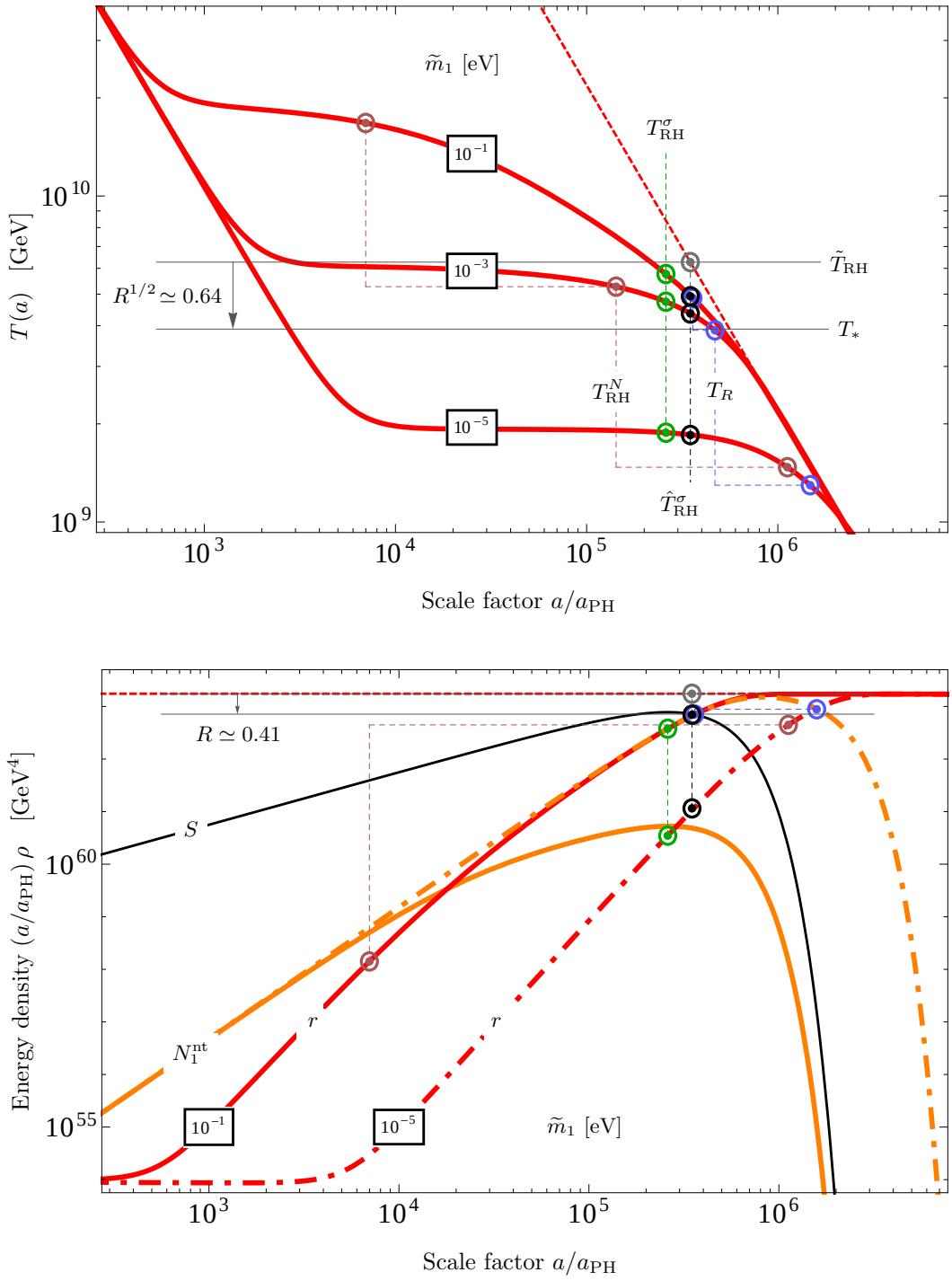

Figure B.1: Evolution of the temperature (upper panel) as well as of the $B-L$ Higgs (S), (s)neutrino ($N_1^{\rm nt}$) and radiation (r) energy densities (lower panel) as functions of the scale factor a for different values of $\widetilde{m}_1$, while keeping $M_1 = m_S/300 = 10^{11}\,\text{GeV}$ and $v_{B-L} = 5 \times 10^{15}\,\text{GeV}$ fixed. The ratio $\Gamma^S_{N_1}/\Gamma^0_S$ consequently is $\Gamma^S_{N_1}/\Gamma^0_S \ll 1$, $\Gamma^S_{N_1}/\Gamma^0_S = \mathcal{O}(1)$, $\Gamma^S_{N_1}/\Gamma^0_S \gg 1$ for $\widetilde{m}_1 = 10^{-5}$, 10^{-3}, 10^{-1} eV, respectively. The coloured markers respectively indicate the values of the various benchmark temperatures as labelled in the upper panel.

The effective kink temperature

In Sec. 4.3, we further introduced the would-be temperature $\tilde{T}_{\rm RH}$ and the effective kink temperature T_*. The continuing decay of the $B-L$ Higgs bosons and heavy neutrinos after $\hat{a}^\sigma_{\rm RH}$ results in the production of further entropy, modifying the naive assumption of an adiabatic expansion. $\tilde{T}_{\rm RH}$ denotes the temperature of the thermal bath would have had at $a = \hat{a}^\sigma_{\rm RH}$ if, extrapolating back in time from the present epoch, no entropy production took place as long as $a \geq \hat{a}^\sigma_{\rm RH}$,

$$\tilde{T}_{\rm RH} = \Delta^{1/3}\, \hat{T}^\sigma_{\rm RH}\,, \tag{B.2}$$

with Δ quantifying the actual entropy production after $a = \hat{a}^\sigma_{\rm RH}$, cf. Eq. (5.21). Explicitly solving the Boltzmann equations yields

$$\Delta \simeq \begin{cases} 2.0 & x > 180 \\ 8.5 \left(\dfrac{M_1}{10^{11}\ \text{GeV}}\right)^{0.65} \left(\dfrac{\widetilde{m}_1}{10^{-4}\ \text{eV}}\right)^{-0.65} & x < 180 \end{cases}, \tag{B.3}$$

with x defined in Eq. (4.3). Combining this with the expression for $\hat{T}^\sigma_{\rm RH}$ in Eq. (4.44), the would-be temperature $\tilde{T}_{\rm RH}$ turns out to be independent of $\widetilde{m}_1$. This can also be understood analytically: In the upper panel of Fig. B.1, $\tilde{T}_{\rm RH}$ is obtained geometrically as the intersection of the extension of the asymptotic behaviour of $T(a)$ at late times (dashed thick red line) and vertical thin black dashed line marking $\hat{a}^\sigma_{\rm RH}$. From Fig. B.1 we see that both quantities (and hence also $\tilde{T}_{\rm RH}$) do not depend on $\widetilde{m}_1$. The reason for this is that they are both directly determined by the initial energy density ρ_0 and the evolution of the scale factor, which will turn out to be insensitive to $\widetilde{m}_1$, cf. Sec. B.2.

Finally, above Eq. (4.59), we introduced the effective kink temperature,

$$T_* = R^{1/2}\, \tilde{T}_{\rm RH}\,, \tag{B.4}$$

as the temperature into which the correction factors Δ and $\alpha_{\rm RH}$ have been absorbed and which directly determines the position of the kink in the GW spectrum, cf. Eq. (4.59). Here, the factor R as introduced in Eq. (4.58) can be geometrically constructed from the lower panel of Fig. B.1. The latter shows the various energy densities, rescaled by a factor a^4, which compensates the expansion at late times. R is then given as the difference between the asymptotic value of energy density in the thermal bath at late times (thick dashed red line) and the energy density in $B-L$ Higgs bosons at $\hat{a}^\sigma_{\rm RH}$ (intersection of thick black curve and thin dashed black vertical line). Transferring this value to the upper panel enables us to identify T_*. From the lower panel of Fig. B.1 we can see that R, and hence T_*, is independent of $\widetilde{m}_1$. This can be traced back to the fact that ρ_S, the asymptotic value of ρ_r and the evolution of the scale factor do not depend on $\widetilde{m}_1$, a point we will prove in the next section. Indeed, R is furthermore also independent of M_1, cf. Sec. B.2. Taking all of this together, we

find

$$T_* \simeq 3.9 \times 10^9 \text{ GeV} \left(\frac{M_1}{10^{11} \text{ GeV}}\right)^{1.5} . \tag{B.5}$$

B.2 The scale factor during reheating

In Sec. 3.4.1 we described our method of numerically determining the scale factor during reheating. The basic idea was to analytically solve the Boltzmann equations for the dominant contributions to the energy density, ρ_S and $\rho^S_{N_1}$, treating the scale factor $a(t)$ as variable. Inserting the solutions for ρ_S and $\rho^S_{N_1}$, cf. Eqs. (3.36) and (3.38), into the Friedmann equation yields an equation for $a(t)$, which can be solved numerically by requiring self-consistency. Now, we add the following observation: In the procedure described above, we introduce an imprecision by ignoring the contribution to the energy density due to the MSSM degrees of freedom produced in the decays of the neutrinos N^S_1. But since both the nonthermal neutrinos N^S_1 as well as the thermal MSSM particles are relativistic degrees of freedom, the Friedmann equation is actually insensitive to the transformation of one to the other.[1] Hence, for the determination of the scale factor, it is sufficient to only differentiate between non-relativistic and relativistic degrees of freedom. The former are described by Eq. (3.36), as in Sec. 3.4.1 and the latter are described by Eq. (3.38) after omitting the term responsible for the decay into MSSM particles. This implies for the energy densities:

$$\rho_S(t) = m_S\, n_S(t)\,, \quad n_S(t) = n_S\left(t_{\rm PH}\right) \left(\frac{a_{\rm PH}}{a(t)}\right)^3 e^{-\Gamma^0_S (t - t_{\rm PH})}\,, \tag{B.6}$$

$$\rho_{\rm rel}(t) = m_S\, \Gamma^0_S \int_{t_{\rm PH}}^{t} dt' \left(\frac{a(t')}{a(t)}\right)^4 n_S(t')\,. \tag{B.7}$$

Inserting these into the Friedmann equation,

$$\left(\frac{\dot{a}}{a}\right)^2 = \frac{1}{3M_P^2}(\rho_S + \rho_{\rm rel})\,, \tag{B.8}$$

and solving for $a(t)$ as described above yields the evolution of the equation of state coefficient ω during reheating, cf. Eq. (3.29), as shown in Fig. B.2. Note that the parameter $\widetilde{m}_1$ does not appear in Eqs. (B.6) to (B.8), and hence the resulting quantities $\rho_S(t)$, $\rho_{\rm rel}(t)$, $a(t)$ and $\omega(a)$ cannot depend on $\widetilde{m}_1$. The same holds for the asymptotic value of ρ_r, $\rho_r(t \gg t_{RH}) = \rho_{\rm rel}(t \gg t_{RH})$. Moreover, Fig. B.2 demonstrates that the shape of $\omega(a)$ is insensitive to M_1, i.e. the three depicted curves differ only by shifts along the horizontal axis.

This has a number of remarkable consequences. First, since the shape of the GW spectrum

[1] This statement holds throughout the parameter space investigated in this paper, cf. Eq. (3.21), since explicitly solving the Boltzmann equations of Sec. 3.4.2 yields that the N^S_1 neutrinos remain relativistic throughout their lifetime. However, for smaller values of Γ^0_N/Γ^0_S, achieved e.g. by lowering the scale of $B-L$ breaking, the neutrinos can live long enough to become non-relativistic, cf. Ref. [73].

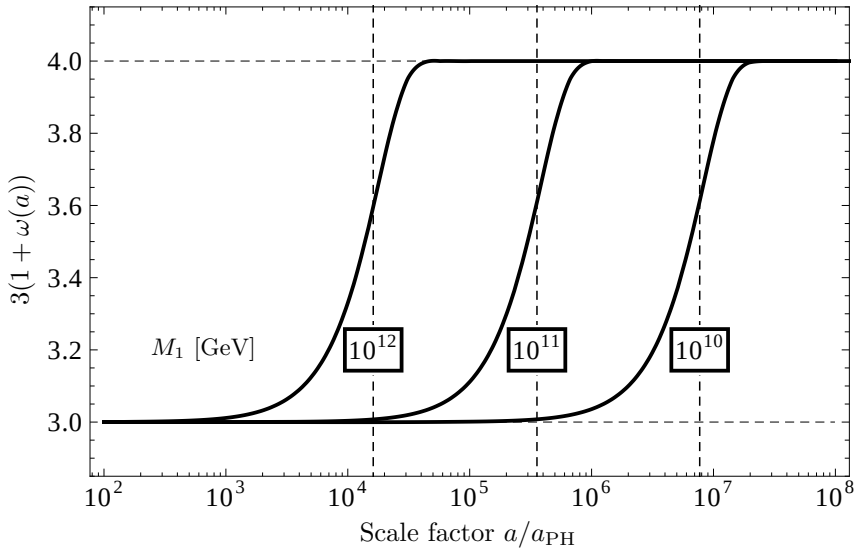

Figure B.2: Evolution of the equation of state coefficient ω as function of the scale factor a for three different values of $M_1 = \eta^2 m_S$. The vertical dashed lines indicate the respective values of $\hat{a}^\sigma_{\rm RH}$, i.e. the times when half of the non-relativistic $B-L$ Higgs particles have decayed.

from inflation is entirely determined by the evolution of the scale factor, the fact that the shape of $a(t)$ is independent of the model parameters directly implies that the coefficients $c_2^{(1)}$ and $c_2^{(2)}$ of the transfer function T_2 must be constant across the entire parameter space. In other words, the shape of the kink in the GW spectrum at $k = k_{\rm RH}$ is insensitive to the details of the reheating process and in particular insensitive to the discrimination between one- and two-stage reheating.

Second, numerically evaluating $a(t)$ as described above, we find[2]

$$\frac{\hat{a}^\sigma_{\rm RH}}{a_{\rm PH}} \propto M_1^{-1.3}\,, \quad H(\hat{a}^\sigma_{\rm RH}) \propto M_1^3\,. \tag{B.9}$$

Exploiting that in our Froggatt-Nielsen model $H_{\rm PH} \propto \sqrt{\lambda} = (M_1/v_{B-L})$, cf. Eq. (4.76), this implies that also the factor $C_{\rm RH} = (a_{\rm PH} H_{\rm PH}^{2/3})/(aH^{2/3})|_{\hat{a}^\sigma_{\rm RH}}$ introduced in Eq. (4.60) to account for the change in the equation of state between $a_{\rm PH}$ and $\hat{a}^\sigma_{\rm RH}$ is independent of all model parameters. An explicit calculation yields $C_{\rm RH} \simeq 1.13$.

Third, rewriting the factor R introduced in Eq. (4.58) as

$$R = \frac{\left(a^4\rho_{\rm rel}\right)_{a=\hat{a}^\sigma_{\rm RH}}}{\left(a^4\rho_{\rm rel}\right)_{a\gg\hat{a}^\sigma_{\rm RH}}} = \frac{I_R\left(t=t_{\rm RH}\right)}{I_R\left(t\gg t_{\rm RH}\right)}\,, \quad I_R(t) = \int_{t_{\rm PH}}^{t} dt'\,\frac{a(t')}{a_{\rm PH}}\,e^{-\Gamma_S^0(t'-t_{\rm PH})}\,, \tag{B.10}$$

[2]In our Froggatt-Nielsen flavour framework, the $B-L$ Higgs decay rate Γ_S^0 also scales as $M_1{}^3$, rendering in directly proportional to $H(\hat{a}^\sigma_{\rm RH})$. An explicit calculation yields $H(\hat{a}^\sigma_{\rm RH}) \simeq 0.58\,\Gamma_S^0$.

and inserting the solution for the scale factor, we find

$$I_R\,(t = t_{\rm RH}) \propto M_1^{-4.3}\,, \quad I_R\,(t \gg t_{\rm RH}) \propto M_1^{-4.3}\,, \qquad \rightarrow R = \text{const.}\,. \tag{B.11}$$

An explicit calculation then yields the value of R used in Sec. 4.3, $R \simeq 0.41$.

Finally, note that the crucial feature of the two-stage reheating process described in Sec. 3.5 was the interplay of the two decay rates $\Gamma_{N_1}^S$ and Γ_S^0. The insensitivity of the quantities calculated in this section to the two-stage nature of the reheating process, can directly be traced back to the fact that for the evolution of the scale factor, governed by Eqs. (B.6) to (B.8), only one of the two decay rates, namely Γ_S^0, plays a role. The decay rate $\Gamma_{N_1}^S$ drops out, because the Friedmann equation does not differentiate between relativistic neutrinos and MSSM radiation. With Γ_S^0 controlled by M_1 (and m_S), but $\Gamma_{N_1}^S$ additionally depending on $\widetilde{m}_1$, the appearance of light neutrino mass scale $\widetilde{m}_1$ turns out to be a good indicator for the importance of the two-stage nature of the reheating process for the various outputs.

B.3 Probing the model parameters with gravitational waves

The kink in the GW spectrum marking the change in the equations of state of the universe after reheating is located at $f_{\rm RH}$, which is per definition directly related to T_*, cf. Eq. (4.63). T_* is related to $\tilde{T}_{\rm RH}$ by the constant factor R, cf. Eqs. (B.4) and (B.11). As described below Eq. (B.3), $\tilde{T}_{\rm RH}$ is determined by $\hat{a}_{\rm RH}^\sigma$ and the asymptotic value of $(a(t)/a_{\rm PH})^4\rho_{\rm rel}$ for late times, both of which are determined by Eqs. (B.6) to (B.8). Exploiting $n_S(t_{\rm PH}) \simeq \rho_0/m_S$, with ρ_0 the vacuum energy density of inflation, one can easily see that both quantities can only depend on the model parameters Γ_S^0 and ρ_0. In the context of our Froggatt-Nielsen model and with v_{B-L} fixed by observations, this implies that a measurement of $f_{\rm RH}$ would determine the $B-L$ Higgs mass m_S and the (s)neutrino mass M_1,

$$m_S \simeq 2.1 \times 10^{13}\,\text{GeV}\left(\frac{f_{\rm RH}}{100\,\text{Hz}}\right)^{0.67}\,, \quad M_1 \simeq 7.1 \times 10^{10}\,\text{GeV}\left(\frac{f_{\rm RH}}{100\,\text{Hz}}\right)^{0.67}\,. \tag{B.12}$$

Assuming that the coefficient $c_2^{(2)}$ of the transfer function T_2, cf. Eq. (4.70), is roughly unity[3], $f_{\rm RH}$ might in practice be determined by measuring the amplitude of the GW spectrum at two frequencies $f_- \ll f_{\rm RH}$ and $f_+ \gg f_{RH}$:

$$f_{\rm RH} \simeq \left[\frac{\Omega_{\rm GW}(f_+)}{\Omega_{\rm GW}(f_-)}\right]^{1/2} f_+\,. \tag{B.13}$$

Although T_* and hence $f_{\rm RH}$ turn out to be insensitive to $\widetilde{m}_1$, this is not the case for

[3]For the GW spectrum from inflation, we found $c_2^{(2)} \simeq 1.04$, cf. Eq. (4.70). Considering the GW spectrum from AH cosmic strings, this value is expected to be slightly modified, depending on the precise shape of $\tilde{C}$, cf. Eq. (4.85) and the footnote on page 87.

the evolution of the temperature during the reheating process in general, as can be seen, for example, from the $\widetilde{m}_1$ dependence of T_{RH}^{N} and $T_{\mathrm{RH}}^{\sigma\,(+)}$. Consequently, a determination of f_{RH} would not suffice to determine the characteristics of the reheating process, and it would in particular still be possible to tune $\widetilde{m}_1$ to modify these. This is an important feature of our two-stage reheating scenario, distinguishing it from the usual scenario of reheating via inflaton decay.

Appendix C

Calculating the Spectral Index in the Jordan Frame

In Sec. 5.3 we calculated the predictions for single-field superconformal D-term inflation in the Einstein frame. Considering the simple structure of the CSS models in the Jordan frame, an obvious question is whether (and how) this calculation can be performed in the Jordan frame. We will address this question in this appendix. Starting from the transformation laws between the Jordan and the Einstein frame, cf. Sec. 5.1.1, we will determine the effective 1-loop scalar potential in the Jordan frame in Sec. C.1. Then, in Sec. C.2, we calculate the observables in the Jordan frame, following Ref. [195].

C.1 One-loop scalar potential in the Jordan frame

In Sec. 5.2.2, we saw that the Coleman-Weinberg 1-loop potential, cf. Eq. (3.6), played a crucial role for the dynamics of the inflaton in the Einstein frame. Let us hence determine the corresponding quantity in the Jordan frame. Since the 1-loop potential is calculated from the tree-level mass matrix of the superfields $S_\pm$, our first task is to determine these masses in the Jordan frame. These can be explicitly calculated from Eqs. (5.18), (5.23), (5.25), (5.30) and (5.37). The background metric in the Jordan frame is $g_{J\mu\nu} = \Omega_0^2\ \eta_{\mu\nu}$, cf. Eqs. (5.33) and (5.40), with $\eta_{\mu\nu}$ the Minkowski metric employed in the corresponding Einstein frame calculation. With this, one easily verifies that the scalar masses $m_\pm^J$ are identical with the masses given in Eq. (5.42),

$$m_\pm^J = m_\pm^E \tag{C.1}$$

According to the sum rule, the same then holds for the fermion mass m_f, cf. Eq. (5.44). This leads to the one-loop correction for the scalar potential $\sqrt{-g_J}\, V_J^{1l} = \sqrt{-g_E}\, V_E^{1l}$, i.e.

$$V_J^{1l} = \Omega_0^{-4}\, V_E^{1l}\,. \tag{C.2}$$

Transforming back to the Einstein frame, one obtains V^{1l} as one-loop correction to the scalar potential, in agreement with the calculation performed directly in the Einstein frame.

At this point it is interesting to understand what mechanism is at work here to ensure that the masses in the Einstein and Jordan frame are equal. To demonstrate this, let us consider a toy CSS model, consisting of a single field S with a kinetic term and a mass term. In the Einstein frame, the Lagrangian is

$$-\mathcal{L}_E = \sqrt{-g_E}\left[K_{S\bar{S}}\, g_E^{\mu\nu}(\partial_\mu S)(\partial_\nu \bar{S}) + V_E\right] = \sqrt{-g_E}\, K_{S\bar{S}}\left[g_E^{\mu\nu}(\partial_\mu S)(\partial_\nu \bar{S}) + m_E^2|S|^2\right] . \quad \text{(C.3)}$$

Rewriting the Lagrangian in the Jordan frame, cf. Secs. 5.1.1 yields

$$-\mathcal{L}_J = \sqrt{-g_J}\left[g_J^{\mu\nu}(\partial_\mu S)(\partial_\nu \bar{S}) + V_J\right] = \Omega^2\sqrt{-g_E}\left[g_E^{\mu\nu}(\partial_\mu S)(\partial_\nu \bar{S}) + m_J^2|S|^2\right] , \quad \text{(C.4)}$$

where we have exploited the feature of conical kinetic terms characteristic for the CSS models, cf. Sec. 5.1.3, and have used $\sqrt{-g_J} = \Omega^4\sqrt{-g_E}$ and $g_J^{\mu\nu} = \Omega^{-2} g_E^{\mu\nu}$. From the requirement $\mathcal{L}_E = \mathcal{L}_J$, we can directly read off $K_{S\bar{S}} m_E^2 = \Omega^2 m_J^2$. Returning to our model of superconformal D-term inflation, cf. Secs. 5.2 and 5.3, we immediately see that on the inflationary trajectory

$$K_{S_+\bar{S}_+}\big|_{S_\pm=0} = K_{S_-\bar{S}_-}\big|_{S_\pm=0} = \Omega_0^2 , \quad \text{(C.5)}$$

and hence $m_J^2 = m_E^2$. As an explicit calculation shows, this does not only work for the toy model above, but indeed for all the contributions to the $S_\pm$ mass matrix, including the FI-term contributions.

C.2 Slow-roll parameters and observables

With the 1-loop scalar potential in the Jordan frame at hand, we can now proceed and calculate the observables, in particular the spectral index. Note that we cannot use Eqs. (3.9) with (3.10), since this is only valid in the Einstein frame. Instead, this section is based on Ref. [195], where the authors derive slow-roll parameters and their relation to the spectral index for a scalar field which is non-minimally coupled to gravity.

According to Ref. [195], the Einstein frame slow-roll parameters ϵ and η entering into

$$n_s = 1 - 6\epsilon + 2\eta ,$$

are instead, in terms of Jordan frame quantities, given by

$$\epsilon = \frac{1}{2\,\Omega_0^2\, f}\left(\frac{V'_{\text{eff}}}{V_J^0}\right)^2 , \qquad \eta = \frac{1}{\Omega_0^5\, f^{1/2}\, V_J^0}\,\frac{d}{d\varphi}\left(\frac{V'_{\text{eff}}\,\Omega_0^3}{f^{1/2}}\right) , \quad \text{(C.6)}$$

with

$$V'_{\text{eff}} \coloneqq \Omega_0^{-4} \frac{d}{d\varphi}(\Omega_0^4 V_J^{1l}), \qquad f \coloneqq 1 + \frac{3}{2}\Omega_0^2 \left[\frac{d}{d\varphi}(\Omega_0^{-2})\right]^2 . \tag{C.7}$$

Here the notation is as in Sec. 5.3, i.e. $V_J^0 = \Omega^{-4} g^2 \xi^2/2$, Ω_0 is given in Eq. (5.40) and φ is the inflaton. Note that V'_{eff} as defined in (C.7) vanishes for $V_J \propto \Omega_0^{-4}$, i.e. for constant V_E. Applying Eqs. (C.6) and (C.7) to our model, we find

$$\begin{aligned}
\epsilon &\simeq 2\left(\frac{g^2 q^2}{8\pi^2}\right)^2 \frac{1}{\varphi^2} \frac{1}{1+\frac{1}{6}\chi(1+\chi)\varphi^2} , \\
\eta &\simeq -\frac{g^2 q^2}{4\pi^2} \frac{1}{\varphi^2} \frac{\left[1-\frac{1}{6}(1+\chi)\varphi^2\right]\left[1+\frac{1}{3}\chi(1+\chi)\varphi^2\right]}{\left[1+\frac{1}{6}\chi(1+\chi)\varphi^2\right]^2} ,
\end{aligned}$$

i.e. just the result found in the Einstein frame, cf. Eq. (5.57). This shows, that the inflationary predictions can be equivalently calculated in both the Einstein and the Jordan frame. In Secs. 5.3 and 5.4 we stick to the Einstein frame, since most readers will be more familiar with Eq. (3.10) than with Eq. (C.6). This is in particular true for the two-field case, when we exploit the extension of Eq. (3.10) to the multi-field case as in [191].[1]

[1] If one wanted to perform a multi-field calculation in the Jordan frame, Ref [196] which extends the analysis of Ref. [195], would probably be a good starting point. For this thesis, this appendix shall however suffice to illustrate the connections between the Einstein and Jordan frame when calculating the observables of slow-roll inflation.

Bibliography

[1] **Planck** Collaboration, P. Ade *et al.*, "Planck 2013 results. XVI. Cosmological parameters," arXiv:1303.5076 [astro-ph.CO].

[2] **Planck** Collaboration, P. Ade *et al.*, "Planck 2013 results. XXV. Searches for cosmic strings and other topological defects," arXiv:1303.5085 [astro-ph.CO].

[3] M. Maggiore, "Gravitational wave experiments and early universe cosmology," *Phys.Rept.* **331** (2000) 283–367, arXiv:gr-qc/9909001 [gr-qc].

[4] W. Buchmuller, K. Schmitz, and G. Vertongen, "Matter and Dark Matter from False Vacuum Decay," *Phys.Lett.* **B693** (2010) 421–425, arXiv:1008.2355 [hep-ph].

[5] A. D. Linde, "Hybrid inflation," *Phys. Rev.* **D49** (1994) 748–754, arXiv:astro-ph/9307002.

[6] G. N. Felder, J. Garcia-Bellido, P. B. Greene, L. Kofman, A. D. Linde, *et al.*, "Dynamics of symmetry breaking and tachyonic preheating," *Phys.Rev.Lett.* **87** (2001) 011601, arXiv:hep-ph/0012142 [hep-ph].

[7] M. Fukugita and T. Yanagida, "Baryogenesis Without Grand Unification," *Phys. Lett.* **B174** (1986) 45.

[8] **Particle Data Group** Collaboration, J. Beringer *et al.*, "Review of Particle Physics (RPP)," *Phys.Rev.* **D86** (2012) 010001.

[9] A. A. Starobinsky, "Relict Gravitation Radiation Spectrum and Initial State of the Universe. (In Russian)," *JETP Lett.* **30** (1979) 682–685.

[10] P. Amaro-Seoane, S. Aoudia, S. Babak, P. Binetruy, E. Berti, *et al.*, "eLISA: Astrophysics and cosmology in the millihertz regime," arXiv:1201.3621 [astro-ph.CO].

[11] Advanced ligo team, advanced ligo reference design (2007), http://www.ligo.caltech.edu/docs/m/m060056-10.pdf.

[12] J. Crowder and N. J. Cornish, "Beyond LISA: Exploring future gravitational wave missions," *Phys.Rev.* **D72** (2005) 083005, arXiv:gr-qc/0506015 [gr-qc].

[13] S. Kawamura, M. Ando, N. Seto, S. Sato, T. Nakamura, *et al.*, "The Japanese space gravitational wave antenna: DECIGO," *Class.Quant.Grav.* **28** (2011) 094011.

[14] R. Kallosh, L. Kofman, A. D. Linde, and A. Van Proeyen, "Superconformal symmetry, supergravity and cosmology," *Class.Quant.Grav.* **17** (2000) 4269–4338, arXiv:hep-th/0006179 [hep-th].

[15] W. Buchmuller, V. Domcke, and K. Schmitz, "Predicting θ_{13} and the Neutrino Mass Scale from Quark Lepton Mass Hierarchies," *JHEP* **1203** (2012) 008, arXiv:1111.3872 [hep-ph].

[16] W. Buchmuller, V. Domcke, and K. Schmitz, "Spontaneous B-L Breaking as the Origin of the Hot Early Universe," *Nucl.Phys.* **B862** (2012) 587–632, arXiv:1202.6679 [hep-ph].

[17] W. Buchmuller, V. Domcke, and K. Schmitz, "WIMP Dark Matter from Gravitino Decays and Leptogenesis," *Phys.Lett.* **B713** (2012) 63–67, arXiv:1203.0285 [hep-ph].

[18] W. Buchmller, V. Domcke, and K. Schmitz, "Superconformal D-Term Inflation," *JCAP* **1304** (2013) 019, arXiv:1210.4105 [hep-ph].

[19] W. Buchmuller, V. Domcke, K. Kamada, and K. Schmitz, "The Gravitational Wave Spectrum from Cosmological B-L Breaking," arXiv:1305.3392 [hep-ph].

[20] S. Glashow, "Partial Symmetries of Weak Interactions," *Nucl.Phys.* **22** (1961) 579–588.

[21] S. Weinberg, "A Model of Leptons," *Phys.Rev.Lett.* **19** (1967) 1264–1266.

[22] A. Salam, "Weak and Electromagnetic Interactions," *Conf.Proc.* **C680519** (1968) 367–377.

[23] H. Fritzsch and P. Minkowski, "Unified Interactions of Leptons and Hadrons," *Annals Phys.* **93** (1975) 193–266.

[24] H. Georgi, "The State of the Art - Gauge Theories. (Talk)," *AIP Conf.Proc.* **23** (1975) 575–582.

[25] G. 't Hooft, "Symmetry breaking through Bell-Jackiw anomalies," *Phys. Rev. Lett.* **37** (1976) 8–11.

[26] G. 't Hooft, "Computation of the quantum effects due to a four- dimensional pseudoparticle," *Phys. Rev.* **D14** (1976) 3432–3450.

[27] V. Kuzmin, V. Rubakov, and M. Shaposhnikov, "On the Anomalous Electroweak Baryon Number Nonconservation in the Early Universe," *Phys.Lett.* **B155** (1985) 36.

[28] M. Hindmarsh, "Signals of Inflationary Models with Cosmic Strings," *Prog.Theor.Phys.Suppl.* **190** (2011) 197–228, arXiv:1106.0391 [astro-ph.CO].

[29] G. Vincent, N. D. Antunes, and M. Hindmarsh, "Numerical simulations of string networks in the Abelian Higgs model," *Phys.Rev.Lett.* **80** (1998) 2277–2280, arXiv:hep-ph/9708427 [hep-ph].

[30] J. Moore, E. Shellard, and C. Martins, "On the evolution of Abelian-Higgs string networks," *Phys.Rev.* **D65** (2002) 023503, arXiv:hep-ph/0107171 [hep-ph].

[31] M. Hindmarsh, S. Stuckey, and N. Bevis, "Abelian Higgs Cosmic Strings: Small Scale Structure and Loops," *Phys.Rev.* **D79** (2009) 123504, arXiv:0812.1929 [hep-th].

[32] A. Albrecht and N. Turok, "Evolution of Cosmic String Networks," *Phys.Rev.* **D40** (1989) 973–1001.

[33] V. Vanchurin, K. D. Olum, and A. Vilenkin, "Scaling of cosmic string loops," *Phys.Rev.* **D74** (2006) 063527, arXiv:gr-qc/0511159 [gr-qc].

[34] K. D. Olum and V. Vanchurin, "Cosmic string loops in the expanding Universe," *Phys.Rev.* **D75** (2007) 063521, arXiv:astro-ph/0610419 [astro-ph].

[35] J. J. Blanco-Pillado, K. D. Olum, and B. Shlaer, "Large parallel cosmic string simulations: New results on loop production," *Phys.Rev.* **D83** (2011) 083514, arXiv:1101.5173 [astro-ph.CO].

[36] **VIRGO, LIGO Scientific** Collaboration, B. Abbott *et al.*, "An Upper Limit on the Stochastic Gravitational-Wave Background of Cosmological Origin," *Nature* **460** (2009) 990, arXiv:0910.5772 [astro-ph.CO].

[37] R. Manchester, G. Hobbs, M. Bailes, W. Coles, W. van Straten, *et al.*, "The Parkes Pulsar Timing Array Project," arXiv:1210.6130 [astro-ph.IM].

[38] J. Wess and J. Bagger, "Supersymmetry and supergravity,". Princeton University Press (1992).

[39] S. Ferrara, R. Kallosh, A. Linde, A. Marrani, and A. Van Proeyen, "Superconformal Symmetry, NMSSM, and Inflation," *Phys.Rev.* **D83** (2011) 025008, arXiv:1008.2942 [hep-th].

[40] F. Bezrukov and M. Shaposhnikov, "The Standard Model Higgs boson as the inflaton," *Phys.Lett.* **B659** (2008) 703–706, arXiv:0710.3755 [hep-th].

[41] S. Ferrara, R. Kallosh, A. Linde, A. Marrani, and A. Van Proeyen, "Jordan Frame Supergravity and Inflation in NMSSM," *Phys.Rev.* **D82** (2010) 045003, arXiv:1004.0712 [hep-th].

[42] M. B. Einhorn and D. T. Jones, "Inflation with Non-minimal Gravitational Couplings in Supergravity," *JHEP* **1003** (2010) 026, arXiv:0912.2718 [hep-ph].

[43] A. A. Starobinsky, "A New Type of Isotropic Cosmological Models Without Singularity," *Phys.Lett.* **B91** (1980) 99–102.

[44] A. H. Guth, "The Inflationary Universe: A Possible Solution to the Horizon and Flatness Problems," *Phys. Rev.* **D23** (1981) 347–356.

[45] A. D. Linde, "A New Inflationary Universe Scenario: A Possible Solution of the Horizon, Flatness, Homogeneity, Isotropy and Primordial Monopole Problems," *Phys. Lett.* **B108** (1982) 389–393.

[46] J. C. Mather, E. Cheng, D. Cottingham, R. Eplee, D. Fixsen, *et al.*, "Measurement of the Cosmic Microwave Background spectrum by the COBE FIRAS instrument," *Astrophys.J.* **420** (1994) 439–444.

[47] **WMAP** Collaboration, E. Komatsu *et al.*, "Seven-Year Wilkinson Microwave Anisotropy Probe (WMAP) Observations: Cosmological Interpretation," *Astrophys.J.Suppl.* **192** (2011) 18, arXiv:1001.4538 [astro-ph.CO].

[48] R. Allahverdi, K. Enqvist, J. Garcia-Bellido, and A. Mazumdar, "Gauge invariant MSSM inflaton," *Phys.Rev.Lett.* **97** (2006) 191304, arXiv:hep-ph/0605035 [hep-ph].

[49] H. Murayama, H. Suzuki, T. Yanagida, and J. Yokoyama, "Chaotic inflation and baryogenesis by right-handed sneutrinos," *Phys. Rev. Lett.* **70** (1993) 1912–1915.

[50] J. R. Ellis, M. Raidal, and T. Yanagida, "Sneutrino inflation in the light of WMAP: Reheating, leptogenesis and flavor-violating lepton decays," *Phys. Lett.* **B581** (2004) 9–18, arXiv:hep-ph/0303242.

[51] S. Antusch, M. Bastero-Gil, S. F. King, and Q. Shafi, "Sneutrino Hybrid Inflation in Supergravity," *Phys. Rev.* **D71** (2005) 083519, arXiv:hep-ph/0411298.

[52] S. Antusch, J. P. Baumann, V. F. Domcke, and P. M. Kostka, "Sneutrino Hybrid Inflation and Nonthermal Leptogenesis," *JCAP* **1010** (2010) 006, arXiv:1007.0708 [hep-ph].

[53] A. Ijjas, P. J. Steinhardt, and A. Loeb, "Inflationary paradigm in trouble after Planck2013," arXiv:1304.2785 [astro-ph.CO].

[54] E. J. Copeland, A. R. Liddle, D. H. Lyth, E. D. Stewart, and D. Wands, "False vacuum inflation with Einstein gravity," *Phys. Rev.* **D49** (1994) 6410–6433, arXiv:astro-ph/9401011.

[55] G. Dvali, Q. Shafi, and R. K. Schaefer, "Large scale structure and supersymmetric inflation without fine tuning," *Phys.Rev.Lett.* **73** (1994) 1886–1889, arXiv:hep-ph/9406319 [hep-ph].

[56] P. Binetruy and G. Dvali, "D term inflation," *Phys.Lett.* **B388** (1996) 241–246, arXiv:hep-ph/9606342 [hep-ph].

[57] E. Halyo, "Hybrid inflation from supergravity D terms," *Phys.Lett.* **B387** (1996) 43–47, arXiv:hep-ph/9606423 [hep-ph].

[58] A. Dolgov and A. D. Linde, "Baryon Asymmetry in Inflationary Universe," *Phys.Lett.* **B116** (1982) 329.

[59] L. Abbott, E. Farhi, and M. B. Wise, "Particle Production in the New Inflationary Cosmology," *Phys.Lett.* **B117** (1982) 29.

[60] L. Kofman, A. D. Linde, and A. A. Starobinsky, "Reheating after inflation," *Phys. Rev. Lett.* **73** (1994) 3195–3198, arXiv:hep-th/9405187.

[61] S. Weinberg, "Cosmological Constraints on the Scale of Supersymmetry Breaking," *Phys.Rev.Lett.* **48** (1982) 1303.

[62] M. Y. Khlopov and A. D. Linde, "Is It Easy to Save the Gravitino?," *Phys. Lett.* **B138** (1984) 265–268.

[63] J. R. Ellis, J. E. Kim, and D. V. Nanopoulos, "Cosmological Gravitino Regeneration and Decay," *Phys. Lett.* **B145** (1984) 181.

[64] J. R. Ellis, D. V. Nanopoulos, and S. Sarkar, "The Cosmology of Decaying Gravitinos," *Nucl. Phys.* **B259** (1985) 175.

[65] T. Moroi, H. Murayama, and M. Yamaguchi, "Cosmological constraints on the light stable gravitino," *Phys. Lett.* **B303** (1993) 289–294.

[66] M. Kawasaki, K. Kohri, and T. Moroi, "Hadronic decay of late-decaying particles and big-bang nucleosynthesis," *Phys. Lett.* **B625** (2005) 7–12, arXiv:0402490.

[67] M. Kawasaki, K. Kohri, and T. Moroi, "Big-Bang nucleosynthesis and hadronic decay of long-lived massive particles," *Phys.Rev.* **D71** (2005) 083502, arXiv:astro-ph/0408426 [astro-ph].

[68] K. Jedamzik, "Big bang nucleosynthesis constraints on hadronically and electromagnetically decaying relic neutral particles," *Phys.Rev.* **D74** (2006) 103509, arXiv:hep-ph/0604251 [hep-ph].

[69] M. Kawasaki, K. Kohri, and N. Sugiyama, "MeV scale reheating temperature and thermalization of neutrino background," *Phys.Rev.* **D62** (2000) 023506, arXiv:astro-ph/0002127 [astro-ph].

[70] S. Hannestad, "What is the lowest possible reheating temperature?," *Phys.Rev.* **D70** (2004) 043506, arXiv:astro-ph/0403291 [astro-ph].

[71] K. Ichikawa, M. Kawasaki, and F. Takahashi, "The Oscillation effects on thermalization of the neutrinos in the Universe with low reheating temperature," *Phys.Rev.* **D72** (2005) 043522, arXiv:astro-ph/0505395 [astro-ph].

[72] M. Bolz, W. Buchmuller, and M. Plumacher, "Baryon asymmetry and dark matter," *Phys.Lett.* **B443** (1998) 209–213, arXiv:hep-ph/9809381 [hep-ph].

[73] W. Buchmuller, K. Schmitz, and G. Vertongen, "Entropy, Baryon Asymmetry and Dark Matter from Heavy Neutrino Decays," *Nucl.Phys.* **B851** (2011) 481–532, arXiv:1104.2750 [hep-ph].

[74] A. D. Sakharov, "Violation of CP Invariance, C Asymmetry, and Baryon Asymmetry of the Universe," *Pisma Zh. Eksp. Teor. Fiz.* **5** (1967) 32–35.

[75] **KATRIN** Collaboration, "KATRIN: A next generation tritium beta decay experiment with sub-eV sensitivity for the electron neutrino mass," arXiv:hep-ex/0109033.

[76] **GERDA** Collaboration, "A New 76Ge Double Beta Decay Experiment at LNGS," arXiv:hep-ex/0404039.

[77] M. Plumacher, "Baryon asymmetry, neutrino mixing and supersymmetric SO(10) unification," *Nucl.Phys.* **B530** (1998) 207–246, arXiv:hep-ph/9704231 [hep-ph].

[78] W. Buchmuller, P. Di Bari, and M. Plumacher, "Leptogenesis for pedestrians," *Annals Phys.* **315** (2005) 305–351, arXiv:hep-ph/0401240 [hep-ph].

[79] G. Lazarides and Q. Shafi, "Origin of matter in the inflationary cosmology," *Phys.Lett.* **B258** (1991) 305–309.

[80] T. Asaka, K. Hamaguchi, M. Kawasaki, and T. Yanagida, "Leptogenesis in inflaton decay," *Phys.Lett.* **B464** (1999) 12–18, arXiv:hep-ph/9906366 [hep-ph].

[81] T. Asaka, K. Hamaguchi, M. Kawasaki, and T. Yanagida, "Leptogenesis in inflationary universe," *Phys.Rev.* **D61** (2000) 083512, arXiv:hep-ph/9907559 [hep-ph].

[82] F. Hahn-Woernle and M. Plumacher, "Effects of reheating on leptogenesis," *Nucl.Phys.* **B806** (2009) 68–83, arXiv:0801.3972 [hep-ph].

[83] G. Bertone, D. Hooper, and J. Silk, "Particle dark matter: Evidence, candidates and constraints," *Phys.Rept.* **405** (2005) 279–390, arXiv:hep-ph/0404175 [hep-ph].

[84] H. Goldberg, "Constraint on the Photino Mass from Cosmology," *Phys.Rev.Lett.* **50** (1983) 1419.

[85] J. R. Ellis, J. S. Hagelin, D. V. Nanopoulos, K. A. Olive, and M. Srednicki, "Supersymmetric relics from the big bang," *Nucl. Phys.* **B238** (1984) 453–476.

[86] H. Pagels and J. R. Primack, "Supersymmetry, Cosmology and New TeV Physics," *Phys.Rev.Lett.* **48** (1982) 223.

[87] M. Drees and G. Gerbier, "Mini-Review of Dark Matter: 2012," arXiv:1204.2373 [hep-ph].

[88] H. Baer, V. Barger, and A. Mustafayev, "Neutralino dark matter in mSUGRA/CMSSM with a 125 GeV light Higgs scalar," *JHEP* **1205** (2012) 091, arXiv:1202.4038 [hep-ph].

[89] J. Jaeckel and A. Ringwald, "The Low-Energy Frontier of Particle Physics," *Ann.Rev.Nucl.Part.Sci.* **60** (2010) 405–437, arXiv:1002.0329 [hep-ph].

[90] L. Randall and R. Sundrum, "Out of this world supersymmetry breaking," *Nucl.Phys.* **B557** (1999) 79–118, arXiv:hep-th/9810155 [hep-th].

[91] G. F. Giudice, M. A. Luty, H. Murayama, and R. Rattazzi, "Gaugino mass without singlets," *JHEP* **9812** (1998) 027, arXiv:hep-ph/9810442 [hep-ph].

[92] M. Ibe and T. T. Yanagida, "The Lightest Higgs Boson Mass in Pure Gravity Mediation Model," *Phys.Lett.* **B709** (2012) 374–380, arXiv:1112.2462 [hep-ph].

[93] K. S. Jeong, M. Shimosuka, and M. Yamaguchi, "Light Higgsino in Heavy Gravitino Scenario with Successful Electroweak Symmetry Breaking," *JHEP* **1209** (2012) 050, arXiv:1112.5293 [hep-ph].

[94] S. Krippendorf, H. P. Nilles, M. Ratz, and M. W. Winkler, "The heterotic string yields natural supersymmetry," *Phys.Lett.* **B712** (2012) 87–92, arXiv:1201.4857 [hep-ph].

[95] **ATLAS** Collaboration, G. Aad *et al.*, "Observation of a new particle in the search for the Standard Model Higgs boson with the ATLAS detector at the LHC," *Phys.Lett.* **B716** (2012) 1–29, arXiv:1207.7214 [hep-ex].

[96] **CMS** Collaboration, S. Chatrchyan *et al.*, "Observation of a new boson at a mass of 125 GeV with the CMS experiment at the LHC," *Phys.Lett.* **B716** (2012) 30–61, arXiv:1207.7235 [hep-ex].

[97] T. Gherghetta, G. F. Giudice, and J. D. Wells, "Phenomenological consequences of supersymmetry with anomaly induced masses," *Nucl.Phys.* **B559** (1999) 27–47, arXiv:hep-ph/9904378 [hep-ph].

[98] M. Ibe, R. Kitano, H. Murayama, and T. Yanagida, "Viable supersymmetry and leptogenesis with anomaly mediation," *Phys.Rev.* **D70** (2004) 075012, arXiv:hep-ph/0403198 [hep-ph].

[99] M. Maggiore, "Gravitational Waves. Vol. 1: Theory and Experiments,". Oxford University Press (2007).

[100] P. Binetruy, A. Bohe, C. Caprini, and J.-F. Dufaux, "Cosmological Backgrounds of Gravitational Waves and eLISA/NGO: Phase Transitions, Cosmic Strings and Other Sources," *JCAP* **1206** (2012) 027, arXiv:1201.0983 [gr-qc].

[101] V. Rubakov, M. Sazhin, and A. Veryaskin, "Graviton Creation in the Inflationary Universe and the Grand Unification Scale," *Phys.Lett.* **B115** (1982) 189–192.

[102] M. S. Turner, M. J. White, and J. E. Lidsey, "Tensor perturbations in inflationary models as a probe of cosmology," *Phys.Rev.* **D48** (1993) 4613–4622, arXiv:astro-ph/9306029 [astro-ph].

[103] R. Saito and S. Shirai, "Gravitational Wave Probe of High Supersymmetry Breaking Scale," *Phys.Lett.* **B713** (2012) 237–243, arXiv:1201.6589 [hep-ph].

[104] K. Nakayama, S. Saito, Y. Suwa, and J. Yokoyama, "Probing reheating temperature of the universe with gravitational wave background," *JCAP* **0806** (2008) 020, arXiv:0804.1827 [astro-ph].

[105] S. Khlebnikov and I. Tkachev, "Relic gravitational waves produced after preheating," *Phys.Rev.* **D56** (1997) 653–660, arXiv:hep-ph/9701423 [hep-ph].

[106] J. Garcia-Bellido and D. G. Figueroa, "A stochastic background of gravitational waves from hybrid preheating," *Phys.Rev.Lett.* **98** (2007) 061302, arXiv:astro-ph/0701014 [astro-ph].

[107] J. F. Dufaux, A. Bergman, G. N. Felder, L. Kofman, and J.-P. Uzan, "Theory and Numerics of Gravitational Waves from Preheating after Inflation," *Phys.Rev.* **D76** (2007) 123517, arXiv:0707.0875 [astro-ph].

[108] J.-F. Dufaux, G. Felder, L. Kofman, and O. Navros, "Gravity Waves from Tachyonic Preheating after Hybrid Inflation," *JCAP* **0903** (2009) 001, arXiv:0812.2917 [astro-ph].

[109] J.-F. Dufaux, D. G. Figueroa, and J. Garcia-Bellido, "Gravitational Waves from Abelian Gauge Fields and Cosmic Strings at Preheating," *Phys.Rev.* **D82** (2010) 083518, arXiv:1006.0217 [astro-ph.CO].

[110] A. Vilenkin, "Gravitational radiation from cosmic strings," *Phys.Lett.* **B107** (1981) 47–50.

[111] D. G. Figueroa, M. Hindmarsh, and J. Urrestilla, "Exact Scale-Invariant Background of Gravitational Waves from Cosmic Defects," *Phys. Rev. Lett. 110,* **101302** (2013) , arXiv:1212.5458 [astro-ph.CO].

[112] T. Damour and A. Vilenkin, "Gravitational wave bursts from cusps and kinks on cosmic strings," *Phys.Rev.* **D64** (2001) 064008, arXiv:gr-qc/0104026 [gr-qc].

[113] X. Siemens, V. Mandic, and J. Creighton, "Gravitational wave stochastic background from cosmic (super)strings," *Phys.Rev.Lett.* **98** (2007) 111101, arXiv:astro-ph/0610920 [astro-ph].

[114] S. Kuroyanagi, K. Miyamoto, T. Sekiguchi, K. Takahashi, and J. Silk, "Forecast constraints on cosmic string parameters from gravitational wave direct detection experiments," *Phys.Rev.* **D86** (2012) 023503, arXiv:1202.3032 [astro-ph.CO].

[115] R. van Haasteren, Y. Levin, G. Janssen, K. Lazaridis, M. K. B. Stappers, *et al.*, "Placing limits on the stochastic gravitational-wave background using European Pulsar Timing Array data," arXiv:1103.0576 [astro-ph.CO].

[116] www.ligo.caltech.edu. Data from s6 run.

[117] M. Hindmarsh and D. T. Jones, "Consistent cosmology with Higgs thermal inflation in a minimal extension of the MSSM," *JCAP* **1303** (2013) 021, arXiv:1301.4890 [hep-ph].

[118] K. Nakayama, F. Takahashi, and T. T. Yanagida, "Constraint on the gravitino mass in hybrid inflation," *JCAP* **1012** (2010) 010, arXiv:1007.5152 [hep-ph].

[119] C. Pallis and Q. Shafi, "Update on Minimal Supersymmetric Hybrid Inflation in Light of PLANCK," arXiv:1304.5202 [hep-ph].

[120] D. Bailin and A. Love, "Supersymmetric gauge field theory and string theory,". Bristol, UK: IOP (1994).

[121] C. Froggatt and H. B. Nielsen, "Hierarchy of Quark Masses, Cabibbo Angles and CP Violation," *Nucl.Phys.* **B147** (1979) 277.

[122] W. Buchmuller and T. Yanagida, "Quark lepton mass hierarchies and the baryon asymmetry," *Phys.Lett.* **B445** (1999) 399–402, arXiv:hep-ph/9810308 [hep-ph].

[123] M. Fujii, K. Hamaguchi, and T. Yanagida, "Leptogenesis with almost degenerate Majorana neutrinos," *Phys. Rev.* **D65** (2002) 115012, arXiv:hep-ph/0202210.

[124] D. Baumann, "TASI Lectures on Inflation," arXiv:0907.5424 [hep-th].

[125] E. J. Copeland, S. Pascoli, and A. Rajantie, "Dynamics of tachyonic preheating after hybrid inflation," *Phys.Rev.* **D65** (2002) 103517, arXiv:hep-ph/0202031 [hep-ph].

[126] J. Garcia-Bellido, M. Garcia Perez, and A. Gonzalez-Arroyo, "Symmetry breaking and false vacuum decay after hybrid inflation," *Phys.Rev.* **D67** (2003) 103501, arXiv:hep-ph/0208228 [hep-ph].

[127] J. Garcia-Bellido and E. Ruiz Morales, "Particle production from symmetry breaking after inflation," *Phys. Lett.* **B536** (2002) 193–202, arXiv:hep-ph/0109230.

[128] J. Berges, D. Gelfand, and J. Pruschke, "Quantum theory of fermion production after inflation," *Phys.Rev.Lett.* **107** (2011) 061301, arXiv:1012.4632 [hep-ph].

[129] F. Lenz, "Topological concepts in gauge theories," *Lect.Notes Phys.* **659** (2005) 7–98, arXiv:hep-th/0403286 [hep-th].

[130] A. Vilenkin, "Cosmic strings and other topological defects,". Cambridge University Press (1994).

[131] S. Kuroyanagi, K. Miyamoto, T. Sekiguchi, K. Takahashi, and J. Silk, "Forecast constraints on cosmic strings from future CMB, pulsar timing and gravitational wave direct detection experiments," *Phys.Rev.* **D87** (2013) 023522, arXiv:1210.2829 [astro-ph.CO].

[132] G. Sigl, K. Jedamzik, D. Schramm, and V. Berezinsky, "Helium photodisintegration and nucleosynthesis: Implications for topological defects, high-energy cosmic rays, and massive black holes," *Phys.Rev.* **D52** (1995) 6682–6693, arXiv:astro-ph/9503094 [astro-ph].

[133] R. Protheroe and T. Stanev, "Limits on topological defects models of the ultrahigh-energy cosmic rays," *Phys.Rev.Lett.* **77** (1996) 3708–3711, arXiv:astro-ph/9605036 [astro-ph].

[134] P. Bhattacharjee, Q. Shafi, and F. Stecker, "TeV and superheavy mass scale particles from supersymmetric topological defects, the extragalactic gamma-ray background, and the highest energy cosmic rays," *Phys.Rev.Lett.* **80** (1998) 3698–3701, arXiv:hep-ph/9710533 [hep-ph].

[135] G. Sigl, S. Lee, P. Bhattacharjee, and S. Yoshida, "Probing grand unified theories with cosmic ray, gamma-ray and neutrino astrophysics," *Phys.Rev.* **D59** (1999) 043504, arXiv:hep-ph/9809242 [hep-ph].

[136] U. Wichoski, J. H. MacGibbon, and R. H. Brandenberger, "High-energy neutrinos, photons and cosmic ray fluxes from VHS cosmic strings," *Phys.Rev.* **D65** (2002) 063005, arXiv:hep-ph/9805419 [hep-ph].

[137] C. T. Hill, H. M. Hodges, and M. S. Turner, "Variational Study of Ordinary and Superconducting Cosmic Strings," *Phys.Rev.Lett.* **59** (1987) 2493.

[138] H. de Vega and F. Schaposnik, "A Classical Vortex Solution of the Abelian Higgs Model," *Phys.Rev.* **D14** (1976) 1100–1106.

[139] N. Bevis, M. Hindmarsh, M. Kunz, and J. Urrestilla, "Fitting CMB data with cosmic strings and inflation," *Phys.Rev.Lett.* **100** (2008) 021301, arXiv:astro-ph/0702223 [astro-ph].

[140] N. Bevis, M. Hindmarsh, M. Kunz, and J. Urrestilla, "CMB power spectrum contribution from cosmic strings using field-evolution simulations of the Abelian Higgs model," *Phys.Rev.* **D75** (2007) 065015, arXiv:astro-ph/0605018 [astro-ph].

[141] T. Asaka, W. Buchmuller, and L. Covi, "False vacuum decay after inflation," *Phys.Lett.* **B510** (2001) 271–276, arXiv:hep-ph/0104037 [hep-ph].

[142] R. A. Battye, B. Garbrecht, and A. Moss, "Constraints on Supersymmetric Models of Hybrid Inflation," *JCAP* **0609** (2006) 007, arXiv:astro-ph/0607339 [astro-ph].

[143] R. Battye, B. Garbrecht, and A. Moss, "Tight constraints on F- and D-term hybrid inflation scenarios," *Phys.Rev.* **D81** (2010) 123512, arXiv:1001.0769 [astro-ph.CO].

[144] R. Jeannerot and M. Postma, "Confronting hybrid inflation in supergravity with CMB data," *JHEP* **0505** (2005) 071, arXiv:hep-ph/0503146 [hep-ph].

[145] R. Battye and A. Moss, "Updated constraints on the cosmic string tension," *Phys.Rev.* **D82** (2010) 023521, arXiv:1005.0479 [astro-ph.CO].

[146] W. Buchmuller, R. Peccei, and T. Yanagida, "Leptogenesis as the origin of matter," *Ann.Rev.Nucl.Part.Sci.* **55** (2005) 311–355, arXiv:hep-ph/0502169 [hep-ph].

[147] F. Hahn-Woernle, M. Plumacher, and Y. Y. Y. Wong, "Full Boltzmann equations for leptogenesis including scattering," *JCAP* **0908** (2009) 028, arXiv:0907.0205 [hep-ph].

[148] L. Covi, E. Roulet, and F. Vissani, "CP violating decays in leptogenesis scenarios," *Phys. Lett.* **B384** (1996) 169–174, arXiv:hep-ph/9605319.

[149] W. Buchmuller and M. Plumacher, "CP asymmetry in Majorana neutrino decays," *Phys.Lett.* **B431** (1998) 354–362, arXiv:hep-ph/9710460 [hep-ph].

[150] M. Bolz, A. Brandenburg, and W. Buchmuller, "Thermal production of gravitinos," *Nucl.Phys.* **B606** (2001) 518–544, arXiv:hep-ph/0012052 [hep-ph].

[151] S. P. Martin, "A Supersymmetry Primer," arXiv:hep-ph/9709356.

[152] N. Arkani-Hamed, A. Delgado, and G. Giudice, "The Well-tempered neutralino," *Nucl.Phys.* **B741** (2006) 108–130, arXiv:hep-ph/0601041 [hep-ph].

[153] J. Hisano, S. Matsumoto, M. Nagai, O. Saito, and M. Senami, "Non-perturbative effect on thermal relic abundance of dark matter," *Phys.Lett.* **B646** (2007) 34–38, arXiv:hep-ph/0610249 [hep-ph].

[154] M. Cirelli, A. Strumia, and M. Tamburini, "Cosmology and Astrophysics of Minimal Dark Matter," *Nucl.Phys.* **B787** (2007) 152–175, arXiv:0706.4071 [hep-ph].

[155] D. Bailin and A. Love, "Cosmology in gauge field theory and string theory,". Bristol, UK: IOP (2004).

[156] F. Borzumati, T. Bringmann, and P. Ullio, "Dark matter from late decays and the small-scale structure problems," *Phys.Rev.* **D77** (2008) 063514, arXiv:hep-ph/0701007 [hep-ph].

[157] M. Kawasaki, K. Kohri, T. Moroi, and A. Yotsuyanagi, "Big-Bang Nucleosynthesis and Gravitino," *Phys.Rev.* **D78** (2008) 065011, arXiv:0804.3745 [hep-ph].

[158] J. Hisano, S. Matsumoto, M. M. Nojiri, and O. Saito, "Direct detection of the Wino and Higgsino-like neutralino dark matters at one-loop level," *Phys.Rev.* **D71** (2005) 015007, arXiv:hep-ph/0407168 [hep-ph].

[159] **XENON100** Collaboration, E. Aprile *et al.*, "Dark Matter Results from 225 Live Days of XENON100 Data," *Phys.Rev.Lett.* **109** (2012) 181301, arXiv:1207.5988 [astro-ph.CO].

[160] H. Baer, V. Barger, and P. Huang, "Hidden SUSY at the LHC: the light higgsino-world scenario and the role of a lepton collider," *JHEP* **1111** (2011) 031, arXiv:1107.5581 [hep-ph].

[161] S. Bobrovskyi, F. Brummer, W. Buchmuller, and J. Hajer, "Searching for light higgsinos with b-jets and missing leptons," *JHEP* **1201** (2012) 122, arXiv:1111.6005 [hep-ph].

[162] T. Moroi and K. Nakayama, "Wino LSP detection in the light of recent Higgs searches at the LHC," *Phys.Lett.* **B710** (2012) 159–163, arXiv:1112.3123 [hep-ph].

[163] T. L. Smith, M. Kamionkowski, and A. Cooray, "Direct detection of the inflationary gravitational wave background," *Phys.Rev.* **D73** (2006) 023504, arXiv:astro-ph/0506422 [astro-ph].

[164] V. Mukhanov, "Physical foundations of cosmology,". Cambridge University Press (2005).

[165] Y. Watanabe and E. Komatsu, "Improved Calculation of the Primordial Gravitational Wave Spectrum in the Standard Model," *Phys.Rev.* **D73** (2006) 123515, arXiv:astro-ph/0604176 [astro-ph].

[166] G. N. Felder and L. Kofman, "Nonlinear inflaton fragmentation after preheating," *Phys.Rev.* **D75** (2007) 043518, arXiv:hep-ph/0606256 [hep-ph].

[167] R. Durrer, M. Kunz, and A. Melchiorri, "Cosmic microwave background anisotropies from scaling seeds: Global defect models," *Phys.Rev.* **D59** (1999) 123005, arXiv:astro-ph/9811174 [astro-ph].

[168] M. Hindmarsh. Private communication.

[169] M. Kramer, "Fundamental physics with the SKA: Strong-field tests of gravity using pulsars and black holes," arXiv:astro-ph/0409020 [astro-ph].

[170] F. Aharonian, T. Arshakian, B. Allen, R. Banerjee, R. Beck, *et al.*, "Pathway to the Square Kilometre Array - The German White Paper -," arXiv:1301.4124 [astro-ph.IM].

[171] Http://www.et-gw.eu/etsensitivities#datafiles.

[172] **LCGT** Collaboration, K. Kuroda, "Status of LCGT," *Class.Quant.Grav.* **27** (2010) 084004.

[173] Y. Izotov and T. Thuan, "The primordial abundance of 4He: evidence for non-standard big bang nucleosynthesis," *Astrophys.J.* **710** (2010) L67–L71, arXiv:1001.4440 [astro-ph.CO].

[174] T. L. Smith, E. Pierpaoli, and M. Kamionkowski, "A new cosmic microwave background constraint to primordial gravitational waves," *Phys.Rev.Lett.* **97** (2006) 021301, arXiv:astro-ph/0603144 [astro-ph].

[175] http://gwcenter.icrr.u tokyo.ac.jp/researcher/parameters.

[176] L. Alabidi, K. Kohri, M. Sasaki, and Y. Sendouda, "Observable Spectra of Induced Gravitational Waves from Inflation," *JCAP* **1209** (2012) 017, arXiv:1203.4663 [astro-ph.CO].

[177] Q. Shafi and A. Vilenkin, "Spontaneously broken global symmetries and cosmology," *Phys.Rev.* **D29** (1984) 1870.

[178] J. Yokoyama, "Inflation can save cosmic strings," *Phys.Rev.Lett.* **63** (1989) 712.

[179] K. Freese, T. Gherghetta, and H. Umeda, "Moduli inflation with large scale structure produced by topological defects," *Phys.Rev.* **D54** (1996) 6083–6087, arXiv:hep-ph/9512211 [hep-ph].

[180] K. Kamada, Y. Miyamoto, and J. Yokoyama, "Evading the pulsar constraints on the cosmic string tension in supergravity inflation," *JCAP* **1210** (2012) 023, arXiv:1204.3237 [astro-ph.CO].

[181] A. Linde, "Chaotic inflation in supergravity and cosmic string production," arXiv:1303.4435 [hep-th].

[182] **Daya Bay** Collaboration, F. An *et al.*, "Improved Measurement of Electron Antineutrino Disappearance at Daya Bay," *Chin. Phys.* **C37** (2013) 011001, arXiv:1210.6327 [hep-ex].

[183] S. Fulling, "Aspects of quantum field theory in curved space-time," *London Math.Soc.Student Texts* **17** (1989) 1–315.

[184] M. B. Einhorn and D. T. Jones, "GUT Scalar Potentials for Higgs Inflation," *JCAP* **1211** (2012) 049, arXiv:1207.1710 [hep-ph].

[185] V. Mukhanov and S. Winitzki, "Introduction to quantum effects in gravity,". Cambridge University Press (2007).

[186] S. Antusch, K. Dutta, and P. M. Kostka, "Tribrid Inflation in Supergravity," *AIP Conf. Proc.* **1200** (2010) 1007–1010, arXiv:0908.1694 [hep-ph].

[187] H. M. Lee, "Chaotic inflation in Jordan frame supergravity," *JCAP* **1008** (2010) 003, arXiv:1005.2735 [hep-ph].

[188] J. Urrestilla, N. Bevis, M. Hindmarsh, and M. Kunz, "Cosmic string parameter constraints and model analysis using small scale Cosmic Microwave Background data," *JCAP* **1112** (2011) 021, arXiv:1108.2730 [astro-ph.CO].

[189] R. Kallosh and A. D. Linde, "P term, D term and F term inflation," *JCAP* **0310** (2003) 008, arXiv:hep-th/0306058 [hep-th].

[190] J. Rocher and M. Sakellariadou, "Supersymmetric grand unified theories and cosmology," *JCAP* **0503** (2005) 004, arXiv:hep-ph/0406120 [hep-ph].

[191] M. Sasaki and E. D. Stewart, "A General analytic formula for the spectral index of the density perturbations produced during inflation," *Prog.Theor.Phys.* **95** (1996) 71–78, arXiv:astro-ph/9507001 [astro-ph].

[192] S. Bobrovskyi, J. Hajer, and S. Rydbeck, "Long-lived higgsinos as probes of gravitino dark matter at the LHC," *JHEP* **1302** (2013) 133, arXiv:1211.5584 [hep-ph].

[193] E. Roulet, L. Covi, and F. Vissani, "On the CP asymmetries in Majorana neutrino decays," *Phys.Lett.* **B424** (1998) 101–105, arXiv:hep-ph/9712468 [hep-ph].

[194] S. Kuroyanagi, K. Nakayama, and S. Saito, "Prospects for determination of thermal history after inflation with future gravitational wave detectors," *Phys.Rev.* **D84** (2011) 123513, arXiv:1110.4169 [astro-ph.CO].

[195] T. Chiba and M. Yamaguchi, "Extended Slow-Roll Conditions and Rapid-Roll Conditions," *JCAP* **0810** (2008) 021, arXiv:0807.4965 [astro-ph].

[196] T. Chiba and M. Yamaguchi, "Extended Slow-Roll Conditions and Primordial Fluctuations: Multiple Scalar Fields and Generalized Gravity," *JCAP* **0901** (2009) 019, arXiv:0810.5387 [astro-ph].

Acknowledgements

First of all, I would like to thank my supervisor Wilfried Buchmüller for his guidance throughout the last few years, for his valuable comments, for pointing out possible flaws in my argumentation and simply for the amazing amount of time he spent in our discussions. He gave me the possibility to work on various different very interesting topics, and looking back, I feel that I have learned really a lot during my time at DESY. He has been an excellent advisor, teacher and mentor.

I further want to thank my other collaborators, Kohei Kamada and Kai Schmitz, for their commitment and for many hours of discussion. I also thank Guido Alterelli, Stefan Antusch, Thorsten Bringmann, Felix Brümmer, Daniel Figueroa, Mark Hindmarsh, Tim Jones, Thomas Konstandin, Fuminobu Takahashi, Gilles Vertongen, Alexander Westphal, Walter Winter and Tsutomu Yanagida for helpful discussions and comments. Moreover, I thank Jan Louis, Juan Garcia-Bellido and Günter Sigl for agreeing to act as referees of my dissertation and disputation. Moreover, I acknowledge support by the German Science Foundation (DFG) within the Collaborative Research Centre (SFB) 676 "Particles, Strings and the Early Universe" as well as by the "Studienstiftung des dt. Volkes", which supported me throughout my studies and while working on this thesis. Furthermore, I want to thank my colleagues who proofread parts of this thesis, namely Kai Schmitz, Clemens Wieck, Felix Brümmer, Elina Fuchs and Sarah Andreas.

Special thanks to the many new friends I have made at DESY, who made this time in Hamburg a really invaluable experience. In particular, to Elina for bringing me into the best office ever and for organizing so many events, to Sarah for the many conversations and for motivating me to go to sport, to Matthias for the amazing cookies, to Václav for enforcing regular coffee breaks, to Aoife and Sara for the regular visits to our office, to Jan He. for the great time at the ICTP and TASI summer schools, to Falk for organizing the BBQs and solving my computer problems, to Jan Ha. for all the discussions after/in various lectures, to Stefano for trying to teach me Italian and to the Italian community of building 67b for fantastic pasta and games of dart. Very special thanks to Kai for answering my questions with an endless patience, for many, many, many hours of discussion and cross-checks in the coffee room and via Skype, for solving my Mathematica problems and finding my missing factors of two. Last but not least, thank you to Sebastian for everything and in particular for the support while finalizing this thesis.